NOVEL IMAGING TECHNIQUES IN THE MANAGEMENT OF THYROID NODULES AND AUTOIMMUNE THYROID DISEASE

EDITED BY: Marek Ruchala, Joanna Klubo-Gwiezdzinska and Ewelina Szczepanek-Parulska

PUBLISHED IN: Frontiers in Endocrinology

frontiers Research Topics

ISSN 1664-8714
ISBN 978-2-88963-330-2
DOI 10.3389/978-2-88963-330-2

About Frontiers

Frontiers is more than just an open-access publisher of scholarly articles: it is a pioneering approach to the world of academia, radically improving the way scholarly research is managed. The grand vision of Frontiers is a world where all people have an equal opportunity to seek, share and generate knowledge. Frontiers provides immediate and permanent online open access to all its publications, but this alone is not enough to realize our grand goals.

Frontiers Journal Series

The Frontiers Journal Series is a multi-tier and interdisciplinary set of open-access, online journals, promising a paradigm shift from the current review, selection and dissemination processes in academic publishing. All Frontiers journals are driven by researchers for researchers; therefore, they constitute a service to the scholarly community. At the same time, the Frontiers Journal Series operates on a revolutionary invention, the tiered publishing system, initially addressing specific communities of scholars, and gradually climbing up to broader public understanding, thus serving the interests of the lay society, too.

Dedication to Quality

Each Frontiers article is a landmark of the highest quality, thanks to genuinely collaborative interactions between authors and review editors, who include some of the world's best academicians. Research must be certified by peers before entering a stream of knowledge that may eventually reach the public - and shape society; therefore, Frontiers only applies the most rigorous and unbiased reviews.
Frontiers revolutionizes research publishing by freely delivering the most outstanding research, evaluated with no bias from both the academic and social point of view. By applying the most advanced information technologies, Frontiers is catapulting scholarly publishing into a new generation.

What are Frontiers Research Topics?

Frontiers Research Topics are very popular trademarks of the Frontiers Journals Series: they are collections of at least ten articles, all centered on a particular subject. With their unique mix of varied contributions from Original Research to Review Articles, Frontiers Research Topics unify the most influential researchers, the latest key findings and historical advances in a hot research area! Find out more on how to host your own Frontiers Research Topic or contribute to one as an author by contacting the Frontiers Editorial Office: researchtopics@frontiersin.org

NOVEL IMAGING TECHNIQUES IN THE MANAGEMENT OF THYROID NODULES AND AUTOIMMUNE THYROID DISEASE

Topic Editors:
Marek Ruchala, Poznan University of Medical Sciences, Poland
Joanna Klubo-Gwiezdzinska, National Institutes of Health (NIH), United States
Ewelina Szczepanek-Parulska, Poznan University of Medical Sciences, Poland

Citation: Ruchala, M., Klubo-Gwiezdzinska, J., Szczepanek-Parulska, E., eds. (2020). Novel Imaging Techniques in the Management of Thyroid Nodules and Autoimmune Thyroid Disease. Lausanne: Frontiers Media SA. doi: 10.3389/978-2-88963-330-2

Table of Contents

frontiers in Endocrinology

EDITORIAL
published: 20 November 2019
doi: 10.3389/fendo.2019.00804

Editorial: Novel Imaging Techniques in the Management of Thyroid Nodules and Autoimmune Thyroid Disease

Ewelina Szczepanek-Parulska[1], *Joanna Klubo-Gwiezdzinska*[2] *and Marek Ruchala*[1]*

[1] *Department of Endocrinology, Metabolism and Internal Medicine, Poznan University of Medical Sciences, Poznan, Poland,* [2] *Thyroid Tumors and Functional Thyroid Disorders Section, National Institute of Diabetes and Digestive and Kidney Diseases (NIDDK), Bethesda, MD, United States*

Keywords: thyroid nodules, thyroid cancer, Graves Disease, subacute thyroiditis, autoimmune thyroid disease

Editorial on the Research Topic

Novel Imaging Techniques in the Management of Thyroid Nodules and Autoimmune Thyroid Disease

The high incidence of thyroid nodules, ranging from about 10 up to 70% of adult population, constitute a major socioeconomic problem (1). Wide access to high-resolution thyroid ultrasonography (US) and other imaging techniques has dramatically raised the detection rate of thyroid lesions (2), but only 8–18% of thyroid nodules in general population are malignant (3). Therefore, an everyday diagnostic challenge for endocrinologists is to identify the patients with higher risk of malignancy, who should undergo prompt diagnostics and surgical management. The gold standard of thyroid nodules diagnostics is conventional ultrasonography followed by fine-needle aspiration biopsy (FNAB) of qualified lesions. However, biopsy is an invasive procedure, which has certain limitations as up to 10–25% patients undergoing biopsy receive inconclusive cytological result (4–6). Hence, there is still a need to search for novel imaging procedures or markers, that would allow a non-invasive estimation of malignancy risk with satisfying sensitivity and specificity. Recent studies have demonstrated that novel imaging techniques might be also used as an additional diagnostic tool to monitor and differentiate different types of thyroiditis (7). The goal of this Research Topic collection is to present current trends and progress that novel techniques of thyroid imaging brings to diagnostics, monitoring and therapy of thyroid nodules and autoimmune thyroid disease (AITD).

In the recent years, the sonoelastography has been introduced as a promising tool to differentiate between benign and malignant thyroid lesions (8, 9). Although current data reveal that diagnostic value of sonoelastography is inferior compared with FNAB, this technique is still considered as a very useful additional method increasing diagnostic accuracy of conventional ultrasound. Consistently, Dobruch-Sobczak et al. in a study including 208 patients with 305 thyroid nodules concludes that decreased elasticity of thyroid nodules is associated with increased risk of malignancy that may justify more aggressive management. In the study by Liu et al. authors employed specific MRI modalities and demonstrated its potential usefulness in differentiation between benign and malignant thyroid nodules. Zonally oblique multi-slice diffusion-weighted imaging (area under curve—AUC = 0.937) proved to be superior to amide proton transfer (AUC = 0.783), $p = 0.028$. Authors conclude that these modalities might constitute a non-invasive, promising method for improving differential diagnosis of thyroid nodules in a clinical setting. Appropriate management of thyroid nodules in pediatric population constitutes a particularly difficult task, i.e., due to possible presence of ectopic intrathyroidal thymic tissue and the similarity

OPEN ACCESS

Edited and reviewed by:
Terry Francis Davies, Icahn School of Medicine at Mount Sinai, United States

***Correspondence:**
Marek Ruchala
mruchala@ump.edu.pl

Specialty section:
This article was submitted to Thyroid Endocrinology, a section of the journal Frontiers in Endocrinology

Received: *22 September 2019*
Accepted: *04 November 2019*
Published: *20 November 2019*

Citation:
Szczepanek-Parulska E, Klubo-Gwiezdzinska J and Ruchala M (2019) Editorial: Novel Imaging Techniques in the Management of Thyroid Nodules and Autoimmune Thyroid Disease. Front. Endocrinol. 10:804. doi: 10.3389/fendo.2019.00804

of its US pattern to thyroid carcinoma. Sonographic features allowing for initial differential diagnosis of such ectopic tissue and malignant lesions are presented in the study by Stasiak et al. The authors also demonstrated a significant role of sonoelastography in differential diagnosis of such lesions, and presented examples of its application.

Another specific subgroup of patients are subjects diagnosed with low-risk papillary thyroid microcarcinoma. There has been an ongoing debate on the possibility of active surveillance (AS) instead of surgical therapy in these patients. That approach is endorsed by the Japanese Thyroid Society as well as by the American Thyroid Association and European guidelines on the management of thyroid nodules and thyroid cancer (6, 10–13). The comprehensive review article by Xue et al. summarizes the current state of knowledge on the role of imaging techniques implemented in AS and involves clues helpful during follow-up of these patients. Authors indicate limited value of US in detecting extra-thyroid extension or lymph node metastases, which could be increased by combining it with computed tomography (CT) scan. Although patients with AS approach are at slightly higher risk of lymph node metastases than those managed surgically, still the incidence remains low in both groups and disease specific survival and overall survival is similar. Moreover, authors underline the role of genetic biomarkers that might be helpful to differentiate between the low and high-risk thyroid cancers and discuss ethical issues concerning the process of qualification of patients to be surveilled instead of surgically managed.

Due to current wider accessibility of MRI, more and more patients would have an incidentally detected thyroid pathology found by this imaging modality. Hence, the MRI-based image characteristics of thyroid nodules and diffuse thyroid pathologies, such as AITD, need to be appropriately recognized and interpreted. Kang et al. addresses this issue and summarizes incidental thyroid findings in a group of 387 patients with neck MRI performed as a part of diagnostic workup for non-thyroidal illness and present the MRI characteristics of the thyroid images found in patients with evidence of AITD. The main MRI characteristics of AITD consist of high and inhomogeneous signal intensity on T2-weighted images. Another study by Malkowski et al. demonstrated that patients with AITD differ from subjects with normal thyroid also in terms of standardized uptake value (SUV-max) of the thyroid parenchyma measured using 18F-FDG-PET/CT. Given increasing accessibility to 18F-FDG-PET/CT imaging worldwide, it is important to correctly interpret and verify increased diffused radioisotope uptake detected in patients undergoing scan for non-thyroidal reasons. According to American Thyroid Association guidelines, focally increased uptake in the thyroid needs verification by US, and lesions above 10 mm in size require FNAB. However, incidentally detected abnormal thyroid PET scan pattern may also be a first manifestation of AITD and requires further diagnostics toward the presence of AITD.

There is an evidence that Color Doppler examination might be a useful predictive factor for Graves' disease (GD) relapse (14). In addition, there is an ongoing effort to identify novel imaging modalities as well as specific serum biomarkers to assist in identification of patients at highest risk of GD relapse. Identification of such predictors would help in clinical decision making to stratify which patients are the best candidates for conservative management with the highest chance for remission on pharmacotherapy, and which may benefit from definitive therapy (ablation with radioiodine or total/near total thyroidectomy). The study by Struja et al. evaluated potential usefulness of application of a high-throughput proton NMR metabolomic profile in prediction of relapse of the GD. However, only a moderate prognostic potential was demonstrated. Out of 227 studied markers, pyruvate and triglycerides in medium VLDL were selected as candidates with acceptable discriminatory strength as predictors with AUCs of 0.73 and 0.67, respectively.

There is an evidence of specific genotypes predisposing to subacute thyroiditis and AITD. However, certain genetic factors are still to be identified. In the study by Stasiak et al. it has been demonstrated that sonographic pattern of subacute thyroiditis might be associated with the specific HLA-haplotype. The authors reported a significant association between the HLA*B18:01 and the US characteristics of subacute thyroiditis. In the study by Jia et al. a novel relationship between CD14 gene polymorphism and AITD has been described. The authors also point out that the allele model, recessive model, and homozygous model of rs2569190 and rs2915863 embodied strong correlations with GD after the adjusting of age and gender. This association was the strongest for female patients and those with a positive family history of GD. Additionally, an analysis of CD14 expression was studied in thyroid tissues derived from thyroidectomized patients with GD, but its role in pathogenesis of GD requires further investigations.

In summary, a constant progress and rising accessibility of modern imaging techniques, as well as identification of novel biochemical and genetic markers gradually improve our understanding of pathogenesis of focal and diffuse thyroid pathologies. Combining standard diagnostic procedures with novel imaging techniques plays more and more important role in the clinical decision making in these patients.

AUTHOR CONTRIBUTIONS

All authors listed have made a substantial, direct and intellectual contribution to the work, and approved it for publication.

REFERENCES

1. Tamhane S, Gharib H. Thyroid nodule update on diagnosis and management. *Clin Diabetes Endocrinol.* (2016) 2:17. doi: 10.1186/s40842-016-0035-7
2. Ruchala M, Szczepanek E. Thyroid ultrasound - a piece of cake? *Endokrynol Pol.* (2010) 61:330–44.
3. Burman KD, Wartofsky L. CLINICAL PRACTICE. Thyroid Nodules. *N Engl J Med.* (2015) 373:2347–56. doi: 10.1056/NEJMcp1415786

4. Borowczyk M, Szczepanek-Parulska E, Debicki S, Budny B, Verburg FA, Filipowicz D, et al. Differences in mutational profile between follicular thyroid carcinoma and follicular thyroid adenoma identified using next generation sequencing. *Int J Mol Sci.* (2019) 20:E3126. doi: 10.3390/ijms20133126
5. Borowczyk M, Szczepanek-Parulska E, Debicki S, Budny B, Verburg FA, Filipowicz D, et al. The genetic heterogeneity of indeterminate thyroid nodules assessed preoperatively with next generation sequencing reflects the diversity of the final histopathological diagnoses. *Pol Arch Intern Med.* (2019). doi: 10.20452/pamw.14979. [Epub ahead of print].
6. Haugen BR, Alexander EK, Bible KC, Doherty GM, Mandel SJ, Nikiforov YE, et al. 2015 American Thyroid Association Management Guidelines for Adult Patients with Thyroid Nodules and Differentiated Thyroid Cancer: the American Thyroid Association Guidelines Task Force on Thyroid Nodules and Differentiated Thyroid Cancer. *Thyroid*. (2016) 26:1–133. doi: 10.1089/thy.2015.0020
7. Ruchala M, Szmyt K, Slawek S, Zybek A, Szczepanek-Parulska E. Ultrasound sonoelastography in the evaluation of thyroiditis and autoimmune thyroid disease. *Endokrynol Pol.* (2014) 65:520–6. doi: 10.5603/EP.2014.0071
8. Szczepanek-Parulska E, Wolinski K, Stangierski A, Gurgul E, Biczysko M, Majewski P, et al. Comparison of diagnostic value of conventional ultrasonography and shear wave elastography in the prediction of thyroid lesions malignancy. *PLoS ONE.* (2013) 8:e81532. doi: 10.1371/journal.pone.0081532
9. Wolinski K, Szczepanek-Parulska E, Stangierski A, Gurgul E, Rewaj-Losyk M, Ruchala M. How to select nodules for fine-needle aspiration biopsy in multinodular goitre. Role of conventional ultrasonography and shear wave elastography - a preliminary study. *Endokrynol Pol.* (2014) 65:114–8. doi: 10.5603/EP.2014.0016
10. Luster M, Aktolun C, Amendoeira I, Barczynski M, Bible KC, Duntas LH, et al. European Perspective on 2015 American Thyroid Association Management Guidelines for adult patients with thyroid nodules and differentiated thyroid cancer: proceedings of an interactive international symposium. *Thyroid.* (2019) 29:7–26. doi: 10.1089/thy.2017.0129
11. Takami H, Ito Y, Okamoto T, Onoda N, Noguchi H, Yoshida A. Revisiting the guidelines issued by the Japanese Society of Thyroid Surgeons and Japan Association of Endocrine Surgeons: a gradual move towards consensus between Japanese and western practice in the management of thyroid carcinoma. *World J Surg.* (2014) 38:2002–10. doi: 10.1007/s00268-014-2498-y
12. Jarzab B, Dedecjus M, Slowinska-Klencka D, Lewinski A, Adamczewski Z, Anielski R, et al. Guidelines of Polish National Societies Diagnostics and treatment of thyroid carcinoma. 2018 update. *Endokrynol Pol.* (2018) 69:34–74. doi: 10.5603/EP.2018.0014
13. Leboulleux S, Tuttle RM, Pacini F, Schlumberger M. Papillary thyroid microcarcinoma: time to shift from surgery to active surveillance? *Lancet Diabetes Endocrinol.* (2016) 4:933–42. doi: 10.1016/S2213-8587(16)30180-2
14. Saleh A, Cohnen M, Furst G, Modder U, Feldkamp J. Prediction of relapse after antithyroid drug therapy of Graves' disease: value of color Doppler sonography. *Exp Clin Endocrinol Diabetes.* (2004) 112:510–3. doi: 10.1055/s-2004-821308

Conflict of Interest: The authors declare that the research was conducted in the absence of any commercial or financial relationships that could be construed as a potential conflict of interest.

frontiers in Endocrinology

ORIGINAL RESEARCH
published: 17 October 2018
doi: 10.3389/fendo.2018.00623

Metabolomics for Prediction of Relapse in Graves' Disease: Observational Pilot Study

Tristan Struja[1], Andreas Eckart[1], Alexander Kutz[1], Andreas Huber[2], Peter Neyer[2], Marius Kraenzlin[3], Beat Mueller[1,4], Christian Meier[3,4], Luca Bernasconi[2†] and Philipp Schuetz[1,4†]*

[1] Division of Endocrinology, Diabetes and Metabolism, Medical University Department, Kantonsspital Aarau, Aarau, Switzerland, [2] Department of Laboratory Medicine, Kantonsspital Aarau, Aarau, Switzerland, [3] Endonet, Basel, Switzerland, [4] Medical Faculty, University of Basel, Basel, Switzerland

Background: There is a lack of biochemical markers for early prediction of relapse in patients with Graves' disease [GD], which may help to direct treatment decisions. We assessed the prognostic ability of a high-throughput proton NMR metabolomic profile to predict relapse in a well characterized cohort of GD patients.

Methods: Observational study investigating patients presenting with GD at a Swiss hospital endocrine referral center and an associated endocrine outpatient clinic. We measured 227 metabolic markers in the blood of patients before treatment initiation. Main outcome was relapse of hyperthyroidism within 18 months of stopping anti-thyroid drugs. We used ROC analysis with AUC to assess discrimination.

Results: Of 69 included patients 18 (26%) patients had a relapse of disease. The clinical GREAT score had an AUC of 0.68 (95% CI 0.63–0.70) to predict relapse. When looking at the metabolomic markers, univariate analysis revealed pyruvate and triglycerides in medium VLDL as predictors with AUCs of 0.73 (95% CI 0.58–0.84) and 0.67 (95% CI 0.53–0.80), respectively. All other metabolomic markers had lower AUCs.

Conclusion: Overall, metabolomic markers in our pilot study had low to moderate prognostic potential for prediction of relapse of GD, with pyruvate and triglycerides being candidates with acceptable discriminatory abilities. Our data need validation in future larger trials.

Keywords: Graves basedow disease, metabolomics, relapse activity, predicable results, retrospective analysis

OPEN ACCESS

Edited by:
Joanna Klubo-Gwiezdzinska, National Institutes of Health (NIH), United States

Reviewed by:
Onyebuchi Okosieme, Cwm Taf University Health Board, United Kingdom
Miloš Žarković, Faculty of Medicine, University of Belgrade, Serbia

****Correspondence:***
Tristan Struja
tristan.struja@gmail.com

† These authors have contributed equally to this work

Specialty section:
This article was submitted to Thyroid Endocrinology, a section of the journal Frontiers in Endocrinology

Received: *28 July 2018*
Accepted: *01 October 2018*
Published: *17 October 2018*

Citation:
Struja T, Eckart A, Kutz A, Huber A, Neyer P, Kraenzlin M, Mueller B, Meier C, Bernasconi L and Schuetz P (2018) Metabolomics for Prediction of Relapse in Graves' Disease: Observational Pilot Study. Front. Endocrinol. 9:623. doi: 10.3389/fendo.2018.00623

INTRODUCTION

Graves' disease [GD] is among the leading causes of hyperthyroidism affecting approximately 0.5% of the general population, especially younger women. It is caused by the presence of autoantibodies to the thyrotropin [TSH] receptor [TRAb] leading to unregulated production and secretion of thyroid hormones (1).

Although treatment with thyroidectomy or radioactive iodine ablation [RAI] provide good cure rates from hyperthyroidism, they are definitive ablative procedures rendering patients subject to lifelong therapy with levothyroxine [T4] (2). On the other hand, anti-thyroid drugs [ATD] provide the chance of cure, albeit, at the cost of a very high relapse rate of approximately 40-60% (1). A more personalized approach would include identifying those who were to benefit most of ATD

therapy before treatment initiation. Various approaches have been studied in the past, such as genome wide association studies, thyroidal blood flow assessed by sonography, numerous TRAb assays, and combinations of biochemical and epidemiological markers (3, 4). So far, none have provided enough predictive power to be widely adopted into clinical practice.

Recently, the concept of extensively mapping the phenotypic metabolic state of an individual (i.e., metabolome) has become available by advances in spectrometric techniques. Some studies have already mapped the metabolic differences of hyperthyroid GD states compared to euthyroidism (5, 6).

In other areas, predictive qualities of metabolomics have already been assessed. One report showed that inclusion of lysophosphatidylcholine (20:4) as marker improved recurrence risk prediction of strokes by 6% (7), whereas another report found elevated levels of decanoylcarnitine and octanoylcarnitine to be associated with a higher stroke recurrence risk (hazard ratios 3.8 and 5.5, respectively) (8). Such findings have also been observed in a rat model of ANCA positive vasculitis (immunized to human myeloperoxidase), where urinary di-methyl-glycine and trimethylamine N-oxide levels at day 56 post immunization increased relapse prediction accuracy from 90.5 to 95.2% (9). Furthermore, a Japanese group measured plasma free amino acids in patients with ulcerative colitis. They observed that lower levels of histidine were associated with an increased risk of relapse within year (10).

We hypothesized that distinct metabolic patterns might predict outcome of ATD therapy with regard to relapse. To our knowledge, this study is the first to assess whether metabolomic differences can be used to predict relapse of hyperthyroidism after a course of ATD.

METHODS

From a previous observational cohort study (11), we had roughly 320 serum aliquots left over at our disposal. Patients were included at an endocrine outpatient clinic and one hospital-based referral center in Switzerland. Patients were treated with ATD in a titration regimen (usually carbimazole or propylthiouracil for 12-18 months). Inclusion criteria were a first episode of GD defined as suppressed TSH (<0.01 mU/l), elevated free T4, and if available, diffuse increased uptake in scintigraphy. Patients with a shorter follow-up period than 24 months after start of ATD treatment were excluded. Also, we excluded patients with ATD treatment duration <12 months, initial ablative therapy (i.e., surgery or radio-active iodine), and time gap between initiation of treatment and blood sample collection over one month. Aforementioned aliquots were analyzed in the current study. After application of the inclusion and exclusion criteria, there were 69 patients left for final analysis. We collected clinical data by medical charts review and if necessary we complemented missing follow-up data by phone calls to patients and general practitioners. The study protocol was approved by the local ethics committee (Ethikkommission Nordwest- und Zentralschweiz (EKNZ) Project No. 2015/227) and has been conducted according to the principles of the Declaration of Helsinki. Need for informed consent was waived due to retrospective nature of analysis with no impact on health outcome.

After blood withdrawal, samples were directly centrifuged and analyzed on serum TSH, fT4, anti-Thyroperoxidase-Antibodies [anti-TPO-Ab] and TRAb levels by standard commercially available laboratory kits (Assays used, are listed in **Supplementary Table 1**). Leftover serum aliquots were stored at−24° Celsius and mean duration storage time was 46 months (median 46 months; 70 to 17 months interquartile range). Two hundred and twenty-seven metabolic biomarkers were quantified from serum using high-throughput proton NMR metabolomics (Nightingale Health Ltd., Helsinki, Finland) (12, 13) (biomarkers assessed are listed in **Supplementary Table 2**). This technique is able to provide excellently reproducible results and analytical accuracy given its limitations regarding sensitivity and resolution as an NMR based method (14, 15). Aliquots were shipped on dry ice by a professional courier service and temperature inside the box was monitored continuously.

To validate our storage conditions and the quality of our samples, Nightingale compared our data with their reference data (see **Supplementary Figure 1**). Reference values were derived from several studies in Scandinavian and UK cohorts with adjacent biobanks [e.g., most recent publication with references to previous works (16)], mainly from the Finnish National Institute of Health and Welfare Biobanks (THL) (17).

Prior to statistical analysis, data was cube root transformed, normalized by the median of each sample, and Pareto scaled to achieve a normal distribution.

The primary outcome of this study was prediction of relapse in GD at ATD treatment initiation. Relapse had to be established by suppressed TSH and elevated peripheral hormones. First, we fitted univariate ROC models for every metabolomic marker. Second, multivariate ROC models were fit by Monte-Carlo cross validation using balanced sub-sampling. We used partial least squares discriminant analysis [PLS-DA] as classification and feature ranking method. Each cross-validation used two thirds of the samples to gauge feature importance. Top important features where then used to build classification models by using the remaining third of samples (18). To account for multiple testing, correction with Benjamini–Hochberg false discovery rate was applied. Statistical significance was set at $\alpha < 0.05$. Statistical analysis was conducted using MetaboAnalyst software version 4.0 (19, 20) and Stata software version 12.1 (Stata Corp., College Station, TX, USA).

RESULTS

Table 1 shows details of the patient population stratified by relapse, the primary endpoint. Previously, we published a validation study of the GREAT score, a combination of epidemiolocal (i.e., age, goiter size) and standard laboratory variables (i.e., fT4, TRAb) to predict relapse (11). It showed an AUC of 0.68 (95% CI 0.63–0.70) to predict relapse.

Comparison of our data with the reference data set revealed relevant differences for omega-3, glutamine, pyruvate, citrate and

TABLE 1 | Baseline characteristics according to relapse status.

		No relapse	Relapse
		***N* = 51**	***N* = 18**
Sex (F/M)	F	41 (80%)	15 (83%)
	M	10 (20%)	3 (17%)
Age (years)		51 ± 13	47± 13
BMI (kg/m^2)		24 ± 4.2	23 ± 2.8
Treatment time (months)		20 (18–22)	19 (18–21)
Follow-up after ATD withdrawal (months)		11 (3.9–28)	1 (0.5–12)
Thyroid volume by sonography (mL)		14 (11–16)	15 (9.8–17)
Goiter size (struma grade, 0-III)	0	24 (56%)	9 (60%)
	I	10 (23%)	5 (33%)
	II	8 (19%)	1 (7%)
	III	1 (2%)	0 (0%)
	Missing	8	3
Orbitopathy		13 (25%)	7 (39%)
Smoking		8 (16%)	1 (6%)
fT4 (pM)		30 (21–36)	38 (21–55)
T3 (pM)		3.5 (2.3–4.3)	2.9 (2.8–7.1)
TPO-AK (U/L)		91 (34–454)	163 (90–357)
TRAb (U/L)		5.2 (2.6–11)	12 (3.5–27)
Additional autoimmune diseases	GIT (IBD, celiac disease, pernicious anemia)	1	1
	Type I Diabetes mellitus	1	0
	Other	1	0

Data presented as counts (percentages), mean (± standard deviation), or median (interquartile range). ATD, anti-thyroid drugs; GIT, gastrointestinal tract; IBD, inflammatory bowel disease; pM, pmol/L.

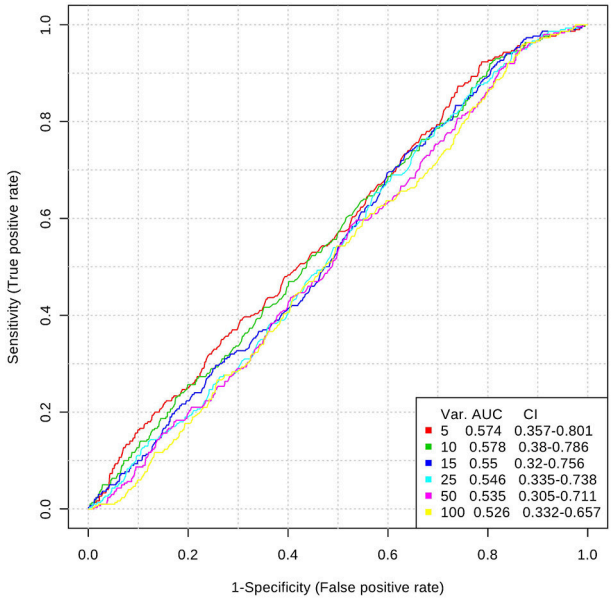

FIGURE 1 | Top 6 ROC models generated by PLS-DA with increasing number of variables. AUC, area under the curve; CI, 95% confidence intervals; PLS-DA, partial least squares-discriminant analysis; Var, number of variables included into model.

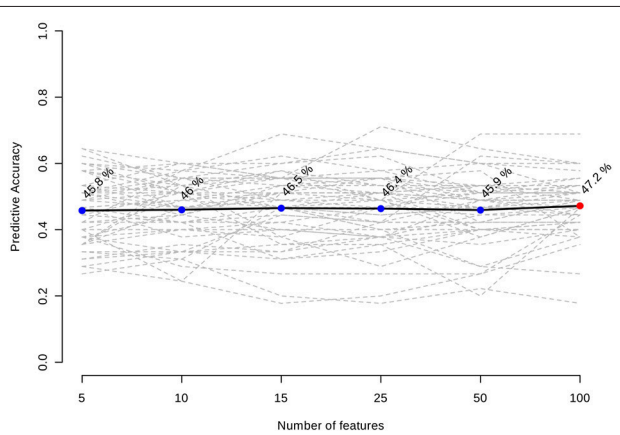

FIGURE 2 | Predictive accuracies of the models with increasing number features included.

acetate. Minor differences were observed for phosphoglycerides, phosphatidylcholines, total cholines, unsaturated fatty acids, and VLDL and LDL diameter, but not in HDL diameter (see **Supplementary Figure 1**).

Univariate analysis only revealed pyruvate and triglycerides in medium VLDL [MVLDLTG] as significant predictors of GD relapse with AUCs of 0.73 (95% CI 0.58–0.84) and 0.67 (95% CI 0.53–0.80), respectively.

Inclusion of multiple variables by multivariate ROC analysis did not yield higher AUCs. **Figure 1** provides an overview of the top six models generated. AUCs ranged from 0.53 (95% CI 0.33–0.66; 100 variables) to 0.57 (95% CI 0.36–0.80; 5 variables), each not being statistically significant. Inclusion of more variables into a model did not result in improved discriminatory power (see **Figure 2**). **Figure 3** displays the frequency of a variable being selected by PLS-DA.

As there were no significant results although PLS-DA tends to overfit data, we abstained from validating the model in a subset of our data.

DISCUSSION

Based on this observational, secondary analysis of blood samples, we were not able to find any metabolomic markers that could predict relapse outcome before ATD treatment initiation with high accuracy. To the best of our knowledge, we are the first to apply the principle of metabolomic phenotyping on relapse prediction in GD.

Although we measured roughly 300 samples, we decided to generate a homogenous cohort by applying stringent inclusion and exclusion criteria leading to many exclusions. We did loosen

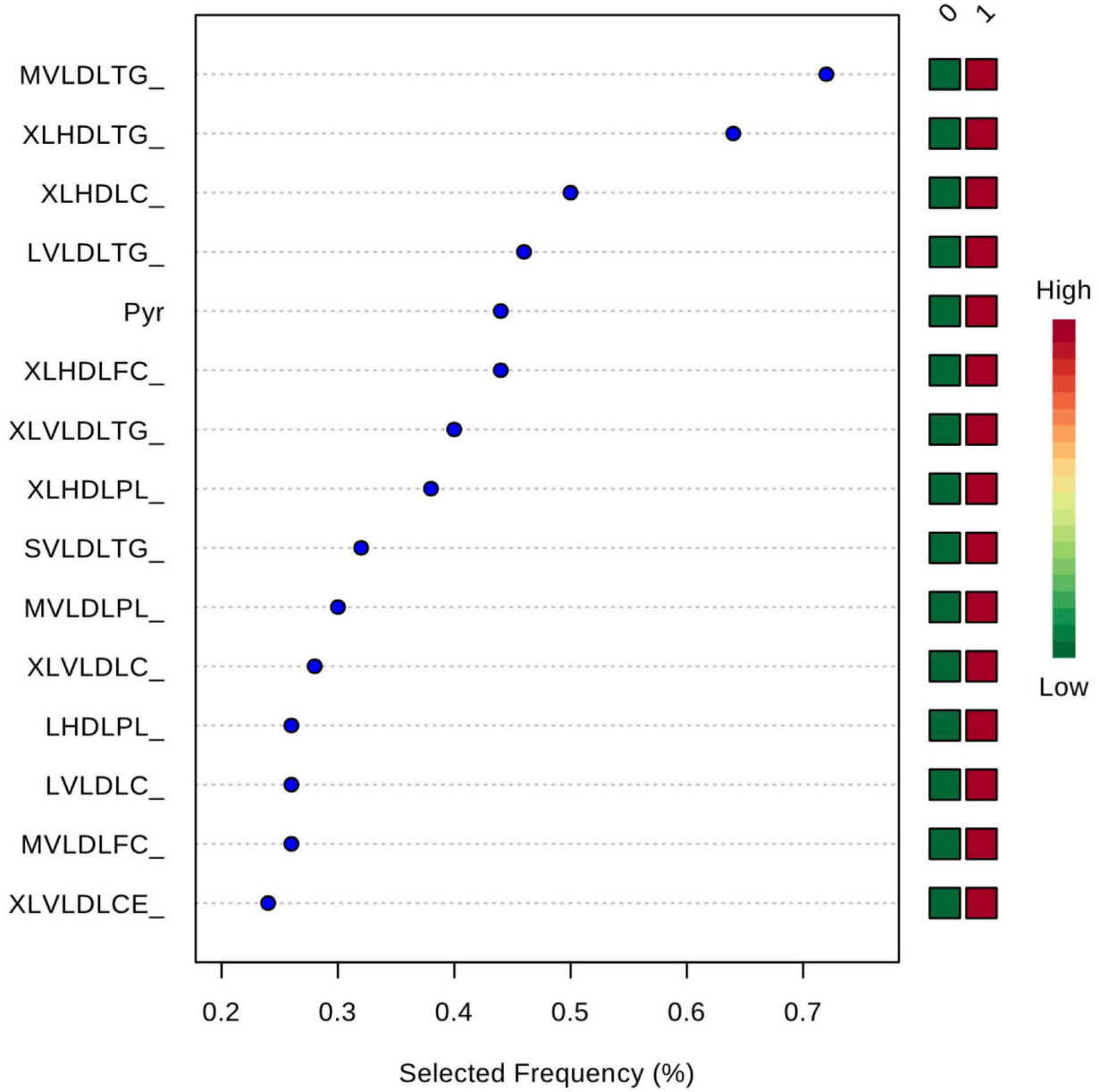

FIGURE 3 | Frequency of a variable being selected by PLS-DA. MVLDLTG, triglycerides in medium VLDL; XLHDLTG, triglycerides in very large HDL; XLHDLC, total cholesterol in very large HDL; LVLDLTG, triglycerides in chylomicrons and extremely large VLDL; Pyr, pyruvate; XLHDLFC, free cholesterol in very large HDL; XLVLDLTG, triglycerides in chylomicrons and extremely large VLDL; XLHDLPL, phospholipids in very large HDL; SVLDLTG, triglycerides in small VLDL; MVLDLPL, phospholipids in medium VLDL; XLVLDLPL, phospholipids in chylomicrons and extremely large VLDL; LHDLPL, phospholipids in very large HDL; LVLDLC, total cholesterol in chylomicrons and extremely large VLDL; MVLDLFC, free cholesterol in medium VLDL; XLVLDLCE, cholesterol esters in chylomicrons and extremely large VLDL.

our exclusion criteria *post-hoc* to include more patients, but this did not influence results in any way.

Our model was not able to generate any predictive properties which is reflected by the AUCs around 0.55. Inclusion of more variables into a ROC model usually leads to better predictive capacities at the cost of decreasing practicability (20). In our case, AUC tended to decrease with a growing number of variables in a model. We assume this is a chance finding as all median values are very close to each other, and CIs do overlap.

While there are already some reports investigating the metabolomic phenotype of hyperthyroid GD patients (5, 6, 21, 22). Not surprisingly, there were distinct differences in metabolic pathways between the euthyroid and hyperthyroid state detected. Besides histamine and nitrogen pathways, amino acid pathways were mainly involved. For instance, Piras et al. reported the

changes from the hyperthyroid to euthyroid state in 15 patients with GD compared to 26 healthy controls (22). They found that GD patients after treatment had significantly lower levels of creatinine, formate, glycerol, histamine, methylamine, and methylsuccinate in plasma as compared to the healthy controls.

Al-Majdoub and colleagues reported changes in the carnitine metabolism of 30 GD patients before treatment compared to 12 months after institution of euthyroidism (5). They observed an increase in short-chain acylcarnitines, whereas medium-chain acylcarnitines were decreased and long-chain acylcarnitines were unchanged after treatment. In general, lysophosphatidylcholines and sphingomyelins were increased in their study. The authors speculated that these changes reflect a starvation like process that was induced by hyperthyroidism.

In 2016, researchers from Singapore published their data on 24 female GD patients transitioning from hyperthyroidism to euthyroidism. In contrast to the previous report, they found a fall of medium- and long-chain acylcarnitines, whereas they observed rises in total cholesterol, LDL, and HDL. The authors postulate that the changes in cholesterol metabolism might be due to increased clearance in hyperthyroidism, whereas the changes in acylcarnitines is based on the T3 induced increased mitochondrial biogenesis and enhanced tricarboxylic acid cycle activity. They also found no changes in branched chain amino acid concentrations (i.e., valine, isoleucine, and leucine). On the other hand, levels of phenylalanine and tyrosine were elevated which might have been due to the increased demand of these amino acid in the synthesis of thyroid hormones (6).

So far there was no investigation looking at the relation to relapse rates. Thus, we studied all markers for their potential to predict relapse with the risk for chance findings. Our data are thus rather hypothesis-generating and need to be validated in future studies. Compared to the previous studies, our laboratory assay put more emphasis on lipid pathways but not carnitine and amino acid metabolism, which might explain our negative findings (see **Supplementary Figure 1** and **Supplementary Table 2**) or it could be due to our limitations in study design. As our focus was prediction of relapse and had only blood samples before the start of treatment, we did not investigate metabolic changes during the transition from hyperthyroidism to euthyroidism.

Our study has three major limitations. First, blood samples were not drawn in a fasting state but randomly. Second, mean storage time of samples was 46 months under sub-optimal conditions (i.e., −24°C instead of −80°C) (23), although other groups reported significant results after storage at −24°C (5). On one hand, suboptimal storage conditions lead to low levels of glutamine, phenylalanine, pyruvate, and acetate. On the other hand, these metabolites are very scarce and at least for lipid components a large coefficient of variation has been reported even under optimal conditions (24). Moreover, glycerol, lactate, and creatinine which are shown to be altered significantly by freeze-thaw cycles in rats (25), have not shown obvious deviations in our cohort.

Furthermore, we did not observe large deviations from the reference sample in fatty acids, especially polyunsaturated fatty acids, which would be other indicators of suboptimal storage and handling (24). Additionally, metabolites such as glucose and lactate that are known to be susceptible to preanalytical errors and have been proposed as a screening tool to assess preanalytical care (26). In our batch, these metabolites were not altogether different from the manufacturer's reference sample.

Third, we had two freeze-thaw cycles during our sample preparation before analysis. From an idealistic standpoint, immediate analysis after blood draw would be the preferable approach which is rarely feasible in routine. Furthermore, a report demonstrated that up to four freeze-thaw cycles did alter samples only slightly (23).

CONCLUSION

Overall, metabolomic markers in our pilot study had only low to moderate prognostic potential for prediction of relapse of GD, with pyruvate and triglycerides being the most promising candidates with acceptable discriminatory ability. Our data need validation in future larger trials.

AUTHOR CONTRIBUTIONS

TS analyzed data and wrote the first draft of the manuscript with primary responsibility for the final content. All authors read and approved the final manuscript.

FUNDING

This study was supported in part by the Swiss National Science Foundation (SNSF Professorship, PP00P3_150531/1) and the Research Council of the Kantonsspital Aarau (1410.000.044).

SUPPLEMENTARY MATERIAL

The Supplementary Material for this article can be found online at: https://www.frontiersin.org/articles/10.3389/fendo.2018.00623/full#supplementary-material

REFERENCES

1. Brent GA. Clinical practice. Graves' disease. *N Engl J Med*. (2008) 358:2594–605. doi: 10.1056/NEJMcp0801880
2. Ross DS, Burch HB, Cooper DS, Greenlee MC, Laurberg P, Maia AL, et al. 2016 American thyroid association guidelines for diagnosis and management of hyperthyroidism and other causes of thyrotoxicosis. *Thyroid* (2016) 26:1343–421. doi: 10.1089/thy.2016.0229
3. Struja T, Fehlberg H, Kutz A, Guebelin L, Degen C, Mueller B, et al. Can we predict relapse in Graves' disease? Results from a systematic review and meta-analysis. *Eur J Endocrinol*. (2017) 176:87–97. doi: 10.1530/EJE-16-0725
4. Struja T, Kutz A, Fischli S, Meier C, Mueller B, Recher M, et al. Is Graves' disease a primary immunodeficiency? New immunological perspectives on an endocrine disease. *BMC Med*. (2017) 15:174. doi: 10.1186/s12916-017-0939-9

5. Al-Majdoub M, Lantz M, Spegel P. Treatment of Swedish patients with Graves' hyperthyroidism is associated with changes in acylcarnitine levels. *Thyroid* (2017) 27:1109–17. doi: 10.1089/thy.2017.0218
6. Chng CL, Lim AY, Tan HC, Kovalik JP, Tham KW, Bee YM, et al. Physiological and metabolic changes during the transition from hyperthyroidism to Euthyroidism in Graves' disease. *Thyroid* (2016) 26:1422–30. doi: 10.1089/thy.2015.0602
7. Jove M, Mauri-Capdevila G, Suarez I, Cambray S, Sanahuja J, Quilez A, et al. Metabolomics predicts stroke recurrence after transient ischemic attack. *Neurology* (2015) 84:36–45. doi: 10.1212/WNL.0000000000001093
8. Seo WK, Jo G, Shin MJ, Oh K. Medium-chain acylcarnitines are associated with cardioembolic stroke and stroke recurrence: a metabolomics study. *Arterioscler Thromb Vasc Biol.* (2018) 38:2245–53. doi: 10.1161/ATVBAHA.118.311373
9. Al-Ani B, Fitzpatrick M, Al-Nuaimi H, Coughlan AM, Hickey FB, Pusey CD, et al. Changes in urinary metabolomic profile during relapsing renal vasculitis. *Sci Rep*. (2016) 6:38074. doi: 10.1038/srep38074
10. Hisamatsu T, Ono N, Imaizumi A, Mori M, Suzuki H, Uo M, et al. Decreased plasma histidine level predicts risk of relapse in patients with ulcerative colitis in remission. *PLoS ONE* (2015) 10:e0140716. doi: 10.1371/journal.pone.0140716
11. Struja T, Kaeslin M, Boesiger F, Jutzi R, Imahorn N, Kutz A, et al. External validation of the GREAT score to predict relapse risk in Graves' disease: results from a multicenter, retrospective study with 741 patients. *Eur J Endocrinol*. (2017) 176:413–9. doi: 10.1530/EJE-16-0986
12. Soininen P, Kangas AJ, Wurtz P, Suna T, Ala-Korpela M. Quantitative serum nuclear magnetic resonance metabolomics in cardiovascular epidemiology and genetics. *Circ Cardiovasc Genet.* (2015) 8:192–206. doi: 10.1161/CIRCGENETICS.114.000216
13. Soininen P, Kangas AJ, Wurtz P, Tukiainen T, Tynkkynen T, Laatikainen R, et al. High-throughput serum NMR metabonomics for cost-effective holistic studies on systemic metabolism. *Analyst* (2009) 134:1781–5. doi: 10.1039/b910205a
14. Nagana Gowda GA, Raftery D. Can NMR solve some significant challenges in metabolomics? *J Magn Reson* (2015) 260:144–60. doi: 10.1016/j.jmr.2015.07.014
15. Gathungu RM, Kautz R, Kristal BS, Bird SS, Vouros P. The integration of LC-MS and NMR for the analysis of low molecular weight trace analytes in complex matrices. *Mass Spectrom Rev*. (2018). doi: 10.1002/mas.21575. [Epub ahead of print].
16. Wang Q, Wurtz P, Auro K, Makinen VP, Kangas AJ, Soininen P, et al. Metabolic profiling of pregnancy: cross-sectional and longitudinal evidence. *BMC Med.* (2016) 14:205. doi: 10.1186/s12916-016-0733-0
17. Puska P, Stahl T. Health in all policies-the Finnish initiative: background, principles, current issues. *Annu Rev Public Health* (2010) 31:315–28 3 p following 328. doi: 10.1146/annurev.publhealth.012809.103658
18. Xia J, Wishart DS. Using metaboanalyst 3.0 for comprehensive metabolomics data analysis. *Curr Protoc Bioinformat.* (2016) 55:14.10.1–14.10.91. doi: 10.1002/cpbi.11
19. Xia J, Wishart DS. Web-based inference of biological patterns, functions and pathways from metabolomic data using MetaboAnalyst. *Nat Protoc.* (2011) 6:743–60. doi: 10.1038/nprot.2011.319
20. Xia J, Broadhurst DI, Wilson M, Wishart DS. Translational biomarker discovery in clinical metabolomics: an introductory tutorial. *Metabolomics* (2013) 9:280–99.
21. Wojtowicz W, Zabek A, Deja S, Dawiskiba T, Pawelka D, Glod M, et al. Serum and urine (1)H NMR-based metabolomics in the diagnosis of selected thyroid diseases. *Sci Rep.* (2017) 7:9108.
22. Piras C, Arisci N, Poddighe S, Liggi S, Mariotti S, Atzori L. Metabolomic profile in hyperthyroid patients before and after antithyroid drug treatment: correlation with thyroid hormone and TSH concentration. *Int J Biochem Cell Biol.* (2017) 93:119–28. doi: 10.1016/j.biocel.2017.07.024
23. Yin P, Peter A, Franken H, Zhao X, Neukamm SS, Rosenbaum L, et al. Preanalytical aspects and sample quality assessment in metabolomics studies of human blood. *Clin Chem.* (2013) 59:833–45. doi: 10.1373/clinchem.2012.199257
24. Zivkovic AM, Wiest MM, Nguyen UT, Davis R, Watkins SM, German JB. Effects of sample handling and storage on quantitative lipid analysis in human serum. *Metabolomics* (2009) 5:507–16. doi: 10.1007/s11306-009-0174-2
25. Torell F, Bennett K, Rannar S, Lundstedt-Enkel K, Lundstedt T, Trygg J. The effects of thawing on the plasma metabolome: evaluating differences between thawed plasma and multi-organ samples. *Metabolomics* (2017) 13:66. doi: 10.1007/s11306-017-1196-9
26. Jobard E, Tredan O, Postoly D, Andre F, Martin AL, Elena-Herrmann B, Boyault S. A Systematic evaluation of blood serum and plasma pre-analytics for metabolomics cohort studies. *Int J Mol Sci.* (2016) 17:2035. doi: 10.3390/ijms17122035

Conflict of Interest Statement: The authors declare that the research was conducted in the absence of any commercial or financial relationships that could be construed as a potential conflict of interest.

frontiers in Endocrinology

ORIGINAL RESEARCH
published: 06 December 2018
doi: 10.3389/fendo.2018.00746

Magnetic Resonance Imaging Features of Normal Thyroid Parenchyma and Incidental Diffuse Thyroid Disease: A Single-Center Study

Taewoo Kang[1], Dong Wook Kim[2], Yoo Jin Lee[2], Young Jun Cho[2], Soo Jin Jung[3], Ha Kyoung Park[4], Tae Kwun Ha[4], Do Hun Kim[5], Ji Sun Park[6], Sung Ho Moon[7], Ki Jung Ahn[8] and Hye Jin Baek[9]*

[1] Department of Surgery (Busan Cancer Center), Pusan National University Hospital, Pusan National University College of Medicine, Busan, South Korea, [2] Department of Radiology, Busan Paik Hospital, Inje University College of Medicine, Busan, South Korea, [3] Department of Pathology, Busan Paik Hospital, Inje University College of Medicine, Busan, South Korea, [4] Department of General Surgery, Busan Paik Hospital, Inje University College of Medicine, Busan, South Korea, [5] Department of Otorhinolaryngology-Head and Neck Surgery, Busan Paik Hospital, Inje University College of Medicine, Busan, South Korea, [6] Department of Nuclear Medicine, Busan Paik Hospital, Inje University College of Medicine, Busan, South Korea, [7] Department of Anesthesiology and Pain Medicine, Busan Paik Hospital, Inje University College of Medicine, Busan, South Korea, [8] Department of Radiation Oncology, Busan Paik Hospital, Inje University College of Medicine, Busan, South Korea, [9] Department of Radiology, Gyeongsang National University School of Medicine and Gyeongsang National University Changwon Hospital, Changwon, South Korea

OPEN ACCESS

Edited by:
Marek Ruchala, Poznan University of Medical Sciences, Poland

Reviewed by:
Salvatore Benvenga, Università degli Studi di Messina, Italy
Rocco Bruno, ASM Matera, Italy

***Correspondence:**
Dong Wook Kim
dwultra@nate.com

Specialty section:
This article was submitted to Thyroid Endocrinology, a section of the journal Frontiers in Endocrinology

Received: *15 October 2018*
Accepted: *26 November 2018*
Published: *06 December 2018*

Citation:
Kang T, Kim DW, Lee YJ, Cho YJ, Jung SJ, Park HK, Ha TK, Kim DH, Park JS, Moon SH, Ahn KJ and Baek HJ (2018) Magnetic Resonance Imaging Features of Normal Thyroid Parenchyma and Incidental Diffuse Thyroid Disease: A Single-Center Study. Front. Endocrinol. 9:746. doi: 10.3389/fendo.2018.00746

Background: No previous studies have investigated the feasibility of magnetic resonance imaging (MRI) diagnosis for detecting incidental diffuse thyroid disease (DTD). This study investigated MRI features of normal thyroid parenchyma and incidental DTD.

Methods: From January 2008 to December 2017, 387 patients underwent neck MRI in our hospital due to tumor/nodal staging ($n = 137$), lymphadenopathy ($n = 122$), inflammatory neck lesion ($n = 85$), congenital neck lesion ($n = 12$), and patient request ($n = 31$). Among them, 375 patients were excluded because of a lack of appropriate histopathological data on the thyroid parenchyma.

Results: Among the patients included, 10 had normal thyroid parenchyma, 1 had Hashimoto thyroiditis, and 1 had diffuse hyperplasia. The common MRI features of normal thyroid parenchyma include iso-/slightly high and homogeneous signal intensity on T1/T2-weighted images, normal anteroposterior diameter of the thyroid gland, smooth margin, and homogeneously increased enhancement as compared to adjacent muscle. Hashimoto thyroiditis exhibited high and inhomogeneous signal intensity on T2-weighted images, while diffuse hyperplasia revealed an increased anteroposterior diameter and lobulated margin of the thyroid gland, and inhomogeneous enhancement.

Conclusions: MRI may be helpful for detection of incidental DTD.

Keywords: thyroid, diffuse thyroid disease, autoimmune, Hashimoto thyroiditis, magnetic resonance imaging

INTRODUCTION

Thyroid disease includes diffuse and nodular types (1). Diffuse thyroid disease (DTD) may be associated with thyroid dysfunction, and the thyroid function test and serology are widely used in evaluating thyroid dysfunction (2). In clinical practice, however, accurate detection of subclinical or asymptomatic DTD is not easy but this detection can be helpful for the appropriate management of thyroid dysfunction (2). Thyroid ultrasonography (US) is widely used to detect and characterize thyroid nodules (3). Although clinical and laboratory findings have played a key role in the diagnosis and treatment of DTD, the use of thyroid US for detecting DTD is feasible (4–7). Moreover, recent studies have demonstrated that computed tomography (CT) may be helpful to detect DTD (8–10). CT detection of DTD may be practical, as CT is widely used in the evaluation of neck lesions. In the literature, magnetic resonance imaging (MRI) is reported to be helpful for differentiating Graves' disease from Hashimoto thyroiditis or painless thyroiditis (11–14). Hashimoto thyroiditis and Graves' disease exhibit increased signal intensity (SI) on T1/T2-weighted images, whereas as the normal thyroid reveals somewhat greater SI than that of adjacent muscle on both images (11, 12). In addition, diffusion-weighted MRI may be helpful for differentiation between Hashimoto thyroiditis, Graves' disease, and painless thyroiditis (13, 14). However, no previous studies have investigated the feasibility of using MRI for detection of incidental DTD.

For evaluating head and neck cancer, contrast-enhanced CT is the most commonly used imaging modality (15). MRI has excellent soft tissue differentiation, but CT provides exceptional anatomical detail with greater spatial resolution than MRI (15). In particular, MRI is commonly used to determine tumor/nodal staging of head and neck cancer, to identify a primary site in patients with unknown primary head and neck cancer, and to evaluate lymphadenopathy in the neck (15). If incidental MRI detection of DTD is possible, as with US and CT, MRI may facilitate appropriate management of DTD.

Therefore, the purpose of this study was to assess the MRI features of normal thyroid parenchyma and incidental DTD.

MATERIALS AND METHODS

Patients

This retrospective study was approved by Busan Paik Hospital institutional review board (IRB 17-0212), and requirement for obtaining informed patient consent was waived because of the retrospective nature of the investigation and the use of anonymized patient data. From January 2008 to December 2017, 387 patients (113 women, 274 men; mean age 57.1 ± 19.3 years [range 1–92 years]) underwent neck MRI in our hospital for tumor/nodal staging (n = 137), lymphadenopathy (n = 122), inflammatory neck lesion (n = 85), congenital neck lesion (n = 12), and by patient request (n = 31). Among them, only the cases with an available histopathological specimen of the thyroid gland, obtained by thyroid surgery, were included. In addition, the interval between neck MRI and thyroid surgery had to be less than 12 months. Ultimately, a total of 12 patients (7 women, 5 men; mean age 49.6 ± 16.2 years [range 22–70 years]) were included in the study.

TABLE 1 | Comparison of magnetic resonance imaging features of normal thyroid parenchyma and diffuse thyroid disease in 12 patients.

MRI features	Normal thyroid parenchyma (n = 10)	Diffuse thyroid disease (n = 2)
SI on T1 WI		
iso-	10 (100)	2 (100)
Low	0 (0)	0 (0)
slightly high	0 (0)	0 (0)
High	0 (0)	0 (0)
SI on T2 WI		
iso-	1 (10)	0 (0)
Low	0 (0)	0 (0)
slightly high	9 (90)	1 (50)
High	0 (0)	1 (50)
HOMOGENEITY on T1 or T2 WI		
Homogeneous	10 (100)	1 (50)
Inhomogeneous	0 (0)	1 (50)
AP DIAMETER OF THE THYROID		
Normal	10 (100)	1 (50)
Increased	0 (0)	1 (50)
Decreased	0 (0)	0 (0)
MARGIN OF THYROID GLAND		
Smooth	10 (100)	1 (50)
Lobulated	0 (0)	1 (50)
DEGREE OF ENHANCEMENT		
iso-	0 (0)	0 (0)
Decreased	0 (0)	0 (0)
Increased	10 (100)	2 (100)
PATTERN OF ENHANCEMENT		
Homogeneous	10 (100)	1 (50)
Inhomogeneous	0 (0)	1 (50)

Data presented in parentheses are percentage of each item. MRI, magnetic resonance imaging; SI, signal intensity; WI, weighted image; AP, anteroposterior.

Magnetic Resonance Imaging Protocol

MRI was performed using 1.5 Tesla units (Gyroscan NT, Philips, Best, Netherlands; and Genesis Signa, GE Healthcare, Chicago, IL, United States) and 3 Tesla units (Skyra, 20-channel phased array coil, Siemens, Erlangen, Germany; and Achieva, Philips, 16-channel phased array coil). MRI at our institution involves image acquisition from the skull base to the tracheal carina. All patients were imaged using a standardized MRI protocol comprising a 3-plane localizer and turbo spin-echo imaging, involving the following sequence: axial and coronal T1-weighted images (TR/TE, 730/10, FOV 220 × 220 cm, matrix 448 × 269, slice thickness 4.0 mm, intersection gap 0.4 mm), axial T2-weighted images (TR/TE, 4530/68, FOV 220 × 220 cm, matrix 448 × 269, slice thickness 4.0 mm, intersection gap 0.4 mm), axial and coronal fat-saturated T2-weighted images, followed by contrast-enhanced axial and coronal T1-weighted images. The same sequence was performed after contrast agent administration

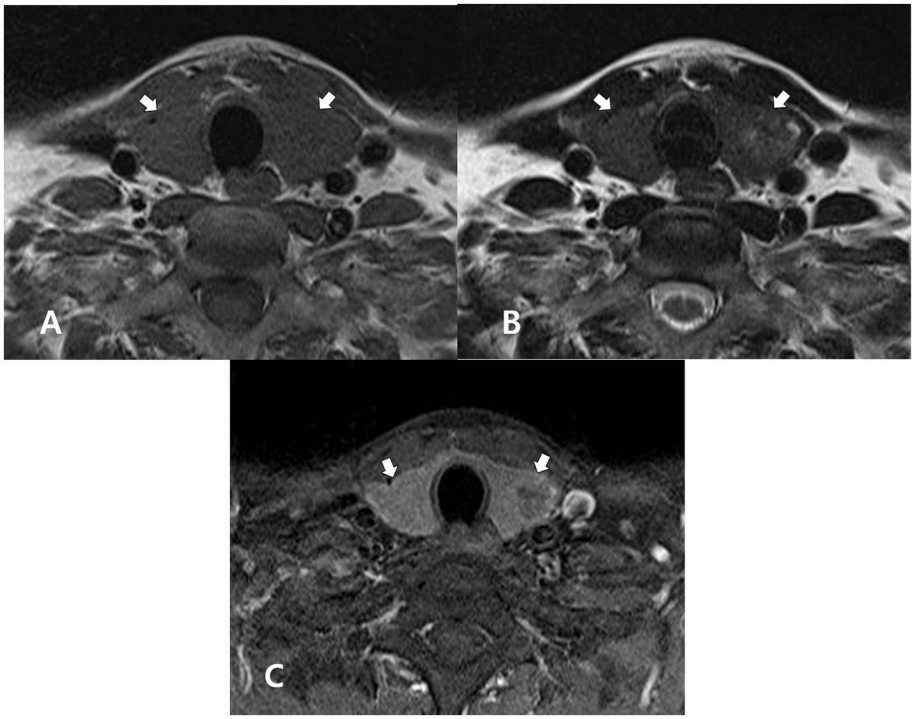

FIGURE 1 | A 51-year-old man with normal thyroid parenchyma confirmed by histopathology after thyroid surgery for the treatment of papillary thyroid carcinoma. In the non-enhanced axial T1- **(A)** and T2- **(B)** weighted images, the thyroid gland (arrows) exhibits homogeneous, iso-, and slightly high signal intensities, respectively, when compared with adjacent muscle. In both images, the thyroid gland (arrows) exhibits a normal size and smooth margin. In the enhanced axial, fat-suppression T1-weighted image **(C)**, the thyroid gland (arrows) exhibits homogeneously increased enhancement, when compared with adjacent muscle.

(0.1 mL/kg of gadobenate dimeglumine, Multihance BRACCO, Milan, Italy, at 2 ml per second, followed by a 20-ml saline flush at the same rate). The first post-contrast sequence began 90 sec after the contrast medium injection, to allow sufficient contrast enhancement.

Magnetic Resonance Imaging Analysis

A single radiologist (with 16 years of experience with thyroid US examination and neck MRI analysis, after obtaining board certification) retrospectively investigated MRI findings of the thyroid gland in the study patients, while being blinded to the US diagnosis of the thyroid gland, clinico-serological information, and the patient's medication history for DTD. The following features were investigated based on MR images, using a picture achieving and computer data system: parenchymal SI (as compared to adjacent muscle and fat; iso- [same SI at that of adjacent muscle], low [low SI relative to adjacent muscle], slightly high [higher SI than adjacent muscle but lower SI than adjacent fat], or high [same SI at that of adjacent fat]; homogeneity on T1- or T2-weighted images (homogeneous and inhomogeneous); anteroposterior diameter of the thyroid gland (normal [1–2 cm], increased [>2 cm], or decreased [<1 cm]); glandular margin (smooth or lobulated); degree of enhancement (as compared to adjacent muscle; iso-, decreased, or increased); and pattern of enhancement (homogeneous or inhomogeneous).

Final Diagnosis of Diffuse Thyroid Disease and Normal Thyroid Parenchyma

Histopathological findings from the thyroid gland were retrospectively analyzed by a single pathologist. Hashimoto thyroiditis was characterized as progressive loss of thyroid follicular cells with replacement by lymphocytes and formation of germinal centers associated with fibrosis. Diffuse hyperplasia was characterized by diffuse hypertrophy and hyperplasia of follicular cells with retention of the lobular architecture and no definite nodule formation. The thyroid gland was considered to have normal thyroid parenchyma when there was no visual evidence of coexisting DTD.

RESULTS

For the 12 patients, the reason for thyroid surgery was suspicious thyroid malignancy in cytology. The mean interval between neck MRI and thyroid surgery was 7.6 ± 2.9 months (range 2–12 months). After thyroid surgery (9 total thyroidectomy and 3 hemithyroidectomy), papillary thyroid carcinoma was confirmed in all patients. Based on the histopathological findings of the thyroid gland, we characterized patients with normal thyroid parenchyma ($n = 10$), Hashimoto thyroiditis ($n = 1$), and diffuse hyperplasia ($n = 1$).

The MRI features of the thyroid gland are listed in **Table 1**. The 9 normal thyroid parenchyma cases exhibited iso-/slightly

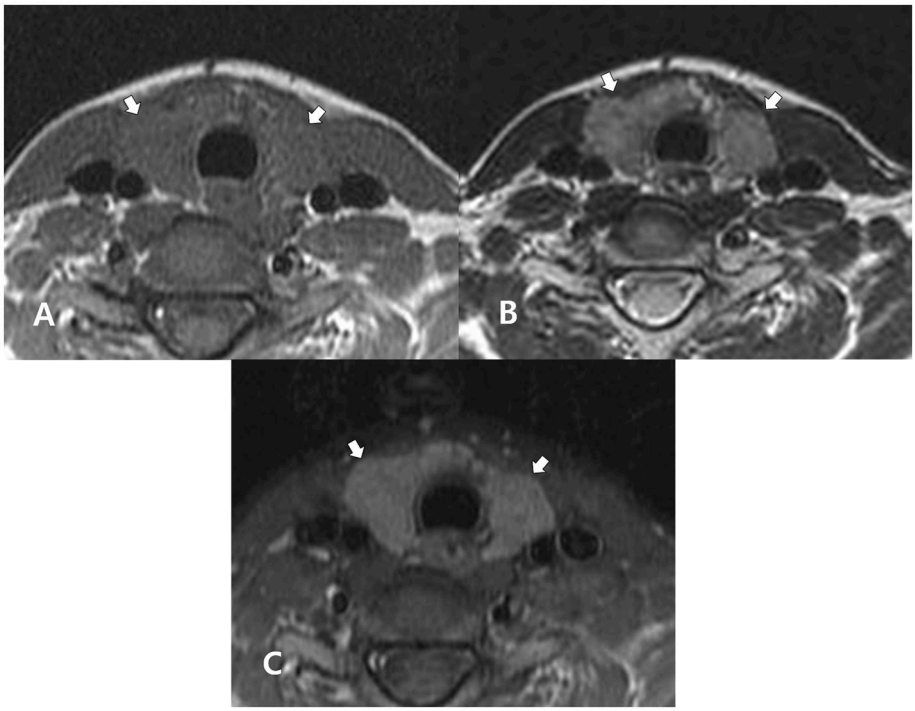

FIGURE 2 | A 27-year-old woman with Hashimoto thyroiditis confirmed in cytology after ultrasound-guided fine-needle aspiration. In the non-enhanced axial T1- **(A)** and T2- **(B)** weighted images, the thyroid gland (arrows) exhibits homogeneous, iso-signal intensity, and inhomogeneous, high signal intensity, respectively, when compared with adjacent muscle. In both images, the thyroid gland (arrows) exhibits a normal gland size and smooth margin. In the enhanced axial, fat-suppression T1-weighted image **(C)**, the thyroid gland (arrows) exhibits homogeneously increased enhancement, when compared with adjacent muscle.

high SI on T1/T2-weighted images, whereas 1 case revealed iso-/slightly high SI on T1/T2-weighted images. In all normal thyroid parenchyma cases, SI was homogeneous, the anteroposterior diameter of the thyroid gland was normal, had a smooth margin, and showed homogeneously increased enhancement as compared with adjacent muscle (**Figure 1**). In contrast, Hashimoto thyroiditis exhibited high and inhomogeneous SI on T2-weighted images (**Figure 2**), and diffuse hyperplasia revealed increased anteroposterior diameter and lobulated margin of the thyroid gland and inhomogeneous enhancement (**Figure 3**).

DISCUSSION

In the literature, the known US features of normal thyroid parenchyma included a fine echotexture, iso-echogenicity, a smooth margin, a normal glandular size, and normal parenchymal vascularity (4–7). In contrast, the known CT features of normal thyroid parenchyma include iso-attenuation, homogeneous attenuation, an anteroposterior diameter of 1–2 cm, smooth margin, and homogeneous enhancement (8–10). In the present MRI study, the thyroid gland was compared with adjacent muscle. The common MRI features of normal thyroid parenchyma include iso-/slightly high SI on T1/T2-weighted images, homogeneous SI, normal anteroposterior diameter of the thyroid gland, smooth margin, and homogeneously increased enhancement. According to previous MRI studies, normal thyroid parenchyma exhibits greater SI than adjacent muscle on T1-weighted images (11, 12). However, all normal thyroid parenchyma cases in the present study exhibited iso-SI on T1-weighted image. The reason for this difference is unclear. To clarify this issue, further studies are required.

In the literature, the reported US features of DTD include increased or decreased parenchymal echogenicity, coarse echotexture or "micronodulation," increased or decreased anteroposterior diameter of the thyroid gland, presence of marginal nodularity, and increased or decreased parenchymal vascularity (4–7). In contrast, the CT features suggestive of DTD include low attenuation, inhomogeneous attenuation, increased glandular size, lobulated margin, and inhomogeneous enhancement (8–10). In the present MRI study, SI, glandular size or margin, and parenchymal enhancement may be different between normal thyroid parenchyma and DTD. Nevertheless, among the numerous studies, no US or CT features with a high sensitivity and specificity for detecting DTD have been found (4–10). Similarly, no specific MRI features for DTD were found. Nevertheless, MRI detection of DTD may be feasible, although only 2 cases of DTD were included. To clarify this issue, a large-scale study is required.

This study had several limitations. First, the sample size was small. In particular, only 2 cases of DTD were included. Secondly, a neck MRI protocol was used in this study. For clarity, a further study using the appropriate MRI protocol for

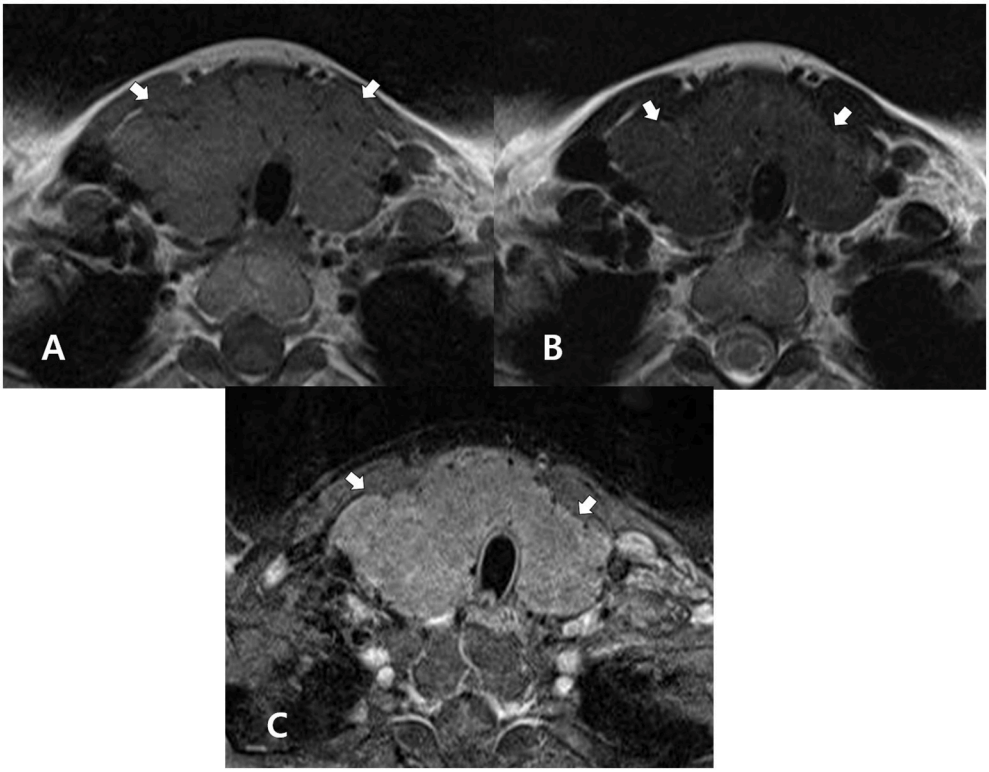

FIGURE 3 | A 44-year-old woman with diffuse hyperplasia confirmed by histopathology after thyroid surgery for the treatment of papillary thyroid carcinoma. In the non-enhanced axial T1- **(A)** and T2-**(B)** weighted images, the thyroid gland (arrows) exhibits homogeneous, iso-. and slightly increased signal intensity, respectively, when compared with the adjacent muscle. In both images, the thyroid gland (arrows) exhibits increased size and a lobulated margin. In the enhanced axial, fat-suppression T1-weighted image **(C)**, the thyroid gland (arrows) exhibits increased, but inhomogeneous enhancement, when compared with adjacent muscle.

the thyroid gland is required. Thirdly, there was a considerable interval between neck MRI and thyroid surgery. Fourthly, a single radiologist performed the image analysis. Finally, only patients who underwent neck MRI and thyroid surgery were included, and thus selection bias was unavoidable.

In conclusion, the results of the present study demonstrated that the MRI features of normal thyroid parenchyma and incidental DTD are different. Thus, MRI may be helpful for detection of incidental DTD.

ETHICS STATEMENT

This study follows the principles expressed in the Declaration of Helsinki. All study participants waived informed consents owing to the retrospective analysis, and the study design was approved by the appropriate ethics review boards.

AUTHOR CONTRIBUTIONS

DWK concept and design. HB, DWK analysis and interpretation of data; TK, DWK manuscript writing; DWK review of final manuscript. All authors acquisition of data, literature review, and refinement of manuscript.

ACKNOWLEDGMENTS

This work was supported by the 2018 Inje University research grant.

REFERENCES

1. Loevner LA. Anatomy and pathology of the thyroid and parathyroid glands. In: Som PM, Curtin HD, editors. *Head and Neck Imaging, 5th Edn*. St. Louis, MO: Mosby (2011). p. 2611–55. doi: 10.1016/B978-0-323-05355-6.00041-0
2. Rosario PW, Bessa B, Valadao MM, Purisch S. Natural history of mild subclinical hypothyroidism: prognostic value of ultrasound. *Thyroid* (2009) 19:9–12. doi: 10.1089/thy.2008.0221
3. Frates MC, Benson CB, Charboneau JW, Cibas ES, Clark OH, Coleman BG, et al. Management of thyroid nodules detected at US: society of radiologists in ultrasound consensus conference statement. *Radiology* (2005) 237:794–800. doi: 10.1148/radiol.2373050220
4. Kim DW, Eun CK, In HS, Kim MH, Jung SJ, Bae SK. Sonographic differentiation of asymptomatic diffuse thyroid disease from normal thyroid: a prospective study. *AJNR Am J Neuroradiol*. (2010) 31:1956–60. doi: 10.3174/ajnr.A2164

5. Kim DW. A comparative study of real-time and static ultrasonography diagnoses for the incidental detection of diffuse thyroid disease. *Endocr Pract*. (2015) 21:910–6. doi: 10.4158/EP15646.OR
6. Pedersen OM, Aardal NP, Larssen TB, Varhaug JE, Myking O, Vik-Mo H. The value of ultrasonography in predicting autoimmune thyroid disease. *Thyroid* (2000) 10:251–9. doi: 10.1089/thy.2000.10.251
7. Schiemann U, Avenhaus W, Konturek JW, Gellner R, Hengst K, Gross M. Relationship of clinical features and laboratory parameters to thyroid echogenicity measured by standardized grey scale ultrasonography in patients with hashimoto's thyroiditis. *Med Sci Monit*. (2003) 9:MT13–17. Available online at: http://www.MedSciMonit.com/pub/vol_9/no_4/3474.pdf
8. Kim DW, Jung SJ, Ha TK, Park HK, Kang T. Comparative study of ultrasound and computed tomography for incidentally detecting diffuse thyroid disease. *Ultrasound Med Biol*. (2014) 40:1778–84. doi: 10.1016/j.ultrasmedbio.2014.02.023
9. Rho MH, Kim DW. Computed tomography features of incidentally detected diffuse thyroid disease. *Int J Endocrinol*. (2014) 2014:921934. doi: 10.1155/2014/921934
10. Kim DW, Lee YJ, Ahn HS, Baek HJ, Ryu JH, Kang T. Comparison of ultrasonography and computed tomography for diagnosing diffuse thyroid disease: a multicenter study. *Radiol Med*. (2018) 123:515–23. doi: 10.1007/s11547-018-0872-9
11. Charkes ND, Maurer AH, Siegel JA, Radecki PD, Malmud LS. MR imaging in thyroid disorders: correlation of signal intensity with Graves' disease activity. *Radiology* (1987) 164:491–4. doi: 10.1148/radiology.164.2.3602391
12. Takashima S, Fukuda H, Tomiyama N, Fujita N, Iwatani Y, Nakamura H. Hashimoto thyroiditis: correlation of MR imaging signal intensity withhistopathologic findings and thyroid function test results. *Radiology* (1995) 197:213–9. doi: 10.1148/radiology.197.1.7568826
13. Ozturk T, Bozgeyik Z, Ozturk F, Burakgazi G, Akyol M, Coskun S, et al. The role of diffusion weighted MR imaging for differentiation between Graves' disease and Hashimoto thyroiditis. *Eur Rev Med Pharmcol Sci*. (2015) 19:2798–803.
14. Abdel Razek AAK, Abd Allah SS, EI-Said AAE. Role of diffusion-weighted magnetic resonance (MR) imaging in differentiation between Graves' disease and painless thyroiditis. *Pol J Radiol*. (2017) 82:536–41. doi: 10.12659/PJR.902416
15. Donta TS, Smoker WR. Head and neck cancer: carcinoma of unknown primary. *Top Magn Reson Imaging* (2007) 18:281–92. doi: 10.1097/RMR.0b0113e3181570c6c

Conflict of Interest Statement: The authors declare that the research was conducted in the absence of any commercial or financial relationships that could be construed as a potential conflict of interest.

frontiers in Endocrinology

ORIGINAL RESEARCH
published: 12 December 2018
doi: 10.3389/fendo.2018.00747

Non-invasive Amide Proton Transfer Imaging and ZOOM Diffusion-Weighted Imaging in Differentiating Benign and Malignant Thyroid Micronodules

Ruijian Liu[1†], Guihuang Jiang[2†], Peng Gao[1†], Guoming Li[2], Linghui Nie[3], Jianhao Yan[2], Min Jiang[1], Renpeng Duan[1], Yue Zhao[1], Jinxian Luo[1], Yi Yin[2] and Cheng Li[1,3]*

[1] Department of General Surgery, Guangdong Second Provincial General Hospital, Guangzhou, China, [2] Department of Medical Imaging, Guangdong Second Provincial General Hospital, Guangzhou, China, [3] Guangdong Traditional Medical and Sports Injury Rehabilitation Research Institute, Guangdong Second Provincial General Hospital, Guangzhou, China

OPEN ACCESS

Edited by:
Ewelina Szczepanek-Parulska, Poznan University of Medical Sciences, Poland

Reviewed by:
Rocco Bruno, ASM Matera, Italy
Takao Ando, Nagasaki University Hospital, Japan

***Correspondence:**
Cheng Li
182838li@163.com

[†] *These authors have contributed equally to this work*

Specialty section:
This article was submitted to Thyroid Endocrinology, a section of the journal Frontiers in Endocrinology

Received: *23 September 2018*
Accepted: *26 November 2018*
Published: *12 December 2018*

Citation:
Liu R, Jiang G, Gao P, Li G, Nie L, Yan J, Jiang M, Duan R, Zhao Y, Luo J, Yin Y and Li C (2018) Non-invasive Amide Proton Transfer Imaging and ZOOM Diffusion-Weighted Imaging in Differentiating Benign and Malignant Thyroid Micronodules. Front. Endocrinol. 9:747. doi: 10.3389/fendo.2018.00747

Background: Pre-operative non-invasive differentiation of benign and malignant thyroid nodules is difficult for doctors. This study aims to determine whether amide proton transfer (APT) imaging and zonally oblique multi-slice (ZOOM) diffusion-weighted imaging (DWI) can provide increased accuracy in differentiating benign and malignant thyroid nodules.

Methods: This retrospective study was approved by the institutional review board and included 60 thyroid nodules in 50 patients. All of the nodules were classified as malignant ($n = 21$) or benign ($n = 39$) based on pathology. It was meaningful to analyze the APT and apparent diffusion coefficient (ADC) values of the two groups by independent t-test to identify the benign and malignant thyroid nodules. The relationship between APT and ZOOM DWI was explored through Pearson correlation analysis. The diagnostic efficacy of APT and ZOOM DWI in determining if thyroid nodules were benign or malignant was compared using receiver operating characteristic (ROC) curve analysis.

Results: The mean APTw value of the benign nodules was 2.99 ± 0.79, while that of the malignant nodules was 2.14 ± 0.73. Additionally, there was a significant difference in the APTw values of the two groups ($P < 0.05$). The mean ADC value of the benign nodules was 1.84 ± 0.41, and was significantly different from that of the malignant nodules, which was 1.21 ± 0.19 ($P < 0.05$). Scatter point and Pearson test showed a moderate positive correlation between the APT and ADC values ($P < 0.05$). The ROC curve showed that the area under the curve (AUC) value of ZOOM DWI (AUC = 0.937) was greater than that of APT (AUC = 0.783) ($P = 0.028$).

Conclusion: APT and ZOOM DWI imaging improved the accuracy of distinguishing between benign and malignant thyroid nodules. ZOOM DWI is superior to APTw imaging ($Z = 2.198$, $P < 0.05$).

Keywords: thyroid nodule, diagnosis, magnetic resonance imaging (MRI), amide proton transfer (APT), diffusion-weighted imaging (DWI)

INTRODUCTION

Thyroid nodules are comm and are found in up to 65% of the general population (1). Surgeons and radiologists are often asked to distinguish between benign and malignant thyroid nodules because it is necessary to be aware of the difference when creating treatment plans and surgical strategies, or when performing conservative monitoring of treatment. Examinations of suspected nodules in the clinic are performed using ultrasound, computed tomography (CT), magnetic resonance imaging (MRI), and positron emission tomography (PET). New iterations of the aforementioned imaging techniques have also been integrated into clinical practice including ultrasound contrast, and perfusion or enhanced CT, The use of ^{18}F-FDG in diffusion-weighted imaging (DWI) and PET/CT has been proposed as a useful tool for the distinguishing benign from malignant thyroid nodules (2–5). However, all these techniques are hampered by a number of limitations. For example, ultrasound has insufficient power for retrosternal goiters. Fine needle aspiration biopsy (FNAB) is highly sensitive and specific, and it is commonly used to identify benign and malignant thyroid nodules (5). However, it is an invasive test that can cause physical discomfort or pain for patients (1), with a 10–15% rate of non-definitive diagnosis (6). CT uses radiation and is not suitable for pregnant women or adolescents. 18FDG-PET uptake in thyroid nodules confirmed by ultrasonography increases the risk of thyroid cancer (5). Contrast-enhanced MRI is forbidden for patients with renal failure and contrast media allergy (7). Therefore, a non-invasive and economical method is urgently needed in the clinic to detect and discern between benign and malignant thyroid nodules.

Amide proton transfer (APT) imaging is a molecular MRI method based on chemical exchange saturation transfer that can be used to detect endogenous mobile proteins and peptides even at relatively low molecular concentrations (8–13). Protein accounts for approximately 18% of the human body weight and performs most cellular functions. These proteins can be divided into two types: semi-solid proteins and mobile proteins. Mobile proteins are the basis of APT imaging. APT imaging has been introduced in the clinic for the imaging of breast cancer (14, 15), brain tumors (9, 10, 13), rectal cancer (16), lung cancer (17, 18), prostate cancer (19, 20), and non-neoplastic diseases, such as stroke (21, 22) and ventral hernia (23). Previous studies have shown that APT imaging, as an MRI biomarker for malignant tumors, can help identify the most active proliferative components in the tumor and predict the response of the tumor to treatment. Although APT imaging has had a positive effect on the diagnosis of diseases, to date, APT images have not been developed for or applied to thyroid nodules.

DWI obtains image contrast by measuring the degree of freedom and diffusion direction of water molecules in tissue (24). The apparent diffusion coefficient (ADC) is an important parameter of DWI images (25), which are commonly used in the diagnosis of the thyroid gland (26). Zonally oblique multi-slice (ZOOM) imaging is a novel DWI imaging method. The ZOOM acquisition method provides better image quality and accuracy than non-ZOOM technology (27). It has been proven that it can be applied to the diagnosis of other diseases by scanning areas of the body such as the cervical spinal cord. A shorter time of repetition (TR) can be obtained when ZOOM DWI is used, along with better image quality, higher blood contrast, and less magnetically sensitive artifacts.

In this study, 60 thyroid nodules were obtained from 50 patients who underwent preoperative MRI. The hypothesis of this confirmatory study is that the two non-invasive advanced MRI techniques, free protein-based APT imaging and water-based molecular diffusion-based ZOOM DWI, can be valuable in differentiating between benign and malignant thyroid nodules. Additionally, ZOOM DWI is superior to APTw imaging.

MATERIALS AND METHODS

Study Population

This study was approved by the Ethics Committee of Guangdong Second People's Hospital. All of the patients signed written informed consent forms prior to inclusion. All of the patients underwent conventional short tau inversion recovery (STIR), T1-weighted and T2-weighted imaging. The latest ZOOM DWI and APTw imaging sequences from *in vitro* MR images for pre-treatment thyroid nodule evaluation from November 2017 to May 2018 were used in the current study. Among 104 patients, 25 patients were excluded because they had no pathological diagnosis due to refusing surgery or undergoing conservative treatment. Five cases of thyroid ^{131}I treatment history or thyroid surgery history were excluded. In the remaining 74 patients, 15 who showed substantial patient motion and inadequate image acquisition were excluded, 8 were excluded because of nodules smaller than 5 mm, and 1 case was excluded because of pathological diagnosis of parathyroid carcinoma. Finally, a total of 50 patients with 60 nodules, including 39 benign thyroid nodules and 21 malignant thyroid nodules, were enrolled in this study, as shown in **Figure 1**.

All of the cases were diagnosed by pathology after surgery. The histologic types of thyroid nodules were as follows: 20 thyroid papillary carcinomas, 1 follicular thyroid cancer, 17 nodular goiter, 20 thyroid adenomas, and 2 cases of Hashimoto's thyroiditis. All of the patients underwent magnetic resonance imaging within 3 days before surgery.

MRI Protocols

All of the cases were subjected to magnetic resonance imaging of the thyroid on a Philips 3T whole-body scanner (Ingenia, 3.0 T; Philips Medical Systems, The Netherlands) with a bore size of 70 cm. In this study, magnetic susceptibility artifacts were reduced in all cases by having patients remove any metal dentures before magnetic resonance imaging. Motion artifacts were reduced by training patients to hold their breath at the appropriate times and avoiding swallowing. A sensitivity-encoding 16-multichannel receiver for head and neck coils was used for thyroid scanning. Our scanning protocol used these sequences to obtain axial imaging: STIR, T1W, T2W, ZOOM

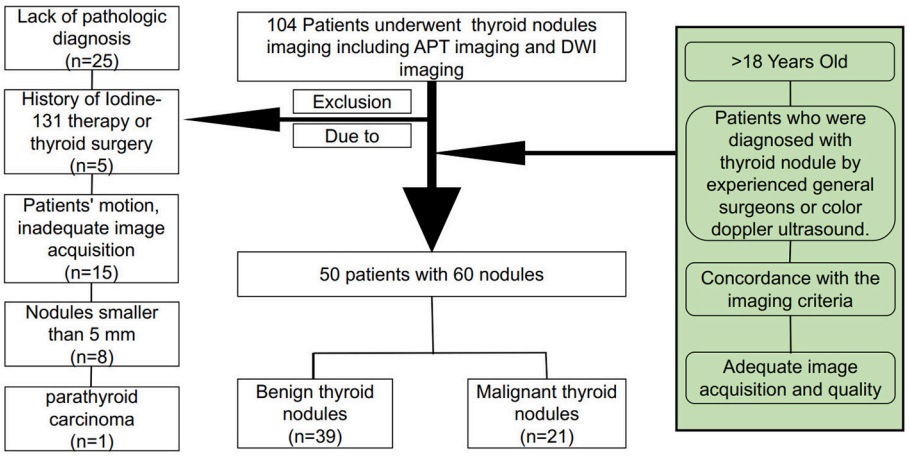

FIGURE 1 | Flowchart of the patient inclusion and exclusion process.

TABLE 1 | Details of the MR parameters.

PARAMETER	APT	STIR	ZOOM DWI	T1W	T2W
FOV(mm)	212 × 182 × 44	220 × 220 × 92	116 × 51 × 79	230 × 218 × 108	220 × 230 × 108
voxel	1.8 × 1.8 × 4.4	0.9 × 0.9 × 4	1.81 × 1.81 × 4	0.9 × 1.1 × 4	0.9 × 1.1 × 4
Matrix	120 × 101 × 10	244 × 219 × 21	64 × 27 × 18	256 × 192 × 24	224 × 200 × 24
NSA	1	1	1	2	2
Fat saturation	SPIR	NO	SPAIR	NO	No
TE	5.9	90	62	18	100
TR	6820	2367	3687	570	2500
Reconstruction matrix	224	400	128	480	528
TSE	158	25	NO	60	23
Flig angle	90	NO	90	90	90
Total time(s)	259	161	221	85	150

DWI, APT, and Gd-enhanced T1-weighted (Gd-T1W) imaging. Gadopentetate dimeglumine (0.2 ml/kg body weight; Magnevist; Bayer Schering, Guangzhou, China) was injected as a bolus via an antecubital vein at a speed of 2.0 mL/s to acquire the axial Gd-T1W images. Specific parameters are given in **Table 1**.

The scan time for each sequence was limited to 5 min, and the imaging acquisition time was intentionally minimized to alleviate patient discomfort. Therefore, gating and anesthesia were not used during the scan. The patient was trained to avoid movement and swallowing before scanning to reduce motion artifacts and improve the image quality.

Image Analysis

The radiologist (Guihua Jiang) and thyroid surgeon (Cheng Li) analyzed each patient's APT and ZOOM DWI images based on post-operative pathology and intra-operative findings. To compare the APT imaging with ZOOM DWI, we analyzed all of the image data using prototype software developed by Philips Medical Systems. The definitions and terms used in this study have been described in previous studies (11, 12, 28–33). APT imaging was quantified by magnetization transfer ratio asymmetry (MTRasym) analysis. The calculated MTRasym (3.5 ppm) image, using B0-corrected magnetization transfer spectral data at the offset of ±3.5 ppm, was deemed the APT image. Philips post-processing software was used to automatically generate ADC diagrams from ZOOM DWI images. The ADC value was automatically calculated after the region of interest (ROI) of each nodule on the ADC map was delimited.

For each imaging method, a combination of surgical findings and pathological results were used. Each ROI was drawn by 1 thyroid surgeon (Cheng Li) and 1 radiologist (Guihua Jiang), who together have 20 years of experience. For each patient, based on the STIR, T1W, and T2W imaging, and enhanced imaging, the ROIs were drawn on the APT imaging and ZOOM DWI images (after removing areas of necrosis, hemorrhage, calcium deposition, and cysts). Each ROI was maximized by placing it at the focus of the entire cross-sectional area of the nodule, thereby minimizing the effects of non-uniformity of the nodule. To minimize the error, each lesion was measured

TABLE 2 | Histological categories and demographic data between benign thyroid individuals and malignant thyroid individuals.

Histological categories	Number (%)	Mean age(years)	Female (%)	Height (m)	Weight (kg)
Benign	39 (65)	43.46 ± 12.79	27 (69.2)	1.62 ± 0.07	60.96 ± 9.13
Thyroid adenoma	20 (33.3)	38.55 ± 11.42	13 (65)	1.64 ± 0.08	59.05 ± 8.86
Nodular goiter	17 (28.3)	50.76 ± 10.9	13 (76.5)	1.59 ± 0.07	62.5 ± 8.06
Hashimoto's thyroiditis	2 (3.3)	30.5 ± 10.61	1 (50)	1.63 ± 0.07	67 ± 21.21
Malignant	21 (35)	39.86 ± 13.08	15 (71.4)	1.61 ± 0.07	59.1 ± 10.71
Thyroid papillary carcinoma	20 (33.3)	38.65 ± 12.16	14 (70)	1.61 ± 0.07	58.9 ± 10.95
Follicular thyroid cancer	1 (1.7)	64	1 (100)	1.56	63
Total	60 (100)	42.2 ± 12.9	42 (70)	1.61 ± 0.07	60.31 ± 9.66

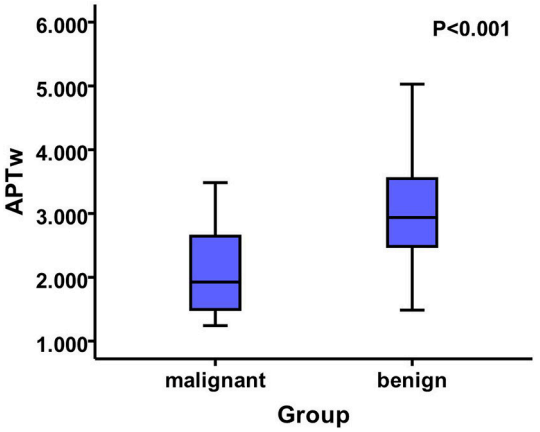

FIGURE 2 | The mean APTw value of the benign nodules was 2.99 ± 0.79, while that of the malignant nodules was 2.14 ± 0.73. Additionally, there was a significant difference between the two groups of APTw values ($P < 0.05$).

3 times, and the values averaged to determine the ADC and APT.

Statistical Analysis

In this study, SPSS 20.0 and MedCalc 15 software were employed for data analysis. The relationship between the molecular parameters, the APTw, and ADC values between different benign and malignant thyroid nodules were analyzed by two-samples *t*-tests. APTw and ADC were statistically evaluated by Pearson correlation. A comparison of diagnostic effects of APT and ZOOM DWI imaging was performed using the receiver operating characteristic (ROC) curve analysis of MedCalc 15. $P < 0.05$ was considered statistically significant.

RESULTS

Demographics and Clinical Characteristics

No significant differences were observed in age, gender distribution, height, or weight between individuals with benign thyroid nodules and those with malignant nodules. Patient demographic data and characteristics are shown in **Table 2**.

Data Analysis of APT Imaging and Zoom DWI

The two-sample *t*-test analysis revealed significantly increased APT values for benign thyroid nodules in comparison to APT values for malignant thyroid nodules ($P < 0.05$) **(Figure 2)**. Additionally, the ADC of malignant thyroid nodules was significantly lower than that of benign nodules ($P < 0.05$) **(Figure 3)**.

Correlation Between APTw and ADC

There was a positive correlation between the mean ADC observed in patients with malignant thyroid nodules and the APTw ($P < 0.001$, $R = 0.536$) **(Figure 4)**.

Comparison of the Diagnostic Performance Between APT Imaging and ZOOM DWI Imaging

Based on the ROC curve of the APT value (area under the curve, AUC = 0.783) and the ADC value (AUC = 0.937), ZOOM DWI imaging was superior to APT imaging in differentiating **between** benign and malignant thyroid nodules **(Figure 5)**.

DISCUSSION

Thyroid doctors cannot formulate the most optimal treatment strategies unless accurate evaluation of benign and malignant thyroid nodules can be performed using non-invasive magnetic resonance imaging. APT imaging is a molecular non-invasive MRI technique based on the chemical exchange saturation transfer (CEST) mechanism that detects endogenous mobile proteins and peptides in biological tissues. In this study, we put forward for the first time that APT imaging is meaningful for the differential diagnosis of benign and malignant thyroid nodules. The APT signal of malignant thyroid nodules is lower than that of benign nodules. Malignant thyroid nodules had lower ADC signal values than those of benign thyroid nodules. In addition, we found a moderate positive correlation between APT values and ADC values. Lastly, there were no significant differences between ZOOM DWI imaging and APT imaging in the diagnosis of benign and malignant thyroid nodules.

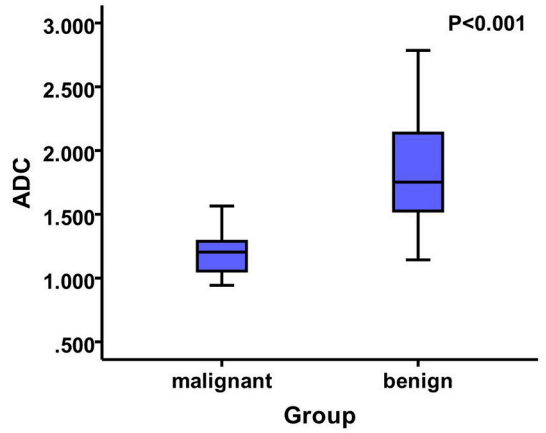

FIGURE 3 | The mean ADC value of the benign nodules was 1.84 ± 0.41, whereas that of the malignant nodules was 1.21 ± 0.19 that showed significant difference among them ($P < 0.05$).

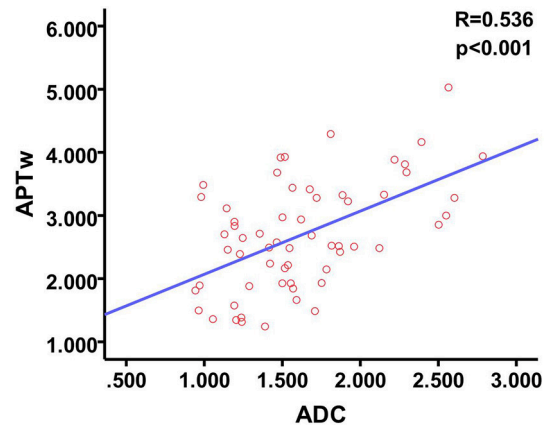

FIGURE 4 | Scatter plot and Pearson test show a moderate positive correlation between APTw and ADC.

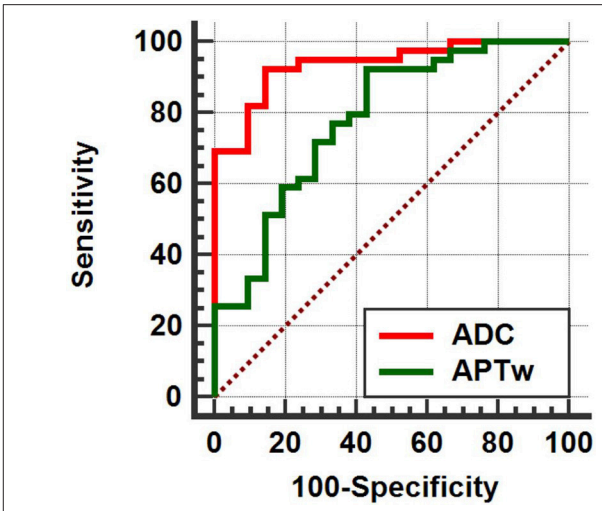

FIGURE 5 | APT (AUC = 0.783) < ADC (AUC = 0.937), ($Z = 2.198$, $P = 0.028$).

In our study, all of our diagnoses came from pathological assessment after thyroidectomy, which is a more accurate reference. In this study, we chose >5 mm nodules rather than >10 mm because we used the latest imaging sequences and an advanced imaging system (Philips 3.0T MRI), in order to obtain the best quality images. Additionally, we reduced imaging artifacts by training patients to remain as immobile as possible during scans.

To date, there have been no studies that have examined the sensitivity and specificity of APT imaging for thyroid nodules. Our APT imaging study of the thyroid is different from similar studies that have examined other parts of the body. Previous studies have shown that APT signals are higher in malignant nodules or malignant tumors of other organs. For example, the APTw values of malignant brain tumors were higher than those of benign brain tumors (9, 11, 12), the APTw values of high-grade gliomas were higher than those of low-grade gliomas (10, 13, 30, 34), the APTw values of moderately differentiated colorectal cancer were higher than those of highly differentiated colorectal cancer (16), and the APTw values for malignant pulmonary lesions were higher than those of benign pulmonary lesions (35). However, there have also been differences in studies, and the APTw value of the prostate cancer Gleason score (GS) in the score 7 group was the highest among the score 6–9 groups (19).

Unlike other malignancies, papillary thyroid cancer is a very latent disease (36–39), Therefore, the slow proliferation of cells accounts for the lower APTw value. In contrast, thyroid adenomas often grow into solitary large nodules, and the nodular goiter is diffusely enlarged. This phenomenon is in line with the principle of APT imaging, which is mainly based on the concentration of free proteins and peptides in the thyroid nodules. The APTw value increases with increases in the concentration of mobile proteins and peptides (40–42). Malignant nodules may destroy the thyroid membrane, thereby affecting the transport and exchange of related microscopic substances. Studies have confirmed by pathology and contrast-enhanced ultrasound that the microvessel density of malignant thyroid nodules is lower than that of benign thyroid nodules. The low microvessel density limits proton exchange between free protein and water, reduces cell growth and metabolism, and results in malignant thyroid nodules. In our study, APT values were lower in malignant thyroid nodules than in benign thyroid nodules. In addition, the nuclei of malignant thyroid nodules are larger, and the proportion of nuclear cytoplasm is increased (43). This may be one reason to account for the decreased APT values in malignant thyroid nodules in comparison to benign thyroid nodules.

Our findings on ZOOM DWI in thyroid nodules are consistent with those of previous studies, where ADC signals for malignant thyroid nodules are lower than those of benign nodules (25, 26, 44, 45), indicating that the diffusion of water

molecules in malignant thyroid nodules is limited. The reduction in microvessel density and the destruction of the thyroid capsule, which occur in thyroid cancer, can also account for lowered ADC signals in malignant thyroid nodules. However, a small number of studies have demonstrated that the differentiation of benign and malignant thyroid nodules based on ADC is ineffective (46). These differences between studies can be ascribed to the different technologies used, including the choice of B values, and the workstations used in ADC computing. The presence of necrotic or hemorrhagic nodules or poor image quality caused by low-field MRI magnets may also account for this difference (39). In addition, we found that there is a moderate positive correlation between APTw values and ADC values. It is possible that both values are related to the exchange of substances, and subsequently increase with increases in the rate of exchange of substances. It was found that ZOOM DWI was superior to APT in the diagnosis of thyroid nodules, which may be explained by APT imaging is a new technology that is not yet fully developed.

This study has several limitations. First, the sample size of the study is relatively small. Future studies will require a larger sample size so as to improve the power of the statistical analysis of our results. In addition, local absorption of heat causes elevated body temperature and results in patients feeling uncomfortable during the examination. Therefore, the specific absorption rate should be considered, which requires the selection of suitable pulse energy and scanning time so that the APT sequence can be further optimized.

CONCLUSIONS

In the current study, APT and ZOOM DWI were compared as two promising imaging methods for evaluating thyroid nodules at the cellular and molecular level. Our results indicate that they provide additional accurate clinical diagnostic information. These important auxiliary methods are of great value for differentiating benign and malignant thyroid nodules. We also found that APT imaging was moderately correlated with ADC values for thyroid nodules.

AUTHOR CONTRIBUTIONS

CL designed experiments; GL, LN, and JY carried out experiments; MJ analyzed experimental results; RD analyzed sequencing data and developed analysis tools. YZ, JL, and YY assisted with collecting data; RL, GJ, and PG wrote the manuscript.

FUNDING

This work was supported by the National Natural Science Foundation of China (81471639, 81771807), Science and Technology Department of Guangdong Province, China (2017ZC0260), Natural Science Foundation of Guangdong Province (2018A0303130129), and Traditional Chinese Medicine department of Guangdong Province, China (20171009, 20171010).

REFERENCES

1. Durante C, Grani G, Lamartina L, Filetti S, Mandel SJ, Cooper DS. The diagnosis and management of thyroid nodules: a review. *JAMA* (2018) 319:914–24. doi: 10.1001/jama.2018.0898
2. Warren FR, Richards M. computed tomography and magnetic resonance imaging of the thyroid and parathyroid glands. *Front Horm Res.* (2016) 45:16–23. doi: 10.1159/000442274
3. Lim HK, Park ST, Ha H, Choi SY. Thyroid nodules detected by contrast-enhanced magnetic resonance angiography: prevalence and clinical significance. *PLoS ONE* (2016) 11:e0149811. doi: 10.1371/journal.pone.0149811
4. Chen L, Xu J, Bao J, Huang X, Hu X, Xia Y, et al. Diffusion-weighted MRI in differentiating malignant from benign thyroid nodules: a meta-analysis. *BMJ Open* (2016) 6:e008413. doi: 10.1136/bmjopen-2015-008413
5. Haugen BR, Alexander EK, Bible KC, Doherty GM, Mandel SJ, Nikiforov YE, et al. 2015 American thyroid association management guidelines for adult patients with thyroid nodules and differentiated thyroid cancer: the american thyroid association guidelines task force on thyroid nodules and differentiated thyroid cancer. *Thyroid Off J Am Thyroid Assoc.* (2015) 156:2165. doi: 10.1089/thy.2015.0020
6. Pacini F, Burroni L, Ciuoli C, Di Cairano G, Guarino E. Management of thyroid nodules: a clinicopathological, evidence-based approach. *Eur J Nucl Med Mol Imaging* (2004) 31:1443–9. doi: 10.1007/s00259-004-1680-0
7. Sourbron SP, Buckley DL. Classic models for dynamic contrast-enhanced MRI. *NMR Biomed.* (2013) 26:1004–27. doi: 10.1002/nbm.2940
8. Zheng Y, Wang X. The applicability of amide proton transfer imaging in the nervous system: focus on hypoxic-ischemic encephalopathy in the neonate. *Cell. Mol. Neurobiol.* (2018) 38:797–807. doi: 10.1007/s10571-017-0552-7
9. Joo B, Han K, Choi YS, Lee S, Ahn SS, Chang JH, et al. Amide proton transfer imaging for differentiation of benign and atypical meningiomas. *Eur. Radiol.* (2018) 28:331–9. doi: 10.1007/s00330-017-4962-1
10. Park JE, Lee JY, Kim HS, Oh J, Jung SC, Kim SJ, et al. Amide proton transfer imaging seems to provide higher diagnostic performance in post-treatment high-grade gliomas than methionine positron emission tomography. *Eur. Radiol.* (2018). doi: 10.1007/s00330-018-5341-2
11. Law B, King AD, Ai QY, Poon D, Chen W, Bhatia KS, et al. Head and neck tumors: amide proton transfer MRI. *Radiology* (2018) 28:3285–95. doi: 10.1148/radiol.2018171528
12. Choi SH. Can amide proton transfer MRI distinguish benign and malignant head and neck tumors? *Radiology* (2018) 288:791–2. doi: 10.1148/radiol.2018180914
13. Choi YS, Ahn SS, Lee S, Chang JH, Kang S, Kim SH, et al. Amide proton transfer imaging to discriminate between low- and high-grade gliomas: added value to apparent diffusion coefficient and relative cerebral blood volume. *Eur. Radiol.* (2017) 27:3181–9. doi: 10.1007/s00330-017-4732-0
14. Klomp DWJ, Dula AN, Arlinghaus LR, Italiaander M, Dortch RD, Zu Z, et al. Amide proton transfer imaging of the human breast at 7T: development and reproducibility. *NMR Biomed.* (2013) 26:1271–7. doi: 10.1002/nbm.2947
15. Dula N, Dewey BE, Arlinghaus LR, Williams JM, Klomp D, Yankeelov TE, et al. Optimization of 7-T chemical exchange saturation transfer parameters for validation of glycosaminoglycan and amide proton transfer of fibroglandular breast tissue. *Radiology* (2015) 275:255–61. doi: 10.1148/radiol.14140762
16. Nishie, Takayama Y, Asayama Y, Ishigami K, Ushijima Y, Okamoto D, et al. Amide proton transfer imaging can predict tumor grade in rectal cancer. *Magn. Reson. Imaging* (2018) 51:96–103. doi: 10.1016/j.mri.2018.04.017
17. Togao O, Kessinger CW, Huang G, Soesbe TC, Sagiyama K, Dimitrov I, et al. Characterization of lung cancer by amide proton transfer (APT) imaging:

an in-vivo study in an orthotopic mouse model. *PLoS ONE* (2013) 8:e77019. doi: 10.1371/journal.pone.0077019
18. Ohno Y, Yui M, Koyama H, Yoshikawa T, Seki S, Ueno Y, et al. Chemical exchange saturation transfer mr imaging: preliminary results for differentiation of malignant and benign thoracic lesions. *Radiology* (2015) 279:578–89. doi: 10.1148/radiol.2015151161
19. Takayama Y, Nishie A, Sugimoto M, Togao O, Asayama Y, Ishigami K, et al. Amide proton transfer (APT) magnetic resonance imaging of prostate cancer: comparison with Gleason scores. *Magn Reson Mater Phys Biol Med.* (2016) 29:671–9. doi: 10.1007/s10334-016-0537-4
20. Jia G, Abaza R, Williams JD, Zynger DL, Zhou J, Shah ZK, et al. Amide proton transfer MR imaging of prostate cancer: a preliminary study. *J. Magn. Reson. Imaging* (2011) 33:647–54. doi: 10.1002/jmri.22480
21. Li H, Zu Z, Zaiss M, Khan IS, Singer RJ, Gochberg DF, et al. Imaging of amide proton transfer and nuclear overhauser enhancement in ischemic stroke with corrections for competing effects. *NMR Biomed.* (2015) 28:200–9. doi: 10.1002/nbm.3243
22. Tee YK, Harston GWJ, Blockley N, Okell TW, Levman J, Sheerin F, et al. Comparing different analysis methods for quantifying the MRI amide proton transfer (APT) effect in hyperacute stroke patients. *NMR Biomed.* (2014) 27:1019–29. doi: 10.1002/nbm.3147
23. Franconi F, Roux J, Garric X, Lemaire L. Early postsurgical visualization of composite mesh used in ventral hernia repair by amide proton transfer MRI. *Magn Reson Med.* (2014) 71:313–7. doi: 10.1002/mrm.24666
24. Iima M, Le Bihan D. Clinical intravoxel incoherent motion and diffusion MR imaging: past, present, and future. *Radiology* (2016) 278:13–32. doi: 10.1148/radiol.2015150244
25. Khizer T, Raza S, Slehria AU. Diffusion-weighted MR imaging and ADC mapping in differentiating benign from malignant thyroid nodules. *J Coll Physicians Surg Pak.* (2015) 25:785–8.
26. Hao Y, Pan C, Chen W, Li T, Zhu W, Qi J. Differentiation between malignant and benign thyroid nodules and stratification of papillary thyroid cancer with aggressive histological features: whole-lesion diffusion-weighted imaging histogram analysis. *J Magn Reson Imaging* (2016) 44:1546–55. doi: 10.1002/jmri.25290
27. Alizadeh M, Poplawski MM, Fisher J, Gorniak R, Dresner A, Mohamed FB, et al. Zonally magnified oblique multislice and non-zonally magnified oblique multislice DWI of the cervical spinal cord. *AJNR Am J Neuroradiol.* (2018) 39:1555–61. doi: 10.3174/ajnr.A5703
28. By S, Barry RL, Smith AK, Lyttle BD, Box BA, Bagnato FR, et al. Amide proton transfer CEST of the cervical spinal cord in multiple sclerosis patients at 3T. *Magn. Reson. Med.* (2018) 79:806–14. doi: 10.1002/mrm.26736
29. Zou T, Yu H, Jiang C, Wang X, Jiang S, Rui Q, et al. Differentiating the histologic grades of gliomas preoperatively using amide proton transfer-weighted (APTW) and intravoxel incoherent motion MRI. *NMR Biomed.* (2018) 31:e3850. doi: 10.1002/nbm.3850
30. Togao O, Hiwatashi A, Yamashita K, Kikuchi K, Keupp J, Yoshimoto K, et al. Grading diffuse gliomas without intense contrast enhancement by amide proton transfer MR imaging: comparisons with diffusion- and perfusion-weighted imaging. *Eur. Radiol.* (2017) 27:578–88. doi: 10.1007/s00330-016-4328-0
31. Park JE, Kim HS, Park KJ, Kim SJ, Kim JH, Smith SA. Pre- and posttreatment glioma: comparison of amide proton transfer imaging with MR spectroscopy for biomarkers of tumor proliferation. *Radiology* (2016) 278:514–23. doi: 10.1148/radiol.2015142979
32. Park JE, Kim HS, Park KJ, Choi CG, Kim SJ. Histogram analysis of amide proton transfer imaging to identify contrast-enhancing low-grade brain tumor that mimics high-grade tumor: increased accuracy of MR perfusion. *Radiology* (2015) 277:151–61. doi: 10.1148/radiol.2015142347
33. Bahl M, Sosa JA, Eastwood JD, Hobbs HA, Nelson RC, Hoang JK. Using the 3-tiered system for categorizing workup of incidental thyroid nodules detected on CT, MRI, or PET/CT: how many cancers would be missed? *Thyroid* (2014) 24:1772–8. doi: 10.1089/thy.2014.0066
34. Jiang S, Yu H, Wang X, Lu S, Li Y, Feng L, et al. Molecular MRI differentiation between primary central nervous system lymphomas and high-grade gliomas using endogenous protein-based amide proton transfer MR imaging at 3 Tesla. *Eur Radiol.* (2016) 26:64–71. doi: 10.1007/s00330-015-3805-1
35. Ohno Y, Kishida Y, Seki S, Yui M, Miyazaki M, Koyama H, et al. Amide proton transfer-weighted imaging to differentiate malignant from benign pulmonary lesions: comparison with diffusion-weighted imaging and FDG-PET/CT. *J Magn Reson Imaging* (2018) 47:1013–21. doi: 10.1002/jmri.25832
36. Ruggiero R, Bosco A, Pirozzi R, Bondanese MC, Gualtieri G, Docimo L. Papillary thyroid microcarcinoma in super obese patient. *G Chir* (2018) 39:173–6. doi: 10.11138/gchir/2017.39.3.173
37. Ito Y, Kudo T, Kihara M, Takamura Y, Kobayashi K, Miya A, et al. Prognosis of low-risk papillary thyroid carcinoma patients: its relationship with the size of primary tumors. *Endocr J.* (2012) 59:119–25. Available online at: https://www.jstage.jst.go.jp/article/endocrj/59/2/59_EJ11-0288/_article
38. Buj R, Mallona I, Díezvillanueva A, Zafón C, Mate JL, Roca M, et al. Kallikreins stepwise scoring reveals three subtypes of papillary thyroid cancer with prognostic applications. *Thyroid* (2018) 28:601–12. doi: 10.1089/thy.2017.0501
39. Ilica T, Artaş H, Ayan A, Günal A, Emer O, Kilbas Z, et al. Initial experience of 3 tesla apparent diffusion coefficient values in differentiating benign and malignant thyroid nodules. *J Magn Reson Imaging* (2013) 37:1077–82. doi: 10.1002/jmri.23913
40. Zhou J, Payen JF, Wilson DA, Traystman RJ, van Zijl PC. Using the amide proton signals of intracellular proteins and peptides to detect pH effects in MRI. *Nat Med.* (2003) 9:1085–90. doi: 10.1038/nm907
41. Kanazawa Y, Fushimi Y, Sakashita N, Okada T, Arakawa Y, Miyazaki M. B1 power optimization for chemical exchange saturation transfer imaging. a phantom study using egg white for amide proton transfer imaging applications in the human brain. *Magn Reson Med Sci.* (2018) 17:86–94. doi: 10.2463/mrms.tn.2016-0069
42. Clark DJ, Smith AK, Dortch RD, Knopp MV, Smith SA. Investigating hydroxyl chemical exchange using a variable saturation power chemical exchange saturation transfer (vCEST) method at 3 T. *Magn Reson Med.* (2016) 76:826–37. doi: 10.1002/mrm.25987
43. Schueller-Weidekamm, Schueller G, Kaserer K, Scheuba C, Ringl H, Weber M, et al. Diagnostic value of sonography, ultrasound-guided fine-needle aspiration cytology, and diffusion-weighted MRI in the characterization of cold thyroid nodules. *Eur J Radiol.* (2010) 73:538–44. doi: 10.1016/j.ejrad.2008.12.013
44. Noda Y, Kanematsu M, Goshima S, Kondo H, Watanabe H, Kawada H, et al. MRI of the thyroid for differential diagnosis of benign thyroid nodules and papillary carcinomas. *AJR Am J Roentgenol.* (2015) 204:W332–5. doi: 10.2214/AJR.14.13344
45. Wu Y, Yue X, Shen W, Du Y, Yuan Y, Tao X, et al. Diagnostic value of diffusion-weighted MR imaging in thyroid disease: application in differentiating benign from malignant disease. *BMC Med Imaging* (2013) 13:23. doi: 10.1186/1471-2342-13-23
46. Sasaki M, Sumi M, Kaneko K, Ishimaru K, Takahashi H, Nakamura T. Multiparametric MR imaging for differentiating between benign and malignant thyroid nodules: initial experience in 23 patients. *J Magn Reson Imaging* (2013) 38:64–71. doi: 10.1002/jmri.23948

Conflict of Interest Statement: The authors declare that the research was conducted in the absence of any commercial or financial relationships that could be construed as a potential conflict of interest.

frontiers in Endocrinology

REVIEW
published: 14 December 2018
doi: 10.3389/fendo.2018.00736

Active Surveillance for Papillary Thyroid Microcarcinoma: Challenges and Prospects

Shuai Xue[1], *Peisong Wang*[1], *Zachary A. Hurst*[2], *Yi Seok Chang*[2] *and Guang Chen*[1]*

[1] *Thyroid Surgery Department, The First Hospital of Jilin University, Changchun, China,* [2] *Department of Physiology and Cell Biology, The Ohio State University, Columbus, OH, United States*

Active surveillance (AS) can be considered as an alternative to immediate surgery in low-risk papillary thyroid microcarcinoma (PTMC) without clinically apparent lymph nodes, gross extrathyroidal extension (ETE), and/or distant metastasis according to American Thyroid Association. However, in the past AS has been controversial, as evidence supporting AS in the management of PTMC was scarce. The most prominent of these controversies included, the limited accuracy and utility of ultrasound (US) in the detection of ETE, malignant lymph node involvement or the advent of novel lymph node malignancy during AS, and disease progression. We summarized publications and indicated: (1) US, performer-dependent, could not accurately diagnose gross ETE or malignant lymph node involvement in PTMC. However, the combination of computed tomography and US provided more accurate diagnostic performance, especially in terms of selection sensitivity. (2) Compared to immediate surgery patients, low-risk PTMC patients had a slightly higher rate of lymph node metastases (LNM), although the overall rate for both groups remained low. (3) Recent advances in the sensitivity and specificity of imaging and incorporation of diagnostic biomarkers have significantly improved confidence in the ability to differentiate indolent vs. aggressive PTMCs. Our paper reviewed current imagings and biomarkers with initial promise to help select AS candidates more safely and effectively. These challenges and prospects are important areas for future research to promote AS in PTMC.

Keywords: active surveillance, papillary thyroid microcarcinoma, imaging, biomarker, recurrence

OPEN ACCESS

Edited by:
Ewelina Szczepanek-Parulska, Poznan University of Medical Sciences, Poland

Reviewed by:
Rocco Bruno, Independent Researcher, Matera, Italy
Trevor Edmund Angell, University of Southern California, United States

***Correspondence:**
Guang Chen
jidayiyuanjzx@sina.com

Specialty section:
This article was submitted to Thyroid Endocrinology, a section of the journal Frontiers in Endocrinology

Received: *16 August 2018*
Accepted: *20 November 2018*
Published: *14 December 2018*

Citation:
Xue S, Wang P, Hurst ZA, Chang YS and Chen G (2018) Active Surveillance for Papillary Thyroid Microcarcinoma: Challenges and Prospects. Front. Endocrinol. 9:736. doi: 10.3389/fendo.2018.00736

INTRODUCTION

In an early era of medicine, cancer was diagnosed at advanced and incurable stages due to poor diagnostic technologies and limited therapeutic options. High mortality from cancer evoked fear and promoted "early detection and curative treatment" as the holy grail for oncologists (1). Improved technology shifted cancer diagnosis to earlier time-points at less advanced stages, the so called "stage migration." Consequently, detection of sub-clinical small cancers became feasible (1, 2). Attributable to improvements in early detection and subsequent increased the number of novel diagnoses, the incidence of localized, *in situ*, cancers (particularly thyroid, melanoma, and kidney) doubled or tripled between 1975 and 2005 according to SEER database (https://seer.cancer.gov/). Despite the increased incidence, thyroid cancer mortality remains stable (3). Moreover, owing to indolent behavior and favorable prognosis of these cancers, high frequency of occult

microcarcinoma in autopsy studies has been also reported (4–9). These evidences indicated that doctors were diagnosing and treating many inert cancers, which would never cause any harm or threaten patient's lives even if left untreated.

Concerns about overdiagnosis and overtreatment lead to the introduction of active surveillance (AS) for indolent cancers, such as low-risk prostate cancer and papillary thyroid cancer, whose 5-year survival rates approached 100%(10). AS has become a routine treatment strategy for localized prostate cancer (11–13). A randomized controlled trial (ProtecT Trial) with median 10-year follow up reported prostate-cancer-specific-mortality was low among different treatment groups (AS, Surgery and Radiotherapy) and no significant difference existed in overall survival among the three treatment strategies. "Low risk" prostate cancer was defined as clinical stage T1-T2a (physical examination and imaging), Gleason Score $\leq$ 6 (biopsy), and prostate specific antigen $<$10 ng/mL (blood test) (14). To date, the most comprehensive study of AS in papillary thyroid microcarcinoma (PTMC) was conducted by the Kuma hospital in Japan. In their prospective trial, 8% of 1,235 PTMC patients demonstrated tumor enlargement $\geq$3 mm and 3.8% demonstrated novel lymph node metastases (LNM) at 10-year follow-up (15). While prognosis for both the immediate surgery and AS cohorts remained excellent, there were significantly less unfavorable events (mainly surgery complications) and medical cost in AS group patients (15). Thus, an increasing number of low-risk PTMC patients in Kuma hospital chose AS as their initial management strategy (16). Per the Kuma hospital criteria, "low risk" PTMC was defined as: no N1 and M1; no sign or symptom of invasion to the recurrent laryngeal nerve (RLN) or trachea; no high-grade malignancy in cytology. In contrast to prostate cancer, this criteria for determining AS candidacy in PTMC was heavily dependent on accuracy of imaging, especially ultrasound. Whether imaging examination could rule out small group of aggressive PTMC from AS candidates reliably remains unknown.

On the basis of these limited data, Leboulleux et al. recommended AS with curative intent should be considered in properly selected PTMC patients (17). However, this suggestion was contested by doctors from United Kingdom, United States, China, and Italy, which meant AS was not equally accepted by all physicians around the world. Clinicians showed little acceptance of AS because they believed evidence to support AS in PTMC was insufficient (18). In contrast to prostate cancer, thyroid cancer patients have better prognoses and lower mortality. However, the utility of AS in thyroid cancer remains controversial. Patients and clinicians alike worry delaying immediate treatment, as would be indicated by AS, may result in more extensive surgical intervention should substantial disease progression occur from the time of initial diagnosis. To address these concerns, it is essential to critically evaluate the ability of diagnostic imaging and biomarkers to accurately stratify risk in PTMC patients.

DIAGNOSTIC ACCURACY OF PREOPERATIVE US

Extrathyroidal Extension (ETE)

ETE, defined as tumor spread outside of the thyroid gland and into the surrounding tissues, occurs in up to 30% of differentiated thyroid cancer cases (19–23). Minimal ETE, detectable only on histological examination, was not a risk factor for disease specific survival and disease related mortality. Gross ETE, or macroscopic ETE, predicted increased recurrence and mortality (24). Thus, the general consensus is to consider gross ETE as an absolute indication for total thyroidectomy and administration of postoperative radioactive iodine (25). Differentiating minimal from gross ETE is essential in the selection of candidates for AS, however, to date, there is no reliable data to evaluate the diagnostic accuracy of ultrasound (US) alone for gross ETE in PTMC. As shown in **Table 1**, several studies assessed diagnostic ability of US for ETE (minimal and gross) in PTC or PTMC (26–33). The sensitivity and specificity of US ranged from 25 to 100% and from 13 to 93%, respectively. The huge variation in accuracy of US among different studies may result from ①: different percentage of minimal and gross ETE; ②: different diagnostic criteria of US; and ③: different levels of experience of the US technicians. Furthermore, we extracted 9 cases of T4 PTC patients from 5 articles and found that only 1 patient was diagnosed correctly by US, as shown in **Table 2** (30, 34–37). That indicates US alone, which is dependent on the experience of the technician and interpreting physician, can't be used to reliably diagnose gross ETE in PTMC.

Tracheal and RLN invasiveness are the most commonly observed gross ETE. Consequently, the Kuma hospital elected to implement "no signs or symptoms of invasion to RLN or trachea" as their selection criteria for AS in PTMC (15). In 2005, a study from Kuma hospital demonstrated US could diagnose tracheal invasion of PTC with extremely favorable sensitivity, specificity, and accuracy of 91, 93, and 93%, respectively (27). Moreover, Ito from Kuma hospital diagnosed tracheal invasion from low-risk PTMC based on the angles between tumor and tracheal wall with 100% sensitivity and 94.5% specificity, while diagnosis of RLN invasion was based on whether the normal rim of the thyroid was clearly present in the direction of RNL with 100% sensitivity and 90.3% specificity. However, 841 (74%) low-risk PTMC patients in this study were diagnosed with help of plain neck computed tomography (CT) because of uncertainty in US imaging. A study enrolled 377 PTC patients demonstrated the combination of US and CT scan decreased the false negative and false positive rates, improving ETE prediction accuracy. In a subgroup of PTMC, the combination of US and CT features also increased positive predictive value (PPV) remarkably (31). Choi et al. demonstrated that contrast-enhanced CT imaging correctly diagnosed a PTC patient as T4, while US alone would have categorized the patient as T3. However, they indicated the combined use of contrast-enhanced CT imaging and US did not improve accuracy for the diagnosis of minimal ETE in PTMC patients (35).

TABLE 1 | Diagnostic accuracy of preoperative ultrasound for extrathyroidal extension in thyroid cancer.

References	Country	Study	Patients	Criteria	SE (%)	SP (%)	PPV (%)	NPV (%)	AC (%)
Shimamoto et al. (26)	Japan	SR	35 of 77 with ETE (minimal and gross)	A	80	73.8	71.8	81.6	76.6
Tomoda et al. (27)	Japan	SR	13 of 509 with TI	C	91	93	25	99	93
Kwak et al. (28)	South Korea	SR	89 of 221 with ETE (N/A)	A	65.2	81.8	70.7	77.7	N/A
Kim et al. (29)	South Korea	SR	67 of 75 with ETE (minimal and gross)	A,C,D	78.5	79.5	46.8	94.1	79.3
Lee et al. (30)	South Korea	SR	174 of 377 with ETE (N/A)	A	66.1	65.1	72.2	58.3	N/A
Lee et al. (31)	South Korea	SR	275 of 568 with ETE (minimal and gross)	A	83.3	68.9	71.6	81.5	75.9
Moon et al. (32)	South Korea	SR	26 of 105 with EFI	E	46.2	97.5	85.7	84.6	84.8
Kamaya et al. (33)	USA	SR	16 of 62 with ETE (minimal and gross)	A,B	25	93	57	78	N/A

Criteria category: A: focal bulging out or disruption of the thyroid capsule by tumor or more than 25% of perimeter of the tumor was abutting the thyroid capsule; B: vessels extending to or from the nodule were seen beyond the capsule on either color or power Doppler images; C: the absence of a clear adventitia, dilatation of the cartilage space or tumor extension into the space, or irregularity of the tracheal mucosa; D: loss of normal esophageal layer by tumor, the tumor was in contact with 180° or more of the circumference of the vessel and tumor invasion into the vessels lumen or a tumor occupying the tracheal esophageal groove; E: the loss of echo-genic perithyroidal fat tissue by tumor. SR, single center retrospective; ETE, extrathyroidal extension; TI, trachea invasion; EFI, extrathyroidal fat invasion; SE, sensitivity; SP, specificity; PPV, positive predictive value; NPV, negative predictive value; AS, accuracy; N/A, not available.

TABLE 2 | Diagnostic accuracy of preoperative ultrasound for pathologic T4 papillary thyroid carcinoma.

References	Country	Study	T4 Patients	Criteria	US accuracy
King et al. (34)	Hong Kong	SP	3/14 of PTC	A	0/3
Choi et al. (35)	South Korea	SR	1/299 of PTC	B	0/1
Park et al. (36)	South Korea	SP	1/94 of PTC	B,C	0/1
Choi et al. (37)	South Korea	SR	1/722 of PTC	B	1/1
Lee et al. (30)	South Korea	SR	3/568 of PTC	B	0/3

Criteria category: A: poorly defined margin with heterogeneous echogenicity in adjacent fat or muscle or tumor invasion into the lumen; B: focal bulging out or disruption of the thyroid capsule by tumor or more than 25% of perimeter of the tumor was abutting the thyroid capsule; C, tumor diameter. SP, single center prospective; SR, single center retrospective; PTC, papillary thyroid carcinoma; US, ultrasound.

Currently, there are very few studies reporting RLN invasion in PTMC, presumably due to the low incidence of RLN invasion in PTMC. Ito et al. found only 9 of 1,143 PTMC patients with RLN invasion, all 9 of whom had a tumor diameter of 7 mm or larger. Consequently, Ito et al. concluded tumors of <7 mm in their largest diameter were unlikely to have RLN invasion. But PTMC was derived from abnormal follicular epithelial cell which meant it could be located anywhere within the thyroid. Small PTMCs (<5 mm) which invade RLN were more likely located in the dorsal part of thyroid. Inaccurate identification for boundaries of small PTMCs and dorsal membrane of thyroid by US may lead to misdiagnosis of gross ETE. Due to limitations in US at the time of evaluation, ETE in these patients was incorrectly assessed. The evidence reminds us of the limited efficacy for US alone in predicting gross ETE and that not all PTMC patients are low risk.

Lymph Node Metastases

LNM to the central and lateral compartments are common occurrences in PTC, and increase the rate of loco-regional recurrence and mortality, especially among old patients (38). Nearly 80% of PTC patients had micrometastatic lymph nodes on postoperative pathologic examination while 30% had clinical lymph nodes on initial presentation (39, 40). However, as shown in **Table 3**, the accuracy of preoperative US for diagnosing metastatic lymph nodes is low (26, 35, 36, 41–52). Appropriate selection of candidates for AS requires high sensitivity in order to prevent the enrollment of higher-risk PTMC patients. To predict central lymph node metastases (CLNM), sensitivity of US ranged from 22.6 to 55%, meaning nearly half of CLNM were not correctly diagnosed. This is perhaps due to the difficulty in detecting metastatic lymph nodes in the retropharynx, superior mediastinum, and deep trachea-esophageal groove. In contrast to CLNM, US sensitivity to detect lateral lymph node metastases (LLNM) was much better (62 to 100%). Of note, micrometastases are less important clinically compared to macrometastases. The benefit of treating incidentally identified micro-metastases are not well-demonstrated. Consequently, the American Thyroid Association (ATA) recommended fine needle aspiration (FNA) only for suspicious cervical lymph nodes larger than 8–10 mm (25). Among the articles we summarized in **Tables 3**, **5** studies focused on metastatic lymph nodes larger than 8–10 mm (26, 35, 47, 50, 52). However, the sensitivity of US for diagnosing CLNM remained low (26–53.2%). US didn't show any advantages in diagnostic ability for larger metastatic lymph nodes compared with the micrometastases.

Shown in **Figure 1** and **Table 4**, standalone CT imaging, or CT combined with US remarkably increased CLNM and LLNM diagnostic sensitivity and accuracy (35, 42, 43, 48, 50). In Choi's study which focused on metastatic lymph nodes larger than 10 mm, combination of US and CT increased sensitivity of CLNM from 53.2 to 73%, and LLNM from 93.9 to 95.9% (35). A separate prospective study from United States demonstrated that the combination of US and CT increased sensitivity of detecting metastatic central and lateral lymph node significantly to 54, 97%, respectively. Accordingly, they suggested combination of US and CT could provide reliable preoperative macroscopic nodal metastasis information to design rational nodal surgery in PTC patients (50).

TABLE 3 | Diagnostic accuracy of preoperative ultrasound for metastatic lymph nodes in thyroid cancer.

References	Country	Study	Patients	Criteria	Compartment	SE (%)	SP (%)	PPV (%)	NPV (%)	AC (%)
Shimamoto et al. (26)	Japan	SR	49 N1 of 77 PTC	A,B	CLNM, LLNM	36.7	89.3	85.7	44.6	55.8
Jeong et al. (35)	South Korea	SP	46 positive LNs of 312 LNs	A	CLNM, LLNM	53.6	97.9	73.7	95	N/A
Kim et al. (41)	South Korea	SR	53 N1 of 165 PTC	A	CLNM	38	93	77	70	71
					LLNM	64	92	83	82	82
Sugitani et al. (42)	Japan	SP	263 N1 of 361 PTC	A	CLNM	29	91	82	47.3	48.3
					LLNM	100	0	98	0	98
Ahn et al. (36)	South Korea	SR	117 positive levels of 183 cervical level	A	CLNM	55	69	77	44	60
					LLNM	62	79	84	55	68
Choi et al. (43)	South Korea	SR	119 N1 of 299 PTC	A,B	CLNM	53.2	79.8	60.8	74.3	69.9
					LLNM	93.9	25	93.9	25	88.7
Park et al. (44)	South Korea	SR	34 N1 of 94 PTC	A	CLNM	22.6	98.6	87.5	74.5	70.1
					LLNM	76.2	75	72.7	78.3	75.6
Choi et al. (45)	South Korea	SR	238 N1 of 589 PTC	A	CLNM	47.2	94.8	90.4	63.5	70.6
					LLNM	69.1	94.8	57.6	96.8	92.4
Lee et al. (46)	Japan	SR	254 positive LNs of 331 LNs	A	CLNM, LLNM	78	99	99.5	58	83
Hwang et al. (47)	USA	SR	30 N1 of 68 PTC	A,B	CLNM	30	86.8	64.3	61.1	N/A
					LLNM	93.8	80	76.5	94.1	N/A
Lee et al. (48)	South Korea	SR	121 N1 of 252 PTC	A	CLNM	23	97	81	72	73
					LLNM	70	84	81	74	77
Yoo et al. (49)	South Korea	SR	51 positive LNs of 124 LNs	A	CLNM	76.4	69.9	63.9	81	72.6
Lesnik et al. (50)	USA	SP	162 PTC	A,B	CLNM	26	95	78	66	N/A
					LLNM	79	87	80	86	N/A
Lee et al. (51)	South Korea	SR	136 N1 of 368 PTC 44 N1 of 48 PTC	A	LLNM	39	88.4	66.3	71.2	70.1
					LLNM	95.5	25	93.3	33.3	89.6
Khokhar et al. (52)	USA	SR	104 N1 of 227 PTC	A,B	CLNM	37.5	90.2	76.5	63.1	66.1

Criteria category: A: heterogeneous inner structure, loss of fatty hilum, rounded shape, taller-than-wide shape, cystic changes, microcalcifications, and peripheral vascularity; B: Lymph node size >6 mm, or 8 mm, or 1 cm; SR, single center retrospective; SP, single prospective; LN, lymph node; PTC, papillary thyroid carcinoma; CLNM, central lymph node metastasis; LLNM, lateral lymph node metastasis; SE, sensitivity; SP, specificity; PPV, positive predictive value; NPV, negative predictive value; AS: accuracy; N/A, not available.

The limitations of US to detect thyroid nodule and cervical lymph nodes were operator-dependent, presumably due to difficultly in evaluating deep anatomic structures such as mediastinum, parapharyngeal, retropharyngeal and infraclavicular regions, acoustically shadowed by bone, calcification or air (66). As a result, the 2015 ATA guideline recommended preoperative CT as an adjunct to US for patients with large or invasive primary tumor or US suspected advanced disease (25). Nevertheless, is it possible to diagnose gross ETE with virtually 100% sensitivity, as reported by the Kuma hospital? Could we diagnose cervical macroscopic LNM with decent sensitivity only by US? As summarized above, it may be possible to approach this high sensitivity through the combination of diagnostic CT and US imaging, which demonstrated significant improvements in diagnostic performance compared to US alone.

Radiologist vs. Surgeon Performed US

Multiple studies demonstrated that radiologist-performed USs were less accurate and provided inadequate preoperative staging when compared to surgeon-performed USs (67–70). Nearly half of patients received incorrect initial surgery with high local recurrence when an operation decision was made only based on radiologist-performed USs. Denise Carneiro-Pla reported surgeon-performed US changed the therapeutic strategy of 45% thyroid cancer patients through the accurate identification of CLNM/LLNM and thyroid intrathoracic extension (69). Rosebel Monteiro demonstrated that metastatic lymph nodes were diagnosed more frequently by CT imaging than US (70.8 vs. 54%). Moreover, surgeon-performed US was only able to detect 45% of metastatic lymph nodes in a cohort comprised of patients with LLNM (67). In the Kuma hospital, US was performed by specially trained sonographers and retrospectively reviewed by surgeons (15). Thus, it is extremely important to note that the appropriate selection of low-risk PTMC patients for AS is limited by the experience, or inexperience, of diagnosing physicians. Addressing this issue means improvements in both imaging technologies and in the education of physicians play important roles in AS candidate selection.

NOVEL LNM DURING AS

Sixteen percent of AS patients will require surgical intervention due to disease progression (71, 72). However, despite disease progression, prognosis in these patients remains remarkably

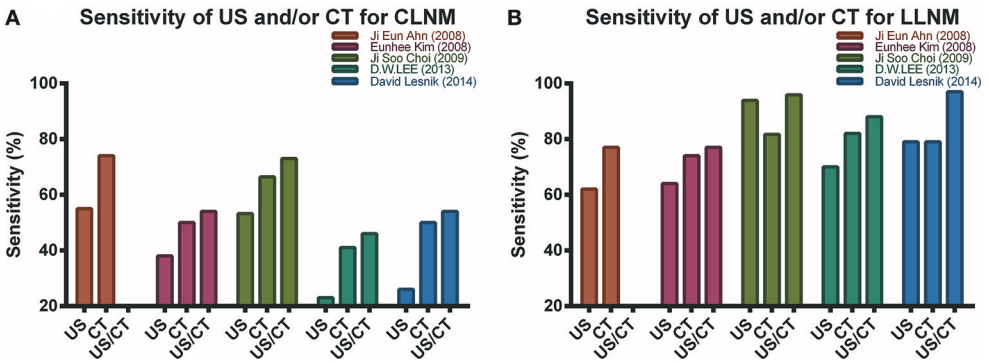

FIGURE 1 | Diagnostic sensitivity was improved by CT alone or combination of US and CT for CLNM **(A)** and LLNM **(B)**. Overall sensitivity of US and/or CT for LLNM was higher than for CLNM. Among Choi (43) and Lesnik (50) studies which only evaluated cervical lymph nodes larger than 10 mm, the combination of US and CT also provided highest sensitivity. The sensitivity for diagnosis of CLNM and LLNM by combination of US and CT was not evaluated in Ahn study (35).

TABLE 4 | Diagnostic accuracy of preoperative ultrasound and computed tomography for metastatic lymph nodes in thyroid cancer.

Study	Criteria	Compartment	SE (%)	SP (%)	PPV (%)	NPV (%)	AC (%)
Author (year): Kim et al. (42) **Country:** South Korea **Type:** SR **Patient:** 53 N1 of 165 PTC	US: A	CLNM	38	93	77	70	71
		LLNM	64	92	83	82	82
	CT:C	CLNM	50	91	79	74	75
		LLNM	74	95	89	86	87
	US+CT: A,C	CLNM	54	84	68	74	72
		LLNM	77	91	84	87	86
Author (year): Ahn et al. (35) **Country:** South Korea **Type:** SR **Patient:** 117 of 183 cervical levels	US: A	CLNM	55	69	77	44	60
		LLNM	62	79	84	55	68
	CT: C	CLNM	74	44	72	47	64
		LLNM	77	70	81	64	74
Author (year): Choi et al. (43) **Country:** South Korea **Type:** SR **Patient:** 119 N1 of 299 PTC	US: A,B	CLNM	53.2	79.8	60.8	74.3	69.9
		LLNM	93.9	25	93.9	25	88.7
	CT: C	CLNM	66.7	79.3	65.5	80.1	74.6
		LLNM	81.7	100	100	30.8	83.1
	US+CT: A,B,C	CLNM	73	70.2	59.1	81.5	71.2
		LLNM	95.9	25	94	33.3	90.6
Author (year): Lee et al. (48) **Country:** South Korea **Type:** SR **Patient:** 121 N1 of 252 PTC	US: A	CLNM	23	97	81	72	73
		LLNM	70	84	81	74	77
	CT: B	CLNM	41	90	66	76	74
		LLNM	82	64	69	78	73
	US+CT: A,B	CLNM	46	88	65	77	74
		LLNM	88	61	69	83	74
Author (year): Lesnik et al. (50) **Country:** USA **Type:** SP **Patient:** 162 PTC	US: A,B	CLNM	26	95	78	66	N/A
		LLNM	79	87	80	86	N/A
	CT: C,D	CLNM	50	94	85	74	N/A
		LLNM	79	83	76	86	N/A
	US+CT: A,B,C,D	CLNM	54	89	77	75	N/A
		LLNM	97	77	74	98	N/A

US criteria category: A: heterogeneous inner structure, loss of fatty hilum, rounded shape, taller-than-wide shape, cystic changes, microcalcifications, and peripheral vascularity; B: Lymph node size <1 cm; CT criteria category: C: round shape, calcification, cystic or necrotic change, heterogeneous enhancement, and strong enhancement without hilar vessel enhancement; D: Short axis >1 cm in axial plane; SR, single center retrospective; SP, single prospective; PTC, papillary thyroid carcinoma; US, ultrasound; CT, computed tomography; CLNM, central lymph node metastasis; LLNM, lateral lymph node metastasis; SE, sensitivity; SP, specificity; PPV, positive predictive value; NPV, negative predictive value; AS, accuracy; N/A, not available.

excellent due to the success of salvage surgery (15). In certain circumstances, most commonly the appearance of a novel LNM in the lateral/central compartment, delayed surgical intervention may increase the risk of subjecting a patient to more invasive surgical procedures, an increased risk of recurrence, and more extensive follow-up. A retrospective study which enrolled 8,808 PTMC in Korea demonstrated 12 PTMC with distant metastases had cervical lymph node involvement. Among them, 10 patients had clinically apparent lateral lymph nodes, while 2 had microscopic CLNM (73). Xu et al. investigated 3,750 non-anaplastic follicular cell-derived thyroid carcinomas and found that, of the 3 PTMC-related deaths, all 3 patients had clinically apparent cervical lymph nodes (74). Clinically apparent cervical lymph nodes were positively related with recurrence, distant metastases, and disease-specific mortality. Consequently, patients in which cervical lymph node involvement is detected during follow-up, no longer benefit from AS, and additional therapeutic intervention should be explored. According to a series of studies from Kuma hospital, the rates of novel lymph node appearance among patients undergoing AS were 1.2, 1.5, and 2.1% with an average of 3.9, 5, and 6.2 years of observation, respectively (72, 75, 76). Ito et al. explained that LNM may occur prior to, or at a very early stage of, PTMC diagnosis. Consequently, immediate surgery will not prevent metastases to the neck lymph node(s) and these patients will have recurrence and require a salvage operation in the future regardless of the initial management strategy (15). However, it is debated as to whether novel LNM during AS are completely comparable to recurrent lymph node involvement in an immediate surgery cohort, as it is difficult to demonstrate whether the tumor cells disseminate into lymph node during AS or before diagnosis.

If early dissemination of tumor cells to a regional or distant lymph node has occurred prior to diagnosis and/or initial thyroidectomy, excision of the primary thyroid cancer is unlikely to prevent recurrent disease localized to the lymph nodes. The parallel progression hypothesis, defined as the capacity of tumor cells to spread to the lymph nodes or more distant sites from the primary tumor site at a very early stage of tumorigenesis leading to the independent progression/evolution of a metastatic site, may explain early dissemination and frequent lymph node recurrence after surgery (77). PTC recurs much more frequently at central or lateral lymph node than thyroid bed after surgery (55, 78, 79), suggesting that recurrent lymph nodes of the neck had an early dissemination event prior to excision of the primary PTC.

Microscopic metastasis in regional lymph nodes was present in up to 63.83% of PTMC patients, although the recurrence rate was much lower to 1–5% (17, 80). The mechanism of lymph node recurrence after initial surgery without prophylactic lymph node dissection was possibly the outgrowth of micro-metastatic deposits into overt tumors. Whether or not a population of microscopic tumor cells can transform into clinically apparent lymph nodes may depend on not only the intrinsic genetic alterations of the cancer cells themselves but also the state of the host environment (81). It is well-known that both the local tissue microenvironment and the systemic physiological environment play significant roles in regulating dormant disseminated tumor cells into gross metastasis. Additionally, the tumor microenvironment can change during multiple steps of tumor progression and metastases, which could either inhibit or facilitate the progression of microscopic lymph nodes to clinically apparent lymph nodes (82–84). Perhaps, however, there exists a connection between persistent tumor foci in the thyroid and the progression of LNM from microscopic to clinically apparent.

We summarized 13 PTMC cohorts, each containing more than 200 patients, who received immediate surgery, shown in **Table 5** (53–65). We hypothesize, that AS patients should have a lower rate of novel clinically apparent metastatic lymph nodes than the rate of recurrent lymph nodes in PTMC cohort with gross ETE and/or palpable lymph nodes. However, as shown in **Figure 2**, we found novel LNM during AS was not less than lymph node recurrence rate among 6 of 11 PTMC cohorts with median follow-up time <10 years. Meanwhile, 5 of these 11 cohorts had relatively higher lymph node recurrence rates than AS group because all of these cohorts had patients with gross ETE and clinical involved lymph nodes. Among these 13 PTMC cohorts, there were two studies which enrolled low-risk PTMC patients without gross ETE or clinically apparent lymph nodes. Their lymph node recurrence rates were 1.2 and 0.7% with 5.4- and 5.8-year follow up, which were less than 1.5 and 2.1% of novel lymph node appearance rate with 5- and 6.2-year observation time in AS cohort from Kuma hospital (64, 65, 72, 76). With limited data, the rate of clinical apparent LNM in low-risk PTMC patients under AS seems to be a little higher than patients with immediate surgery. Considering cofounders between different patient's cohorts, this preliminary result needs to be supported and proved by more evidence in the future. Oda et al. compared clinicopathological and prognostic features of low-risk PTMC between AS and immediate surgery groups with a comparable experimental timeline. They found novel LNM appeared in 6 of 1179 AS patients (0.5%), whereas only 2 of 974 (0.2%) patients choosing immediate surgery experienced recurrence in cervical lymph nodes although this difference was not statistically significant (85). A study from Italy which enrolled 312 very low-risk PTMC (No family history of thyroid cancer; No history of head and neck irradiation; Tumor staging: T1 1 cm or less, N0, M0; No extension beyond thyroid capsule; Unifocal; Not aggressive histologic subtype; Not locally invasive) with 6.7-year follow up demonstrated none of the patients had lymph node recurrence (86). In addition, another study from Kuma hospital found up to 11% of PTMC in cohort of young patients aged 20 to 29 had novel LNM with median 5.5-year follow up (87). If novel LNM in AS group was completely comparable with lymph node recurrence in an immediate surgery cohort, should 11% of low-risk PTMC in 20 s group who underwent immediate surgery have lymph node recurrence after 5.5-year follow up? Patient age was believed to be predictor for novel lymph node appearance during AS (72, 87). However, age was not a risk factor for cervical lymph node recurrence in PTMC patients (79, 88).

In contrast to AS, the benefits of immediate surgery may include: ① A more accurate risk stratification can be made using information gathered from histological or genetic evaluation of a biopsy obtained from surgery, than can be obtained from imaging data alone. ② TSH suppression after surgery would

TABLE 5 | Cervical lymph node recurrence rate in different papillary thyroid microcarcinoma cohorts with immediate surgery.

References	Country	No. of patients	Gross ETE (n, %)	Clinical LN (n, %)	RAI (n, %)	FU (years)	TR (n, %)	LNR (n, %)
Wada et al. (53)	Japan	259	N/A	24 (9.3)	N/A	5.1	6 (2.3)	5(1.9)
Pelizzo et al. (54)	Italy	403	N/A	N/A	260 (60.5)	8.5	6(1.5)	1(0.2)
Hay et al. (55)	USA	900	N/A	131 (14.6)	155 (17)	17.2	51(5.7)	36 (4)
Besic et al. (56)	Slovenia	254	N/A	51 (20.1)	124 (49)	4.7	7 (2.7)	6(2.4)
Mercante et al. (57)	Italy	445	N/A	37 (8.3)	389 (87.4)	5.3	17(3.8)	13(2.9)
So et al. (58)	South Korea	551	4 (0.7)	0	444 (80.6)	3.4	1(0.2)	0
Moon et al. (59)	South Korea	288	0	10 (3.5)	114 (39.6)	6	12 (4.2)	7(2.4)
Londero et al. (60)	Denmark	406	N/A	N/A	161(40)	8	15(3.7)	7(1.7)
Lee et al. (61)	South Korea	2014	18 (0.9)	N/A	51(2.5)	11.2	126(6.3)	98(4.9)
Gschwandtner et al. (62)	Austria	1391	N/A	N/A	255 (18.3)	7	5(0.4)	5(0.4)
Kim et al. (63)	South Korea	5656	210 (3.7)	N/A	N/A	5.1	126(2.2)	122(2.2)
Cecoli et al. (64)	Italy	437	0	0	152 (38.7)	5.8	6(1.4)	3(0.7)
Kim et al. (65)	South Korea	8676	0	0	3,863 (44.5)	5.4	139(1.6)	105 (1.2)

ETE, extrathyroidal extension; LN, lymph node; RAI, radioactive iodine; FU, follow up; TR, total recurrence; LNR, lymph node recurrence; N/A, not available.

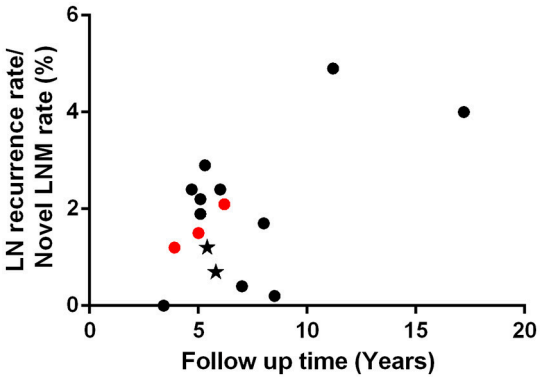

FIGURE 2 | Cervical lymph node recurrence rates (black dots and stars) among 13 different PTMC cohorts and novel LNM rates (red dots) in AS groups. With <10-year follow up, 5 PTMC cohorts had relatively higher lymph node recurrence than novel LNM rate in AS patients because all of these 5 cohorts had small group of PTMC with gross ETE and/or clinical apparent lymph node (detail seen **Table 5**). The lymph node recurrence rates of "low-risk" cohorts (black stars), which excluded patients with gross ETE and clinical apparent lymph node, were relatively less than novel LNM rates in AS groups.

decrease recurrence risk in contralateral lobe and neck lymph node. ③ Serum Tg is an accurate and reliable biomarker of tumor burden in Tg auto-antibody negative patients who received a total thyroidectomy. ④ For PTMC patients with lymph node recurrence, metastatic lymph nodes were stable for many years (89). At this time, it may be more feasible to use serum Tg levels during AS for monitoring recurrent lymph nodes.

ETHICAL ISSUES

In 2000, Emanuel et al. argued the most important ethical concerns in clinical trials was "the potential benefits to individuals must outweigh the risks (90)." However, with only US and FNA, we have little prognostic information, with the exception of age and tumor size, to evaluate the safety of AS. Consequently, Stack and Angelos recommended implementing only institutional review board-approved research protocols or surveillance contracts for educating patients, codifying the relationship between clinician and patient, and establishing medicolegal protections (91). But Morris et al. disagreed, instead believing these documents would jeopardize patient autonomy and influence their choice (92). Supporters of AS think higher risk among a small number of patients will and should be balanced by the advantage of avoiding surgery in a larger number of patients (93). However, is it ethical to risk the health of some patients, even a minority, for the greater good? Recently, Dr. Akira estimated the lifetime disease progression probabilities, stratified by patient age, of PTMC during AS, which were 60.3% (20 s), 37.1% (30 s), 27.3% (40 s), 14.9% (50 s), 9.9% (60 s), and 3.5% (70 s) (87). This study provided significant information for AS patients selection. In the future, we need more information from imaging and molecular signatures to provide more accurate risk stratifications of the clinical behavior and the risk for disease progression of PTMC patients during AS.

IMPROVEMENTS IN IMAGING

US

In terms of diagnostic accuracy, 3-dimensional (3D) US outperformed 2-dimensional (2D) US when compared to patients' final histopathological outcome (94). A single sweep of 3D US provided imaging for reconstruction and overcame the major limitations of 2D US. Kim et al. evaluated 91 thyroid nodules from 85 consecutive patients and compared sensitivity and specificity between 3D and 2D US. They found 3D US had significantly higher sensitivities than 2D in predicting ETE (94). In contrast, a separate study from South Korea reported 3D US with tomographic ultrasound imaging algorithms alone was not superior to real-time 2D US (95). This discrepancy is perhaps attributable to the differences that variable image reconstruction

parameters have on US interpretation. Slapa et al. summarized the advantages of 3D US as follows: distinct separation between imaging acquisition and analysis, better remote consultation, less operator dependency, and increased diagnostic accuracy (96).

Recently, shear wave elastography (SWE) has emerged to diagnose and predict the pathologic prognostic factors of PTC using quantitative information about thyroid nodule elasticity. It is operator-independent and can display elastograms of estimated tissue stiffness. Yun et al. enrolled 208 PTC patients and found ETE was associated with the elasticity index determined by SWE, and quantification of the elasticity index could accurately predict pathologic ETE (97). Diagnostic accuracy of cervical lymph nodes was also significantly improved by SWE. Woo et al. reported the elasticity indices of SWE were significantly correlated with not only malignant lymph nodes, but also the number, size and ETE of involved lymph nodes. They concluded quantitative SWE could predict pathologic prognostic factors of cervical LNM (98). Azizi et al. evaluated 270 lymph nodes from 236 patients with both conventional US and SWE. Using single shear wave velocity cut off of 2.93 m/s, SWE could improve diagnostic sensitivity and specificity to 92.59 and 75.46%, respectively. Lymph node stiffness measured by SWE is reported to be an independent predictor of malignant lymph node (99). Xu from China also found predictive performance for CLNM in PTC was markedly improved with the combination of conventional US and SWE, which indicated SWE would be a useful tool for treatment planning (100).

CT and MRI

Liu et al. evaluated cervical metastatic lymph nodes using dual-energy spectral CT and found venous phase λ_{HU} (slope of the spectral Hounsfield unit curve) was the best parameter for diagnosis with sensitivity, specificity of 62.0 and 91.1%, respectively. Compared to conventional CT, quantitative assessment with gemstone spectral CT parameters improved accuracy for detecting cervical metastatic lymph nodes of PTC (101). Considering MRI, several studies have reported the apparent diffusion coefficient (ADC) derived from diffusion-weighted imaging (DWI) could be used as a predictor for thyroid cancer aggressiveness (102–104). Hao et al. evaluated the predictive performance of ADC for ETE of PTCs in a cohort of 23 PTMC patients. PTCs with ETE had significant lower median ADC, 5th percentile ADC, and 25th percentile ADC while PTMCs had significant lower ADC only in 5th percentile ADC (102). Another study used DWI histogram analysis of whole tumor ADC to investigate the relationships between ADC parameters with histopathological features like LNM, ETE, Ki-67, and p53. They found ADC mean, ADC max, ADC median, ADC modus, ADC p75, and ADC p90 were all related significantly with p53, which was prognostic marker for thyroid cancer. Moreover, they identified an inverse correlation between ADC max, ADC p90, and Ki-67, which was regarded as predictor for disease progression during AS (105). Importantly, ADC histogram skewness and kurtosis were also identified to be parameters for predicting LNM (104). Meyer et al. demonstrated MRI texture analysis, which was a novel imaging technique derived from extensive data provided by conventional sequences, was a very useful tool to predict histopathological features in thyroid cancer although they only enrolled 13 thyroid cancer patients (4 PTC; 4FTC; and 5 ATC) (103).

IMPROVEMENTS IN BIOMARKER

BRAF

Braf, as a member of RAF kinase family, served as a growth signal transduction protein kinase. $Braf^{V600E}$ composed nearly 90% of all somatic mutated Braf and played an important oncogenic role in thyroid tumorigenesis (106). The replacement of valine with glutamate at codon 600 resulted from the substitution of thymine with adenine at nucleotide 1799, then activated its serine/threonine kinase constitutively, leading to further activation of MAPK pathway (107). The downstream effectors of mutated Braf, such as Mek and Erk, will be phosphorylated and take part in thyroid tumorigenesis (106, 107). Moreover, $Braf^{V600E}$ could promote tumor formation and aggressiveness by regulating the expression of other genes epigenetically, either through hyper- or hypomethylation. The interaction between $Braf^{V600E}$ and epigenetic alterations, which downregulated tumor suppressor genes (like T1MP3, SLC5A8, DAPK1, RARβ2) and upregulated oncogenes (like HMGB2 and FDG1), increased tumor cell proliferation and invasion (108, 109).

In 2015, a meta-analysis was performed to investigate the correlation between $Braf^{V600E}$ and clinical features for PTMC (110). In Li et al, the authors analyzed 3437 PTMC patients across 19 studies after searching PubMed, EMBASE, and the Cochrane library. They found that $Braf^{V600E}$ mutation was associated with aggressive clinicopathological features like multifocality, ETE, LNM, and advanced stage of PTMC. Consequently, they suggested $Braf^{V600E}$ could be used as a risk factor for the stratification and management of PTMC (110). Lee et al. predicted gross ETE of PTMC with 100% sensitivity through the use of tumor size, US features, and $Braf^{V600E}$ mutation status. They categorized US features of the primary tumor into four groups: A: intraparechymal; B, tumor abutting the capsule <50% of diameter; C: tumor abutting >50% of diameter; and D: tumor destroyed the capsule. In a subgroup of $Braf^{V600E}$negative patients, a tumor size of 0.7 cm and US categorizations B and C were cut-off values for gross ETE, with 100% sensitivity, whereas US categorizations A and B as cutoff value had 100% sensitivity for predicting gross ETE in the $Braf^{V600E}$ mutation positive patients (111). Besides clinical risk features, Chen et al. also found PTMCs with $Braf^{V600E}$ mutation were more likely to recur (OR 2.09 [95% CI:1.31–3.33]) by a meta-analysis of 2,247 PTMC patients from 4 published studies and 2 institutional cohort primary data (112). Niemeier et al. developed a molecular-pathological score (including superficial tumor location, intraglandular tumor spread/multifocality, tumor fibrosis, and Braf status) to stratify PTMC into different risk groups and successfully predict recurrence rate. In the diagnosis of aggressive PTMC, the combination of histologic features and Braf status increased diagnostic sensitivity from 77 to 96% and specificity from 68 to 80% (113). With mounting evidence, revisions to the ATA guidelines in 2015 began to consider $Braf^{v600e}$ status as a risk

factor of structural disease recurrence in PTMC patients after initial therapy (25).

However, Miyauchi et al. in the Kuma hospital detected $BRAF^{V600E}$ status in 11 PTMC patients without disease progression, 10 PTMC with tumor size progression, and 5 with novel LNM. The percentage of $Braf^{V600E}$ was 64, 70, and 80% in each group, respectively (114). Consequently, the use of $BRAF^{V600E}$ alone is insufficient to accurately stratify risk in PTMC patients. If using $Braf^{V600E}$ alone as biomarker for selecting AS candidates, nearly 60% of PTMCs who may never have disease progression will be categorized wrongly. Considering high prevalence of $Braf^{v600e}$ mutation among PTMC, $Braf^{V600E}$ alone cannot be used as reliable biomarker for differentiating aggressive PTMC from indolent ones, and identifying potential disease progression cases from stable ones during AS. A possible reason may be that the oncogenic event driving PTMC aggressiveness requires additional mutations acting in conjunction with $BRAF^{V600E}$ and the MAPK signaling pathway (115). Thus, the identification of additional genetic variants, which are less abundant than $BRAF^{V600E}$, could be important in predicting PTMC aggressiveness.

TERT

Telomerase reverse transcriptase (TERT) is the catalytic protein subunit of telomerase, which can maintain chromosomal integrity and genome stability (116). Malignant cancer cells, which were replicative immortal, required activation of telomerase and regulation of other growth controlling genes, pathways and molecular by TERT (117). First reported in 2013, TERT promoter mutation (C228T and C250T) in thyroid cancer has progressed rapidly in recent 5 years (118). Many studies have demonstrated TERT mutation was associated with more aggressive clinicopathological features of thyroid cancer, such as male gender, ETE, LNM, advanced stage, distant metastasis, recurrence, and mortality (119–122). Two meta-analyses in 2016 investigated clinicopathological significance of TERT promoter mutations in PTC and found the average prevalence of TERT promoter mutation was around 10%. Additionally, PTC patients with TERT promoter mutation displayed more aggressive histopathological features (121, 122). Kim et al. developed an effective risk stratification system using TERT promoter mutation status that reliably predicted structural recurrence and mortality in DTC patients (119).

Of note, the co-occurrence of Braf and TERT promoter mutations enhanced the predictive ability for prognosis of PTC. Moon et al. performed a meta-analysis including 13 studies with 4,347 PTC patients and found the co-occurrence of Braf and TERT promoter mutations was more significantly associated with aggressive clinicopathological features than either mutation alone (123). Accordingly, they believed these two mutations had a synergistic effect on prognosis and were useful in risk stratification of PTC. Liu et al. categorized 1,051 PTC patients according to mutation status of Braf and TERT promoter and demonstrated deaths per 1,000-person years in PTC patients with neither mutation, $Braf^{V600E}$ alone, TERT mutation alone, or both mutations were 0.80, 3.08, 6.62, and 29.86, respectively. Simple 4-genotype classification can predict disease-specific mortality accurately (124). Recently, this synergistic effect of BRAF and TERT promoter has been demonstrated as $Braf^{V600E} \rightarrow$ MAPK pathway $\rightarrow$ FOS $\rightarrow$ GABP $\rightarrow$ TERT signaling/transcription axis in human cancers (125). Firstly, mutated $Braf^{V600E}$ activated MAPK pathway, which phosphorylated FOS to be an active transcription factor for activating the GABPB promotor. Then increased expression of GABPB and formation of GABPA-GABPB complex activated the mutant TERT promoter. In this axis, phosphorylated FOS played important oncogenic bridging role between $Braf^{V600E}$ and TERT promoter mutations (125).

However, de Biase et al. detected TERT promoter mutations with next-generation sequencing in 431 PTMC patients assembled from six different institutions. They found the prevalence of TERT promoter mutations among PTMC was only 4.7%, less than the 10% reported in PTC patients. Moreover, the presence of TERT promoter mutations was not associated with unfavorable clinicopathological features (126). Also in Miyauchi's study, no PTMC patients undergoing AS were positive for TERT promoter mutations, even in a subgroup of patients with increased tumor sizes and/or novel lymph node appearance (114). Therefore, with regard to its low prevalence in PTMC, TERT promoter mutations are unlikely to be reliable molecular markers of tumor aggressiveness/progression.

MicroRNA

MicroRNA is defined as a group of small endogenous, single stranded non-coding RNAs of 19–25 nucleotides that can exclusively regulate their proprietary mRNA expression (127). The miRNA-221-222 cluster, downstream of the MAPK pathway, played an important role in tumorigenesis and aggressiveness for PTC (128). Located on the X chromosome, miRNA-221-222 cluster was regulating PTC formation and invasion through negative regulation of p27 (129). Multiple studies have demonstrated that upregulated miR-221-222 cluster was associated with more unfavorable clinicopathological features, treatment resistance, increased recurrence rate, and worse prognosis (130–133). Because of that, the miRNA-221-222 cluster was considered as a potential biomarker for aggressive PTC. Additionally, miRNA-146b is another well-studied and overexpressed microRNA in PTC. Its expression level was positively associated with tumor aggressiveness and poor prognosis (131, 133). Study has shown miRNA-146b functioned in PTC through binding with the 3′UTR region of retinoic acid receptor beta (RARβ) (134). Moreover, advanced PTC patients could receive benefit from retinoic acid (a RARβ ligand) treatment. Retinoic acid treatment resulted in tumor shrinkage and increased radioiodine uptake in 38% and 26% of patients, respectively (135). These studies suggested that miRNA-146b might play important role in thyroid cancer initiation and progression. In addition to the two microRNAs discussed above, there are also other microRNAs which have been identified to be associated with tumor aggressiveness (especially ETE, LNM and distant metastasis) including miRNA135-b, 146-a, 146-5p and several others (**Table 6**) (129, 136–155).

The upregulation of miRNA-221-222 cluster and miRNA-146b in $BRAF^{V600E}$ positive tumors, was suggested to be attributable to activation via the NF-κB pathway (156, 157). In

TABLE 6 | Tissue microRNA as predictor for aggressiveness in papillary thyroid carcinoma.

MicroRNA	Change in APTC	ETE	LNM	DM	Target molecular	References
MiR-126-3p	↓	*			ADAM9,SLC7A5	(136)
MiR-130b	↓	*			N/D	(137)
MiR-135b	↑	*			N/D	(138)
MiR-146a	↑	*	*		RARβ,PRKCE	(137, 139–142)
MiR-146b	↑	*	*	*	KIT, SMAD4, ZNRF3,IRAK1, RARβ	(137–140, 142–148)
MiR-16	↓	*			ITGA2	(145)
MiR-199b-5p	↑	*	**		N/D	(149)
MiR-221	↑	*	*	*	p27,TIMP3	(129, 132, 137, 138, 143, 145, 150)
MiR-222	↑	*	*		p27, PPP2R2A,TIMP3	(129, 132, 137, 138, 143, 145, 151)
MiR-2861	↑		**		N/D	(152)
MiR-30a-3p	↓		*		N/D	(149)
MiR-34b	↓	*			N/D	(137)
MiR-363-3p	↓		*		PIK3CA	(153)
MiR-451	↑		**		N/D	(152)
MiR-613	↓	*			FN1	(145)
MiR-622	↓		*		VEGFA	(154)

*APTC, aggressive papillary thyroid carcinoma; ETE, extrathyroidal extension; LNM, lymph node metastases; DM, distant metastases; N/D, not determinated. ↑, up-regulated in aggressive PTC. ↓, down-regulated in aggressive PTC. *, related with aggressive features, **Related with central and lateral neck lymph node metastases.*

TABLE 7 | Long Non-coding RNA as predictor for aggressiveness in papillary thyroid carcinoma.

LncRNA	Change in APTC	ETE	LNM	DM	Target molecular	References
ATB	↑		*		N/D	(167)
CASC2	↓		*		N/D	(168)
CNALPTC1	↑		*		miR-30 family	(169)
GAS8-AS1	↑		*		N/D	(170)
HIT000218960	↑		*		HMGA2	(165)
HOXD-AS1	↑		*	*	N/D	(171)
LINC00271	↓	*	*		N/D	(166)
LINC01061	↑		*		miR-4316	(172)
LOC100507661	↑		*		N/D	(163)
MALAT1	↑		*		N/D	(173)
MEG3	↓		*		Rac1	(174)
NONHSAT037832	↓		*		N/D	(175)
NONHSAT076754	↑		*		N/D	(176)
NONHSAT129183	↑		*		N/D	(177)
NONHSAT076747	↑		*		N/D	(178)
NONHSAT122730	↑		*		N/D	(178)
NR_036575.1	↑	*			N/D	(179)
PVT1	↑	*	*		IGF1R	(180)
RP11-402L6.1	↑		*		N/D	(181)
XLOC_051122	↑		*		N/D	(182)
XLOC_006074	↑		*		N/D	(182)

*APTC, aggressive papillary thyroid carcinoma; ETE, extrathyroidal extension; LNM, lymph node metastases; DM, distant metastases; N/D, not determinated. ↑, up-regulated in aggressive PTC. ↓, down-regulated in aggressive PTC. *, related with aggressive features.*

$Braf^{V600E}$ PTMC patients, it remains unknown what molecular events trigger disease progression during AS. Would it be possible to increase our ability to predict PTMC disease progression by screening FNA biopsies for clinically actionable somatic mutations and/or the expression of miRNAs?

Serum Circulating Biomarkers

Compared with inherent instability of mRNA, circulating miRNA is subjected to nuclease activity and resistant to environment. Because of that, miRNA, which can be readily detected in bloodstream, is believed as a potential ideal candidate serum biomarker for PTC (158). Yu et al. detected serum miRNA expression by Solexa sequencing and found increased miR-151-5p, detected in the serum, was associated with LNM of PTC (159). However, the evidence of using circulating miRNA to predict disease progression of PTMC during AS was absent. In addition, a prospective observational pilot study found circulating myeloid-derived suppressor cells, which were detected preoperatively by novel flow cytometry-based immunoassay, were positively associated with a higher TNM stage and disease recurrence (160). Lubitz et al. reported they only detected 63% circulating $Braf^{V600E}$ mutation by novel RNA-based blood assay compared with conventional tissue assays on surgical specimens. They concluded detecting circulating $Braf^{V600E}$ could be a surrogate for conventional FNA detection (161). In contrast, a separate study found only 37.3% of PTC patients with locally advanced and metastasis were detected to have circulating $Braf^{V600E}$ mutation. These patients didn't get any benefits from analysis of circulating tumor DNA (162). Accordingly, there are several challenges about the application of serum circulating biomarkers for PTMC which include: ① Molecular FNA diagnostics with biomarkers have high concordance with pathological results. In contrast, serum circulating biomarkers demonstrate only partial concordance with FNA determined pathology. Consequently, circulating biomarkers from blood are not superior to FNA biopsies in predicting aggressiveness. ② All studies about detecting serum circulating biomarkers enrolled cancer patients with advanced stage or distant metastasis. However, the serum circulating biomarkers identified in high-risk patients may not be detectable in low-risk PTMC patients. ③ Genetic background and alternations in circulating cells may be different with those in the primary tumor. Some cancer cells derived from the primary tumor may undergo changes that facilitate blood vessel invasion and then turn to circulating cells. ④ Other malignant tumors shared the same circulating miRNA or DNA with thyroid cancer. Differentiating where these circulating biomarkers came from is difficult.

Other Novel Targets

Besides genetic alternations, LncRNAs, which is defined as a class of RNAs containing over 200 nucleotides, play important roles in tumor progression (163). Kim et al. reported LOC100507661 expression was positively related with LNM and $Braf^{V600E}$ mutation in PTC patients (164). High expression of HOTAIR in thyroid cancer was associated with larger tumor size, more metastatic lymph nodes, and poorer outcome after a meta-analysis of TCGA and GEO databases (165). PTC patients with high expression of HIT000218960 had more multifocality, LNM and advanced TNM stage (166). Down-regulation of LINC00271 was identified as an independent risk factor for ETE, LNM, TNM stage and recurrence (167). Other LncRNAs, which related with aggressiveness of PTC, were also identified and summarized in **Table 7** (164, 166–183).

Epigenetic changes, particularly methylation of DAPK, REC8, TIMP3, CDH1, FGFR2 were also reported to be associated with aggressive behavior of PTC (184). Whether we can predict the aggressiveness of PTMC using these biomarkers derived from PTC patients remains to be investigated.

CONCLUSION

The utility of AS for low-risk PTMC patients requires improvements our abilities to accurate and confidently stratify patient risk. Due to the substantially improved diagnostic performance in identifying gross ETE and macroscopic cervical LNM, the combined use of US and CT imaging modalities is strongly recommended for use in AS. Patients should be informed and educated fairly and objectively according to the data that is currently available. Dynamic monitoring, risk stratification, and personal follow-up schedules are tantamount in minimizing the potential risks incurred by recommending patients against immediate surgery. Furthermore, the advent of increasingly sophisticated imaging technologies, and the screening for novel prognostic biomarkers have shown great promise, although future validation studies are warranted.

AUTHOR CONTRIBUTIONS

All authors listed have made a substantial, direct and intellectual contribution to the work, and approved it for publication.

REFERENCES

1. Klotz L. Cancer overdiagnosis and overtreatment. *Curr Opin Urol.* (2012) 22:203–9. doi: 10.1097/MOU.0b013e32835259aa
2. Esserman LJ, Thompson IM Jr, Reid B. Overdiagnosis and overtreatment in cancer: an opportunity for improvement. *JAMA* (2013) 310:797–8. doi: 10.1001/jama.2013.108415
3. Welch HG, Black WC. Overdiagnosis in cancer. *J Natl Cancer Inst.* (2010) 102:605–13. doi: 10.1093/jnci/djq099
4. Harach HR, Franssila KO, Wasenius VM. Occult papillary carcinoma of the thyroid. A "normal" finding in Finland. A systematic autopsy study. *Cancer* (1985) 56:531–8. doi: 10.1002/1097-0142(19850801)56:3<531::AID-CNCR2820560321>3.0.CO;2-3
5. Kovács GL, Gonda G, Vadasz G, Ludmany E, Uhrin K. Epidemiology of thyroid microcarcinoma found in autopsy series conducted in areas of different iodine intake. *Thyroid* (2005) 15:152–7. doi: 10.1089/thy.2005.15.152
6. Martinez-Tello FJ, Martinezcabruja R, Fernandezmartin J, Lassooria C, Ballestincarcavilla C. Occult carcinoma of the thyroid. A systematic autopsy study from Spain of two series performed with two different methods. *Cancer* (1993) 71:4022–9. doi: 10.1002/1097-0142(19930615)71:12<4022::AID-CNCR2820711236>3.0.CO;2-O
7. Stamatiou K, Alevizos A, Agapitos E, Sofras F. Incidence of impalpable carcinoma of the prostate and of non-malignant and precarcinomatous lesions in Greek male population: an autopsy study. *Prostate* (2006) 66:1319–28. doi: 10.1002/pros.20339
8. Welch HG, Black WC. Using autopsy series to estimate the disease "reservoir" for ductal carcinoma in situ of the breast: how much more breast cancer can we find? *Ann Intern Med.* (1997) 127:1023–8. doi: 10.7326/0003-4819-127-11-199712010-00014
9. Yamamoto Y, Maeda T, Izumi K, Otsuka H. Occult papillary carcinoma of the thyroid. A study of 408 autopsy cases. *Cancer* (1990) 65:1173–9. doi: 10.1002/1097-0142(19900301)65:5<1173::AID-CNCR2820650524>3.0.CO;2-2
10. Haymart MR, Miller DC, Hawley ST. Active surveillance for low-risk cancers - a viable solution to overtreatment? *N Engl J Med.* (2017) 377:203–6. doi: 10.1056/NEJMp1703787
11. Bul M, Zhu X, Valdagni R, Pickles T, Kakehi Y, Rannikko A, et al. Active surveillance for low-risk prostate cancer worldwide: the PRIAS study. *Eur Urol.* (2013) 63:597–603. doi: 10.1016/j.eururo.2012.11.005
12. Tosoian JJ, Carter HB, Lepor A, Loeb S. Active surveillance for prostate cancer: current evidence and contemporary state of practice. *Nat Rev Urol.* (2016) 13:205–15. doi: 10.1038/nrurol.2016.45
13. Welty CJ, Cowan JE, Nguyen H, Shinohara K, Perez N, Greene KL, et al. Extended followup and risk factors for disease reclassification in a large active surveillance cohort for localized prostate cancer. *J Urol.* (2015) 193:807–11. doi: 10.1016/j.juro.2014.09.094
14. Hamdy FC, Donovan JL, Lane JA, Mason M, Metcalfe C, Holding P, et al. 10-year outcomes after monitoring, surgery, or radiotherapy for localized prostate cancer. *N Engl J Med.* (2016) 375:1415–24. doi: 10.1056/NEJMoa1606220
15. Miyauchi A, Ito Y, Oda H. Insights into the management of papillary microcarcinoma of the thyroid. *Thyroid* (2018) 28:23–31. doi: 10.1089/thy.2017.0227
16. Ito Y, Miyauchi A, Kudo T, Oda H, Yamamoto M, Sasai H, et al. Trends in the implementation of active surveillance for low-risk papillary thyroid microcarcinomas at Kuma Hospital: gradual increase and heterogeneity in the acceptance of this new management option. *Thyroid* (2018) 28:488–95. doi: 10.1089/thy.2017.0448
17. Leboulleux S, Tuttle RM, Pacini F, Schlumberger M. Papillary thyroid microcarcinoma: time to shift from surgery to active surveillance? *Lancet Diabetes Endocrinol.* (2016) 4:933–42. doi: 10.1016/s2213-8587(16)30180-2
18. Nickel B, Brito JP, Barratt A, Jordan S, Moynihan R, McCaffery K. Clinicians' views on management and terminology for papillary thyroid microcarcinoma: a qualitative study. *Thyroid* (2017) 27:661–71. doi: 10.1089/thy.2016.0483
19. Chow SM, Law SC, Chan JK, Au SK, Yau S, Lau WH. Papillary microcarcinoma of the thyroid-Prognostic significance of lymph node metastasis and multifocality. *Cancer* (2003) 98:31–40. doi: 10.1002/cncr.11442
20. Pyo JS, Sohn JH, Kang G. Detection of tumor multifocality is important for prediction of tumor recurrence in papillary thyroid microcarcinoma: a retrospective study and meta-analysis. *J Pathol Transl Med.* (2016) 50:278–86. doi: 10.4132/jptm.2016.03.29
21. Riss JC, Peyrottes I, Chamorey E, Haudebourg J, Sudaka A, Benisvy D, et al. Prognostic impact of tumour multifocality in thyroid papillary microcarcinoma based on a series of 160 cases. *Eur Ann Otorhinolaryngol Head Neck Dis.* (2012) 129:175–8. doi: 10.1016/j.anorl.2011.11.003

22. So YK, Kim MW, Son YI. Multifocality and bilaterality of papillary thyroid microcarcinoma. *Clin Exp Otorhinolaryngol.* (2015) 8:174–8. doi: 10.3342/ceo.2015.8.2.174
23. Zhao Q, Ming J, Liu C, Shi L, Xu X, Nie X, et al. Multifocality and total tumor diameter predict central neck lymph node metastases in papillary thyroid microcarcinoma. *Ann Surg Oncol.* (2013) 20:746–52. doi: 10.1245/s10434-012-2654-2
24. Diker-Cohen T, Hirsch D, Shimon I, Bachar G, Akirov A, Duskin-Bitan H, et al. Impact of minimal extra-thyroid extension in differentiated thyroid cancer: systematic review and meta-analysis. *J Clin Endocrinol Metab.* (2018) 103:2100–6. doi: 10.1210/jc.2018-00081
25. Haugen BR, Alexander EK, Bible KC, Doherty GM, Mandel SJ, Nikiforov YE, et al. 2015 American Thyroid Association Management Guidelines for adult patients with thyroid nodules and differentiated thyroid cancer: The American Thyroid Association Guidelines Task Force on thyroid nodules and differentiated thyroid cancer. *Thyroid* (2016) 26:1–133. doi: 10.1089/thy.2015.0020
26. Shimamoto K, Satake H, Sawaki A, Ishigaki T, Funahashi H. Preoperative staging of thyroid papillary carcinoma with ultrasonography. *Eur J Radiol.* (1998) 29:4–10. doi: 10.1016/S0720-048X(97)00184-8
27. Tomoda C, Uruno T, Takamura Y, Ito Y, Miya A, Kobayashi K, et al. Ultrasonography as a method of screening for tracheal invasion by papillary thyroid cancer. *Surg Today* (2005) 35:819–22. doi: 10.1007/s00595-005-3037-0
28. Kwak JY, Kim E-K, Youk JH, Kim MJ, Son EJ. Extrathyroid extension of well-differentiated papillary thyroid microcarcinoma on US. *Thyroid* (2008) 18:609–14. doi: 10.1089/thy.2007.0345
29. Kim H, Kim JA, Son EJ, Youk JH, Chung TS, Park CS, et al. Preoperative prediction of the extrathyroidal extension of papillary thyroid carcinoma with ultrasonography versus MRI: a retrospective cohort study. *Int J Surg.* (2014) 12:544–8. doi: 10.1016/j.ijsu.2014.03.003
30. Lee CY, Kim SJ, Ko KR, Chung KW, Lee JH. Predictive factors for extrathyroidal extension of papillary thyroid carcinoma based on preoperative sonography. *J Ultrasound Med.* (2014) 33:231–8. doi: 10.7863/ultra.33.2.231
31. Lee DY, Kwon TK, Sung MW, Kim KH, Hah JH. Prediction of extrathyroidal extension using ultrasonography and computed tomography. *Int J Endocrinol.* (2014) 2014:351058. doi: 10.1155/2014/351058
32. Moon SJ, Kim DW, Kim SJ, Ha TK, Park HK. Ultrasound assessment of degrees of extrathyroidal extension in papillary thyroid microcarcinoma. *Endocr Practice* (2014) 20:1037–43. doi: 10.4158/EP14016.OR
33. Kamaya A, Tahvildari AM, Patel BN, Willmann JK, Jeffrey RB, Desser TS. Sonographic detection of extracapsular extension in papillary thyroid cancer. *J Ultrasound Med.* (2015) 34:2225–30. doi: 10.7863/ultra.15.02006
34. King AD, Ahuja AT, To EW, Tse GM, Metreweli C. Staging papillary carcinoma of the thyroid: magnetic resonance imaging vs ultrasound of the neck. *Clin Radiol.* (2000) 55:222–6. doi: 10.1053/crad.1999.0373
35. Choi JS, Kim J, Kwak JY, Kim MJ, Chang HS, Kim EK. Preoperative staging of papillary thyroid carcinoma: comparison of ultrasound imaging and CT. *AJR Am J Roentgenol.* (2009) 193:871–8. doi: 10.2214/AJR.09.2386
36. Park JS, Son KR, Na DG, Kim E, Kim S. Performance of preoperative sonographic staging of papillary thyroid carcinoma based on the sixth edition of the AJCC/UICC TNM classification system. *AJR Am J Roentgenol.* (2009) 192:66–72. doi: 10.2214/AJR.07.3731
37. Choi JS, Chung WY, Kwak JY, Moon HJ, Kim MJ, Kim EK. Staging of papillary thyroid carcinoma with ultrasonography: performance in a large series. *Ann Surg Oncol.* (2011) 18:3572–8. doi: 10.1245/s10434-011-1783-3
38. Zaydfudim V, Feurer ID, Griffin MR, Phay JE. The impact of lymph node involvement on survival in patients with papillary and follicular thyroid carcinoma. *Surgery* (2008) 144:1070–7; discussion:7–8. doi: 10.1016/j.surg.2008.08.034
39. Pereira JA, Jimeno J, Miquel J, Iglesias M, Munne A, Sancho JJ, et al. Nodal yield, morbidity, and recurrence after central neck dissection for papillary thyroid carcinoma. *Surgery* (2005) 138:1095–100; discussion:100–1. doi: 10.1016/j.surg.2005.09.013
40. Sancho JJ, Lennard TW, Paunovic I, Triponez F, Sitges-Serra A. Prophylactic central neck disection in papillary thyroid cancer: a consensus report of the European Society of Endocrine Surgeons (ESES). *Langenbecks Arch Surg.* (2014) 399:155–63. doi: 10.1007/s00423-013-1152-8
41. Jeong HS, Baek CH, Son YI, Choi JY, Kim HJ, Ko YH, et al. Integrated 18F-FDG PET/CT for the initial evaluation of cervical node level of patients with papillary thyroid carcinoma: comparison with ultrasound and contrast-enhanced CT. *Clin Endocrinol.* (2006) 65:402–7. doi: 10.1111/j.1365-2265.2006.02612.x
42. Ahn JE, Lee JH, Yi JS, Shong YK, Hong SJ, Lee DH, et al. Diagnostic accuracy of CT and ultrasonography for evaluating metastatic cervical lymph nodes in patients with thyroid cancer. *World J Surg.* (2008) 32:1552–8. doi: 10.1007/s00268-008-9588-7
43. Kim E, Park JS, Son K-R, Kim JH, Jeon SJ. Preoperative diagnosis of cervical metastatic lymph nodes in papillary thyroid carcinoma: comparison of ultrasound, computed tomography, and combined ultrasound with computed tomography. *Thyroid* (2008) 18:411–8. doi: 10.1089/thy.2007.0269
44. Sugitani I, Fujimoto Y, Yamada K, Yamamoto N. Prospective outcomes of selective lymph node dissection for papillary thyroid carcinoma based on preoperative ultrasonography. *World J Surg.* (2008) 32:2494–502. doi: 10.1007/s00268-008-9711-9
45. Choi YJ, Yun JS, Kook SH, Jung EC, Park YL. Clinical and imaging assessment of cervical lymph node metastasis in papillary thyroid carcinomas. *World J Surg.* (2010) 34:1494–9. doi: 10.1007/s00268-010-0541-1
46. Lee K, Kawata R, Nishikawa S, Yoshimura K, Takenaka H. Diagnostic criteria of ultrasonographic examination for lateral node metastasis of papillary thyroid carcinoma. *Acta Otolaryngol.* (2010) 130:161–6. doi: 10.3109/00016480903015143
47. Hwang HS, Orloff LA. Efficacy of preoperative neck ultrasound in the detection of cervical lymph node metastasis from thyroid cancer. *Laryngoscope* (2011) 121:487–91. doi: 10.1002/lary.21227
48. Lee DW, Ji YB, Sung ES, Park JS, Lee YJ, Park DW, et al. Roles of ultrasonography and computed tomography in the surgical management of cervical lymph node metastases in papillary thyroid carcinoma. *Eur J Surg Oncol.* (2013) 39:191–6. doi: 10.1016/j.ejso.2012.07.119
49. Yoo YH, Kim JA, Son EJ, Youk JH, Kwak JY, Kim EK, et al. Sonographic findings predictive of central lymph node metastasis in patients with papillary thyroid carcinoma: influence of associated chronic lymphocytic thyroiditis on the diagnostic performance of sonography. *J Ultrasound Med.* (2013) 32:2145–51. doi: 10.7863/ultra.32.12.2145
50. Lesnik D, Cunnane ME, Zurakowski D, Acar GO, Ecevit C, Mace A, et al. Papillary thyroid carcinoma nodal surgery directed by a preoperative radiographic map utilizing CT scan and ultrasound in all primary and reoperative patients. *Head Neck* (2014) 36:191–202. doi: 10.1002/hed.23277
51. Lee YJ, Kim DW, Park HK, Kim DH, Jung SJ, Oh M, et al. Pre-operative ultrasound diagnosis of nodal metastasis in papillary thyroid carcinoma patients according to nodal compartment. *Ultrasound Med Biol.* (2015) 41:1294–300. doi: 10.1016/j.ultrasmedbio.2015.01.003
52. Khokhar MT, Day KM, Sangal RB, Ahmedli NN, Pisharodi LR, Beland MD, et al. Preoperative high-resolution ultrasound for the assessment of malignant central compartment lymph nodes in papillary thyroid cancer. *Thyroid* (2015) 25:1351–4. doi: 10.1089/thy.2015.0176
53. Wada N, Duh QY, Sugino K, Iwasaki H, Kameyama K. Lymph node metastasis from 259 papillary thyroid microcarcinomas: frequency, pattern of occurrence and recurrence, and optimal strategy for neck dissection. *Ann Surg.* (2003) 237:399–407. doi: 10.1097/01.SLA.0000055273.58908.19
54. Pelizzo MR, Boschin IM, Toniato A, Piotto A, Bernante P, Pagetta C, et al. Papillary thyroid microcarcinoma (PTMC): prognostic factors, management and outcome in 403 patients. *Eur J Surg Oncol.* (2006) 32:1144–8. doi: 10.1016/j.ejso.2006.07.001
55. Hay ID, Hutchinson ME, Gonzalez-Losada T, McIver B, Reinalda ME, Grant CS, et al. Papillary thyroid microcarcinoma: a study of 900 cases observed in a 60-year period. *Surgery* (2008) 144:980–7; discussion:7–8. doi: 10.1016/j.surg.2008.08.035
56. Besic N, Zgajnar J, Hocevar M, Petric R. Extent of thyroidectomy and lymphadenectomy in 254 patients with papillary thyroid microcarcinoma: a single-institution experience. *Ann Surg Oncol.* (2009) 16:920–8. doi: 10.1245/s10434-009-0332-9

57. Mercante G, Frasoldati A, Pedroni C, Formisano D, Renna L. Prognostic factors affecting neck lymph node recurrence and distant metastasis in papillary microcarcinoma of the thyroid: results of a study in 445 patients. *Thyroid* (2009) 19:707–16. doi: 10.1089/thy.2008.0270
58. So YK, Son YI, Hong SD, Seo MY, Baek CH, Jeong HS, et al. Subclinical lymph node metastasis in papillary thyroid microcarcinoma: a study of 551 resections. *Surgery* (2010) 148:526–31. doi: 10.1016/j.surg.2010.01.003
59. Moon HJ, Kim EK, Chung WY, Yoon JH, Kwak JY. Minimal extrathyroidal extension in patients with papillary thyroid microcarcinoma: is it a real prognostic factor? *Ann Surg Oncol.* (2011) 18:1916–23. doi: 10.1245/s10434-011-1556-z
60. Londero SC, Krogdahl A, Bastholt L, Overgaard J, Trolle W, Pedersen HB, et al. Papillary thyroid microcarcinoma in Denmark 1996-2008: a national study of epidemiology and clinical significance. *Thyroid* (2013) 23:1159–64. doi: 10.1089/thy.2012.0595
61. Lee J, Park JH, Lee CR, Chung WY, Park CS. Long-term outcomes of total thyroidectomy versus thyroid lobectomy for papillary thyroid microcarcinoma: comparative analysis after propensity score matching. *Thyroid* (2013) 23:1408–15. doi: 10.1089/thy.2012.0463
62. Gschwandtner E, Klatte T, Swietek N, Bures C, Kober F, Ott J, et al. Increase of papillary thyroid microcarcinoma and a plea for restrictive treatment: a retrospective study of 1,391 prospective documented patients. *Surgery* (2016) 159:503–11. doi: 10.1016/j.surg.2015.06.015
63. Kim SK, Park I, Woo JW, Lee JH, Choe JH, Kim JH, et al. Predictive Factors for Lymph Node Metastasis in Papillary Thyroid Microcarcinoma. *Ann Surg Oncol.* (2016) 23:2866–73. doi: 10.1245/s10434-016-5225-0
64. Cecoli F, Ceresola EM, Altrinetti V, Cabria M, Cappagli M, Montepagani A, et al. Therapeutic strategies and clinical outcome in papillary thyroid microcarcinoma: a multicenter observational study. *Eur Thyroid J.* (2016) 5:180–6. doi: 10.1159/000446746
65. Kim SK, Park I, Woo JW, Lee JH, Choe JH, Kim JH, et al. Total thyroidectomy versus lobectomy in conventional papillary thyroid microcarcinoma: analysis of 8,676 patients at a single institution. *Surgery* (2017) 161:485–92. doi: 10.1016/j.surg.2016.07.037
66. Yeh MW, Bauer AJ, Bernet VA, Ferris RL, Loevner LA, Mandel SJ, et al. American Thyroid Association statement on preoperative imaging for thyroid cancer surgery. *Thyroid* (2015) 25:3–14. doi: 10.1089/thy.2014.0096
67. Monteiro R, Han A, Etiwy M, Swearingen A, Krishnamurthy V, Jin J, et al. Importance of surgeon-performed ultrasound in the preoperative nodal assessment of patients with potential thyroid malignancy. *Surgery* (2018) 163:112–7. doi: 10.1016/j.surg.2017.10.005
68. Kumbhar SS, O'Malley RB, Robinson TJ, Maximin S, Lalwani N. Why thyroid surgeons are frustrated with radiologists: lessons learned from pre- and postoperative US. *Radiographics* (2016) 36:2141–53. doi: 10.1148/rg.2016150250
69. Carneiro-Pla D, Amin S. Comparison between preconsultation ultrasonography and office surgeon-performed ultrasound in patients with thyroid cancer. *World J Surg.* (2014) 38:622–7. doi: 10.1007/s00268-013-2251-y
70. Oltmann SC, Schneider DF, Chen H, Sippel RS. All thyroid ultrasound evaluations are not equal: sonographers specialized in thyroid cancer correctly label clinical N0 disease in well differentiated thyroid cancer. *Ann Surg Oncol.* (2015) 22:422–8. doi: 10.1245/s10434-014-4089-4
71. Sugitani I, Toda K, Yamada K, Yamamoto N, Ikenaga M, Fujimoto Y. Three distinctly different kinds of papillary thyroid microcarcinoma should be recognized: our treatment strategies and outcomes. *World J Surg.* (2010) 34:1222–31. doi: 10.1007/s00268-009-0359-x
72. Ito Y, Miyauchi A, Kihara M, Higashiyama T, Kobayashi K, Miya A. Patient age is significantly related to the progression of papillary microcarcinoma of the thyroid under observation. *Thyroid* (2014) 24:27–34. doi: 10.1089/thy.2013.0367
73. Jeon MJ, Kim WG, Choi YM, Kwon H, Lee YM, Sung TY, et al. Features Predictive of Distant Metastasis in Papillary Thyroid Microcarcinomas. *Thyroid* (2016) 26:161–8. doi: 10.1089/thy.2015.0375
74. Xu B, Ibrahimpasic T, Wang L, Sabra MM, Migliacci JC, Tuttle RM, et al. Clinicopathologic features of fatal non-anaplastic follicular cell-derived thyroid carcinomas. *Thyroid* (2016) 26:1588–97. doi: 10.1089/thy.2016.0247
75. Ito Y, Uruno T, Nakano K, Takamura Y, Miya A. An observation trial without surgical treatment in patients with papillary microcarcinoma of the thyroid. *Thyroid* (2003) 13:381–7. doi: 10.1089/105072503321669875
76. Ito Y, Miyauchi A, Inoue H, Fukushima M, Kihara M, Higashiyama T, et al. An observational trial for papillary thyroid microcarcinoma in Japanese patients. *World J Surg.* (2010) 34:28–35. doi: 10.1007/s00268-009-0303-0
77. Ghajar CM, Bissell MJ. Pathways of parallel progression Metastasis. *Nature* (2016) 540:528–9. doi: 10.1038/nature21104
78. Kim H, Kim TH, Choe JH, Kim JH, Kim JS, Oh YL, et al. Patterns of initial recurrence in completely resected papillary thyroid carcinoma. *Thyroid* (2017) 27:908–14. doi: 10.1089/thy.2016.0648
79. Mehanna H, Al-Maqbili T, Carter B, Martin E, Campain N, Watkinson J, et al. Differences in the recurrence and mortality outcomes rates of incidental and nonincidental papillary thyroid microcarcinoma: a systematic review and meta-analysis of 21 329 person-years of follow-up. *J Clin Endocrinol Metab.* (2014) 99:2834–43. doi: 10.1210/jc.2013-2118
80. Sun W, Lan X, Zhang H, Dong W, Wang Z, He L, et al. Risk factors for central lymph node metastasis in CN0 papillary thyroid carcinoma: a systematic review and meta-analysis. *PLoS ONE* (2015) 10:e0139021. doi: 10.1371/journal.pone.0139021
81. McAllister SS, Weinberg RA. The tumour-induced systemic environment as a critical regulator of cancer progression and metastasis. *Nat Cell Biol.* (2014) 16:717–27. doi: 10.1038/ncb3015
82. Bissell MJ, Hines WC. Why don't we get more cancer? A proposed role of the microenvironment in restraining cancer progression. *Nat Med.* (2011) 17:320–9. doi: 10.1038/nm.2328
83. Valastyan S, Weinberg RA. Tumor metastasis: molecular insights and evolving paradigms. *Cell* (2011) 147:275–92. doi: 10.1016/j.cell.2011.09.024
84. Wirtz D, Konstantopoulos K, Searson PC. The physics of cancer: the role of physical interactions and mechanical forces in metastasis. *Nat Rev Cancer* (2011) 11:512–22. doi: 10.1038/nrc3080
85. Oda H, Miyauchi A, Ito Y, Yoshioka K, Nakayama A, Sasai H, et al. Incidences of unfavorable events in the management of low-risk papillary microcarcinoma of the thyroid by active surveillance versus immediate surgery. *Thyroid* (2016) 26:150–5. doi: 10.1089/thy.2015.0313
86. Durante C, Attard M, Torlontano M, Ronga G, Monzani F, Costante G, et al. Identification and optimal postsurgical follow-up of patients with very low-risk papillary thyroid microcarcinomas. *J Clin Endocrinol Metab.* (2010) 95:4882–8. doi: 10.1210/jc.2010-0762
87. Miyauchi A, Kudo T, Ito Y, Oda H, Sasai H, Higashiyama T, et al. Estimation of the lifetime probability of disease progression of papillary microcarcinoma of the thyroid during active surveillance. *Surgery* (2018) 163:48–52. doi: 10.1016/j.surg.2017.03.028
88. Siddiqui S, White MG, Antic T, Grogan RH, Angelos P, Kaplan EL, et al. Clinical and pathologic predictors of lymph node metastasis and recurrence in papillary thyroid microcarcinoma. *Thyroid* (2016) 26:807–15. doi: 10.1089/thy.2015.0429
89. Tomoda C, Sugino K, Matsuzu K, Uruno T, Ohkuwa K, Kitagawa W, et al. Cervical lymph node metastases after thyroidectomy for papillary thyroid carcinoma usually remain stable for years. *Thyroid* (2016) 26:1706–11. doi: 10.1089/thy.2016.0225
90. Emanuel EJ, Wendler D, Grady C. What makes clinical research ethical? *JAMA* (2000) 283:2701–11. doi: 10.1001/jama.283.20.2701
91. Stack BC Jr, Angelos P. The ethics of disclosure and counseling of patients with thyroid cancer. *JAMA Otolaryngol Head Neck Surg* (2015) 141:957–8. doi: 10.1001/jamaoto.2015.2419
92. Morris LG, Wong RJ, Tuttle RM. Ethical considerations when counseling patients with thyroid cancer about surgery vs observation. *JAMA Otolaryngol Head Neck Surg.* (2016) 142:406–7. doi: 10.1001/jamaoto.2016.0038
93. Leboulleux S, Tuttle RM, Pacini F, Schlumberger M. Papillary thyroid microcarcinoma and active surveillance – Authors' reply. *Lancet Diabetes Endocrinol.* (2016) 4:976–7. doi: 10.1016/s2213-8587(16)30326-6
94. Kim SC, Kim JH, Choi SH, Yun TJ, Wi JY, Kim SA, et al. Off-site evaluation of three-dimensional ultrasound for the diagnosis of thyroid nodules: comparison with two-dimensional ultrasound. *Eur Radiol.* (2016) 26:3353–60. doi: 10.1007/s00330-015-4193-2
95. Yi YS, Kim SS, Kim WJ, Bae MJ, Kang JH, Choi BG, et al. Comparison of two- and three-dimensional sonography for the prediction of the extrathyroidal

extension of papillary thyroid carcinomas. *Korean J Intern Med.* (2016) 31:313–22. doi: 10.3904/kjim.2014.363

96. Slapa RZ, Jakubowski WS, Slowinska-Srzednicka J, Szopinski KT. Advantages and disadvantages of 3D ultrasound of thyroid nodules including thin slice volume rendering. *Thyroid Res.* (2011) 4:1. doi: 10.1186/1756-6614-4-1
97. Park YJ, Kim JA, Son EJ, Youk JH, Park CS. Quantitative shear wave elastography as a prognostic implication of papillary thyroid carcinoma (PTC): elasticity index can predict extrathyroidal extension (ETE). *Ann Surg Oncol.* (2013) 20:2765–71. doi: 10.1245/s10434-013-2927-4
98. Jung WS, Kim JA, Son EJ, Youk JH, Park CS. Shear wave elastography in evaluation of cervical lymph node metastasis of papillary thyroid carcinoma: elasticity index as a prognostic implication. *Ann Surg Oncol.* (2015) 22:111–6. doi: 10.1245/s10434-014-3627-4
99. Azizi G, Keller JM, Mayo ML, Piper K, Puett D, Earp KM, et al. Shear wave elastography and cervical lymph nodes: predicting malignancy. *Ultrasound Med Biol.* (2016) 42:1273–81. doi: 10.1016/j.ultrasmedbio.2016.01.012
100. Xu JM, Xu XH, Xu HX, Zhang YF, Guo LH, Liu LN, et al. Prediction of cervical lymph node metastasis in patients with papillary thyroid cancer using combined conventional ultrasound, strain elastography, and acoustic radiation force impulse (ARFI) elastography. *Eur Radiol.* (2016) 26:2611–22. doi: 10.1007/s00330-015-4088-2
101. Liu X, Ouyang D, Li H, Zhang R, Lv Y. Papillary thyroid cancer: dual-energy spectral CT quantitative parameters for preoperative diagnosis of metastasis to the cervical lymph nodes. *Radiology* (2015) 275:167–76. doi: 10.1148/radiol.14140481
102. Hao Y, Pan C, Chen W, Li T, Zhu W, Qi J. Differentiation between malignant and benign thyroid nodules and stratification of papillary thyroid cancer with aggressive histological features: Whole-lesion diffusion-weighted imaging histogram analysis. *J Magn Reson Imaging* (2016) 44:1546–55. doi: 10.1002/jmri.25290
103. Meyer HJ, Schob S, Hohn AK, Surov A. MRI texture analysis reflects histopathology parameters in thyroid cancer - a first preliminary study. *Transl Oncol.* (2017) 10:911–6. doi: 10.1016/j.tranon.2017.09.003
104. Schob S, Meyer HJ, Dieckow J, Pervinder B, Pazaitis N, Hohn AK, et al. Histogram analysis of diffusion weighted imaging at 3T is useful for prediction of lymphatic metastatic spread, proliferative activity, and cellularity in thyroid cancer. *Int J Mol Sci.* (2017) 18:E821. doi: 10.3390/ijms18040821
105. Hirokawa M, Kudo T, Ota H, Suzuki A, Miyauchi A. Pathological characteristics of low-risk papillary thyroid microcarcinoma with progression during active surveillance. *Endocr J.* (2016) 63:805–10. doi: 10.1507/endocrj.EJ16-0097
106. Xing M. BRAF mutation in thyroid cancer. *Endocr Relat Cancer* (2005) 12:245–62. doi: 10.1677/erc.1.0978
107. Xing M. BRAF mutation in papillary thyroid cancer: pathogenic role, molecular bases, and clinical implications. *Endocr Rev.* (2007) 28:742–62. doi: 10.1210/er.2007-0007
108. Hou P, Liu D, Xing M. Genome-wide alterations in gene methylation by the BRAF V600E mutation in papillary thyroid cancer cells. *Endocr Relat Cancer* (2011) 18:687–97. doi: 10.1530/ERC-11-0212
109. Hu S, Liu D, Tufano RP, Carson KA, Rosenbaum E, Cohen Y, et al. Association of aberrant methylation of tumor suppressor genes with tumor aggressiveness and BRAF mutation in papillary thyroid cancer. *Int J Cancer* (2006) 119:2322–9. doi: 10.1002/ijc.22110
110. Li F, Chen G, Sheng C, Gusdon AM, Huang Y, Lv Z, et al. BRAFV600E mutation in papillary thyroid microcarcinoma: a meta-analysis. *Endocr Relat Cancer* (2015) 22:159–68. doi: 10.1530/ERC-14-0531
111. Lee DY, Hwang SM, An JH, Son KR, Baek SK, Kim SG, et al. Predicting Extrathyroidal Extension in Patients With Papillary Thyroid Microcarcinoma According to a BRAF Mutation. *Clin Exp Otorhinolaryngol.* (2017) 10:174–80. doi: 10.21053/ceo.2015.01655
112. Chen Y, Sadow PM, Suh H, Lee KE, Choi JY, Suh YJ, et al. BRAF(V600E) Is correlated with recurrence of papillary thyroid microcarcinoma: a systematic review, multi-institutional primary data analysis, and meta-analysis. *Thyroid* (2016) 26:248–55. doi: 10.1089/thy.2015.0391
113. Niemeier LA, Kuffner Akatsu H, Song C, Carty SE, Hodak SP, Yip L, et al. A combined molecular-pathologic score improves risk stratification of thyroid papillary microcarcinoma. *Cancer* (2012) 118:2069–77. doi: 10.1002/cncr.26425
114. Yabuta T, Matsuse M, Hirokawa M, Yamashita S, Mitsutake N, Miyauchi A. TERT promoter mutations were not found in papillary thyroid microcarcinomas that showed disease progression on active surveillance. *Thyroid* (2017) 27:1206–7. doi: 10.1089/thy.2016.0645
115. Li D, Gao M, Li X, Xing M. Molecular aberrance in papillary thyroid microcarcinoma bearing high aggressiveness: identifying a "Tibetan Mastiff Dog" from puppies. *J Cell Biochem.* (2016) 117:1491–6. doi: 10.1002/jcb.25506
116. Heidenreich B, Kumar R. TERT promoter mutations in telomere biology. *Mutat Res.* (2017) 771:15–31. doi: 10.1016/j.mrrev.2016.11.002
117. Pestana A, Vinagre J, Sobrinho-Simoes M, Soares P. TERT biology and function in cancer: beyond immortalisation. *J Mol Endocrinol.* (2017) 58:R129–46. doi: 10.1530/JME-16-0195
118. Liu X, Bishop J, Shan Y, Pai S, Liu D, Murugan AK, et al. Highly prevalent TERT promoter mutations in aggressive thyroid cancers. *Endocr Relat Cancer* (2013) 20:603–10. doi: 10.1530/ERC-13-0210
119. Kim TH, Kim YE, Ahn S, Kim JY, Ki CS, Oh YL, et al. TERT promoter mutations and long-term survival in patients with thyroid cancer. *Endocr Relat Cancer* (2016) 23:813–23. doi: 10.1530/ERC-16-0219
120. Kim TH, Ki CS, Kim HS, Kim K, Choe JH, Kim JH, et al. refining dynamic risk stratification and prognostic groups for differentiated thyroid cancer with TERT promoter mutations. *J Clin Endocrinol Metab.* (2017) 102:1757–64. doi: 10.1210/jc.2016-3434
121. Liu C, Liu Z, Chen T, Zeng W, Guo Y, Huang T. TERT promoter mutation and its association with clinicopathological features and prognosis of papillary thyroid cancer: a meta-analysis. *Sci Rep.* (2016) 6:36990. doi: 10.1038/srep36990
122. Yin DT, Yu K, Lu RQ, Li X, Xu J, Lei M, et al. Clinicopathological significance of TERT promoter mutation in papillary thyroid carcinomas: a systematic review and meta-analysis. *Clin Endocrinol.* (2016) 85:299–305. doi: 10.1111/cen.13017
123. Moon S, Song YS, Kim YA, Lim JA, Cho SW, Moon JH, et al. Effects of Coexistent BRAF(V600E) and TERT promoter mutations on poor clinical outcomes in papillary thyroid cancer: a meta-analysis. *Thyroid* (2017) 27:651–60. doi: 10.1089/thy.2016.0350
124. Liu R, Bishop J, Zhu G, Zhang T, Ladenson PW, Xing M. Mortality risk stratification by combining BRAF V600E and TERT promoter mutations in papillary thyroid cancer: genetic duet of BRAF and TERT promoter mutations in thyroid cancer mortality. *JAMA Oncol.* (2017) 3:202–208. doi: 10.1001/jamaoncol.2016.3288
125. Liu R, Zhang T, Zhu G, Xing M. Regulation of mutant TERT by BRAF V600E/MAP kinase pathway through FOS/GABP in human cancer. *Nat Commun.* (2018) 9:579. doi: 10.1038/s41467-018-03033-1
126. de Biase D, Gandolfi G, Ragazzi M, Eszlinger M, Sancisi V, Gugnoni M, et al. TERT promoter mutations in papillary thyroid microcarcinomas. *Thyroid* (2015) 25:1013–9. doi: 10.1089/thy.2015.0101
127. Boufraqech M, Klubo-Gwiezdzinska J, Kebebew E. MicroRNAs in the thyroid. *Best Pract Res Clin Endocrinol Metab.* (2016) 30:603–19. doi: 10.1016/j.beem.2016.10.001
128. Zhang R, Hardin H, Chen J, Guo Z, Lloyd RV. Non-coding RNAs in thyroid cancer. *Endocr Pathol.* (2016) 27:12–20. doi: 10.1007/s12022-016-9417-8
129. Visone R, Russo L, Pallante P, De Martino I, Ferraro A, Leone V, et al. MicroRNAs (miR)-221 and miR-222, both overexpressed in human thyroid papillary carcinomas, regulate p27Kip1 protein levels and cell cycle. *Endocr Relat Cancer* (2007) 14:791–8. doi: 10.1677/ERC-07-0129
130. Fuziwara CS, Kimura ET. MicroRNA deregulation in anaplastic thyroid cancer biology. *Int J Endocrinol.* (2014) 2014:743450. doi: 10.1155/2014/743450
131. Chruscik A, Lam AK. Clinical pathological impacts of microRNAs in papillary thyroid carcinoma: a crucial review. *Exp Mol Pathol.* (2015) 99:393–8. doi: 10.1016/j.yexmp.2015.08.013
132. Liang L, Zheng X, Hu M, Cui Y, Zhong Q, Wang S, et al. MiRNA-221/222 in thyroid cancer: a meta-analysis. *Clin Chim Acta* (2018) 484:284–92. doi: 10.1016/j.cca.2018.06.012
133. Lee JC, Zhao JT, Clifton-Bligh RJ, Gill A, Gundara JS, Ip JC, et al. MicroRNA-222 and microRNA-146b are tissue and circulating biomarkers

of recurrent papillary thyroid cancer. *Cancer* (2013) 119:4358–65. doi: 10.1002/cncr.28254
134. Oridate N, Lotan D, Xu XC, Hong WK, Lotan R. Differential induction of apoptosis by all-trans-retinoic acid and N-(4-hydroxyphenyl)retinamide in human head and neck squamous cell carcinoma cell lines. *Clin Cancer Res.* (1996) 2:855–63.
135. Simon D, Korber C, Krausch M, Segering J, Groth P, Gorges R, et al. Clinical impact of retinoids in redifferentiation therapy of advanced thyroid cancer: final results of a pilot study. *Eur J Nucl Med Mol Imaging* (2002) 29:775–82. doi: 10.1007/s00259-001-0737-6
136. Xiong Y, Kotian S, Zeiger MA, Zhang L, Kebebew E. miR-126-3p inhibits thyroid cancer cell growth and metastasis, and is associated with aggressive thyroid cancer. *PLoS One* (2015) 10:e0130496. doi: 10.1371/journal.pone.0130496
137. Yip L, Kelly L, Shuai Y, Armstrong MJ, Nikiforov YE, Carty SE, et al. MicroRNA signature distinguishes the degree of aggressiveness of papillary thyroid carcinoma. *Ann Surg Oncol.* (2011) 18:2035–41. doi: 10.1245/s10434-011-1733-0
138. Wang Z, Zhang H, He L, Dong W, Li J, Shan Z, et al. Association between the expression of four upregulated miRNAs and extrathyroidal invasion in papillary thyroid carcinoma. *Onco Targets Ther.* (2013) 6:281–7. doi: 10.2147/OTT.S43014
139. Sun M, Fang S, Li W, Li C, Wang L. Associations of miR-146a and miR-146b expression and clinical characteristics in papillary thyroid carcinoma. *Cancer Biomark.* (2015) 15:33–40. doi: 10.3233/CBM-140431
140. Qiu Z, Li H, Wang J, Sun C. miR-146a and miR-146b in the diagnosis and prognosis of papillary thyroid carcinoma. *Oncol Rep.* (2017) 38:2735–40. doi: 10.3892/or.2017.5994
141. Zhang X, Li D, Li M, Ye M, Ding L, Cai H, et al. MicroRNA-146a targets PRKCE to modulate papillary thyroid tumor development. *Int J Cancer* (2014) 134:257–67. doi: 10.1002/ijc.28141
142. Czajka AA, Wojcicka A, Kubiak A, Kotlarek M, Bakula-Zalewska E, Koperski L, et al. Family of microRNA-146 regulates RARbeta in papillary thyroid carcinoma. *PLoS ONE* (2016) 11:e0151968. doi: 10.1371/journal.pone.0151968
143. He H, Jazdzewski K, Li W, Liyanarachchi S, Nagy R, Volinia S, et al. The role of microRNA genes in papillary thyroid carcinoma. *Proc Natl Acad Sci USA.* (2005) 102:19075–80. doi: 10.1073/pnas.0509603102
144. Chou CK, Chen RF, Chou FF, Chang HW, Chen YJ. miR-146b is highly expressed in adult papillary thyroid carcinomas with high risk features including extrathyroidal invasion and the BRAF(V600E) mutation. *Thyroid* (2010) 20:489–94. doi: 10.1089/thy.2009.0027
145. Yang Z, Yuan Z, Fan Y, Deng X, Zheng Q. Integrated analyses of microRNA and mRNA expression profiles in aggressive papillary thyroid carcinoma. *Mol Med Rep.* (2013) 8:1353–8. doi: 10.3892/mmr.2013.1699
146. Geraldo MV, Yamashita AS, Kimura ET. MicroRNA miR-146b-5p regulates signal transduction of TGF-beta by repressing SMAD4 in thyroid cancer. *Oncogene* (2012) 31:1910–22. doi: 10.1038/onc.2011.381
147. Deng X, Wu B, Xiao K, Kang J, Xie J, Zhang X, et al. MiR-146b-5p promotes metastasis and induces epithelial-mesenchymal transition in thyroid cancer by targeting ZNRF3. *Cell Physiol Biochem.* (2015) 35:71–82. doi: 10.1159/000369676
148. Chou CK, Chi SY, Huang CH, Chou FF, Huang CC, Liu RT, et al. IRAK1, a target of miR-146b, reduces cell aggressiveness of human papillary thyroid carcinoma. *J Clin Endocrinol Metab.* (2016) 101:4357–66. doi: 10.1210/jc.2016-2276
149. Peng Y, Li C, Luo DC, Ding JW, Zhang W, Pan G. Expression profile and clinical significance of microRNAs in papillary thyroid carcinoma. *Molecules* (2014) 19:11586–99. doi: 10.3390/molecules190811586
150. Diao Y, Fu H, Wang Q. MiR-221 Exacerbate cell proliferation and invasion by targeting TIMP3 in papillary thyroid carcinoma. *Am J Ther.* (2017) 24:e317-e28. doi: 10.1097/MJT.0000000000000420
151. Huang Y, Yu S, Cao S, Yin Y, Hong S, Guan H, et al. MicroRNA-222 promotes invasion and metastasis of papillary thyroid cancer through targeting protein phosphatase 2 regulatory subunit B alpha expression. *Thyroid* (2018) 28:1162–73. doi: 10.1089/thy.2017.0665
152. Wang Z, Zhang H, Zhang P, Li J, Shan Z, Teng W. Upregulation of miR-2861 and miR-451 expression in papillary thyroid carcinoma with lymph node metastasis. *Med Oncol.* (2013) 30:577. doi: 10.1007/s12032-013-0577-9
153. Liu J, Li Q, Li R, Ren P, Dong S. MicroRNA-363-3p inhibits papillary thyroid carcinoma progression by targeting PIK3CA. *Am J Cancer Res.* (2017) 7:148–58.
154. Wang R, Ma Q, Ji L, Yao Y, Ma M, Wen Q. miR-622 suppresses tumor formation by directly targeting VEGFA in papillary thyroid carcinoma. *Onco Targets Ther.* (2018) 11:1501–9. doi: 10.2147/OTT.S156810
155. Rosignolo F, Memeo L, Monzani F, Colarossi C, Pecce V, Verrienti A, et al. MicroRNA-based molecular classification of papillary thyroid carcinoma. *Int J Oncol.* (2017) 50:1767–77. doi: 10.3892/ijo.2017.3960
156. Pacifico F, Crescenzi E, Mellone S, Iannetti A, Porrino N, Liguoro D, et al. Nuclear factor-{kappa}B contributes to anaplastic thyroid carcinomas through up-regulation of miR-146a. *J Clin Endocrinol Metab.* (2010) 95:1421–30. doi: 10.1210/jc.2009-1128
157. Bommarito A, Richiusa P, Carissimi E, Pizzolanti G, Rodolico V, Zito G, et al. BRAFV600E mutation, TIMP-1 upregulation, and NF-kappaB activation: closing the loop on the papillary thyroid cancer trilogy. *Endocr Relat Cancer* (2011) 18:669–85. doi: 10.1530/ERC-11-0076
158. Nixon AM, Provatopoulou X, Kalogera E, Zografos GN, Gounaris A. Circulating thyroid cancer biomarkers: Current limitations and future prospects. *Clin Endocrinol.* (2017) 87:117–26. doi: 10.1111/cen.13369
159. Yu S, Liu Y, Wang J, Guo Z, Zhang Q, Yu F, et al. Circulating microRNA profiles as potential biomarkers for diagnosis of papillary thyroid carcinoma. *J Clin Endocrinol Metab.* (2012) 97:2084–92. doi: 10.1210/jc.2011-3059
160. Angell TE, Lechner MG, Smith AM, Martin SE, Groshen SG, Maceri DR, et al. Circulating myeloid-derived suppressor cells predict differentiated thyroid cancer diagnosis and extent. *Thyroid* (2016) 26:381–9. doi: 10.1089/thy.2015.0289
161. Lubitz CC, Parangi S, Holm TM, Bernasconi MJ, Schalck AP, Suh H, et al. Detection of circulating BRAF(V600E) in patients with papillary thyroid carcinoma. *J Mol Diagn.* (2016) 18:100–8. doi: 10.1016/j.jmoldx.2015.08.003
162. Condello V, Macerola E, Ugolini C, De Napoli L, Romei C, Materazzi G, et al. Analysis of circulating tumor DNA does not improve the clinical management of patients with locally advanced and metastatic papillary thyroid carcinoma. *Head Neck* (2018). doi: 10.1002/hed.25155
163. Sui F, Ji M, Hou P. Long non-coding RNAs in thyroid cancer: Biological functions and clinical significance. *Mol Cell Endocrinol.* (2018) 469:11–22. doi: 10.1016/j.mce.2017.07.020
164. Kim D, Lee WK, Jeong S, Seol MY, Kim H, Kim KS, et al. Upregulation of long noncoding RNA LOC100507661 promotes tumor aggressiveness in thyroid cancer. *Mol Cell Endocrinol.* (2016) 431:36–45. doi: 10.1016/j.mce.2016.05.002
165. Li H-m. Overexpression of LncRNA HOTAIR is associated with poor prognosis in thyroid carcinoma: a study based on TCGA and GEO data. *Hormone Metab Res.* (2017) 49:388–99. doi: 10.1055/s-0043-103346
166. Li T, Yang XD, Ye CX, Shen ZL, Yang Y, Wang B, et al. Long noncoding RNA HIT000218960 promotes papillary thyroid cancer oncogenesis and tumor progression by upregulating the expression of high mobility group AT-hook 2 (HMGA2) gene. *Cell Cycle* (2017) 16:224–31. doi: 10.1080/15384101.2016.1261768
167. Ma B, Liao T, Wen D, Dong C, Zhou L, Yang S, et al. Long intergenic non-coding RNA 271 is predictive of a poorer prognosis of papillary thyroid cancer. *Sci Rep.* (2016) 6:36973. doi: 10.1038/srep36973
168. Fu XM, Guo W, Li N, Liu HZ, Liu J. The expression and function of long noncoding RNA lncRNA-ATB in papillary thyroid cancer. *Eur Rev Med Pharmacol Sci.* (2017) 21:3239–46.
169. Zhou T, Zhong M, Zhang S, Wang Z, Xie R, Xiong C, et al. LncRNA CASC2 expression is down- regulated in papillary thyroid cancer and promotes cell invasion by affecting EMT pathway. *Cancer Biomark* (2018) 23:185–91. doi: 10.3233/CBM-181198
170. Chen C, Zhou L, Wang H, Chen J, Li W, Liu W, et al. Long noncoding RNA CNALPTC1 promotes cell proliferation and migration of papillary thyroid cancer via sponging miR-30 family. *Am J Cancer Res.* (2018) 8:192–206.
171. Zhang D, Liu X, Wei B, Qiao G, Jiang T, Chen Z. Plasma lncRNA GAS8-AS1 as a potential biomarker of papillary thyroid carcinoma in chinese patients. *Int J Endocrinol.* (2017) 2017:2645904. doi: 10.1155/2017/2645904

172. Xu K, Feng Y. HOXD-AS1 is a predictor of clinical progression and functions as an oncogenic lncRNAs in papillary thyroid cancer. *J Cell Biochem* (2018). doi: 10.1002/jcb.27809. [Epub ahead of print].
173. Wu X, Yan Y, Li H, Ji N, Yu T, Huang Y, et al. DNA copy number gain-mediated lncRNA LINC01061 upregulation predicts poor prognosis and promotes papillary thyroid cancer progression. *Biochem Biophys Res Commun.* (2018) 503:1247–53. doi: 10.1016/j.bbrc.2018.07.032
174. Liu J, Dong H, Yang Y, Qian Y, Liu J, Li Z, et al. Upregulation of long noncoding RNA MALAT1 in papillary thyroid cancer and its diagnostic value. *Future Oncol.* (2018). doi: 10.2217/fon-2018-0416. [Epub ahead of print].
175. Wang C, Yan G, Zhang Y, Jia X, Bu P. Long non-coding RNA MEG3 suppresses migration and invasion of thyroid carcinoma by targeting of Rac1. *Neoplasma* (2015) 62:541–9. doi: 10.4149/neo_2015_065
176. Lan X, Sun W, Zhang P, He L, Dong W, Wang Z, et al. Downregulation of long noncoding RNA NONHSAT037832 in papillary thyroid carcinoma and its clinical significance. *Tumour Biol.* (2016) 37:6117–23. doi: 10.1007/s13277-015-4461-4
177. Xia S, Wang C, Ni X, Ni Z, Dong Y. NONHSAT076754 aids ultrasonography in predicting lymph node metastasis and promotes migration and invasion of papillary thyroid cancer cells. *Oncotarget* (2017) 8:2293–306. doi: 10.18632/oncotarget.13725
178. Ding J, Wang F, Xiang T, Qiao M. Expression and function of long noncoding RNA NONHSAT129183 in papillary thyroid cancer. *Oncol Res.* (2018) 26:1047–53. doi: 10.3727/096504018X15152037713570
179. Wang Q, Yang H, Wu L, Yao J, Meng X, Jiang H, et al. Identification of specific long non-coding RNA expression: profile and analysis of association with clinicopathologic characteristics and BRAF mutation in papillary thyroid cancer. *Thyroid* (2016) 26:1719–32. doi: 10.1089/thy.2016.0024
180. Sun W, Lan X, Wang Z, Dong W, He L, Zhang T, et al. Overexpression of long non-coding RNA NR_036575.1 contributes to the proliferation and migration of papillary thyroid cancer. *Med Oncol.* (2016) 33:102. doi: 10.1007/s12032-016-0816-y
181. Feng K, Liu Y, Xu LJ, Zhao LF, Jia CW, Xu MY. Long noncoding RNA PVT1 enhances the viability and invasion of papillary thyroid carcinoma cells by functioning as ceRNA of microRNA-30a through mediating expression of insulin like growth factor 1 receptor. *Biomed Pharmacother.* (2018) 104:686–98. doi: 10.1016/j.biopha.2018.05.078
182. Du Y, Xia W, Zhang J, Wan D, Yang Z, Li X. Comprehensive analysis of long noncoding RNA-mRNA co-expression patterns in thyroid cancer. *Mol Biosyst.* (2017) 13:2107–15. doi: 10.1039/c7mb00375g
183. Liyanarachchi S, Li W, Yan P, Bundschuh R, Brock P, Senter L, et al. Genome-wide expression screening discloses long noncoding RNAs involved in thyroid carcinogenesis. *J Clin Endocrinol Metab.* (2016) 101:4005–13. doi: 10.1210/jc.2016-1991
184. Asa SL, Ezzat S. The epigenetic landscape of differentiated thyroid cancer. *Mol Cell Endocrinol.* (2018) 469:3–10. doi: 10.1016/j.mce.2017.07.012

Conflict of Interest Statement: The authors declare that the research was conducted in the absence of any commercial or financial relationships that could be construed as a potential conflict of interest.

frontiers in Endocrinology

ORIGINAL RESEARCH
published: 16 January 2019
doi: 10.3389/fendo.2018.00811

Variations in CD14 Gene Are Associated With Autoimmune Thyroid Diseases in the Chinese Population

Xi Jia[1], *Bing Wang*[1], *Qiuming Yao*[1], *Qian Li*[1] *and Jinan Zhang*[2]*

[1] *Department of Endocrinology, Jinshan Hospital of Fudan University, Shanghai, China,* [2] *Department of Endocrinology, Shanghai University of Medicine and Health Sciences Affiliated Zhoupu Hospital, Shanghai, China*

Autoimmune thyroid diseases (AITDs) are chronic organ-specific autoimmune diseases and mainly include Graves' disease (GD) and Hashimoto's thyroiditis (HT). CD14 is an important component of the immune system as a receptor for gram-negative lipopolysaccharide (LPS). The genetic polymorphisms of CD14 have been confirmed to be associated with a variety of autoimmune diseases. However, its relationship with AITDs is still unclear. The study was aimed to determine whether four single nucleotide polymorphisms (rs2915863, rs2569190, rs2569192, and rs2563298) of CD14 are associated with AITDs and its subgroups of GD and HT. The results showed significant association of rs2915863 and rs2569190 with GD. The frequencies of rs2915863 genotypes and T allele in patients with GD differed significantly from their controls ($P = 0.007$ and $P = 0.021$, respectively). For rs2569190, frequencies of genotypes and G allele in GD patients also showed positive *P*-values ($P = 0.038$ and $P = 0.027$, respectively). The correlations between these two loci and GD are more pronounced in female GD patients and patients with a family history. In genetic model analysis, the allele model, recessive model, and homozygous model of rs2569190 and rs2915863 embodied strong correlations with GD after the adjusting of age and gender ($P = 0.014$, $P = 0.015$, $P = 0.009$, and $P = 0.014$, $P = 0.001$, $P = 0.006$, respectively). However, these four sites are not related to HT. We firstly discovered the relationship between CD14 gene polymorphism and GD, and the results indicate that CD14 is an important risk locus for AITD and its SNPs may contribute to host's genetic predisposition to GD.

Keywords: CD14, single nucleotide polymorphisms, autoimmune thyroid diseases, Graves' disease, Hashimoto's thyroiditis

OPEN ACCESS

Edited by:
Marek Ruchala, Poznan University of Medical Sciences, Poland

Reviewed by:
Takao Ando, Nagasaki University Hospital, Japan
Agathocles Tsatsoulis, University of Ioannina, Greece

***Correspondence:**
Jinan Zhang
zhangjinan@hotmail.com

Specialty section:
This article was submitted to Thyroid Endocrinology, a section of the journal Frontiers in Endocrinology

Received: *19 August 2018*
Accepted: *24 December 2018*
Published: *16 January 2019*

Citation:
Jia X, Wang B, Yao Q, Li Q and Zhang J (2019) Variations in CD14 Gene Are Associated With Autoimmune Thyroid Diseases in the Chinese Population. Front. Endocrinol. 9:811. doi: 10.3389/fendo.2018.00811

INTRODUCTION

Autoimmune thyroid diseases (AITDs) are chronic thyroid-specific autoimmune diseases and mainly include Graves' disease (GD) and Hashimoto's thyroiditis (HT) (1). The prevalence of AITDs is estimated to be 5% in general population and 5–10 times in women than in men (2, 3). The specific pathogeny of AITDs is still unclear and may be related to genetic susceptibility, immunopathogenic mechanisms, and environmental factors (4, 5).

The cluster differentiation antigen 14 (CD14) gene is localized on chromosome 5q31.1 region and encodes a glycosylphosphatidylinositol-anchored membrane glycoprotein (6). As a pattern recognition factor, CD14 protein is constitutively expressed in majority of innate immune response cells, and plays a central role in innate immunity through recognition of bacterial lipopolysaccharide (LPS) (6, 7). CD14 protein exists mainly in membrane form (mCD14) or soluble form (sCD14) (8). Membrane CD14 is expressed primarily on the surface of monocytes, macrophages, and neutrophils, while sCD14 is predominantly in serum (8). Detection of sCD14 in serum can partially reflect the expression of CD14 gene *in vivo*. As an important component of innate immunity, alterations in CD14 expression appear to correlate with aberrant immune responses and autoimmune diseases. The role of CD14 polymorphisms in autoimmune disorders has been widely explored, including inflammatory bowel disease (IBD) (9–11), multiple sclerosis (MS) (12), rheumatoid arthritis (RA) (13–15), juvenile idiopathic arthritis (16), systemic lupus erythematosus (15), and type 1 diabetes mellitus (T1DM) (17). Different autoimmune diseases often share some common immunological mechanisms. Therefore, it is reasonable to speculate that CD14 polymorphisms may contribute to AITDs. This study was conducted to explore the association of four CD14 polymorphisms (rs2915863, rs2569190, rs2569192, and rs2563298) with the AITDs in the population of south China, and to explore its mechanisms though bioinformatics analysis.

MATERIALS AND METHODS

Patients and Healthy Individuals

In our study, we conduct an anonymized cohort involving 847 Chinese Han AITDs patients and 715 healthy Chinese Han controls. The AITDs patients included 522 GD patients (363 males and 159 females) and 325 HT patients (49 males and 276 females). The male to female ratio of our sample is in consistent with that in general population. In order to exclude sampling bias, all of them were randomly recruited individuals living in the same geographic region (Shanghai, China), without any genetic relationship. All AITDs patients were recruited from the Out-patient Department of Endocrinology of Jinshan Hospital. Healthy controls were consecutively enrolled from the Healthy Check-Up Center of the same hospital with ethnically and geographically matching. The control group participating in the study did not have any history of immune diseases or other chronic diseases. The study was approved by the ethical committees of Jinshan Hospital. All enroll individuals in the AITDs group and the control group provided verbal and written informed consent.

The diagnosis criteria of GD used in this study included clinical manifestations of thyrotoxicosis, biochemical indicators of hyperthyroidism, positive circulating thyroid-stimulating hormone receptor antibody (TRAb) and diffuse goiter of the thyroid observed by B-ultrasound or palpation. HT cases were defined on the basis of enlarged thyroid and elevated level of either thyroid peroxidase antibody (TPOAb) or thyroglobulin antibody (TgAb).

DNA Sample Collection and Extraction

Genomic DNA was extracted from 2 ml peripheral venous blood of each participants using the Relax Gene Blood DNA System (Tiangen Biotech Co., Ltd., Beijing, China). The concentration and purity of DNA was measured using Nano Drop 2,000 Spectra-photometer (Thermo Scientific Company, Waltham, MA, USA).

SNP Selection and Genotyping

Four SNPs of CD14 were investigated in the present study, including rs2915863, rs2569190, rs2569192, and rs2563298. In the light of previously published literature, significant associations of these loci with multiple autoimmune diseases have been identified. Therefore, there have a theoretical basis for us to speculate that they may also have correlations with the susceptibility of AITDs. The Hardy-Weinberg equilibrium *P*-values (HWpval) of these four SNPs met the criteria of HWpval > 0.05. The target DNA sequences were amplified by multiplex polymerase chain reaction (PCR) method using specific primers with sequences shown in **Table 1**.

Genotyping-Clinical Phenotype Analysis

Different clinical manifestations may have different genetic backgrounds. In order to more accurately investigate the relationship between SNPs and different clinical phenotypes of AITDs, the clinical classifications of GD and HT in the current study were set as (i) presence or absence of thyrotoxic exophthalmos in the GD group; (ii) the thyroid goiter degree or normal volume; and (iii) presence or absence of AITD family

TABLE 1 | specific primer sequences of SNPs.

SNPs	Primer
rs2915863	Forward Primer- TCTCAAAGTGCTGGGATTACAG Reverse Primer- AAATACAAAATTAGCCGGGTGTAG
rs2569190	Forward Primer- CCTCTGTGAACCCTGATCACCTCC Reverse Primer- CGCCTGAGTCATCAGGACACTGC
rs2569192	Forward Primer- ACTCACAGCTTGATTCAACAAATG Reverse Primer- TTGGTTTCTCTTCTTTTAAGAGCC
rs2563298	Forward Primer- GATAGGGTTTCTTAGGGAGTTAGG Reverse Primer- AATAATGAATGGACTCAAACTGCC

TABLE 2 | Demographic statistics and clinical phenotypes of subjects in case group.

	AITDs (%)	GD (%)	HT (%)
Number	847	522	325
GENDER			
Female	639 (75.44)	363 (69.54)	276 (84.92)
Male	208 (24.56)	159 (30.46)	49 (15.08)
Age	41.87 ± 14.53	41.39 ± 14.79	42.60 ± 14.06
Ophthalmopathy (+)	86 (10.15)	83 (15.90)	3 (0.92)
Family history (+)	162 (19.13)	108 (20.69)	54 (16.62)

AITDs, autoimmune thyroid diseases; GD, Graves' disease; HT, Hashimoto's thyroiditis.

TABLE 3 | Associations of rs2915863, rs2569190, rs2569192, and rs2563298 in CD14 gene with AITDs, GD, and HT.

SNP	Genotype or allele	NC	AITD	*P*-value	GD	*P*-value	HT	*P*-value
		n (%)	*n* (%)	AITD vs. NC	*n* (%)	GD vs. NC	*n* (%)	HT vs. NC
rs2915863	CC	225 (31.47)	258 (30.46)	0.060	153 (29.31)	**0.007**	105 (32.31)	0.889
	TC	370 (51.75)	407 (48.05)		244 (46.74)		163 (50.15)	
	TT	120 (16.78)	182 (21.49)		125 (23.95)		57 (17.54)	
	C	820 (57.34)	923 (54.49)	0.109	550 (52.68)	**0.021**	373 (57.38)	0.986
	T	610 (42.66)	771 (45.51)		494 (47.32)		277 (42.62)	
rs2569190	AA	270 (37.76)	311 (36.72)	0.109	178 (34.10)	**0.038**	133 (40.92)	0.358
	AG	353 (49.37)	395 (46.64)		250 (47.89)		145 (44.62)	
	GG	92 (12.87)	141 (16.65)		94 (18.01)		47 (14.46)	
	A	893 (62.45)	1,017 (60.04)	0.168	606 (58.05)	**0.027**	411 (63.23)	0.732
	G	537 (37.55)	677 (39.96)		438 (41.95)		239 (36.77)	
rs2569192	GG	554 (77.48)	650 (76.74)	0.929	396 (75.86)	0.775	254 (78.15)	0.784
	CG	155 (21.68)	189 (22.31)		122 (23.37)		67 (20.2)	
	CC	6 (0.84)	8 (0.94)		4 (0.77)		4 (1.23)	
	G	1,263 (88.32)	1,489 (87.90)	0.716	914 (87.55)	0.559	575 (88.46)	0.927
	C	167 (11.68)	205 (12.10)		130 (12.45)		75 (11.54)	
rs2563298	CC	552 (77.20)	649 (76.62)	0.955	396 (75.86)	0.866	253 (77.85)	0.695
	AC	158 (22.10)	190 (22.43)		122 (23.37)		68 (20.92)	
	AA	5 (0.70)	8 (0.94)		4 (0.77)		4 (1.23)	
	C	1,262 (88.25)	1,488 (87.84)	0.841	914 (87.55)	0.675	574 (88.31)	0.846
	A	168 (11.75)	206 (12.16)		130 (12.45)		76 (11.69)	

AITDs, autoimmune thyroid diseases; GD, Graves' disease; HT, Hashimoto's thyroiditis; NC, Normal Controls. Bold represents a positive P value.

history (disease in the first-degree relatives). The characteristics of all experimental subjects are summarized in **Table 2**.

Graves' ophthalmopathy (GO), also called thyroid-associated opthalmopathy, is a common extra-thyroid manifestation of GD, mainly manifested as inflammation and swelling of the extraocular muscles, chemosis, eyelid edema, proptosis, excess tearing, and episcleral vascular injection (1, 18). Graves' ophthalmopathy (GO) was diagnosed by the clinical assessment criteria for GO from Williams Textbook of Endocrinology (19).

Statistical Analysis

All odds ratios (OR), 95% confidence interval (95%CI), and *P*-values were calculated using the Stata version 12.1 software (Stata, Inc.), based on the two-tailed Pearson chi-square test (X^2 test) for genotype/allele frequency of each SNP. $P < 0.05$ was considered statistically significant. For each SNP, deviation from Hardy-Weinberg equilibrium (HWE) was estimated using the HWE program (http://ihg.gsf.de/cgi-bin/hw/hwa1.pl) in controls and cases separately. Linkage analysis and haplotype analysis were also performed in this study. A linkage disequilibrium (LD) test was conducted using Haploview Software (version 4.2, Broad Institute, Cambridge, MA, USA). To consolidate the evidence, significant findings were further examined by multiple logistic regression (Stata 12.1, Inc.) and adjusted for potential interfering factors (gender and age) simultaneously.

Bioinformatics Analysis

Associations of CD14 Expression Level With Key Immune Cells in GD Tissues

The correlations of CD14 expression level with key immune cells in 18 GD thyroid tissues were studied through using GSE9340 from Gene Expression Omnibus (GEO) database (20). Macrophages, plasma B cells, T follicular helper cells (Tfh) and regulatory T cells (Tregs) in GD tissues were estimated from the gene expression profiles in GSE9340 by CIBERSORT tool (21). Th1 and Th2 in D tissues were estimated from the gene expression profiles in GSE9340 by Cell tool (22). To further assess the roles of CD14 in GD, the correlations of its expression and intrathyroidal immune cells were analyzed using Spearson correlation analysis.

Functional Pathways Related to CD14 in GD Tissues

Gene set enrichment analysis (GSEA) was done to identify crucial functional pathways related to CD14 through using gene expression profiling of 18 GD tissues from GSE9340 (23). GSEA analysis was performed with GSEA v3.0, and GO biological process (4,436 genes sets) were used as predefined genes sets. Gene sets with both an Enrichment score (ES) more than 0.70 and false discovery rate (FDR) $q < 0.05$ were considered significantly enriched pathways.

RESULTS

Association of CD14 rs2915863 and rs2569190 With GD

In the current study, we examined the frequency distribution for each allele and analyzed the association for each SNP in a case-control manner. Associations of SNPs in CD14 gene with AITDs, GD and HT are shown in **Table 3**. Although there are no significant association between these four SNPs (rs2915863, rs2569190, rs2569192, and rs2563298) and AITDs, rs2915863 and rs2569190 are significantly correlated with GD. Both genotyping

TABLE 4 | Associations of rs2915863 and rs2569190 in CD14 gene with female GD patients and GD patients with family history.

SNP	Genotype or allele	NC	Female GD patients	*P*-value	GD with family history	*P*-value
		n (%)	*n* (%)		*n* (%)	
rs2915863	CC	225 (31.47)	108 (29.75)	0.005	25 (23.15)	0.024
	TC	370 (51.75)	164 (45.18)		54 (50.00)	
	TT	120 (16.78)	91 (25.07)		29 (26.85)	
	C	820 (57.34)	307 (42.29)	0.000	104 (48.15)	0.011
	T	610 (42.66)	419 (57.71)		112 (51.85)	
rs2569190	AA	270 (37.76)	119 (32.78)	0.026	29 (26.85)	0.011
	AG	353 (49.37)	176 (48.48)		55 (50.93)	
	GG	92 (12.87)	68 (18.73)		24 (22.22)	
	A	893 (62.45)	414 (57.02)	0.015	113 (52.31)	0.004
	G	537 (37.55)	312 (42.98)		103 (47.69)	

AITDs, autoimmune thyroid diseases; GD, Graves' disease; HT, Hashimoto's thyroiditis; NC, Normal Controls.

and allele analyses of rs2915863 showed significant *P*-values ($P_{genetyping} = 0.007$ and $P_{allele} = 0.021$, respectively). Moreover, rs2569190 also obtained similar results, and the *P*-values of the genotyping and allele analyses were 0.038 and 0.027.

Since rs2915863 and rs2569190 are significantly associated with GD and different clinical subpopulations may have different genetic backgrounds, we further analyzed the gender and family history subgroups of GD patients. As shown in **Table 4**, for rs2915863, female GD patients show a stronger positive *P*-value ($P_{genetyping} = 0.005$, $P_{allele} = 0.000$) than GD patients in general population ($P_{genetyping} = 0.007$, $P_{allele} = 0.021$). Similarly, rs2569190 also has stronger association with female GD patients ($P = 0.026$) as well as GD patients with a positive family history ($P = 0.011$) than in general GD patients ($P = 0.038$). Moreover, this difference is more pronounced in the allele analysis. The *P*-values for female GD patients and GD patients with family history are 0.015 and 0.004, respectively, much more significant than that for GD patients in general population ($P = 0.027$).

To further understand the roles of rs2915863 and rs2569190 in GD, we analyzed the relationship between SNPs and GD in different genetic models, as shown in which **Tables 5**, **6**, correspondingly. In **Table 5**, we can see that in the model analysis of CD14 and AITDs, only the recessive model of rs2915863 has obvious positive results, and the *P*-values before and after correction are 0.019 and 0.012, respectively. It is clear from **Table 6** that rs2915863 has strong association with GD in the allele model, recessive model and homozygous model before ($P = 0.013$, $P = 0.001$, and $P = 0.006$, respectively) and even after ($P = 0.014$, $P = 0.001$, and $P = 0.006$, respectively) adjustment for possible cofounders (age and gender) and rs2569190 also display strong correlations with GD in the allele model, recessive model and homozygous model before ($P = 0.012$, $P = 0.015$, and $P = 0.008$, respectively) and after ($P = 0.014$, $P = 0.015$, and $P = 0.009$, respectively) adjustment for the possible cofounders (age and gender). Furthermore, both rs2915863 and rs2569190 are not related to HT ($P > 0.05$), and both rs2569192 and rs2563298 of CD14 are not related to AITDs, GD, and HT.

Correlations of CD14 With Intrathyroidal Immune Cells

CD14 expression level was positively correlated the proportion of M1 cell ($r = 0.66$, $P = 0.003$) and M1/M2 ratio ($r = 0.56$, $P = 0.014$) in GD tissues (**Figure 1**). Additionally, CD14 expression level was also positively correlated with the proportion of Tfh cell ($r = 0.49$, $P = 0.04$) and Th2 ($r = 0.82$, $P < 0.0001$) in GD tissues (**Figure 1**). CD14 was not correlated with the proportion of Th1 cell ($r = 0.05$, $P = 0.84$) in GD tissues (**Figure 1**).

Functional Pathways Related to CD14 in GD Pathogenesis

GSEA analysis suggested that there were a total of 93 significantly enriched pathways related to CD14 in GD tissues (**Supplementary Table 1**). Most of those enriched pathways were immunity-related pathways, suggesting the critical role of CD14 in the development of GD through regulating immune response. **Table 7** showed the top 10 significantly enriched pathways in the GSEA analysis, such as Interferon-gamma-mediated signaling pathway, Regulation of toll-like receptor signaling pathway, and Positive regulation of interleukin-6 production (**Figures 2–4**, **Table 7**).

DISCUSSION

CD14 is a receptor that recognizes LPS and other bacterial wall components (8). In CD14 gene, rs2915863 or CD14/−1720 is located in 5' near gene region, while rs2569190, also known as CD14/−260 or C(−159)T, is located in the promoter region (24). Both rs2915863 and rs2569190 can affect the expression level of CD14 *in vivo*, supported by the fact that they are associated with altered levels of sCD14 (25–29). sCD14 is an acute phase protein mainly produced by liver, and can reflect inflammatory disease activity (30). In the present study, we found that two variants rs2915863 and rs2569190 in CD14 gene show significant associations with GD, especially for females GD patient and GD patients with family history. The frequencies of

TABLE 5 | Odds ratios (ORs) of the associations of polymorphisms in CD14 gene with AITD before and after adjustment for confounders (age and gender).

Comparison models	Unadjusted estimates		Adjusted estimates	
	OR (95%CI)	*P*-values	OR (95%CI)	*P*-values
rs2915863				
Allele model	1.12 (0.97–1.29)	0.108	1.13 (0.98–1.31)	0.098
Dominant model	1.05 (0.85–1.30)	0.668	1.04 (0.84–1.30)	0.714
Recessive model	1.36 (1.05–1.75)	**0.019**	1.40 (1.07–1.81)	**0.012**
Homozygous model	1.15 (0.99–1.33)	0.060	1.16 (1.1–1.35)	0.050
Additive model	0.96 (0.76–1.20)	0.720	0.94 (0.75–1.19)	0.618
rs2569190				
Allele model	1.10 (0.95–1.28)	0.183	1.12 (0.98–1.28)	0.255
Dominant model	1.03 (0.83–1.26)	0.810	1.03 (0.83–1.27)	0.807
Recessive model	1.33 (1.00–1.78)	0.048	1.32 (0.99–1.77)	0.063
Homozygous model	1.15 (0.99–1.35)	0.070	1.15 (0.99–1.35)	0.075
Additive model	0.97 (0.78–1.21)	0.794	0.98 (0.79–1.22)	0.863
rs2569192				
Allele model	1.04 (0.82–1.32)	0.709	1.02 (0.81–1.28)	0.857
Dominant model	1.04 (0.55–1.60)	0.728	1.02 (0.80–1.30)	0.879
Recessive model	1.13 (0.39–3.26)	0.826	1.10 (0.37–3.23)	0.863
rs2563298				
Allele model	1.04 (0.83–1.30)	0.716	1.02 (0.81–1.28)	0.888
Dominant model	1.03 (0.82–1.31)	0.787	1.00 (0.79–1.28)	0.973
Recessive model	1.35 (0.44–4.15)	0.596	1.36 (0.44–4.24)	0.597

Allele model = G vs. C; Dominant model = (GG+GC) vs. CC; Recessive model = GG vs. (GC+CC); Homozygous model = GG vs. CC; Additive model = GC vs. CC. Bold represents a positive P value.

TABLE 6 | Odds ratios (ORs) of the associations of four polymorphisms in the CD14 gene with GD before and after adjusting for confounders (age and gender).

Comparison models	Unadjusted estimates		Adjusted estimates	
	OR(95%CI)	*P*-values	OR (95%CI)	*P*-values
rs2915863				
Allele model	1.21 (1.04–1.41)	**0.013**	1.21 (1.04–1.40)	**0.014**
Dominant model	1.12 (0.89–1.41)	0.329	1.11 (0.88–1.39)	0.391
Recessive model	1.53 (1.18–1.98)	**0.001**	1.55 (1.20–2.00)	**0.001**
Homozygous model	1.23 (1.06–1.43)	**0.006**	1.23 (1.06–1.43)	**0.006**
Additive model	0.99 (0.77–1.26)	0.919	0.97 (0.76–1.24)	0.791
rs2569190				
Allele model	1.21 (1.04–1.42)	**0.012**	1.21 (1.04–1.41)	**0.014**
Dominant model	1.22 (0.98–1.52)	0.073	1.21 (0.97–1.51)	0.089
Recessive model	1.42 (1.07–1.89)	**0.015**	1.42 (1.07–1.90)	**0.015**
Homozygous model	1.24 (1.06–1.45)	**0.008**	1.23 (1.05–1.45)	**0.009**
Additive model	1.13 (0.90–1.43)	0.281	1.12 (0.89–1.42)	0.335
rs2569192				
Allele model	1.08 (0.86–1.37)	0.495	1.08 (0.86–1.37)	0.501
Dominant model	1.11 (0.86–1.42)	0.417	1.11 (0.86–1.42)	0.424
Recessive model	0.80 (0.25–2.55)	0.700	0.80 (0.25–2.57)	0.709
rs2563298				
Allele model	1.07 (0.85–1.36)	0.546	1.07 (0.85–1.36)	0.557
Dominant model	1.08 (0.85–1.39)	0.495	1.09 (0.85–1.40)	0.509
Recessive model	0.88 (0.27–2.89)	0.839	0.90 (0.27–2.93)	0.855

Allele model = G vs. C; Dominant model = (GG+GC) vs. CC; Recessive model = GG vs. (GC+CC); Homozygous model = GG vs. CC; Additive model = GC vs. CC. Bold represents a positive P value.

rs2915863 minor allele T and rs2569190 minor allele G are greatly increased in patients with GD. Genetic model analysis shows that rs2915863 and rs2569190 have strong correlations with GD in allele model, recessive model and homozygous model, suggesting that polymorphisms rs2915863 and rs2569190 of CD14 gene may be contributors to the causes of GD.

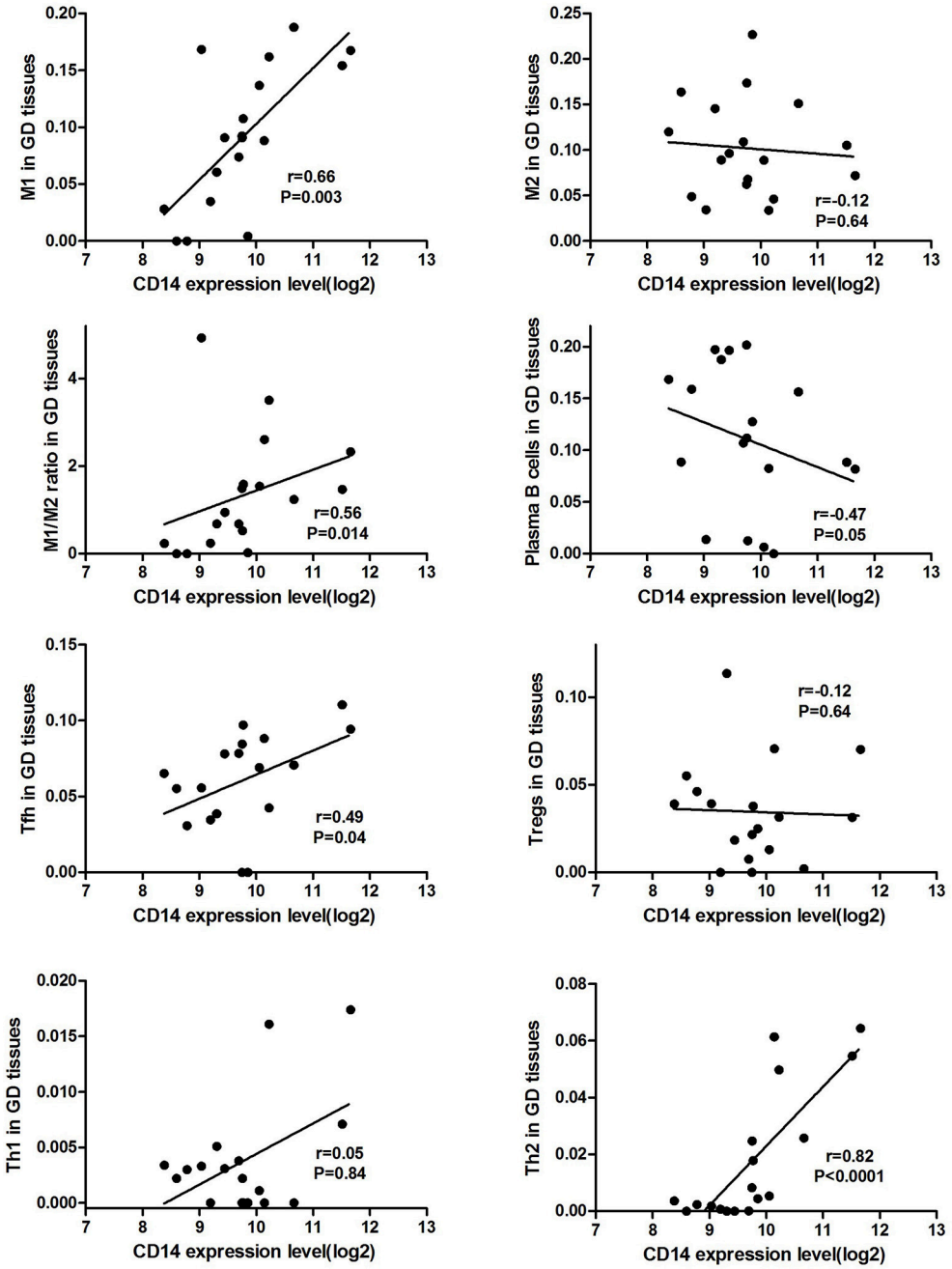

FIGURE 1 | Correlations of CD14 with key intrathyroidal immune cells in GD tissues.

AITDs are classic autoimmune diseases, with multiple factors involved. AITDs have been confirmed to be associated with SNPs of various immune genes, including CD40, CTLA4, and IL-21 and so on (31–33). Since autoimmune diseases have a certain degree of similarity in immune imbalance and genetic background, a SNP is often found to be associated with multiple autoimmune diseases. Previous studies have found that rs2915863 is associated with symptomatic airway hyper-responsiveness, which may be related to endotoxin exposure and elevated IgE (34–36), and rs2569190 may contribute to allergic rhinitis (37), allergic asthma (24), and IBD (11). In this study, we, for the first time, found that rs2915863 and rs2569190 are significantly related to GD, especially in female patients. Our findings that the role of rs2915863 and rs2569190 in promoting GD are more pronounced in female patients is consistent with the universal acceptance that there is a gender difference in the incidence of GD. The mechanism of preponderance of females in GD has not yet been fully elucidated, and may be related

TABLE 7 | Top 10 significantly enriched pathways in the GSEA analysis.

Gene set	ES	Nominal *P*-value	FDR *q*-value
Negative regulation of lipid catabolic process	0.84	<0.001	0.002
Interferon-gamma-mediated signaling pathway	0.81	0.002	0.022
Response to interferon-gamma	0.73	0.004	0.015
Regulation of toll-like receptor signaling pathway	0.75	0.002	0.016
High-density lipoprotein particle remodeling	0.78	<0.001	0.016
Cellular response to interferon-gamma	0.72	0.006	0.014
Regulation of mast cell activation	0.74	<0.001	0.013
Positive regulation of interleukin-6 production	0.70	0.002	0.012
Regulation of natural killer cell mediated immunity	0.75	0.006	0.014
Positive regulation of toll-like receptor signaling pathway	0.83	0.002	0.014

ES, Enrichment score; FDR, false discovery rate.

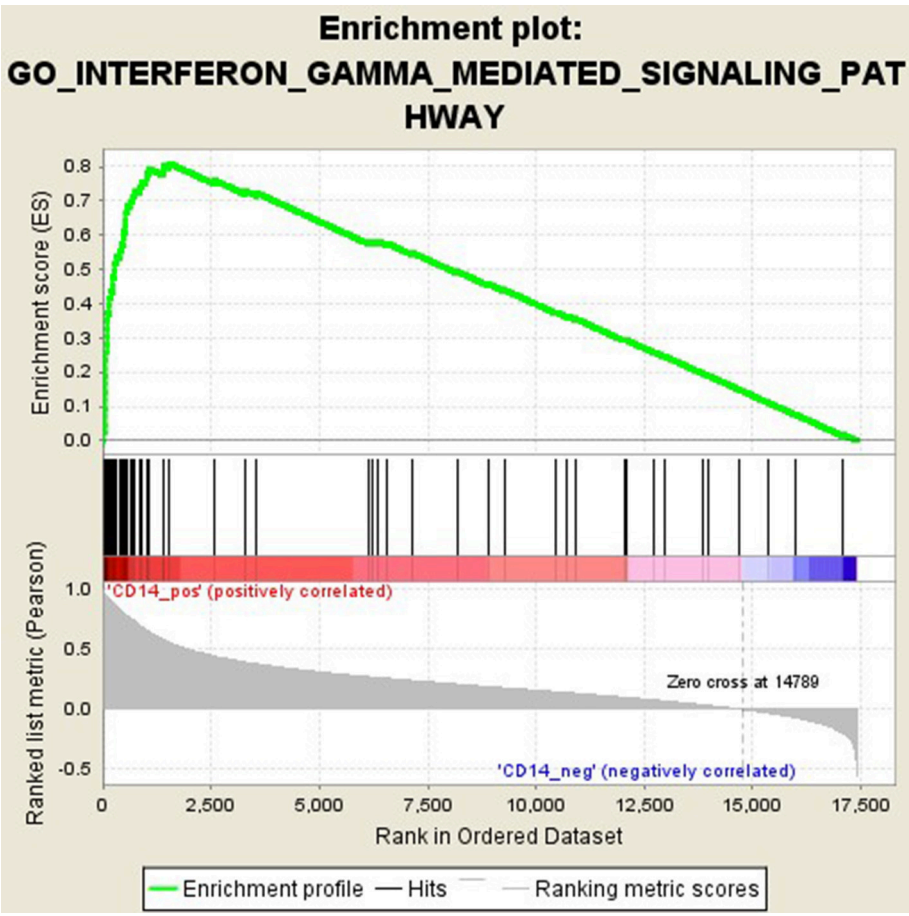

FIGURE 2 | Enrichment plot for the gene set of "Interferon-gamma-mediated signaling pathway".

to sex hormones, genetic susceptibility and mental factors (3, 38). Although GD is not a genetic disease in the traditional sense, it has a certain degree of genetic predisposition (2). The family aggregation of GD supports the importance of genetic factors in its pathogenesis. Moreover, our study found that the relationship between CD14 polymorphisms and GD is more pronounced in patients with family history. Compared with the general GD group, the susceptible allele T in rs2915863 and the susceptible allele G in rs2569190 have stronger positive *P*-values in patients with family history. Thus, mutations in the rs2915863 and rs2569190 loci of CD14 gene may have family aggregation and may play a greater role in GD patients with family history.

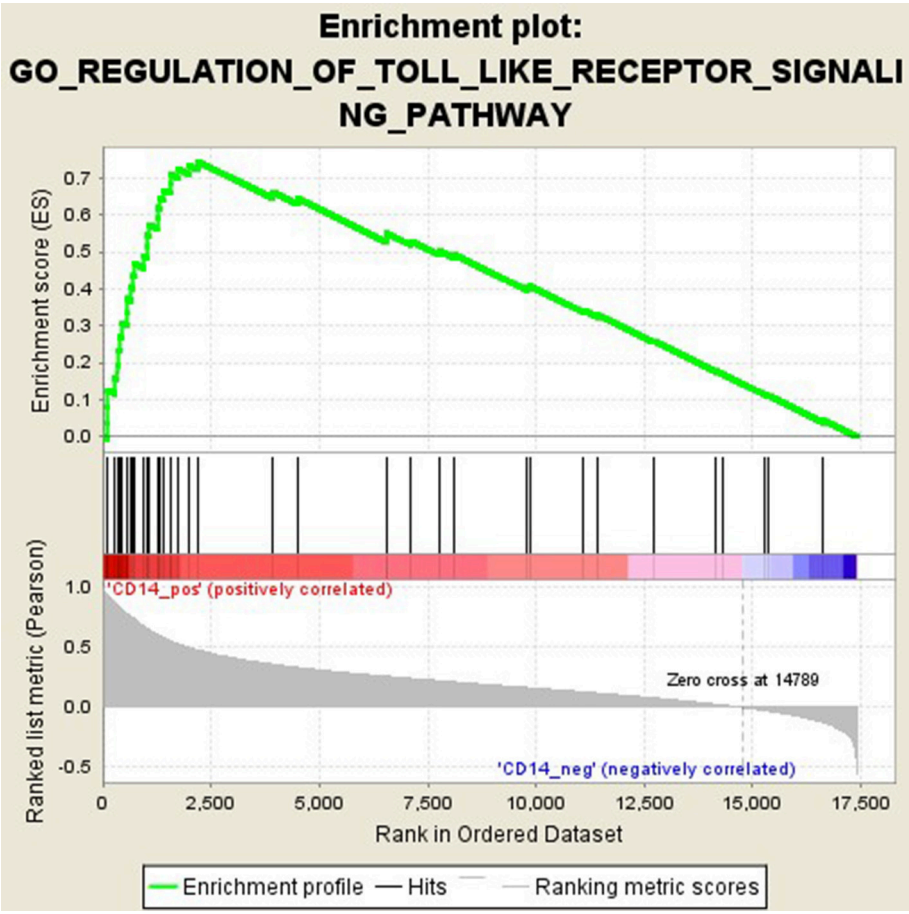

FIGURE 3 | Enrichment plot for the gene set of "Regulation of toll-like receptor signaling pathway".

There is sufficient evidence to support that mutations at these two sites can cause changes in CD14 expression levels and methylation levels, suggesting that they can affect CD14 function (39–41). As an important component of the innate immune system, CD14 has been demonstrated to be involved in infectious and immune-related diseases (42, 43). Membrane CD14 is mainly expressed on the surface of monocyte macrophages, and is one of the specific molecular markers of monocytes/macrophages (44, 45). Macrophages are important antigen-presenting cells (APCs) that mediate homeostasis of the immune system and can currently be divided into two subgroups, M1 and M2 cells (44, 46). CD14, LPS, and LPS binding proteins bind to form a ligand complex that is recognized by the Toll-like receptor-4 (TLR-4)/MD-2 receptor, mediates antigen presentation, stimulates T cell activation and promotes B cell production of antibodies (43, 47). AITDs are chronic organ-specific autoimmune diseases characterized by the production of autoimmune antibodies that attack thyroid cells (1). A variety of immune cells mediate the pathogenesis of AITDs, and macrophages in which membrane CD14 is located are one of the hotspots of recent research. We found through bioinformatics analysis that CD14 expression level was positively correlated the proportion of macrophages M1 cell and M1/M2 ratio in GD tissues (**Figure 1**), suggesting that CD14 is an important molecule mediating macrophage homeostasis in thyroid tissue of patients with GD. Excessive activation of macrophages, especially its M1 subtype, is closely related to the occurrence of autoimmune diseases, including systemic lupus erythematosus, inflammatory bowel disease, rheumatoid arthritis, and multiple sclerosis (46, 48–53). In GD, infiltrating macrophages were observed in thyroid tissue of AITD patients and in the periorbital tissues of patients with GO (54–56). Infiltrating macrophages can directly destroy thyroid follicular cells (57) or kill thyroid cells through the autologous apoptosis pathway (58).

Activation of T cells is also one of the diverse immune functions of CD14. CD14 can promote the early polarization toward Th1 and downregulating Th2 immune responses by stimulating the secretion of tumor necrosis factor-α (TNF-α) and interleukin-6 (IL-6) (43). We found that CD14 expression level was positively correlated with the proportion of Tfh cell and Th2 in GD tissues but not correlated with the proportion of Th1 cell in GD tissues (**Figure 1**). The involvement of Th1 cell and Th2 cell in the pathogenesis of GD and HT is

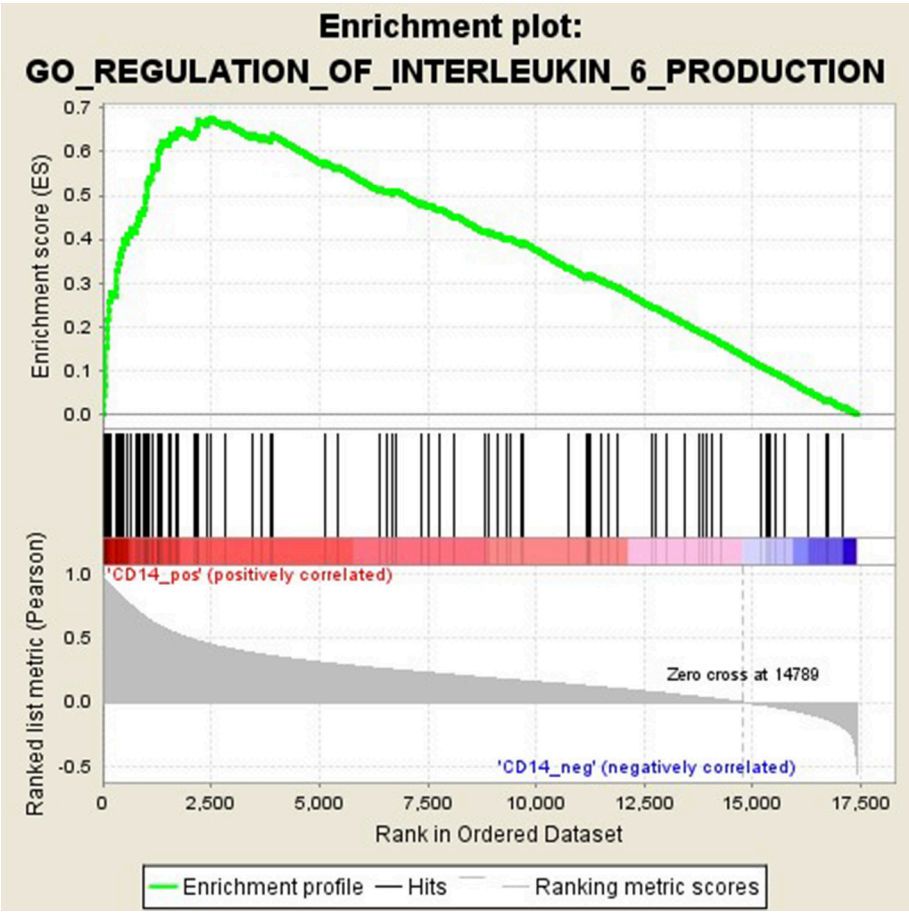

FIGURE 4 | Enrichment plot for the gene set of "Positive regulation of interleukin-6 production".

currently recognized, but its specific mechanism remains to be seen (1) and our findings can bring more information in this area. We have further discovered that there were a total of 93 significantly enriched pathways related to CD14 in GD tissues (**Supplementary Table 1**). Most of those enriched pathways were immunity-related pathways, suggesting the critical role of CD14 in the development of GD through regulating immune response. Interferon-gamma-mediated signaling pathway, Regulation of toll-like receptor signaling pathway and Positive regulation of interleukin-6 production ranks in the top three, with the greatest relationship with GD. We first discovered that CD14 may mediate the pathogenesis of GD through these pathways.

In conclusion, we, for the first time, demonstrated the significant association between genetic variations in CD14 and GD, and this relationship is more pronounced in female GD patients and GD patients with family history. To further demonstrate the role of CD14 in GD, we conducted a bioinformatics analysis and found that CD14 expression level was positively correlated the proportion of macrophages M1 cell and M1/M2 ratio in GD thyroid tissues. Additionally, CD14 expression level was also positively correlated with the proportion of Tfh cell and Th2 but not correlated with the proportion of Th1 cell in GD tissues. We also found that there were many pathways related to CD14 in GD tissues and most of them were immunity-related. However, the more in-depth mechanism of CD14 in the pathogenesis of GD requires more experimental research. Moreover, to further verify the role of CD14 gene variations in GD, it is necessary to conduct studies with larger sample sizes and more ethnicity.

ETHICS STATEMENT

All patients and healthy controls have signed informed consent. The study was approved by the ethical committees of Jinshan Hospital.

AUTHOR CONTRIBUTIONS

XJ was responsible for the experimental design. BW, QY, and QL participated in sample collection. JZ played the guiding role.

ACKNOWLEDGMENTS

The present work was supported by grants from the National Natural Science Foundation of China (Nos. 81670722 and 81471004).

SUPPLEMENTARY MATERIAL

The Supplementary Material for this article can be found online at: https://www.frontiersin.org/articles/10.3389/fendo.2018.00811/full#supplementary-material

REFERENCES

1. Smith TJ, Hegedus L. Graves' disease. *N Engl J Med.* (2016) 375:1552–65. doi: 10.1056/NEJMra1510030
2. McLeod DS, Cooper DS. The incidence and prevalence of thyroid autoimmunity. *Endocrine* (2012) 42:252–65. doi: 10.1007/s12020-012-9703-2
3. Gabrielson AT, Sartor RA, Hellstrom WJG. The impact of thyroid disease on sexual dysfunction in men and women. *Sex Med Rev.* (2019) 7:57–70. doi: 10.1016/j.sxmr.2018.05.002
4. Effraimidis G, Wiersinga WM. Mechanisms in endocrinology: autoimmune thyroid disease: old and new players. *Eur J Endocrinol.* (2014) 170:R241–52. doi: 10.1530/EJE-14-0047
5. Tomer Y. Mechanisms of autoimmune thyroid diseases: from genetics to epigenetics. *Annu Rev Pathol.* (2014) 9:147–56. doi: 10.1146/annurev-pathol-012513-104713
6. Haziot A, Ferrero E, Kontgen F, Hijiya N, Yamamoto S, Silver J, et al. Resistance to endotoxin shock and reduced dissemination of gram-negative bacteria in CD14-deficient mice. *Immunity* (1996) 4:407–14. doi: 10.1016/S1074-761380254-X
7. Bazil V, Horejsi V, Baudys M, Kristofova H, Strominger JL, Kostka W, et al. Biochemical characterization of a soluble form of the 53-kDa monocyte surface antigen. *Eur J Immunol.* (1986) 16:1583–9. doi: 10.1002/eji.1830161218
8. Wright SD, Ramos RA, Tobias PS, Ulevitch RJ, Mathison JC. CD14, a receptor for complexes of lipopolysaccharide (LPS) and LPS binding protein. *Science* (1990) 249:1431–3. doi: 10.1126/science.1698311
9. Wang Z, Hu J, Fan R, Zhou J, Zhong J. Association between CD14 gene C-260T polymorphism and inflammatory bowel disease: a meta-analysis. *PLoS ONE* (2012) 7:1–15. doi: 10.1371/journal.pone.0045144
10. Olivares M, Laparra JM, Sanz Y. Host genotype, intestinal microbiota and inflammatory disorders. *Br J Nutr.* (2013) 109 (Suppl. 2):S76–80. doi: 10.1017/S0007114512005521
11. Bank S, Andersen PS, Burisch J, Pedersen N, Roug S, Galsgaard J, et al. Associations between functional polymorphisms in the NFkappaB signaling pathway and response to anti-TNF treatment in Danish patients with inflammatory bowel disease. *Pharmacogenomics J.* (2014) 14:526–34. doi: 10.1038/tpj.2014.19
12. Kurne A, Sayat G, Aydin OF, Turgutoglu N, Terzi M, Sackesen C, et al. Lack of association of the CD14/C – 159T polymorphism with susceptibility and progression parameters in Turkish multiple sclerosis patients. *J Neuroimmunol.* (2012) 250:83–6. doi: 10.1016/j.jneuroim.2012.05.005
13. Takeuchi F, Nakaue N, Kobayashi N, Kuwata S, Murayama T, Kawasugi K, et al. Genetic contribution of the CD14−159C/T dimorphism in the promoter region in Japanese RA. *Clin Exp Rheumatol.* (2008) 26:337–9.
14. Mikuls TR, LeVan TD, Sayles H, Yu F, Caplan L, Cannon GW, et al. Soluble CD14 and CD14 polymorphisms in rheumatoid arthritis. *J Rheumatol.* (2011) 38:2509–16. doi: 10.3899/jrheum.110378
15. Dhaouadi T, Sfar I, Haouami Y, Abdelmoula L, Turki S, Hassine LB, et al. Polymorphisms of Toll-like receptor-4 and CD14 in systemic lupus erythematosus and rheumatoid arthritis. *Biomark Res.* (2013) 1:20–32. doi: 10.1186/2050-7771-1-20
16. Zeng HS, Chen XY, Luo XP. The association with the−159C/T polymorphism in the promoter region of the CD14 gene and juvenile idiopathic arthritis in a Chinese Han population. *J Rheumatol.* (2009) 36:2025–8. doi: 10.3899/jrheum.081093
17. Dezsofi A, Szebeni B, Hermann CS, Kapitany A, Veres G, Sipka S, et al. Frequencies of genetic polymorphisms of TLR4 and CD14 and of HLA-DQ genotypes in children with celiac disease, type 1 diabetes mellitus, or both. *J Pediatr Gastroenterol Nutr.* (2008) 47:283–7. doi: 10.1097/MPG.0b013e31816de885
18. De Leo S, Lee SY, Braverman LE. Hyperthyroidism. *Lancet* (2016) 388:906–18. doi: 10.1016/S0140-673600278-6
19. Melmed S, Polonsky KS, Reed Larsen P, Kronenberg HM. *Williams Textbook of Endocrinology, 13th ed.* Amsterdam: Elsevier (2015).
20. Wescombe L, Lahooti H, Gopinath B, Wall JR. The cardiac calsequestrin gene (CASQ2) is up-regulated in the thyroid in patients with Graves' ophthalmopathy–support for a role of autoimmunity against calsequestrin as the triggering event. *Clin Endocrinol.* (2010) 73:522–8. doi: 10.1111/j.1365-2265.2009.03753.x
21. Newman AM, Liu CL, Green MR, Gentles AJ, Feng W, Xu Y, et al. Robust enumeration of cell subsets from tissue expression profiles. *Nat Methods* (2015) 12:453–7. doi: 10.1038/nmeth.3337
22. Aran D, Hu Z, Butte AJ. xCell: digitally portraying the tissue cellular heterogeneity landscape. *Genome Biol.* (2017) 18:220–32. doi: 10.1186/s13059-017-1349-1
23. Subramanian A, Tamayo P, Mootha VK, Mukherjee S, Ebert BL, Gillette MA, et al. Gene set enrichment analysis: a knowledge-based approach for interpreting genome-wide expression profiles. *Proc Natl Acad Sci USA.* (2005) 102:15545–50. doi: 10.1073/pnas.0506580102
24. Nieto-Fontarigo JJ, Salgado FJ, San-Jose ME, Cruz MJ, Casas-Fernandez A, Gomez-Conde MJ, et al. The CD14 (-159 C/T) SNP is associated with sCD14 levels and allergic asthma, but not with CD14 expression on monocytes. *Sci Rep.* (2018) 8:4147. doi: 10.1038/s41598-018-20483-1
25. Koenig W, Khuseyinova N, Hoffmann MM, Marz W, Frohlich M, Hoffmeister A, et al. CD14 C(-260)–>T polymorphism, plasma levels of the soluble endotoxin receptor CD14, their association with chronic infections and risk of stable coronary artery disease. *J Am Coll Cardiol.* (2002) 40:34–42. doi: 10.1016/S0735-1097(02)01937-X
26. LeVan TD, Guerra S, Klimecki W, Vasquez MM, Lohman IC, Martinez FD, et al. The impact of CD14 polymorphisms on the development of soluble CD14 levels during infancy. *Genes Immun.* (2006) 7:77–80. doi: 10.1038/sj.gene.6364276
27. Levan TD. Michel O, Dentener M, Thorn J, Vertongen F, Beijer L, et al. Association between CD14 polymorphisms and serum soluble CD14 levels: effect of atopy and endotoxin inhalation. *J Allergy Clin Immunol.* (2008) 121:434–40 e431. doi: 10.1016/j.jaci.2007.08.050
28. Raunio T, Knuuttila M, Karttunen R, Vainio O, Tervonen T. Serum sCD14, polymorphism of CD14(-260) and periodontal infection. *Oral Dis.* (2009) 15:484–9. doi: 10.1111/j.1601-0825.2009.01573.x
29. Alavi-Naini R, Salimi S, Sharifi-Mood B, Davoodikia AA, Moody B, Naghavi A. Association between the CD14 gene C-159T polymorphism and serum soluble CD14 with pulmonary tuberculosis. *Int J Tuberc Lung Dis.* (2012) 16:1383–7. doi: 10.5588/ijtld.11.0827
30. Bas S, Gauthier BR, Spenato U, Stingelin S, Gabay C. CD14 is an acute-phase protein. *J Immunol.* (2004) 172:4470–9. doi: 10.4049/jimmunol.172.7.4470
31. Zhang J, Xiao WX, Zhu YF, Muhali FS, Xiao L, Jiang WJ, et al. Polymorphisms of interleukin-21 and interleukin-21-receptor genes confer risk for autoimmune thyroid diseases. *BMC Endocr Disord.* (2013) 13:26. doi: 10.1186/1472-6823-13-26
32. Wang D, Chen J, Zhang H, Zhang F, Yang L, Mou Y. Role of different CD40 polymorphisms in Graves' disease and Hashimoto's Thyroiditis. *Immunol Invest.* (2017) 46:544–51. doi: 10.1080/08820139.2017.1319382
33. Ramgopal S, Rathika C, Padma MR, Murali V, Arun K, Kamaludeen MN, et al. Interaction of HLA-DRB1* alleles and CTLA4 (+49 AG) gene polymorphism in autoimmune thyroid disease. *Gene* (2018) 642:430–8. doi: 10.1016/j.gene.2017.11.057

34. Smit LA, Heederik D, Doekes G, Koppelman GH, Bottema RW, Postma DS, et al. Endotoxin exposure, CD14 and wheeze among farmers: a gene–environment interaction. *Occup Environ Med.* (2011) 68:826–31. doi: 10.1136/oem.2010.060038
35. Kljaic-Bukvic B, Blekic M, Aberle N, Curtin JA, Hankinson J, Semic-Jusufagic A, et al. Genetic variants in endotoxin signalling pathway, domestic endotoxin exposure and asthma exacerbations. *Pediatr Allergy Immunol.* (2014) 25:552–7. doi: 10.1111/pai.12258
36. Sahiner UM, Semic-Jusufagic A, Curtin JA, Birben E, Belgrave D, Sackesen C, et al. Polymorphisms of endotoxin pathway and endotoxin exposure: *in vitro* IgE synthesis and replication in a birth cohort. *Allergy* (2014) 69:1648–58. doi: 10.1111/all.12504
37. Chen ML, Zhao H, Huang QP, Xie ZF. Single nucleotide polymorphisms of IL-13 and CD14 genes in allergic rhinitis: a meta-analysis. *Eur Arch Otorhinolaryngol.* (2018) 275:1491–500. doi: 10.1007/s00405-018-4975-7
38. De Leo S, Pearce EN. Autoimmune thyroid disease during pregnancy. *Lancet Diabetes Endocrinol.* (2018) 6:575–86. doi: 10.1016/S2213-858730402-3
39. Simpson A, John SL, Jury F, Niven R, Woodcock A, Ollier WE, et al. Endotoxin exposure, CD14, and allergic disease: an interaction between genes and the environment. *Am J Respir Crit Care Med.* (2006) 174:386–92. doi: 10.1164/rccm.200509-1380OC
40. Simpson A, Martinez FD. The role of lipopolysaccharide in the development of atopy in humans. *Clin Exp Allergy* (2010) 40:209–23. doi: 10.1111/j.1365-2222.2009.03391.x
41. Friedrich K, Smit M, Brune M, Giese T, Rupp C, Wannhoff A, et al. CD14 is associated with biliary stricture formation. *Hepatology* (2016) 64:843–52. doi: 10.1002/hep.28543
42. Romagnani S. T-cell subsets (Th1 versus Th2). *Ann Allergy Asthma Immunol.* (2000) 85:9–18. doi: 10.1016/S1081-120662426-X
43. Zanoni I, Granucci F. Role of CD14 in host protection against infections and in metabolism regulation. *Front Cell Infect Microbiol.* (2013) 3:32. doi: 10.3389/fcimb.2013.00032
44. Kiss M, Czimmerer Z, Nagy L. The role of lipid-activated nuclear receptors in shaping macrophage and dendritic cell function: from physiology to pathology. *J Allergy Clin Immunol.* (2013) 132:264–86. doi: 10.1016/j.jaci.2013.05.044
45. Tundup S, Srivastava L, Nagy T, Harn D. CD14 influences host immune responses and alternative activation of macrophages during *Schistosoma mansoni* infection. *Infect Immun.* (2014) 82:3240–51. doi: 10.1128/IAI.01780-14
46. Ip WKE, Hoshi N, Shouval DS, Snapper S, Medzhitov R. Anti-inflammatory effect of IL-10 mediated by metabolic reprogramming of macrophages. *Science* (2017) 356:513–9. doi: 10.1126/science.aal3535
47. Kim D, Kim JY. Anti-CD14 antibody reduces LPS responsiveness via TLR4 internalization in human monocytes. *Mol Immunol.* (2014) 57:210–5. doi: 10.1016/j.molimm.2013.09.009
48. Hucke S, Eschborn M, Liebmann M, Herold M, Freise N, Engbers A, et al. Sodium chloride promotes pro-inflammatory macrophage polarization thereby aggravating CNS autoimmunity. *J Autoimmun.* (2016) 67:90–101. doi: 10.1016/j.jaut.2015.11.001
49. Li F, Zhu X, Yang Y, Huang L, Xu J. TIPE2 alleviates systemic lupus erythematosus through regulating macrophage polarization. *Cell Physiol Biochem.* (2016) 38:330–9. doi: 10.1159/000438633
50. Tostanoski LH, Gosselin EA, Jewell CM. Engineering tolerance using biomaterials to target and control antigen presenting cells. *Discov Med.* (2016) 21:403–10.
51. Park SY, Lee SW, Lee SY, Hong KW, Bae SS, Kim K, et al. SIRT1/adenosine monophosphate-activated protein kinase alpha signaling enhances macrophage polarization to an anti-inflammatory phenotype in rheumatoid arthritis. *Front Immunol.* (2017) 8:1135. doi: 10.3389/fimmu.2017.01135
52. Van Welden S, De Vos M, Wielockx B, Tavernier SJ, Dullaers M, Neyt S, et al. Haematopoietic prolyl hydroxylase-1 deficiency promotes M2 macrophage polarization and is both necessary and sufficient to protect against experimental colitis. *J Pathol.* (2017) 241:547–58. doi: 10.1002/path.4861
53. Aparicio-Soto M, Montserrat-de la Paz S, Sanchez-Hidalgo M, Cardeno A, Bermudez B, Muriana FJG, et al. Virgin olive oil and its phenol fraction modulate monocyte/macrophage functionality: a potential therapeutic strategy in the treatment of systemic lupus erythematosus. *Br J Nutr.* (2018) 120:681–92. doi: 10.1017/S0007114518001976
54. Sugenoya A, Silverberg J, Trokoudes K, Row VV, Volpe R. Macrophage-lymphocyte interaction in Graves' disease and Hashimoto's thyroiditis. *Acta Endocrinol.* (1979) 91:99–108. doi: 10.1530/acta.0.0910099
55. Totterman TH, Andersson LC, Hayry P. Evidence for thyroid antigen-reactive T lymphocytes infiltrating the thyroid gland in Graves' disease. *Clin Endocrinol.* (1979) 11:59–68. doi: 10.1111/j.1365-2265.1979.tb03046.x
56. van Steensel L, Paridaens D, van Meurs M, van Hagen PM, van den Bosch WA, Kuijpers RW, et al. Orbit-infiltrating mast cells, monocytes, and macrophages produce PDGF isoforms that orchestrate orbital fibroblast activation in Graves' ophthalmopathy. *J Clin Endocrinol Metab.* (2012) 97:E400–8. doi: 10.1210/jc.2011-2697
57. Ben-Skowronek I, Szewczyk L, Kulik-Rechberger B, Korobowicz E. The differences in T and B cell subsets in thyroid of children with Graves' disease and Hashimoto's thyroiditis. *World J Pediatr.* (2013) 9:245–50. doi: 10.1007/s12519-013-0398-0
58. Berghi NO. Immunological mechanisms implicated in the pathogenesis of chronic Urticaria and Hashimoto Thyroiditis. *Iran J Allergy Asthma Immunol.* (2017) 16:358–66.

Conflict of Interest Statement: The authors declare that the research was conducted in the absence of any commercial or financial relationships that could be construed as a potential conflict of interest.

frontiers in Endocrinology

ORIGINAL RESEARCH
published: 23 January 2019
doi: 10.3389/fendo.2019.00003

Sonographic Pattern of Subacute Thyroiditis Is HLA-Dependent

*Magdalena Stasiak[1], Bogusław Tymoniuk[2], Zbigniew Adamczewski[1,3], Bartłomiej Stasiak[4] and Andrzej Lewiński[1,3]**

[1] Department of Endocrinology and Metabolic Diseases, Polish Mother's Memorial Hospital Research Institute, Lodz, Poland, [2] Department of Immunology, Rheumatology and Allergy, Medical University of Lodz, Lodz, Poland, [3] Department of Endocrinology and Metabolic Diseases, Medical University of Lodz, Lodz, Poland, [4] Institute of Information Technology, Lodz University of Technology, Lodz, Poland

Background: Since 1977 the susceptibility to SAT has been known to be HLA-B*35-related in ∼70% of patients. Recently it has been demonstrated that SAT is associated with the presence of HLA-B*18:01 and DRB1*01, as well as with HLA-C*04:01. The association between the type of genetic SAT background and sonographic pattern of the disease has never been analyzed. The aim of the study was to evaluate the potential correlation between the presence of individual HLA haplotypes and the sonographic SAT pattern, and to provide the US characteristics of the analyzed SAT cases.

Methods: HLA-A, -B, -C, -DQB1, and -DRB1 were genotyped using a next-generation sequencing method in 46 SAT patients. All patients were divided into the following groups according to the HLA haplotype: 1. HLA-B*35 and/or HLA-C*04, but without any other of the analyzed antigens; 2. HLA-DRB1*01, regardless of the co-presence of HLA-B*35 or C*04:01, but without HLA-B*18:01; 3. HLA-B*18:01 only, without any other of the analyzed antigens; 4. HLA-B*18:01 plus B*35, regardless of the presence of any other analyzed antigens. The US patterns of SAT thyroid lesions were compared among the groups.

Results: The US image of SAT lesions in Groups 1 and 2 were similar. The typical SAT features for these groups were as follows: hypoechoic, strongly heterogeneous, bilateral, multiple areas, with decreased vascularization, usually oval with blurred margins, infrequently affecting the whole lobe, or having nodule-like pattern. Several features of Group 3 were different from the other groups. In 60% of cases lesions were rather homogeneous, and in 100%–hypoechoic, in 80% of patients there was only one unilateral single SAT area filling the whole affected lobe. On the contrary to the other groups, in Group 4 no lesion was oval in shape.

Conclusions: Our results provide for the first time the evidence that the US pattern of SAT lesions depends on HLA, and the determining factor is the presence of HLA-B*18:01. The deviations from the typical SAT US image are mostly pronounced in patients with the presence of only HLA-B*18:01, without any other analyzed haplotype. Further research is necessary to explain this phenomenon.

Keywords: HLA-B*35, HLA-B*18:01, HLA-DRB1*01, HLA-C*04:01, subacute thyroiditis, ultrasound

OPEN ACCESS

Edited by:
Ewelina Szczepanek-Parulska, Poznan University of Medical Sciences, Poland

Reviewed by:
Trevor Edmund Angell, University of Southern California, United States
Roberto Vita, Università degli Studi di Messina, Italy

***Correspondence:**
Andrzej Lewiński
alewin@csk.umed.lodz.pl

Specialty section:
This article was submitted to Thyroid Endocrinology, a section of the journal Frontiers in Endocrinology

Received: *06 December 2018*
Accepted: *07 January 2019*
Published: *23 January 2019*

Citation:
Stasiak M, Tymoniuk B, Adamczewski Z, Stasiak B and Lewiński A (2019) Sonographic Pattern of Subacute Thyroiditis Is HLA-Dependent. Front. Endocrinol. 10:3. doi: 10.3389/fendo.2019.00003

INTRODUCTION

Subacute thyroiditis (SAT) (also called de Quervain thyroiditis) is a thyroid inflammatory disease, associated with the presence of certain types of human leukocyte antigens (HLA). Previous viral infection (occurring ∼2–6 weeks earlier) is considered a triggering factor in genetically predisposed individuals. The prevalence of SAT is the highest in middle-aged women, and male to female ratio varies from 1:4 (1) to 1:7 (2). The most common presentation is the anterior neck pain radiating ipsilaterally up to the jaw and ear, and down to the upper part of the chest (3, 4). Fever is usually present, frequently reaching over 39°C, and rising especially at night. Patients often complain of asthenia, and some symptoms of thyrotoxicosis are often present. Typical laboratory findings include high erythrocyte sedimentation rate (ESR). The level of C reactive protein (CRP) is also elevated and laboratory markers of hyperthyroidism are often present but the blood concentration of thyroid antibodies is normal in most patients (3, 4).

Sonographic findings in SAT can be very diverse. In most cases, the ultrasound (US) features include hypoechoic and heterogeneous areas, poorly vascularized on color Doppler, usually with blurred margins and without microcalcifications (5, 6). High tissue stiffness in sonoelastography is characteristic for the disease (7). Blurred, heterogeneous areas of different shape and size can be described as "lava-flow" sonographic pattern (5). The SAT lesions can be bilateral or unilateral, sometimes switching the affected side in the course of the disease. However, the US pattern of SAT is sometimes non-characteristic, and SAT-associated thyroid lesions may mimic thyroid nodules, sometimes with suspicious US features (6).

Since 1977 the susceptibility to SAT has been known to be HLA-B*35-related in ∼70% of patients (8–10). Recently, our research group demonstrated that SAT is associated with the presence of HLA-B*18:01 and DRB1*01, as well as with HLA-C*04:01, with the latter being in linkage disequilibrium with HLA-B*35 (Stasiak et al., under review). Haplotypes HLA-B*18:01 and DRB1*01 are HLA-B*35-independent SAT risk factors (Stasiak et al., under review). These four (4) antigens allow confirmation of the genetic basis in almost all patients with SAT. However, the association between the type of genetic SAT background and sonographic pattern of the disease has never been analyzed.

The aim of the study was to evaluate the potential correlation between the presence of SAT-associated HLA haplotypes, i.e., HLA-B*18:01, DRB1*01, B*35, and C*04:01, and the sonographic SAT pattern, and to provide the US characteristics of the analyzed SAT cases.

MATERIALS AND METHODS

High resolution HLA typing was performed in 46 patients who were diagnosed with SAT between 2003 and 2018 in the Department of Endocrinology and Metabolic Diseases, Polish Mother's Memorial Hospital—Research Institute, Lodz, Poland. HLA-A, -B, -C, -DQB1, and -DRB1 were genotyped using a next-generation sequencing method on Illumina platform (Illumina, USA). Sequencing-based HLA typing of the HLA genes A, B, C, DQB1, and DRB1 was carried out in 96-well format within a semi-automated workflow by using MiaFora Flex5 typing kits (Immucor, USA). Long-range PCR amplification of five HLA loci was performed on DNA extracted from blood samples.

The diagnosis of SAT was based on the diagnostic criteria recently proposed by our research group (2). These criteria were as follows: elevation of ESR (or at least CRP) plus hypoechoic area/areas with blurred margin and decreased vascularization in US, plus cytological confirmation of SAT (or at least cytological exclusion of malignancy), plus at least one of the following: hard thyroid swelling and/or pain and tenderness of the thyroid gland/lobe, and/or elevation of serum free thyroxine (FT4) and suppression of thyrotropin (TSH), and/or decreased radioiodine uptake (RAIU). Serum levels of TSH and FT4 were measured by electrochemiluminescence immunoassay (ECLIA), Cobas e601 analyzer (Roche Diagnostics, USA), ESR was determined with Ves-Matic Cube 30 (Diesse, Italy), CRP was determined by VITROS® 4600 Chemistry System (Ortho Clinical Diagnostics, USA).

Ultrasound examination (US) was performed in every patient, in a supine position, using a Toshiba Aplio XG scanner (Toshiba, Japan), with high frequency 7–14 MHz linear transducer with field of view width of 38 mm (PLT 1204 BT). The US examinations were performed with standard settings optimized for thyroid imaging. The protocol included the B-mode presentation with application of image improvement techniques such as spatial compound imaging and differential tissue harmonics. In Power Doppler US, a pulse repetition frequency (PRF) 14.1 KHz and color gain 60 were routinely used for evaluating thyroid lesions vascularity. The Power Doppler gain was controlled so that perithyroidal tissues did not display any random color artifacts. The mean size of SAT lesions was calculated on the basis of the largest of the three dimensions of the analyzed lesions. The analyzed US features were defined as follows: 1. echogenicity: moderately hypoechoic were lesions darker than the normal surrounding thyroid parenchyma, but less dark than the surrounding muscles; markedly hypoechoic were lesions at least as dark as the surrounding strap muscles; 2. strongly heterogeneous were lesions with mixed isoechoic, hypoechoic and strongly hypoechoic echogenicity; 3. microcalcifications were calcifications smaller than 1 mm; 4. shape: lesion was considered as oval if its anteroposterior diameter was shorter than the transverse diameter on both transverse and longitudinal planes; lesion was considered as round if its anteroposterior and transverse diameters were equal on both transverse and longitudinal planes; lesion was considered as patchy if its shape was entirely irregular and could not be classified as oval or round; 5. margins: margins were considered as blurred if there was no clear separation from the surrounding thyroid parenchyma; margins were considered as lobulated if at least one oval or round protrusion of the margin was present; margins were considered as smooth if they were

Abbreviations: CRP, C reactive protein; ESR, erythrocyte sedimentation rate; FNAB, fine needle aspiration biopsy; FT4, free thyroxine; HLA, human leukocyte antigens; MHC, major histocompatibility complex; RAIU, radioiodine uptake; SAT, subacute thyroiditis; TSH, thyrotropin; US, ultrasound.

TABLE 1 | Sonographic characteristics of the SAT lesions in each group and comparison with all the other subjects.

Sonographic feature of SAT lesions	Group 1 ($n = 25$)	*p*-value*	Group 2 ($n = 10$)	*p*-value*	Group 3 ($n = 5$)	*p*-value*	Group 4 ($n = 6$)	*p*-value*
Echogenicity		0.788		0.294		0.408		0.359
Moderately hypoechoic	88%		80%		100%		100%	
Markedly hypoechoic	12%		20%		0%		0%	
Strongly heterogeneous	84%	0.303	80%	0.880	40%	**0.028**	83.3%	0.747
Microcalcifications	4%	0.353	0%	0.594	0%	0.724	0%	0.695
Shape		0.909		0.785		0.656		**0.027**
Oval	73.3%		66.7%		100%		0%	
Patchy	20%		33.3%		0%		50%	
Round	6.7%		0%		0%		50%	
Margin		0.937		0.572		0.602		0.062
Blurred	80%		100%		66.7%		50%	
Lobulated	13.3%		0%		33.3%		0%	
Smooth	6.7%		0%		0%		50%	
Bilateral	84%	0.170	70%	0.610	20%	**0.002**	100%	0.141
Whole lobe affected	48%	0.141	70%	0.606	80%	**0.003**	66.7%	0.777
Nodule-like pattern	8%	0.855	10%	0.869	0%	0.465	16.7%	0.457
Blurred areas	28%	0.747	40%	0.257	0%	0.159	16.7%	0.573
Separated areas	36%	0.592	30%	0.842	60%	0.166	0%	0.068
No. of areas		0.506						
Single area	16%		10%	0.389	80%	**<0.0005**	0%	0.195
Multiple areas	84%		90%		20%		100%	
Vascularity								
Decreased	84%	0. 786	90%	0.486	60%	0.431	83.3%	0.960
Normal or increased	12%	0.385	0%	0.270	0%	0.915	16.7%	0.457
Absent	4%	0.217	10%	0.869	40%	0.073	0.0%	0.418

**As compared to all other groups.*
$p < 0.05$ was considered as statistically significant.
*Group 1. HLA-B*35 and/or HLA-C*04, but without any other of the analyzed antigens;*
*Group 2. HLA-DRB1*01, regardless of the co-presence of HLA-B*35 or C*04:01, but without B*18:01;*
*Group 3. HLA-B*18:01 only, without any other analyzed antigen;*
*Group 4. HLA-B*35 plus B*18, regardless of the presence of any other analyzed antigens.*

clearly separated from the surrounding thyroid parenchyma; 6. the lesions were considered as nodule-like if they resembled thyroid nodules but disappeared with SAT resolution and were previously cytologically confirmed as SAT; 7. the areas were considered as blurred if their shape and margins were difficult to determine; the areas were considered as separated if their shape and margins could be clearly determined, even if the shape was irregular. Vascularity was determined with Power Doppler. The following definitions for vascularity were used: 1. decreased—blood flow within the lesion present but decreased as compared to the normal thyroid parenchyma; 2. normal or increased—blood flow within the lesion present with the same or increased intensity as compared to the normal thyroid parenchyma; 3. absent—no flow detected within the lesion.

Fine needle aspiration biopsy (FNAB) was performed in all SAT patients using a 23-gauge needle. For cytology, hematoxylin-eosin staining was used for evaluation. The smear was considered as diagnostic if at least five groups of well-preserved follicular cells, containing at least 10 cells each, were visible. Smears were cytologically evaluated, and the presence of multinucleated giant cells together with mononucleated macrophages, and follicular epithelial cells against acute and chronic inflammatory dirty background was considered as a result typical for SAT. Cytological confirmation of microcalcification was possible if characteristic violet calcium salt deposit was visible in hematoxylin-eosin stained FNAB material.

All patients were divided into the following groups according to the HLA haplotype: 1. HLA-B*35 and/or HLA-C*04, but without any other of the analyzed antigens; 2. HLA-DRB1*01, regardless of the co-presence of HLA-B*35 or C*04:01, but without HLA-B*18:01; 3. HLA-B*18:01 only, without any other of the analyzed antigens; 4. HLA-B*18:01 plus B*35, regardless of the presence of any other analyzed antigens.

For each HLA group the difference in US pattern of SAT thyroid lesions between this group and all the remaining cases was analyzed. Additionally, a pair-wise comparison was also done for every possible pair of groups. Statistical analysis of several

TABLE 2 | Comparison of sonographic features of the SAT lesions in pairs of the analyzed groups.

Sonographic feature	*p*-value for groups 1 and 2	*p*-value for groups 1 and 3	*p*-value for groups 1 and 4	*p*-value for groups 2 and 3	*p*-value for group 2 and 4	*p*-value for groups 3 and 4
Echogenicity	0.541	0.414	0.372	0.283	0.242	1.000
Strongly heterogenous	0.777	**0.034**	0.968	0.121	0.869	0.137
Microcalcifications	0.521	0.649	0.618	1.000	1.000	1.000
Shape	0.688	0.598	0.084	0.257	0.108	0.082
Margin	0.497	0.651	0.193	0.134	0.064	0.329
Bilateral	0.350	**0.003**	0.294	0.067	0.137	**0.006**
Whole lobe affected	0.490	**0.004**	0.714	0.060	0.982	0.079
Nodule-like pattern	0.849	0.513	0.519	0.464	0.696	0.338
Blurred areas	0.490	0.177	0.569	0.099	0.330	0.338
Separated areas	0.735	0.317	0.081	0.264	0.137	**0.026**
Single/multiple areas	0.647	**0.003**	0.294	**0.007**	0.424	**0.006**
Vascularity						
Decreased	0.647	0.221	0.968	0.171	0.696	0.387
Normal	0.252	0.414	0.759	1.000	0.182	0.338
Absent	0.490	**0.014**	0.618	0.171	0.424	0.087

$p < 0.05$ was considered as statistically significant.
*Group 1. HLA-B*35 and/or HLA-C*04, but without any other of the analyzed antigens;*
*Group 2. HLA-DRB1*01, regardless of the co-presence of HLA-B*35 or C*04:01, but without B*18:01;*
*Group 3. HLA-B*18:01 only, without any other analyzed antigen;*
*Group 4. HLA-B*35 plus B*18, regardless of the presence of any other analyzed antigens.*

US SAT features was performed for each group individually. The respective variables were mostly categorical, usually concerning the presence/absence of a particular feature. SAT lesion size was the only numerical parameter, for which descriptive statistics, including mean, standard deviation, minimum and maximum values, were computed in each group. Student's *t*-test was applied to determine the statistical significance of the differences between groups, while for the categorical variables chi-square test was used for this purpose. In all the tests the value of $p < 0.05$ was considered significant.

Written informed consents for all the performed procedures were obtained from all the patients.

The study was approved by Local Medical Ethics Committee.

RESULTS

General Sonographic Characteristics

Hypoechogenicity of SAT lesions was characteristic for all the cases, and in 5 patients (11%) SAT lesions were deeply hypoechoic. Among 46 patients, in 36 (78.3%) the SAT lesions were strongly heterogeneous, and in 10 (21.7%) they were rather homogeneous in their hypoechogenicity. Microcalcifications (confirmed cytologically) were present in one case only (2.2%). The mean size of SAT lesions was 38.2 mm (ranging from 9 to 70 mm). In 27 patients (58.7%) the SAT lesion/lesions completely filled one or both of the thyroid lobes. In patients in whom the SAT lesion did not fill the whole affected lobe, the shapes of the lesions were as follows: oval—in 69.2%, patchy—in 23.1% and round—in 7.7%, while the margins were blurred in 80.8%, lobulated—in 11.5% and smooth—in 7.7%. SAT lesions were bilateral in 76% and unilateral in 24%. The SAT lesions resembled thyroid nodules in 8.7%. Among SAT-typical areas, in 19.6% of the cases there was one isolated area corresponding to tender palpable nodule. In all the remaining cases the areas were multiple. The vascularization of SAT lesions were decreased in 82.6% of the cases, normal or increased in 8.7% and absent in 8.7%.

HLA-Dependent Sonographic Characteristics

All the evaluated SAT features in the analyzed groups have been presented in **Table 1**, along with the comparison of every single group with all the other subjects. Comparisons between individual groups have been presented in **Table 2.**

The US images of SAT lesions in Groups 1 and 2 were similar (**Table 1**), with no statistically significant differences between these two Groups (**Table 2**). The typical SAT features for these Groups were as follows: hypoechoic (88% in Group 1 vs. 80% in Group 2), strongly heterogeneous (84 vs. 80%), bilateral (84 vs. 70%), multiple (84 vs. 90%) areas, with decreased vascularization (84 vs. 90%), usually oval (73.3 vs. 66.7%) with blurred margins (80 vs. 100%), infrequently affecting the whole lobe (48 vs. 70%), rarely with nodule-like pattern (8 vs. 10%) (**Figure 1**).

Several features of Group 3 were different from the other groups (**Tables 1**, **2**). In only 40% of the cases, lesions were strongly heterogeneous ($p = 0.028$ as compared to the other groups), while in 60% they were rather homogenous, and in 100% hypoechoic. Only 20% of these patients had bilateral lesions ($p = 0.002$ as compared to other groups), but in 80% of them there was only one single SAT area ($p < 0.0005$ as compared to other groups), filling the whole affected

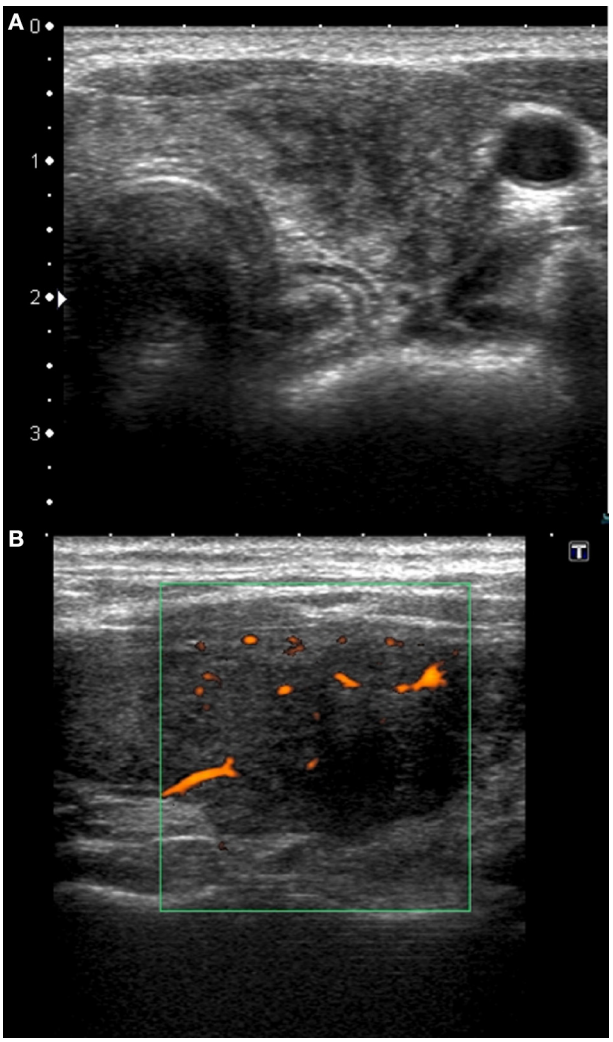

FIGURE 1 | Typical sonographic patterns of SAT in patients with HLA-B*35, C*04:01, and DRB1*01, without HLA-B*18:01. **(A)** Hypoechoic, strongly heterogeneous, areas with poorly defined margins; **(B)** hypoechoic blurred areas with decreased or absent vascularization.

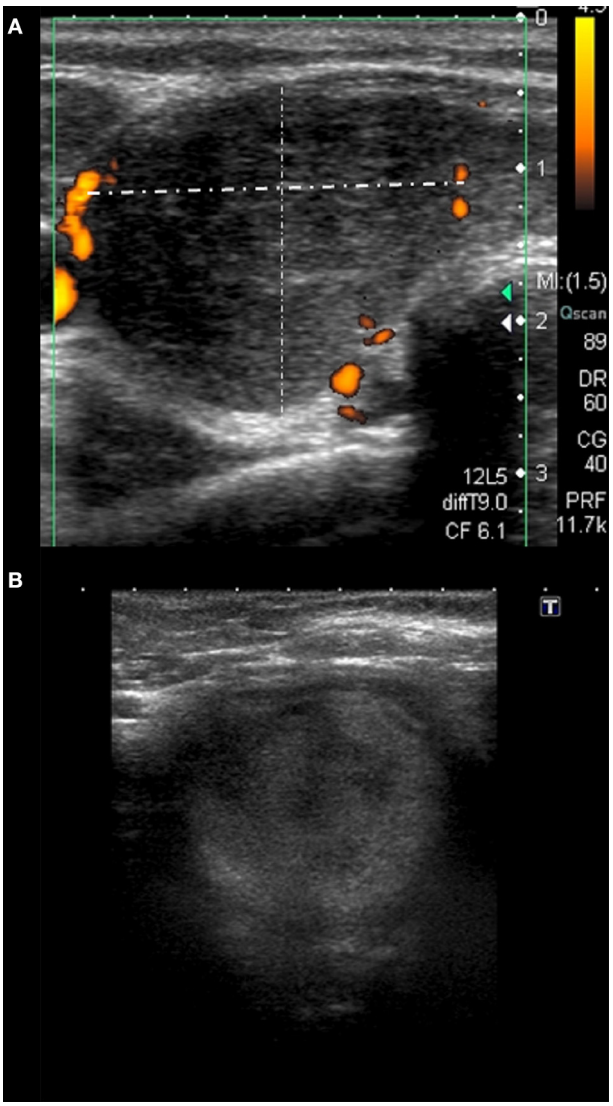

FIGURE 2 | Different sonographic pattern observed in patient with HLA-B*18:01 only. **(A)** Homogeneously hypoechoic single area filling the whole right lobe; **(B)** moderately hypoechoic single SAT area filling the whole thyroid lobe, mimicking a nodule affecting the whole lobe.

lobe ($p = 0.003$, as compared to other groups) (**Figure 2**). In Group 3, the vascularization was absent in as much as 40% of patients, although the difference was statistically significant only in comparison with Group 1 ($p = 0.014$). Other US findings were similar as in the other groups (**Tables 1**, **2**). In contrast to all other groups, in Group 4 no lesion was oval in shape ($p = 0.027$ as compared to other groups). Other differences were not statistically significant (**Tables 1**, **2**).

In comparison of both HLA-B*18:01-positive Groups (3 and 4), significant differences were observed in lateralization, as 80% of the patients in Group 3 had unilateral lesions, while 100% of the patients in Group 4 had bilateral lesions ($p = 0.006$) (**Table 2**). Moreover, single (80%), separated (60%) areas were typical for Group 3, while these features were absent in Group 4 ($p = 0.006$ and $p = 0.026$, respectively) (**Table 2**).

There were no statistically significant differences in the SAT lesion size between the groups (**Table 3**).

DISCUSSION

Ultrasound evaluation plays an important role in the diagnostic process and in monitoring of SAT. Clinical SAT symptoms may be non-characteristic and US examination helps to make the proper diagnosis. The typical sonographic findings of SAT are bilateral or unilateral, focal or multifocal, poorly defined hypoechoic areas (5, 6, 11, 12) in the enlarged thyroid gland. In some cases, nodular lesions can be observed, sometimes mimicking thyroid malignancy (13, 14). SAT lesions were

TABLE 3 | Size of the SAT lesions in the analyzed group of patients.

	Mean (mm)	SD	Min (mm)	Max (mm)	*p*-value*
Group 1	38.13	16.94	9.0	70.0	0.934
Group 2	34.10	15.99	13.0	62.0	0.361
Group 3	42.40	15.66	25.0	66.0	0.564
Group 4	42.67	14.84	19.0	63.0	0.471

**As compared to all other groups.*
$p < 0.05$ was considered as statistically significant.
*Group 1. HLA-B*35 and/or of HLA-C*04, but without any other of the analyzed antigens;*
*Group 2. HLA-DRB1*01, regardless of the co-presence of HLA-B*35 or C*04:01, but without B*18:01;*
*Group 3. HLA-B*18:01 only, without any other analyzed antigen;*
*Group 4. HLA-B*35 plus B*18, regardless of the presence of any other analyzed antigens.*
max, maximum size; min, minimum size; SD, standard deviation.

typically hypoechoic in all our cases, and in 5 patients (11%) they were even deeply (markedly) hypoechoic. Lee and Kim (11) observed markedly hypoechoic lesions only in patients with the nodule-like US pattern of SAT. On the contrary, in our group, all markedly hypoechoic lesions were blurred areas, while all nodule-like lesions were moderately hypoechoic. These discrepancies are most probably the result of different criteria of lesion qualification as nodule-like one, since Lee and Kim described nodular US pattern of SAT as more frequent than non-nodular (11). In our study, SAT lesions resembled thyroid nodules only in 8.7%, and all the remaining lesions were non-nodular areas. Similarly to other authors' observations (5, 6, 12), most of the SAT lesions (78.3%) were strongly heterogeneous and microcalcifications were an extremely rare finding.

The mean size of the SAT lesions was 38.2 mm (ranging from 9 to 70 mm). Similar size range was observed by Vural et al. (6) who described lesions sized 7–75 mm in a group of 20 SAT patients, reporting also that the largest lesions filled the whole thyroid lobe, sometimes even together with isthmus. In our cohort, 58.7% of the patients had lesions that completely filled one or both thyroid lobes. In patients, in whom the SAT lesion did not fill the whole affected lobe, the lesions had various shapes. In our study, oval lesions were the most common type, occurring in 69.2%, while patchy, and round lesions constituted 23.1 and 7.7%, respectively. Lee and Kim (11) reported all non-nodular lesions as patchy in shape, and round areas were not observed.

Bilateral occurrence of SAT lesions is common, usually exceeding 70% of patients (5, 11, 12) and in our study the prevalence of bilateral SAT lesions was 76%. Interestingly, Park et al. (15) demonstrated the presence of bilateral SAT lesions only in 14.8% of patients. This discrepancy in the scale of thyroid involvement, as compared to our observations, may result from the lower SAT severity in the study group analyzed by Park et al. (15), as compared to ours. This conclusion seems to be supported by the fact that the ESR in the group of Park et al. (15) was only slightly elevated, with a mean value of 37 mm/hr (normal range 0–20), and in 25% of the patients the ESR was even normal, which can question SAT diagnosis in the cases without elevated ESR. For comparison, in our group, all the patients had elevated ESR, and the mean value was 66 mm/h, with the upper normal limit of 12 mm/h (data not presented in this paper).

The vascularization of SAT lesions is usually decreased (82.6% of our cases) or even absent (8.7% of our cases) although several authors reported normal to increases blood flow in a few SAT lesions, as well (11, 12, 16). Prior studies suggested that decreased vascularization is typical for the acute SAT phase and the increased blood flow is a feature of the recovery phase (12, 16). However, this explanation cannot be applied to our patients, because the analyzed US image was the first one, performed to diagnose the disease in the acute phase (confirmed by increased inflammation markers, including markedly increased ESR in all the cases), and yet we observed increased or normal vascularization in 8.7% of patients.

The occurrence of SAT is associated with genetic predisposition, encoded in the sixth chromosome fragment responsible for the HLA tissue compatibility antigen system. Correlation between SAT and HLA-B*35 has widely been described (8, 17–22) but the genetic SAT background in HLA-B*35-negative patient was unknown. Recently, the strong association between SAT and HLA-B*18:01, DRB1*01 and HLA-C*04:01 was demonstrated by our study team (Stasiak et al., under review) and—therefore—currently the HLA-dependent background of SAT is possible to be determined in almost all patients.

No data regarding the association of HLA haplotype and US pattern of SAT was available, because until recently, only HLA-B*35 was unequivocally considered to be a genetic SAT background. In most studies analyzing this relationship, no US examination was performed, or no description of the sonographic findings was available. The first reports on the relationship of SAT and HLA-B*35 date back to the 1970's, when the US examination was not widely available. The authors of the subsequent articles regarding the significance of HLA-B*35 in SAT used RAIU in the diagnosis of the disease, or the diagnosis was based only on the clinical presentation, elevated ESR and laboratory features of thyrotoxicosis (8, 17–20, 22). Therefore, only very few thyroid US images are described in SAT patients with confirmed presence of HLA-B*35. Hamaguchi et al. (21) reported HLA-B*35-positive twins with SAT, in whom the thyroid was enlarged in US, with unilateral hypoechoic areas corresponding to tender, firm, palpable nodules. Unfortunately, no details concerning the size or shape of the areas were provided (21). In our study, HLA-B*35 and HLA-C*04:01 were analyzed together in the same group, as HLA-C*04:01 is in linkage disequilibrium with HLA-B*35. The typical sonographic pattern for this group included multiple hypoechoic, strongly heterogeneous, areas, with decreased vascularization, usually oval, with blurred margins, infrequently affecting the whole lobe. In contrast to the observations of Hamaguchi et al. (21), in our Group 1 SAT lesions were often bilateral (84%). It should be stressed, however, that a single description of identical twins cannot be compared to the analysis of our group, containing 25 patients. The US pattern of SAT lesions in our Group 1 corresponds to the typical SAT sonographic findings. Interestingly, the same typical pattern was found in HLA-DRB1*01-positive group, although this haplotype belongs to class II of the major histocompatibility complex (MHC), while all other HLA-related SAT risk haplotypes belong to class I MHC. It could have been expected that the main differences in the US image should be found between haplotypes

from various MHC classes. However, it seems that the effect of haplotypes HLA-B*35, C*04:01 and DRB1*01 on the US image of SAT lesions is similar.

It is worth noticing that no statistically significant differences in patient age between the analyzed four groups has been found (data not presented in the present paper). Recently Vita et al. (23) reported that among patients with remission of Graves' disease, carriers of the alleles B35 or DR1 (serotyping) were the youngest and the oldest, respectively. However, the peak incidence age is different for each of the two diseases, and therefore discrepancies in age-dependence are expectable.

The presence of HLA-B*18:01 seems to be a key factor that changes the thyroid US image in SAT, because the differences in sonographic findings are expressed most strongly in patients with HLA-B*18:01 only. Less expressed differences from the typical SAT US pattern are visible in patients with the coexistence of HLA-B*18:01 and B*35, while in patients without HLA-B*18:01 sonographic findings are SAT-typical. Several features of SAT lesions in patients with the presence of HLA-B*18:01 only were different from patients without HLA-B*18:01 haplotype or even from patients with simultaneous presence of HLA-B*18:01 and B*35. In most cases with HLA-B*18:01 only, there was unilateral homogenously hypoechoic single SAT area, which filled the whole affected lobe, mimicking the large thyroid nodule. Vascularization of these lesions was SAT-typical—decreased or frequently absent. In patients with co-presence of HLA-B*18:01 and B*35, the main difference, as compared to the other groups, concerned the shape of the SAT lesions. In the whole group of our patients, the most common SAT lesion shape was oval, but no lesion in HLA-B*18:01 plus B*35 patients was oval in shape. The lesions were patchy or round—the latter shape being very rare in SAT lesions.

Our results have clearly shown that the presence of HLA-B*18:01 is the main factor changing the typical SAT sonographic pattern to a different one. The co-occurrence of HLA-B*35 reduces many of the above described differences, although the presence of HLA-B*18:01 still alters the US pattern, which remains—to some extent—different from the one typical for SAT. It is to be noted that the differences between the US image in HLA-B*18:01-positive patients with and without HLA-B*35 are very significant. Firstly, in 80% of patients with HLA-B*18:01 only, SAT lesions were unilateral, while in patients with additional presence of HLA-B*35 all lesions were bilateral. Secondly, in the HLA-B*18:01 group, most lesions were single, separated, homogenously hypoechoic areas filling the whole thyroid lobe, while for patients with HLA-B*18:01 and B*35, multiple heterogeneous areas were a typical US finding. Now, it is difficult, to speculate why the occurrence of HLA-B*18:01 changes the US SAT image in such a great extent. Perhaps the decisive role is played by subpopulations of immune cells that are involved in the inflammatory process in SAT. The presence on the cell membrane of MHC class I molecules presenting own peptides that resemble pathogen antigens increases the risk of antigen presentation, effector cell activation and the occurrence of the inflammatory process. Further research is required to precisely explain this phenomenon—first of all, our future work will focus on evaluation of the inflammatory cells subpopulation in the FNAB material obtained in the active phase of SAT inflammation in patients with particular HLA haplotypes.

When analyzing the conclusions drawn on the basis of the obtained results, the limitations of this study should be taken into account. Firstly, it should be noted that all the patients taking part in the study were Caucasians, and the direct transposition of the obtained results to other populations may not be fully possible. Secondly, ultrasound examination was performed by the authors, so it was not blinded for SAT diagnosis. However, it was fully blinded for HLA antigens, because no HLA results were known at the time of US examination in the acute phase of the disease. Moreover, the pathology review was unblinded as the suspicion of SAT was always stated on the cytology request form. Additionally, the analysis of the obtained data must be done with care in regard to the statistical significance, as—despite the relatively large number of the analyzed parameters—no correction for multiple comparisons was applied. However, in most of the cases marked bold in **Tables 1**, **2** we can assume that the presented *p*-values indicate the true, existing differences between the groups with high probability.

In conclusion, our results provide for the first time evidence that the US image of SAT depends on HLA haplotype, and the determining factor is the presence of HLA-B*18:01. The deviations from the typical SAT US image are mostly pronounced in patients with the presence of only HLA-B*18:01, without any other analyzed haplotypes. Further research is necessary to explain the cause of this phenomenon.

ETHICS STATEMENT

This study was carried out in accordance with the recommendations of WHO Standards and operational guidance for ethics review of health-related research with human participants with written informed consent from all subjects. All subjects gave written informed consent in accordance with the Declaration of Helsinki. The protocol was approved by the Ethics Committee of the Polish Mother's Memorial Hospital—Research Institute, Lodz, Poland.

AUTHOR CONTRIBUTIONS

MS was responsible for study design, data collection, data analysis, and writing of the manuscript. BT, ZA, and BS contributed to data collection and data analysis. AL contributed to study design, and writing of the manuscript. All authors were involved in writing the paper and approved the submitted final versions.

FUNDING

The study was financially supported by the statutory funds from the Polish Mother's Memorial Hospital—Research Institute, Lodz, Poland, and from the Medical University of Lodz, Lodz, Poland 503/1-107-03/503-11-001-18.

REFERENCES

1. Samuels MH. Subacute, silent, and postpartum thyroiditis. *Med Clin North Am.* (2012) 96:223–33. doi: 10.1016/j.mcna.2012.01.003
2. Stasiak M, Michalak R, Stasiak B, Lewinski A. Clinical characteristics of subacute thyroiditis is different than it used to be – current state based on 15 years own material. *Neuro Endocrinol Lett.* (2018) 39.
3. Alfadda AA, Sallam RM, Elawad GE, Aldhukair H, Alyahya MM. Subacute thyroiditis: clinical presentation and long term outcome. *Int J Endocrinol.* (2014) 2014:794943. doi: 10.1155/2014/794943
4. Fatourechi V, Aniszewski JP, Fatourechi GZ, Atkinson EJ, Jacobsen SJ. Clinical features and outcome of subacute thyroiditis in an incidence cohort: Olmsted County, Minnesota study. *J Clin Endocrinol Metab.* (2003) 88:2100–5. doi: 10.1210/jc.2002-021799
5. Cappelli C, Pirola I, Gandossi E, Formenti AM, Agosti B, Castellano M. Ultrasound findings of subacute thyroiditis: a single institution retrospective review. *Acta Radiol.* (2014) 55:429–33. doi: 10.1177/0284185113498721
6. Vural Ç, Paksoy N, Gök ND, Yazal K. Subacute granulomatous (De Quervain's) thyroiditis: fine-needle aspiration cytology and ultrasonographic characteristics of 21 cases. *Cytojournal* (2015) 12:9. doi: 10.4103/1742-6413.157479
7. Ruchala M, Szczepanek-Parulska E, Zybek A, Moczko J, Czarnywojtek A, Kaminski G et al. The role of sonoelastography in acute, subacute and chronic thyroiditis: a novel application of the method. *Eur J Endocrinol.* (2012) 166:425–32. doi: 10.1530/EJE-11-0736
8. Nyulassy S, Hnilica P, Buc M, Guman M, Hirschová V, Stefanovic J. Subacute (de Quervain's) thyroiditis: association with HLA-Bw35 antigen and abnormalities of the complement system, immunoglobulins and other serum proteins. *J Clin Endocrinol Metab.* (1977) 45:270–4.
9. Ohsako N, Tamai H, Sudo T, Mukuta T, Tanaka H, Kuma K, et al. Clinical characteristics of subacute thyroiditis classified according to human leukocyte antigen typing. *J Clin Endocrinol Metab.* (1995) 80:3653–6. doi: 10.1210/jcem.80.12.8530615
10. Kobayashi N, Tamai H, Nagai K, Matsubayashi S, Matsuzuka F, Kuma K, et al. Studies on the pathogenesis of subacute thyroiditis. *Nihon Naibunpi Gakkai Zasshi* (1985) 61:737–43. doi: 10.1507/endocrine1927.61.7_737
11. Lee YJ, Kim DW. Sonographic characteristics and interval changes of subacute thyroiditis. *J Ultrasound Med.* (2016) 35:1653–9. doi: 10.7863/ultra.15.09049
12. Frates MC, Marqusee E, Benson CB, Alexander EK. Subacute granulomatous (de Quervain) thyroiditis: grayscale and color Doppler sonographic characteristics. *J Ultrasound Med.* (2013) 32:505–11. doi: 10.7863/jum.2013.32.3.505
13. Zacharia TT, Perumpallichira JJ, Sindhwani V, Chavhan G. Gray-scale and color Doppler sonographic findings in a case of subacute granulomatous thyroiditis mimicking thyroid carcinoma. *J Clin Ultrasound.* (2002) 30:442–4. doi: 10.1002/jcu.10087
14. Park HK, Kim DW, Lee YJ, Ha TK, Kim DH, Bae SK, et al. Suspicious sonographic and cytological findings in patients with subacute thyroiditis: two case reports. *Diagn Cytopathol.* (2015) 43:399–402. doi: 10.1002/dc.23230
15. Park SY, Kim EK, Kim MJ, Kim BM, Oh KK, Hong SW, et al. Ultrasonographic characteristics of subacute granulomatous thyroiditis. *Korean J Radiol.* (2006) 7:229–34. doi: 10.3348/kjr.2006.7.4.229
16. Hiromatsu Y, Ishibashi M, Miyake I, Soyejima E, Yamashita K, Koike N, et al. Color Doppler ultrasonography in patients with subacute thyroiditis. *Thyroid* (1999) 9:1189–93. doi: 10.1089/thy.1999.9.1189
17. Yeo PP, Chan SH, Aw TC, Lui KF, Rauff A, Mathew T, et al. HLA and Chinese patients with subacute (De Quervain's) thyroiditis. *Tissue Antigens* (1981) 17:249–50. doi: 10.1111/j.1399-0039.1981.tb00694.x
18. Goto H, Uno H, Tamai H, Kuma K, Hayashi Y, Matsubayashi S, et al. Genetic analysis of subacute (de Quervain's) thyroiditis. *Tissue Antigens* (1985) 26:110–3. doi: 10.1111/j.1399-0039.1985.tb00942.x
19. Tamai H, Goto H, Uno H, Sasazuki T, Kuma K, Hayashi Y, et al. HLA in Japanese patients with subacute (De Quervain's) thyroiditis. *Tissue Antigens* (1984) 24:58–9. doi: 10.1111/j.1399-0039.1984.tb00398.x
20. Zein EF, Karaa SE, Megarbane A. Familial occurrence of painful subacute thyroiditis associated with human leukocyte antigen-B35. *Presse Med.* (2007) 36:808–9. doi: 10.1016/j.lpm.2007.02.011
21. Hamaguchi E, Nishimura Y, Kaneko S, Takamura T. Subacute thyroiditis developed in identical twins two years apart. *Endocr J.* (2005) 52:559–62. doi: 10.1507/endocrj.52.559
22. Kramer AB, Roozendaal C, Dullaart RP. Familial occurrence of subacute thyroiditis associated with human leukocyte antigen-B35. *Thyroid* (2004) 14:544–7. doi: 10.1089/1050725041517048
23. Vita R, Lapa D, Trimarchi F, Vita G, Fallahi P, Antonelli A, et al. Certain HLA alleles are associated with stress-triggered Graves' disease and influence its course. *Endocrine* (2017) 55:93–100. doi: 10.1007/s12020-016-0909-6

Conflict of Interest Statement: The authors declare that the research was conducted in the absence of any commercial or financial relationships that could be construed as a potential conflict of interest.

frontiers in Endocrinology

ORIGINAL RESEARCH
published: 11 March 2019
doi: 10.3389/fendo.2019.00127

Integration of Sonoelastography Into the TIRADS Lexicon Could Influence the Classification

Katarzyna Sylwia Dobruch-Sobczak[1,2], Agnieszka Krauze[3], Bartosz Migda[3], Krzysztof Mlosek[3], Rafał Zenon Słapa[3], Elwira Bakuła-Zalewska[4], Zbigniew Adamczewski[5,6], Andrzej Lewiński[5,6], Wiesław Jakubowski[3] and Marek Dedecjus[7]*

[1] Radiology Department II, The Maria Sklodowska-Curie Memorial Cancer Center and Institute of Oncology, Warsaw, Poland, [2] Ultrasound Department, Institute of Fundamental Technological Research, Polish Academy of Science, Warsaw, Poland, [3] Department of Imaging Diagnostics, Medical University of Warsaw, Warsaw, Poland, [4] Department of Pathology, The Maria Sklodowska-Curie Memorial Cancer Center and Institute of Oncology, Warsaw, Poland, [5] Department of Endocrinology and Metabolic Diseases, Medical University of Lodz, Łódź, Poland, [6] Department of Endocrinology and Metabolic Diseases, Research Institute, Polish Mother's Memorial Hospital, Łódź, Poland, [7] Department of Oncological Endocrinology and Nuclear Medicine, The Maria Sklodowska-Curie Memorial Cancer Center and Institute of Oncology, Warsaw, Poland

OPEN ACCESS

Edited by:
Joanna Klubo-Gwiezdzinska, National Institutes of Health (NIH), United States

Reviewed by:
Trevor Edmund Angell, University of Southern California, United States
Miloš Žarković, University of Belgrade, Serbia

***Correspondence:**
Katarzyna Sylwia Dobruch-Sobczak
kdsobczak@gmail.com

Specialty section:
This article was submitted to Thyroid Endocrinology, a section of the journal Frontiers in Endocrinology

Received: *02 December 2018*
Accepted: *11 February 2019*
Published: *11 March 2019*

Citation:
Dobruch-Sobczak KS, Krauze A, Migda B, Mlosek K, Słapa RZ, Bakuła-Zalewska E, Adamczewski Z, Lewiński A, Jakubowski W and Dedecjus M (2019) Integration of Sonoelastography Into the TIRADS Lexicon Could Influence the Classification. Front. Endocrinol. 10:127. doi: 10.3389/fendo.2019.00127

Aim: Numerous TIRADS (Thyroid Image Reporting and Data System) classifications have been developed, and various ultrasound (US) parameters are employed in different countries. The aim of our study was to introduce risk classification and management in a native population based on the Guidelines of Polish National Societies Diagnostics and Treatment of Thyroid Carcinoma but with the addition of sonoelastography.

Materials and Methods: We examined prospectively 208 patients with 305 thyroid lesions employing B-mode ultrasound and sonoelastography (SE). Nodule composition, echogenicity, margins, shape, presence or absence of calcifications, thyroid capsule, nodule size were assessed using B-mode ultrasound. Moreover, sonoelastography results were presented using the Asteria scale.

Results: In univariate analysis, the following US features were significantly associated with malignancy: >50% solid /solid component, marked hypoechogenicity, ill-defined margins, micro and macrocalcification, taller-than wide shape, no/partial halo pattern, infiltration of the capsule and an Asteria score of 4. Multivariate logistic regression analysis of B-mode features revealed that ill-defined margins (OR 10.77), markedly hypoechogenicity (OR 5.12), microcalcifications (OR 4.85), thyroid capsule infiltrations (OR 3.2), macrocalcifications (OR 3.01), and hard lesion in SE (OR 6.85) were associated with a higher Odds Ratio (OR) for malignancy. Multivariate logistic regression analysis revealed that combining two features increases the OR and the best combination was irregular margins and Asteria scale 4 (OR 20.21). Adding a third feature did not increase the OR.

Conclusions: Sonoelastography increases the value risk of predicted malignancy, with consequent different approach to further clinical investigation and management. A solitary feature (Asteria 4) in a solid tumor can result in its categorization as TIRADS 4, but coexistence with high risk features allows it to be upgraded to TIRADS 5. The irregular

margin was the strongest single feature which allowed for the assignment of a solid tumor into TIRADS 5 category. The highest accuracy was found by combining the features of age, margin, echogenicity (markedly hypoechoic), capsule infiltration, microcalcifications and sonoelastography (Asteria 3,4) of the tumors.

Keywords: TIRADS classification, thyroid cancer, thyroid nodules, ultrasonography, sonoelastography

INTRODUCTION

In Poland, 3,529 new cases of thyroid cancer were diagnosed in 2015. The annual incidence rate has increased from 3.8 per 100,000 in 2000 to 9.2 per 100,000 in 2015 (1, 2). Therefore, it is crucial to increase the accuracy of detection and surveillance in patients with thyroid disease.

Ultrasound examination (US) significantly improves the detection of thyroid nodules. According to reports in the literature, the percentage of thyroid nodules in adult patient's ranges from 33 to 68% and is higher when using higher frequency probes (1, 3). Most of these lesions are benign and reports indicate that malignant tumors below 10 mm in size are often characterized by non-aggressive behavior (2, 4), supporting the need for non- and minimally invasive diagnostic tools in patients with thyroid nodules. Currently, numerous recommendations for the risk stratification of thyroid nodules and their management are available in the literature (5–8). Most often, confirmation of the suspicious character of the nodule requires a cytological examination of the material using a fine needle aspiration biopsy (FNAB) which is the preferred the first line confirmatory investigation. Depending on the risk of malignancy in thyroid nodules, pathological verification may be recommended and a clinical decision in favor of surgery made (8). Currently, US, in combination with FNAB are considered to be the principle diagnostic tools for the diagnosis of thyroid nodules (9–12).

However, the use of US in the differentiation of malignant and benign lesions is characterized by low specificity (13). Moreover, lesions without suspicious ultrasound features, <10 mm in size, without additional clinical factors to suggest increased risk such as the presence of metastatic lymph nodes or distant metastases, neck radiation in the past, family history of thyroid cancer, appearance of a thyroid nodule before 20 or after 60 years of age or significant increase in nodule size, could be observed conservatively without proceeding with FNAB (8, 10, 14).

Currently, the basic US technique used to assess thyroid nodules is gray-scale imaging (B-mode). The features that are suspicious of malignancy in terms of US B-mode include solid composition, low or markedly low echogenicity (in relation to thyroid parenchyma and strap muscles); irregular or lobulated margins, vertical shape of the lesion (taller-than-wide) and the presence of microcalcifications and capsule infiltration (10, 15, 16). In recent years, new ultrasound techniques have appeared, such as elastography and ultrasound contrast agents to assess stiffness and micro vascularization of tissues. These techniques improve the diagnostic accuracy of US, but with some limitations (17–22).

An important step in the standardization of the assessment of the malignancy risk in thyroid nodules based on the US examination was the introduction of the TIRADS (Thyroid Imaging Reporting and Data System) classification based on the widely accepted BIRADS classification (Breast Imaging Reporting and Data System). It describes the risk of malignancy of focal lesions on an incremental scale from 0 to 6 (23). TIRADS was first proposed in 2009 (24, 25) and was the subject of further refinement in the following years (26–29). Different TIRADS classifications were published in the literature (25–27). The most recent two were proposed by the European Thyroid Association, EU-TIRADS (30), and by the American College of Radiology, ACR-TIRADS (31, 32). The above recommendations are based on a current review of the literature and expert opinion. However, there are some differences in these recommendations, even though they both utilized similar US features for predicting malignancy. In the ACR-TIRADS, experts assessed (on a scale 1–3 points, where 3 points are given for the highest risk of malignancy) the composition, echogenicity, shape, margins and the presence of echogenic foci. As an example, for the lesion to be categorized as TIRADS 5, at least 7 points are required in total. In the EU-TIRADS, it is sufficient to identify one of the high-risk US features (non-oval shape, irregular margins, microcalcification and marked hypoechogenicity) to categorize a nodule as TIRADS 5. In both guidelines sonoelastography (SE) may be used as a complementary tool for assessing nodules for FNAB but they do not precise how integrate them into risk stratification system.

In our country, Guidelines of Polish National Societies Diagnostics and Treatment of Thyroid Carcinoma recommend the use of clinical and ultrasound features, including SE (if available), in qualifying for FNAB (8).

Therefore, an attempt was made to introduce new TIRADS classification and assessment the risk of malignancy in thyroid nodules with the addition of sonoelastography in a group of polish patients.

MATERIALS AND METHODS

Patients

In this prospective study, patients gave informed consent to participate in the research, and the institutional Review Board of the Maria Sklodowska-Curie Institute–Cancer Center, Warsaw, Poland (MSCI) approved the study. From May 2014 to November 2017, 208 patients (54 men, 154 women) with a total of 305 thyroid nodules were included in the study. The US examinations were conducted in the Department of Oncological Endocrinology and Nuclear Medicine MSCI and in Department of Imaging Diagnostics at the Medical University of Warsaw.

The inclusion criteria for the study were a thyroid nodule with suspicious features on US examination or a nodule after US-guided FNAB (according to the Guidelines of Polish National Societies) (8), with Bethesda IV-VI results and patients with Bethesda II with clinical symptoms. The exclusion criteria for the study were completely cystic lesions, lesions with eggshell calcifications, or lesions with non-diagnostic cytology results. The researchers during examination and assessment the B-mode films were blinded—not aware neither of the FNAB nor histological results. We did not use the TIRADS classification and elastography as a criterion which qualified the patient to the surgery.

Histology

Out of 305 nodules, 126 were single nodules (126 patients), and multiple nodules (179) were found in the remaining 82 patients. Histological verification was performed in 153 thyroid nodules (including all CV-CVI lesions), and cytological confirmation was performed in 152 thyroid nodules. Histological and cytological findings were used as study endpoints. All patients with cytological confirmation of malignancy were verified by histological examination after surgery. For patients with benign FNAB results, US follow-up examination was performed within 6 months. FNABs were performed with the capillary fill, free hand technique using 22- to 24-gauge needles, and aspirates were immediately fixed in 75% ethanol and stained with haematoxylin and eosin (H&E). The cytological results were reported according to the Bethesda classification I-VI category (CI-CVI) (33). FNAB was repeated for nodules classified as CI, CIII, and small C IV nodule (<10mm). Additionally, 55/207 nodules confirmed as benign (CII) were operated on due to clinical diagnosis of compressive symptoms from an enlarged thyroid.

Cytological results (CV and CVI) were verified by an independent pathologist. The pathologist was blinded to the results of the US examination. Surgical specimens were immediately fixed in 10% buffered formalin. Representative sections from these specimens were processed and routinely stained with H&E for histopathologic (microscopic) examinations.

Conventional B-Mode and US Examinations

Five radiologists, with experience in thyroid B-mode imaging ranging from 6 to 22 years and with experience in US elastography from 1 to 7 years performed the examinations of the thyroid glands and the cervical regions using a 5–12 MHz linear array transducer (iU22 US machine, Philips Medical Systems, Bothell, WA). During the examination, patients were in the supine position. Transverse and longitudinal sections of the lesions were investigated. During the sonoelastography, the US probe was gently placed on the thyroid and examiners avoided pressing on the thyroid with the probe, according to recommended device requirements, to reduce false-positive findings. This SE technique does not require compression and de-compression and is, therefore, operator independent. Radiologists who performed the US examinations prospectively analyzed gray-scale conventional B-mode US, color Doppler (CD) and SE (using Asteria four-point scale criteria) (17).

The following lesion features were assessed in the US examinations according to the Polish Ultrasound Society and Guidelines of Polish National Societies (8).

-composition: solid, almost solid, cystic portion <50%, cystic portion >50%, spongiform (in solid-cystic lesions the echogenicity, margins, spongiform character, angle of the wall and vascularity of the solid part were assessed);
-echogenicity: hyperechoic, isoechoic, hypoechoic—compared to surrounding thyroid tissue and markedly hypoechoic compared to strap muscle;
-margins: well-defined, irregular (spicular, jagged, angular, lobular);
-shape (taller-than-wide—tall/wide, wider-than-tall—wide/tall);
-presence or absence of calcifications (micro- or macrocalcifications) shadowing and comet- tail artifacts;
-color Doppler pattern: peripheral, central, mixed, none;
-thyroid capsule: infiltration, deformation, none;
-nodule size: volume of the nodule;

In order to calculate the volume of nodules, their shape was assumed to be ellipsoidal. The three axes of symmetry for each nodule were determined as the largest lengths of each lesion in three perpendicular directions. The three axes are referred to in the paper as "tall," "wide," and "long." Finally, the volume was calculated using the ellipsoid formula.

$$\left(V = \frac{4}{3}\,\pi\,\frac{\text{tall}}{2}\,\frac{\text{wide}}{2}\,\frac{\text{long}}{2} \right).$$

Strain sonoelastography of the tumors and surrounding tissue was performed after B-mode examinations. The lesions were placed in the middle of the field of view (FOV). After 5–10 s of image stabilization, the 10 s films were recorded, and the radiologists evaluated those records containing transversal and longitudinal B-mode cross sections. Using the color map (where blue indicates hard tissue and red indicates soft tissue), the Asteria scale was reported as following:

-elasticity score (ES)-1: the nodule is displayed homogenously in red; indicating elasticity in the entire lesion;
-elasticity score (ES)-2: the nodule is displayed predominantly in green with a few blue areas/spots; indicating elasticity in a large part of the lesion;
-elasticity score (ES)-3: the nodule is displayed predominantly in blue with a few green areas/spots; indicating stiffness in a large part of the lesion;
-elasticity score (ES)-4: the nodule is displayed completely in blue (hard); indicating a lesion without elasticity;

Finally, after statistical analysis, the US features and the sonoelastography of the nodules were categorized according to independent predictors of malignancy and a new approach for classifying TIRADS risk factors was proposed.

We sorted the tumors into intermediate, high and highest risk of malignancy (TIRADS 3, 4 and 5 categories) according to the

results from statistical analysis (accuracy) of the B-mode features and SE descriptors (**Figure 1**).

Statistical Analysis

Statistical analysis was completed with the STATISTICA v 13.1 software package. Significance level $\alpha = 0.05$ was used for testing of statistical hypothesis.

In the analyzed material for each continuous variable: number, arithmetic mean, standard deviation, median, lower and upper quartile, minimum value, maximum value and skewness and kurtosis coefficients were calculated. For each discrete variable, the number and the structure index were calculated. To compare means, the Student's *t*-test, Mann-Whitney *U* test and one-way analysis of variance were used. Homogeneity variance was tested using *F*-test and Brown-Forsythe's test. Scheffe's test was used as a *post-hoc* test.

Analysis of the interdependencies between a pair of discrete variables was based on the contingency table and calculations for them: row percentages, column percentages and Pearson chi-square independence test values or Fisher's exact test for four-field tables.

Odds ratios (OR) with relative 95% confidence intervals were calculated to determine the relevance of all potential predictors of outcome.

For the assessment of usability of individual US features in differentiation of benign and malignant lesions, using the contingency table, called the classification matrix, sensitivity, specificity, positive predictive value (PPV), negative predictive value (NPV) and accuracy and Youden index were calculated.

The assessment of the impact of individual independent variables on the dichotomous dependent variable based on the logistic regression model (univariate and multivariate analysis) was performed to determine independent predictors of malignancy from US features that showed statistical significance and the power of individual US features.

Finally, benign and malignant lesions were divided into two groups: lesions smaller or equal to 10 mm and those greater than 10 mm, and were compared according to US features.

RESULTS

Patients

A total of 305 thyroid lesions (207 benign, 98 malignant) were identified in 208 patients with mean age 50.4 years (range 15–86 years, SD: 14.73 years). The mean age of the patients with benign lesions was 52.0 years (range 15–82 years, SD; 14.27 years). The mean age of the patients with malignant lesions was 47.8 years (range 20–86 years; SD; 15.22 years). The mean volume of all lesions was 2.67 ml (range 0.01–44.6 ml; SD; 5.51 ml); the mean volumes of malignant and benign lesions were 2.52 ml (range 0.01–28.18ml, SD; 5.08 ml) and 2.73 ml (range 0.03–44.60 ml; SD; 5.70 mm), respectively. There were 126 single nodules and 179

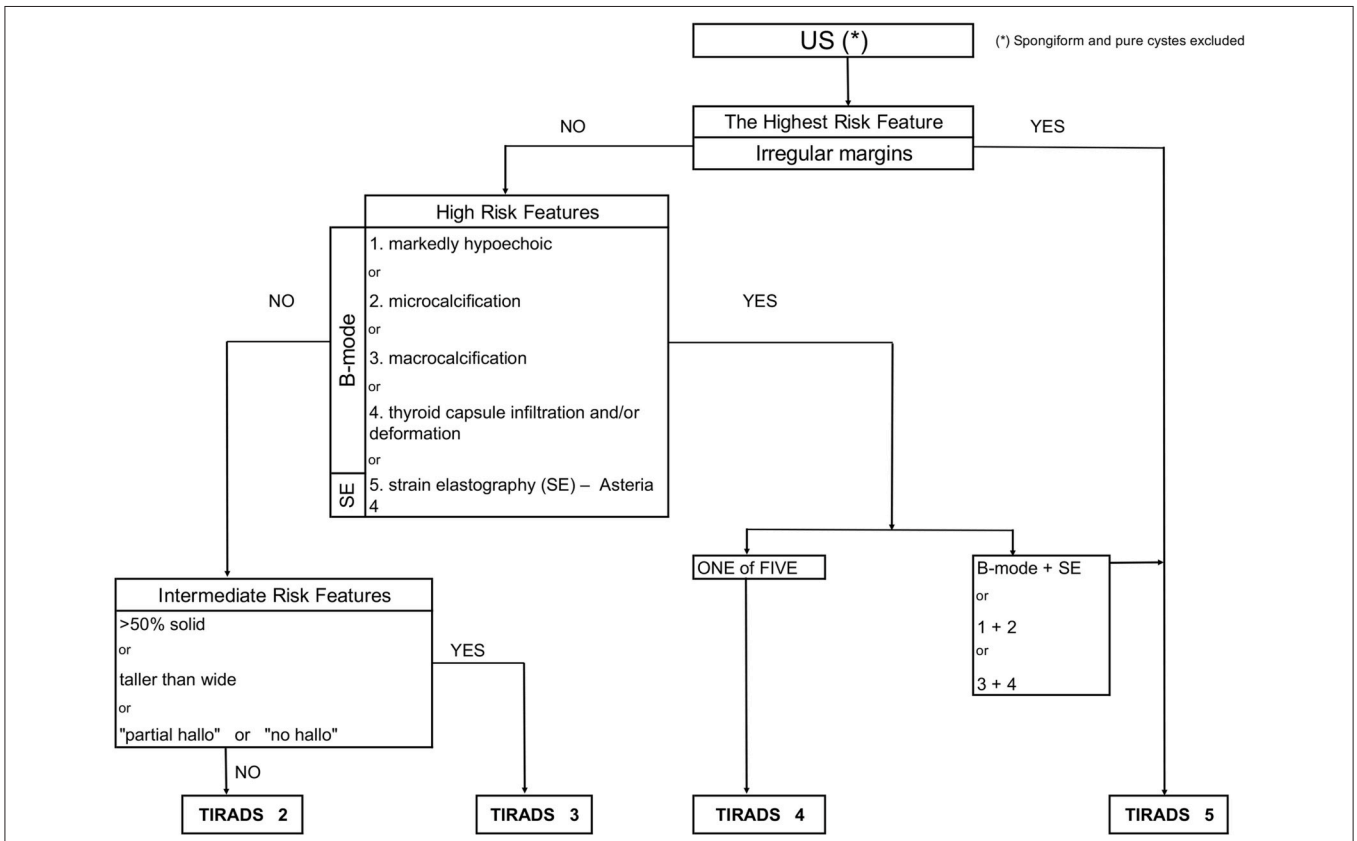

FIGURE 1 | Flowchart concerning the integration of sonoelastography into the modified TIRADS classification.

TABLE 1 | Histopathological and/or cytological results of 305 thyroid lesions.

Pathology	No.
Benign lesions	207
Nodular hyperplasia	181
Adenoma	18
Focal thyroiditis	8
Malignant lesions	98
Papillary carcinoma	81
Follicular variant	5
Follicular carcinoma	9
Medullary carcinoma	8
Total	305

were in a multinodular goiter. The histological and cytological results for the 305 lesions are presented in **Table 1**. The Bethesda category distributions were: VI (18), V (39), IV (35), III (43), II (166), I (24).

Conventional B-Mode US Examination

The data in **Table 2** presents the characteristics of the benign and malignant nodules.

It can be noticed that malignant tumors more often are solid, are taller-than-wide, are hypoechogenic, have irregular margins, have micro- and macrocalcifications, lack halo and are stiff on SE ($p < 0.05$) when compared to benign ones.

Benign lesions were significantly more cystic-solid (>50% solid component), iso-and hyperechoic, with well define margins, wider-than-tall without micro- and macrocalcifications, with halo and deformable on sonoelastography ($p < 0.05$) (**Table 2**).

In univariate analysis, the following US features were significantly associated with malignancy; with sensitivity, specificity and accuracy as follows: >50 solid /solid component (66.39, 46.86, 54.10%), marked hypoechogenicity (28.57, 92.75, 72.13%), ill-defined margins (66.33, 84.54, 78.69%), microcalcification (64.29, 72.95, 70.16%), macrocalcification (38.78, 82.61, 68.52%), taller-than wide shape (68.37, 48.31, 54.75%), no/partial halo pattern (94.90, 21.74, 45.25%), infiltration the capsule (37.75, 84.06, 69.18%) and Asteria 4 score (44.90, 89.37, 75.08%) (**Tables 3**, **4**).

Using ORs (multivariate logistic regression analysis) for the association of significant predictors with the odds of malignant outcome, we determined that irregular margins (OR, 10.77; $p < 0.01$) had the highest OR. Then, marked hypoechogenicity (OR, 5.12; $p < 0.01$), microcalcifications (OR, 4.85; $p < 0.01$), thyroid capsule infiltrations (OR, 3.2; $p < 0.01$), macrocalcifications (OR, 3.01; $p < 0.01$), and hard lesion in SE (Asteria 4) (OR, 6.85; $p < 0.01$) independently predicted the malignancy (**Table 4**).

Using the logistic regression model, we combined the aforementioned features and demonstrated a sensitivity of 67.35%, specificity of 91.30%, PPV of 78.57%, NPV of 85.52%, accuracy of 83.61%, OR of 21.656, and a 95% CI (11.369–41.253).

TABLE 2 | The structure of the US features data; *p*-values produced by chi-square test.

Parameter	Malignant lesion (%)	Benign lesion (%)	*p*-value
Composition			0.004
3= >50%Solid/Solid	68 (38.20)	110 (61.80)	
2= >50%Cystic/Almost Solid	30 (26.32)	84 (73.68)	
1= Cystic/Spongiform	0 (0.00)	13 (100.00)	
Echo pattern (in comparision to muscles)			<0.001
1=Hypoechoic	28 (65.12)	15 (34.88)	
2=Izoechoic	16 (37.21)	27 (62.79)	
3=Hyperechoic	54 (24.66)	165 (75.34)	
Echo pattern (in comparision to thyroid)			<0.001
1=Hypoechoic	85 (39.35)	131 (60.65)	
2=Izoechoic	9 (12.16)	65 (87.84)	
3=Hyperechoic	4 (26.67)	11 (73.33)	
Margins			<0.001
0=Ill-define	65 (67.01)	32 (32.99)	
1=Well-define	33 (15.87)	175 (84.13)	
Tall/wide			0.006
1= Tall/wide >= 1	67 (38.51)	107 (61.49)	
0= Tall/wide < 1	31 (23.66)	100 (76.34)	
Microcalcifications			<0.001
1=Present	63 (52.94)	56 (47.06)	
0=Absent	35 (18.82)	151 (81.18)	
Makrocalcifications			<0.001
1=Present	38 (51.35)	36 (48.65)	
0=Absent	60 (25.97)	171 (74.03)	
Color doppler pattern			0.404
3=Mixed	55 (33.95)	107 (66.05)	
2=Central	11 (28.95)	27 (71.05)	
1=Peripheral	26 (27.96)	67 (72.04)	
0=Absent	6 (50.00)	6 (50.00)	
Thyroid capsule			<0.001
2=Infiltration	12 (92.31)	1 (7.69)	
1=Deformation	25 (43.86)	32 (56.14)	
0=Not disturb	61 (25.96)	174 (74.04)	
"Halo" pattern			<0.001
2=Partial/No	93 (36.47)	162 (63.53)	
1=Yes	5 (10.00)	45 (90.00)	
Asteria scale			<0.001
4	44 (66.67)	22 (33.33)	
3	35 (35.00)	65 (65.00)	
2	16 (14.16)	97 (85.84)	
1	3 (11.54)	23 (88.46)	

Findings of Combined Conventional B-Mode US Features and Combined With SE

To improve the accuracy of predicting malignancy in thyroid lesions, we combined the conventional US B-mode parameters with the results from SE. Multivariate logistic regression analysis revealed that combining two features: margins and Asteria (3,4 score) scale, increased OR to 20.21 (OR for margins

TABLE 3 | Descriptive statistics of B-mode and elastographic parameters discriminating benign from malignant thyroid lesions (PPV, positive predictive value; NPV, negative predictive value; sensitivity, specificity, Youden index, sum-sensitivity+specificity).

Parameter	Youden index	Sensitivity (%)	95% CI (sensitivity)	Specificity (%)	95% CI (specificity)	PPV (%)	95% CI (PPV)	NPV (%)	95% CI (NPV)	Sum
Margins	0.51	66.33	56.51–74.91	84.54	78.99–88.83	67.01	57.16–75.56	84.13	78.56–88.47	302.01
Markedly hypoechoic	0.21	28.57	20.57–38.19	92.75	88.39–95.56	65.12	50.17–77.58	73.28	67.62–78.28	259.72
Microcalcifications	0.37	64.29	54.43–73.07	72.95	66.52–78.54	52.94	44.02–61.68	81.18	74.96–86.15	271.36
Thyroid capsule infiltration	0.22	37.76	28.79–47.64	84.06	78.46–88.42	52.86	41.32–64.10	74.04	68.08–79.23	248.71
Macrocalcifications	0.21	38.78	29.73–48.67	82.61	76.86–87.17	51.35	40.18–62.39	74.03	68.01–79.25	246.76
Asteria scale	0.34	44.90	35.43–54.75	89.37	84.43–92.88	66.67	54.66–76.84	77.41	71.69–82.25	278.34
"Halo" pattern	0.17	94.90	88.61–97.80	21.74	16.66–27.85	36.47	30.80–42.54	90.00	78.64–95.65	243.11
Composition (solid)	0.16	69.39	59.68–77.64	46.86	40.18–53.65	38.20	31.38–45.52	76.38	68.28–82.92	230.83
Tall/wide	0.17	68.37	58.62–76.73	48.31	41.59–55.09	38.51	31.60–45.91	76.34	68.37–82.80	231.52

10.77, for Asteria scale 6.85). Also, combining another two features, echo pattern in comparison to muscles and the presence of microcalcifications significantly increased OR to 13.27 (OR for echo pattern 5.12, for microcalcifications 4.85), and macrocalcification and thyroid capsule infiltration to 7.60, respectively (OR for macrocalcification 3.00, for thyroid capsule infiltration 3.19). Adding the third feature did not increase the OR. Otherwise, combining irregular margins, which had the highest OR, with all US features did not improved statistical parameters (including OR) in differentiation the character of the lesions. The detailed findings are presented in **Table 5**.

We sorted the tumors into intermediate, high and highest risk of malignancy.

Logistic regression analysis showed the lowest accuracy (<55%) for three features including composition (solid or >50% solid), shape (taller-than-wide) and halo pattern (without halo or partial halo). Therefore, we proposed a TIRADS 3 (intermediate risk) category for lesions with these features. **Table 6** demonstrates that in this group 4/64 tumor were malignant, and the risk of malignancy was 6.25%. In SE, all of the tumors were found to be not suspicious (Asteria 1 and 2).

Ill-defined margins as a single feature resulted in the highest accuracy (78.69) and also highest OR (10.77)—therefore, we proposed assigning them into TIRADS 5, the category for highest risk of malignancy.

The features such as: markedly hypoechoic, microcalcifications, thyroid capsule infiltration, or macrocalcification and Asteria 4, were assigned into TIRADS 4, the high risk of malignancy category (accuracy from 68 to 76%).

The goal was to assess the influence of the SE on proposed TIRADS 3, 4, 5 category results. Initially, according to the accuracy results for B-mode and SE features, the proposed TIRADS categories were preassigned for all tumors. Then we excluded the lesions with Asteria 4 as a single feature from TIRADS 4 category, because they were associated with increased risk of malignancy (**Table 6**). Afterwards, we assessed the "new" risk of malignancy, adding the SE result.

Using a logistic regression model, we combined all US features with age (<34 years) to obtain the highest accuracy. Combining the features of age, margin, echogenicity (markedly hypoechoic) capsule infiltration, and microcalcifications, we demonstrated sensitivity 69.39%, specificity 92.24%, PPV 82.93%, NPV 86.55%, accuracy 85.57%, AUC 0.871, 95%CI (0.829–0.907).

Finally, malignant and benign lesions were divided into two groups: smaller or equal to 10 mm and greater than 10 mm, and were compared according to US features. In comparison of groups of the lesions measuring <10 mm in diameter only thyroid capsule infiltration or/and deformation were statistically significantly different ($p = 0.03$) (**Table 7**).

DISCUSSION

The TIRADS classification was first introduced by Horvath, and the goal of this approach was to group thyroid lesions into different categories depending on the likelihood of malignancy to precisely select thyroid nodules for biopsy or to avoid

TABLE 4 | Logistic regression analysis of Asteria Scale parameter and B-mode risk factors in predicting malignancy of thyroid lesions (*p*-values were calculated by Chi-square tests).

Parameter	Malignant if	OR	95% CI	*p*-value	Accuracy (%)
Margins	=0	10.77	6.12–18.97	<0.001	78.69
Markedly hypoechoic	=1	5.12	2.58–10.18	<0.001	72.13
Microcalcifications	=1	4.85	2.90–8.14	<0.001	70.16
Thyroid capsule infiltration	>0	3.20	1.84–5.57	<0.001	69.18
Macrocalcifications	=1	3.01	1.74–5.19	<0.001	68.52
Asteria Scale	=4	6.85	3.77–12.45	<0.001	75.08
"Halo" pattern	=2	5.17	1.97–13.53	<0.001	45.25
Composition (solid)	=3	2.00	1.20–3.33	0.007	54.10
Tall/wide	>=1	2.02	1.22–3.36	0.006	54,75

TABLE 5 | Logistic regression analysis of combined elastographic and B-mode parameters in predicting malignancy of thyroid lesions (OR).

Parameter	OR	Combined OR	Combined OR 95% CI	Malignant if	Malignant, *n* True (+)
Margins	10.77	20.21	10.37–39.37	0	75 (60)
Asteria Scale (4 degree)	6.85			3, 4	
Markedly hypoechoic	5.12	13.27	3.75–46.99	1	19 (16)
Microcalcifications	4.85			1	
Thyroid capsule infiltration	3.19	11.18	6.33–19.76	2, 1, 0	96 (65)
Asteria Scale (4 degree)	6.85			(3, 4), (3, 4), (4).	
Asteria Scale (4 degree)	6.85	9.45	4.71–18.95	4	51 (38)
Markedly hypoechoic	5.12			1	
Microcalcifications	4.85	8.62	4.81–15.46	1	76 (52)
Asteria Scale (4 degree)	6.85			3, 4	
Macrocalcifications	3.00	8.69	4.99–15.14	1	94 (61)
Asteria Scale (4 degree)	6.85			3, 4	
Macrocalcifications	3.00	7.63	3.26–17.86	2	
Thyroid capsule infiltration	3.19			0,1	31 (23)

TABLE 6 | Risk of malignant tumors and their frequency according to B-mode features and combination of B-mode features and sonoelastography (Asteria 3, 4).

		TIRADS–B-mode			Combination B-mode+Sonoelastography		
		Number of nodules (*n* = 255)	Number of malignant nodules (*n* = 94)	Malignancy risk (%)	Number of nodules	Number of malignant nodules	Malignancy risk (%)
TIRADS 3		64	4	6.25	0	0	
	Composition >50%Solid/Solid	55	3	5.45	0	0	x
	Tall/wide	6	1	16.67	0	0	x
	"Halo" pattern partial//no	3	0	0	0	0	x
TIRADS 4		94	24	25.53	41	14	34.14
	Markedly hypoechoic	20	8	40	12	6	50
	Microcalcifications	53	12	22.64	21	5	23.81
	Capsule:infiltration; deformation	18	4	22.22	6	3	50
	Macrocalcifications	3	0	0	2	0	0
TIRADS 5		97	65	67.01	75	60	80

Table does not include 50 tumors (including 5 malignancy) Asteria 4 scores, which were qualified into TIRADS 4 category as a single high risk feature.

TABLE 7 | Comparing analysis, the frequency of occurring US features of the thyroid lesion regarding maximal measurement ≤1 cm and >1 cm (*p*-values were calculated by Chi-square tests).

Parameter	Analyzed feature	Lesion >10 mm		Lesion ≤10 mm		*p*-value
		Benign (%)	Malignant (%)	Benign (%)	Malignant (%)	
Composition	>50%Solid; Solid	78 (66.10)	40 (33.90)	32 (53.33)	28 (46.67)	0.098
Echo pattern	Markedly hypoechoic	11 (39.29)	17 (60.71)	4 (26.67)	11 (73.33)	0.408
Echo pattern	Hypoechoic	85 (63.43)	49 (36.57)	46 (56.10)	36 (43.90)	0.284
Margins	Ill-define	21 (35.00)	39 (65.00)	11 (29.73)	26 (70.27)	0.592
Tall/wide	>0.9565	67 (61.47)	42 (38.53)	40 (61.54)	25 (38.46)	0.993
Microcalcifications	Present	42 (48.84)	44 (51.16)	14 (42.42)	19 (57.58)	0.530
Macrocalcifications	Present	26 (46.43)	30 (53.57)	10 (55.56)	8 (44.44)	0.500
Thyroid capsule	Infiltration; Deformation	32 (52.46)	29 (47.54)	1 (11.11)	8 (88.89)	0.030
"Halo" pattern	Partial; No	111 (66.07)	57 (33.93)	51 (58.62)	36 (41.38)	0.241
Asteria Scale	3,4	64 (57.14)	48 (42.86)	23 (42.59)	31 (57.41)	0.079
Asteria Scale	4	15 (39.47)	23 (60.53)	7 (25.00)	21 (75.00)	0.239

unnecessary biopsy. The main objective was to standardize and simplify reporting and improve communication between radiologists and endocrinologists. The authors described 10 patterns of thyroid nodules, but this proposal was not widely accepted and applied. Therefore, other authors proposed a new classification. Park et al. introduce the equation for calculating the probability of malignancy in thyroid nodules based on 12 dichotomic US features (25).

Kwak et al. proposed a classification based on the number of suspicious US features (27). The authors proposed a TIRADS classification, which relies on counting the number of suspicious US features, beginning from TIRADS 4. The authors subdivided the category TIRADS 4 into a, b, c, where one, two, three or four suspicious features were assigned to a subcategory of category 4, respectively. They demonstrated that, using multivariate analysis, the values of fitted probabilities and risk of malignancies increased with the number of suspicious US features. Elastography was not recommended. Our results are dissimilar to the Kwak risk stratification, where the number of suspicious features higher than two did not increase the predicted risk of malignancy, but adding sonoelastography significantly increased the predicted risk of malignancy.

In 2017, two societies, the European Thyroid Association and American College of Radiology, independently published their guidelines, the EU-TIRADS and ACR TI-RADS system for risk stratification, respectively. In 2018 in Poland, recommendations according to the Guidelines of Polish National Societies prepared on the initiative of the Polish Group for Endocrine Tumors were released. They contain the clinical and US suspicious features of thyroid nodules and indications for biopsy, but the TIRADS classification is not followed in routine practice by endocrinologists and radiologists.

Our results demonstrate that inclusion of sonoelastography suspicious features (Asteria 3,4) in the TIRADS classification system increases the risk for malignancy in TIRADS 4 and TIRADS 5 category. Unfortunately, in TIRADS 3 lesions, the inclusion of elastography features did not increase the risk of the malignancy (all lesions had sonoelastography scores of Asteria 1 or 2). There were four false negative results for elastography in this group. Therefore, for a TIRADS 3 (intermediate risk) category, FNAB is still recommended upon B-mode features finding (mean risk of malignancy 6.25%) is advocated regardless of sonoelastography results.

Ill-defined margins as a single feature resulted in the highest accuracy and highest OR (10.77)—therefore, we proposed assigning them into TIRADS 5, the category with the highest risk of malignancy, and recommended performing FNAB. When combining this features with sonoelastography (Asteria 3, 4 scores) the risk of malignancy increased even more (from 67.01 to 80.00%).

As an example, adding sonoelastography results (Asteria scale 3, 4) to ill-defined margins, reduced false positive results from 32 tumors, for ill-defined margin alone, to 10 tumors (**Tables 2**, **5**).

The occurrence of at least one of the high-risk features in a nodule should lead to consideration of assignment to TIRADS 4 category and performance of an FNAB should be considered.

The combined analyses of SE (Asteria 3, 4 scores) with the following high risk TIRADS 4 category B-mode features: infiltration of the capsule, markedly hypoechoic microcalcification and macrocalcification, resulted in an increased prediction of malignancy using the risk of malignancy (the risk of malignancy increased from 25.53 to 34.14%). Also, the combination of two B-mode features, such as marked hypoechogenicity with microcalcification (OR = 13.27) or macrocalcification and thyroid capsule infiltration (OR 7.60) increased the OR—therefore, we recommended a classification of TIRADS5 category for tumors with these features independently, based on the size of the lesions. In the case of a non-diagnostic, or negative result, FNAB should be repeated.

Our results and proposed algorithm for TIRADS suggest that sonoelastography could be integrated into the TIRADS classification system and used in daily practice, and also as an independent risk predictor in daily practice.

If nodules are predominantly cystic or spongiform and have no features of intermediate or high risk of malignancy, then TIRADS 2 category is appropriate and surveillance recommended (7, 32).

In the EU-TIRADS, if at least one of the high-risk features: non-oval shape, irregular margins, microcalcifications or marked hypoechogenicity is present, it is recommended that the lesion should be classified into the high-risk category of EU-TIRADS 5. Only a mildly hypoechoic pattern without any feature of high risk is recommended for classification as EU-TIRADS 4 category with intermediate risk, and an FNAB is recommended for nodules >15 mm. Our results are partially concordant with the EU-TIRADS if the suspicious US B-mode features are analyzed. However, we suggest dividing them into intermediate, high and the highest risk of malignancy.

Haugen BR at al. published an ATA (American Thyroid Association) risk stratification scale of thyroid nodules, dividing them into 5 categories (benign, very low suspicion, low suspicion, intermediate suspicion and high suspicion) (7). Our results are only partially compatible with the ATA recommendations. In our study, similar to the Haugen et al. study, the group of highly suspicious features include: ill-defined margin, hypoechogenicity, microcalcifications and extra-thyroidal extension. We achieved an inconsistent result with shape (taller-then-wide), >50% solid tumor composition and halo "pattern"(partial or no), which we categorized it into intermediate risk group, and despite the difference in the risk stratification the recommendation for the biopsy was similar. In ATA guidelines shape (taller-then-wide) in solid hypoechoic or solid hypoechoic component of a partially cystic nodule is the high suspicion features group. In the most recent published paper comparing the different TIRADS classification, Ha EJ et al. concluded that ATA guidelines afford relatively moderate sensitivity for thyroid cancer detection, compared to the 2016 KTA (Korean Thyroid Association) and 2017 ACR guidelines. This limitation could arise due to the examined population—different region (different biology of the thyroid disease) and different hospitals (differences in equipment).

This work has some limitations. Firstly, we had a high percentage of malignant lesions, 32% higher than normal prevalence in population. That could have some impact on our statistics. That is why further prospective exploration of our results is needed. Secondly, we used strain elastography that is considered more operator dependent and requires more experience for accurate interpretation. Both this technique together with shear wave elastography are recommended by World Federation of Ultrasound in Medicine and Biology according to stratification of thyroid nodules (34). Thirdly, it should be noted that the possibility of false negatives was not completely avoidable, as patients with Bethesda Category II and no changes in B-mode US examination within 1 year did not undergo surgery.

CONCLUSIONS

Our work has demonstrated that three B-mode features, such as composition (solid or >50% solid), shape (taller-than-wide) and halo pattern (without halo or partial halo), correspond to an intermediate risk of malignancy (TIRADS 3). The highest risk factor for cancer malignancy (TIRADS 5), turned out to be associated with margin (ill-defined) as the strongest single feature. A high risk of malignancy (TIRADS 4) was associated with echo pattern (markedly hypoechoic), microcalcifications (present), thyroid capsule (infiltration), macrocalcification (present), and Asteria scale (4 degree). There has been disagreement regarding the integration of sonoelastography into the TIRADS system in previous classifications. In our study, sonoelastography increases the predicted risk of malignancy especially in nodules in TIRADS 4 and 5 categories. Asteria 4 as a solitary feature in a solid tumor could result in its categorization as TIRADS 4 category, but coexistence with high risk features allows it to be upgraded to TIRADS 5 category. Lesion in TIRADS 5 category and suspicious sonoelastography (Asteria 3,4) indicates a highly increased risk of malignancy.

ETHICS STATEMENT

This study was carried out in accordance with the recommendations of the Institutional Review Board of the Maria Sklodowska-Curie Institute - Cancer Center, Warsaw, Poland (MSCI), and all subjects gave written informed consent in accordance with the Declaration of Helsinki.

AUTHOR CONTRIBUTIONS

K-DS contributed conception and design of the study, wrote the first draft and sections of the manuscript. MD contributed conception and design of the study, organized the database. BM, KM, and RS organized the database. BM wrote sections of the manuscript. AK wrote sections of the manuscript. EB-Z organized the pathological analysis. AK organized the database. ZA contributed conception of the study. All authors contributed to manuscript revision, read, and approved the submitted version.

ACKNOWLEDGMENTS

We thank Zbysław Chrabałowski for the valuable advice regarding statistical analyses.

REFERENCES

1. Reiners C, Wegscheider K, Schicha H, Theissen P, Vaupel R, Wrbitzky R, et al. Prevalence of thyroid disorders in the working population of Germany: ultrasonography screening in 96,278 unselected employees. *Thyroid.* (2004) 14:926–32. doi: 10.1089/thy.2004.14.926
2. Ito Y, Uruno T, Nakano K, Takamura Y, Miya A, Kobayashi K, et al. An observation trial without surgical treatment in patients with papillary microcarcinoma of the thyroid. *Thyroid.* (2003) 13:381–7. doi: 10.1089/105072503321669875
3. Guth S, Theune U, Aberle J, Galach A, Bamberger CM. Very high prevalence of thyroid nodules detected by high frequency (13 MHz) ultrasound examination. *Eur J Clin Invest.* (2009) 39:699–706. doi: 10.1111/j.1365-2362.2009.02162.x
4. Smith-Bindman R, Lebda P, Feldstein VA, Sellami D, Goldstein RB, Brasic N, et al. Risk of thyroid cancer based on thyroid ultrasound imaging

characteristics: results of a population-based study. *JAMA Intern Med.* (2013) 173:1788–96. doi: 10.1001/jamainternmed.2013.9245
5. Perros P, Boelaert K, Colley S, Evans C, Evans RM, Gerrard Ba G, et al. Guidelines for the management of thyroid cancer. *Clin Endocrinol.* (2014) 81(Suppl 1):1–122. doi: 10.1111/cen.12515
6. Gharib H, Papini E, Garber JR, Duick DS, Harrell RM, Hegedus L, et al. American Association of Clinical Endocrinologists, American College of Endocrinology, and Associazione Medici Endocrinologi Medical Guidelines for Clinical Practice for the Diagnosis and Management of Thyroid Nodules—2016 Update. *Endocr Pract*. (2016) 22:622–39. doi: 10.4158/EP161208.GL
7. Haugen BR, Alexander EK, Bible KC, Doherty GM, Mandel SJ, Nikiforov YE, et al. 2015 American Thyroid Association Management Guidelines for Adult Patients with Thyroid Nodules and Differentiated Thyroid Cancer: The American Thyroid Association Guidelines Task Force on Thyroid Nodules and Differentiated Thyroid Cancer. *Thyroid.* (2016) 26:1–133. doi: 10.1089/thy.2015.0020
8. Jarzab B, Dedecjus M, Slowinska-Klencka D, Lewinski A, Adamczewski Z, Anielski R, et al. Guidelines of Polish National Societies diagnostics and treatment of thyroid carcinoma. 2018 update. *Endokrynol Pol*. (2018) 69:34–74. doi: 10.5603/EP.2018.0014
9. Choi YJ, Yun JS, Kim DH. Clinical and ultrasound features of cytology diagnosed follicular neoplasm. *Endocrine J.* (2009) 56:383–9. doi: 10.1507/endocrj.K08E-310
10. Kim EK, Park CS, Chung WY, Oh KK, Kim DI, Lee JT, et al. New sonographic criteria for recommending fine-needle aspiration biopsy of nonpalpable solid nodules of the thyroid. *AJR Am J Roentgenol.* (2002) 178:687–91. doi: 10.2214/ajr.178.3.1780687
11. Moon HJ, Kwak JY, Kim MJ, Son EJ, Kim EK. Can vascularity at power Doppler US help predict thyroid malignancy? *Radiology.* (2010) 255:260–9. doi: 10.1148/radiol.09091284
12. Adamczewski Z, Lewinski A. The risk of malignancy of the thyroid nodule/focal lesion–an assessment by ultrasound, based on our own scoring system. *Thyroid Res.* (2013) 6:A1. doi: 10.1186/1756-6614-6-S2-A1
13. Morris LF, Ragavendra N, Yeh MW. Evidence-based assessment of the role of ultrasonography in the management of benign thyroid nodules. *World J. Surg.* (2008) 32:1253–63. doi: 10.1007/s00268-008-9494-z
14. Iannuccilli JD, Cronan JJ, Monchik JM. Risk for malignancy of thyroid nodules as assessed by sonographic criteria: the need for biopsy. *J Ultrasound Med*. (2004) 23:1455–64. doi: 10.7863/jum.2004.23.11.1455
15. Kwak JY, Han KH, Yoon JH, Moon HJ, Son EJ, Park SH, et al. Thyroid imaging reporting and data system for US features of nodules: a step in establishing better stratification of cancer risk. *Radiology.* (2011) 260:892–9. doi: 10.1148/radiol.11110206
16. Moon WJ, Jung SL, Lee JH, Na DG, Baek JH, Lee YH, et al. Benign and malignant thyroid nodules: US differentiation–multicenter retrospective study. *Radiology.* (2008) 247:762–70. doi: 10.1148/radiol.2473070944
17. Asteria C, Giovanardi A, Pizzocaro A, Cozzaglio L, Morabito A, Somalvico F, et al. US-elastography in the differential diagnosis of benign and malignant thyroid nodules. *Thyroid.* (2008) 18:523–31. doi: 10.1089/thy.2007.0323
18. Bae U, Dighe M, Dubinsky T, Minoshima S, Shamdasani V, Kim Y. Ultrasound thyroid elastography using carotid artery pulsation: preliminary study. *J Ultrasound Med.* (2007) 26:797–805. doi: 10.7863/jum.2007.26.6.797
19. Zhang B, Jiang Y-X, Liu J-B, Yang M, Dai Q, Zhu Q-L, et al. Utility of contrast-enhanced ultrasound for evaluation of thyroid nodules. *Thyroid.* (2010) 20:51–7. doi: 10.1089/thy.2009.0045
20. Bhatia K, Rasalkar D, Lee Y, Wong K, King A, Yuen H, et al. Cystic change in thyroid nodules: a confounding factor for real-time qualitative thyroid ultrasound elastography. *Clin Radiol.* (2011) 66:799–807. doi: 10.1016/j.crad.2011.03.011
21. Migda B, Słapa R, Bierca J, Slowinska-Srzednicka J, Migda A, Dobruch-Sobczak K, et al. Differentiation of thyroid nodules in multinodular goiter with the application of technical ultrasound advances—initial results. *Endokrynol Polska.* (2016) 67:157–65. doi: 10.5603/EP.a2016.0026
22. Dobruch-Sobczak K, Zalewska EB, Guminska A, Słapa RZ, Mlosek K, Wareluk P, et al. Diagnostic performance of shear wave elastography parameters alone and in combination with conventional B-mode ultrasound parameters for the characterization of thyroid nodules: a prospective, dual-center study. *Ultrasound Med. Biol.* (2016) 42:2803–11. doi: 10.1016/j.ultrasmedbio.2016.07.010
23. D'Orsi CJ, Sickles EA, Mendelson EB, Morris EA. *ACR BI-RADS Atlas: Breast Imaging Reporting and Data System*. Reston, VA: American College of Radiology (2013).
24. Horvath E, Majlis S, Rossi R, Franco C, Niedmann JP, Castro A, et al. An ultrasonogram reporting system for thyroid nodules stratifying cancer risk for clinical management. *J Clin Endocrinol Metab*. (2009) 94:1748–51. doi: 10.1210/jc.2008-1724
25. Park JY, Lee HJ, Jang HW, Kim HK, Yi JH, Lee W, et al. A proposal for a thyroid imaging reporting and data system for ultrasound features of thyroid carcinoma. *Thyroid.* (2009) 19:1257–64. doi: 10.1089/thy.2008.0021
26. Friedrich-Rust M, Meyer G, Dauth N, Berner C, Bogdanou D, Herrmann E, et al. Interobserver agreement of Thyroid Imaging Reporting and Data System (TIRADS) and strain elastography for the assessment of thyroid nodules. *PLoS ONE.* (2013) 8:e77927. doi: 10.1371/journal.pone.0077927
27. Kwak JY, Jung I, Baek JH, Baek SM, Choi N, Choi YJ, et al. Image reporting and characterization system for ultrasound features of thyroid nodules: multicentric Korean retrospective study. *Korean J Radiol*. (2013) 14:110–7. doi: 10.3348/kjr.2013.14.1.110
28. Russ G, Royer B, Bigorgne C, Rouxel A, Bienvenu-Perrard M, Leenhardt L. Prospective evaluation of thyroid imaging reporting and data system on 4550 nodules with and without elastography. *Eur J Endocrinol*. (2013) 168:649–55. doi: 10.1530/EJE-12-0936
29. Na DG, Baek JH, Sung JY, Kim JH, Kim JK, Choi YJ, et al. Thyroid imaging reporting and data system risk stratification of thyroid nodules: categorization based on solidity and echogenicity. *Thyroid.* (2016) 26:562–72. doi: 10.1089/thy.2015.0460
30. Russ G, Bonnema SJ, Erdogan MF, Durante C, Ngu R, Leenhardt L. European thyroid association guidelines for ultrasound malignancy risk stratification of thyroid nodules in adults: the EU-TIRAD. *Eur Thyroid J.* (2017) 6:225–37. doi: 10.1159/000478927
31. Grant EG, Tessler FN, Hoang JK, Langer JE, Beland MD, Berland LL, et al. Thyroid ultrasound reporting lexicon: white paper of the ACR Thyroid Imaging, Reporting and Data System (TIRADS) Committee. *J Am Coll Radiol*. (2015) 12:1272–9. doi: 10.1016/j.jacr.2015.07.011
32. Tessler FN, Middleton WD, Grant EG, Hoang JK, Berland LL, Teefey SA, et al. ACR Thyroid Imaging, Reporting and Data System (TI-RADS): white paper of the ACR TI-RADS Committee. *J Am Coll Radiol*. (2017) 14:587–95. doi: 10.1016/j.jacr.2017.01.046.
33. Straccia P, Rossi ED, Bizzarro T, Brunelli C, Cianfrini F, Damiani D, et al. A meta-analytic review of the Bethesda system for reporting thyroid cytopathology: has the rate of malignancy in indeterminate lesions been underestimated? *Cancer Cytopathol.* (2015) 123:713–22. doi: 10.1002/cncy.21605
34. Cosgrove D, Barr R, Bojunga J, Cantisani V, Chammas MC, Dighe M, et al. WFUMB guidelines and recommendations on the clinical use of ultrasound elastography: Part 4. Thyroid. *Ultrasound Med Biol.* (2017) 43:4–26. doi: 10.1016/j.ultrasmedbio.2016.06.022

Conflict of Interest Statement: The authors declare that the research was conducted in the absence of any commercial or financial relationships that could be construed as a potential conflict of interest.

frontiers in Endocrinology

ORIGINAL RESEARCH
published: 05 April 2019
doi: 10.3389/fendo.2019.00208

The Role of ^{18}F-FDG PET/CT in the Management of the Autoimmune Thyroid Diseases

Bogdan Małkowski[1], *Zbigniew Serafin*[2], *Rafał Glonek*[3]*, *Szymon Suwała*[3], *Rita Łopatto*[1] *and Roman Junik*[3]

[1] Department of Nuclear Medicine, Oncology Centre, prof. Łukaszczyk Memorial Hospital, Bydgoszcz, Poland, [2] Department of Radiology and Diagnostic Imaging, University of Nicolaus Copernicus in Torun, Collegium Medicum in Bydgoszcz, Bydgoszcz, Poland, [3] Department of Endocrinology and Diabetology, University of Nicolaus Copernicus in Torun, Collegium Medicum in Bydgoszcz, Bydgoszcz, Poland

Objective: It is a well-known fact that positron emission tomography (PET) is an effective tool in the assessment of thyroid focal lesions, however only few studies so far have investigated its role in monitoring of autoimmune thyroid diseases (AITDs). The aim of this study is to assess if PET scan may be useful for the assessment of the thyroid gland in patients with an AITD—Hashimoto's thyroiditis.

Methods: We evaluated twenty subjects with diagnosed Hashimoto's thyroiditis (proven by presence of elevated thyroid antibodies level and by thyroid imaging). The maximum standardized uptake value (SUV-max) of the thyroid parenchyma was measured using ^{18}F-FDG-PET/CT. Control group consisted of patients who have been in carcinoma remission for other reasons than thyroid cancer and who had been investigated by PET scan to exclude carcinoma recurrence.

All control group subjects had their thyroid glands intact, none of them had a medical history of thyroid disease including thyroid nodules. AITDs had been excluded in all control group subjects. STATISTICA 13.1 software was used for statistical analysis.

Results: Results: The SUV-max was significantly higher in patients with an AITD than in healthy subjects (median SUV-max 3.94 vs. 1.95; $p = 0.005$).

Conclusions: ^{18}F-FDG-PET/CT scan may differentiate normal thyroid parenchyma from the diffused inflammatory changes of the thyroid gland in patients with AITDs. However, the researchers must be continued.

Keywords: thyroid, ultrasound, autoimmune thyroid disease, 18FDG-PET, Hashimoto's disease

OPEN ACCESS

Edited by:
Joanna Klubo-Gwiezdzinska, National Institutes of Health (NIH), United States

Reviewed by:
Roberto Vita, University of Messina, Italy
Silvia Martina Ferrari, University of Pisa, Italy

***Correspondence:**
Rafał Glonek
rafalglonek@wp.pl

Specialty section:
This article was submitted to Thyroid Endocrinology, a section of the journal Frontiers in Endocrinology

Received: *10 December 2018*
Accepted: *14 March 2019*
Published: *05 April 2019*

Citation:
Małkowski B, Serafin Z, Glonek R, Suwała S, Łopatto R and Junik R (2019) The Role of ^{18}F-FDG PET/CT in the Management of the Autoimmune Thyroid Diseases. Front. Endocrinol. 10:208. doi: 10.3389/fendo.2019.00208

INTRODUCTION

Autoimmune thyroid diseases (AITDs) is a wide group of autoimmune thyroid disorders like hyperthyroid Graves' disease, Hashimoto's thyroiditis or atrophic autoimmune hypothyroidism (1). The most common type of an AITD in Poland is Hashimoto's thyroiditis (referred to as AITD, throughout this article), which is much more common in women. Its prevalence is estimated at 2% in all age groups with an annual incidence of 0.3–1.5 per thousand people, however, a statistical growth of its incidence has been recently observed (2). AITD may result in hyperthyroidism, subclinical dysfunction or, most commonly, in hypothyroidism. The common hypothyroidism

signs and symptoms include deterioration of well-being, excessive weight gain, dry skin, hair loss and many more. Moreover, AITDs may be a prelude to the subsequent development of thyroid hormone disorders. There is no ideal test for diagnosis of AITDs. Currently the diagnosis of AITD is based on the coexistence of clinical symptoms, presence of antibodies against thyroid antigens (thyroperoxidase, thyroglobulin) and characteristic ultrasound image (3). Therefore, it is undoubtedly worth looking for new methods of diagnosing and monitoring the disease. AITD can be associated with other autoimmune diseases in the same patient such as vitiligo, chronic autoimmune gastritis, rheumatoid arthritis or polymyalgia rheumatica (4).

It is a well-known fact that positron emission tomography (PET) is an effective tool in the assessment of thyroid focal lesions (5), especially in the diagnosis of advanced differentiated thyroid carcinoma (6).

However, we also know that the PET scan may be useful in the imaging of inflammatory lesions including thyroiditis (in some of the previous studies this case has been referred as "false-positive PET uptake") (7, 8). Under normal conditions, uptake of FDG in the thyroid tissue is low or absent. The PET scans may present increased focal or diffuse pattern of FDG uptake. Diffusely increased uptake of FDG may be associated with AITDs or with the hypothyroidism (9–12). Focal increased uptake of FDG represents higher risk of malignancy (13).

PET scan is not a standard test used in diagnosing and monitoring of AITD patients. However, results of this imaging studies may be valuable in some cases.

The aim of this study was to assess if PET scan may be useful for the assessment of the thyroid gland in patients with AITD.

MATERIALS AND METHODS

We conducted 18-FDG-PET scan in twenty patients of our endocrinology clinic between September and November 2018, in which we diagnosed Hashimoto's in advance. The disease has been identified by elevated thyroid peroxidase antibodies level and by the hypoechoic pattern of the thyroid gland assessed by ultrasound imaging. Thyroid ultrasonography was performed using the Sonoscape E2 ultrasonograph device with 7.5 MHz linear probe.

Control subjects were six patients (exclusively women) who have been in carcinoma remission and underwent neck imaging with a PET scan due to reasons other than assessment of thyroid disease. AITDs had been excluded in all control group subjects. All control group subjects had their thyroid glands intact, none of them had a medical history of thyroid disorders.

Written informed consent was obtained from the every participant of this study. Bioethics Committee of the Nicolaus Copernicus University in Torun functioning at Collegium Medicum in Bydgoszcz stated their positive opinion on our research.

To assess the ^{18}FDG uptake, the SUV-max was measured in the thyroid area. Nuclear medicine imaging was performed on the whole-body high-resolution PET/CT scanner Biograph 6. The images were acquired 60 min after radiotracer administration. To ensure the results proper interpretation, nuclear medicine specialist assessed them.

All data obtained were subjected to a statistical analysis with usage of STATISTICA 13.1. Differences in SUV-max values between a group of AITDs subjects and a group of healthy subjects were analyzed by the Mann-Whitney *U*-test and the aforementioned difference has been considered statistically significant at the p-value <0.05.

RESULTS

Median age of subjects with Hashimoto's thyroiditis was 41.56 $\pm$ 13.09 years. There were no age-related statistical differences in the ^{18}FDG uptake in thyroid parenchyma ($p = 0.57$). The SUVmax has been measured in the thyroid area for all the subjects included in the study. SUV-max was significantly higher in patients with an AITD than in control subjects (median SUV-max 3.94 vs. 1.95; $p = 0.005$). The differences between SUV-max in the group of patients with an AITD- Hashimoto's thyroiditis and in control group patients was presented in **Figure 1**.

DISCUSSION

Positron emission tomography (PET) scan is widely used and a valuable method in work-up of patients with thyroid carcinoma or cancer screening in healthy patients (14). Nowadays, there are more than 5000 PET-CT systems available all over the world. In clinical oncology PET-CT may be used as a diagnostic tool which may reduce amount of unnecessary surgical interventions (15).

PET-CT scanning uses isotopes such as oxygen-15, fluorine-18 or gallium-68. In our research we used 18-fluorodeoxyglucose (^{18}F-FDG) as a radiotracer. ^{18}F-FDG has short half-live ($\sim$110 min) and it has been established that increased uptake of ^{18}F-FDG was noted in cells with enhanced metabolism such as inflammatory cells and cancer cells measured as the maximum standardized uptake value (SUVmax) (10, 16, 17).

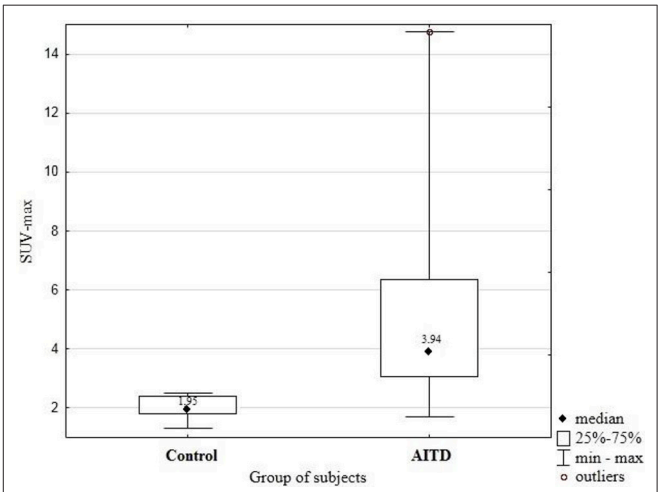

FIGURE 1 | Difference of SUV-max between group of patients with AITD and control group subjects.

Most studies about thyroid PET scan have been focused on differentiation between benign and malignant lesions such as: thyroid incydentalomas or thyroid papillary carcinoma (17–19). Nevertheless, there have been only few reports of autoimmune thyroid disorders (AITDs) ^{18}F-FDG -PET scan. Akosmana and al. described thyroid lymphoma associated with Hashimoto's disease in 44-year-old man. PET scan performed in this patient showed increased diffuse FDG uptake in thyroid gland (SUVmax−17.6). After treatment—third cycle of chemotherapy—FDG uptake by thyroid remained increased (SUVmax−5.1) (20). While Schmid et al. reported increased 18F-FDG uptake mimicking thyroid cancer in a patient with Hashimoto's thyroiditis (21).

The most common of AITDs in Poland is Hashimoto's thyroiditis, its prevalence has been estimated at 2%. It is frequent to notice hormonal abnormalities as hypothyroidism or presence of elevated thyroid antibodies serum level before the occurrence of the clinical symptoms such as weight gain, hair loss, mental disorders (3). In our research we studied if ^{18}F-FDG PET scan can differentiate normal thyroid parenchyma from parenchymal changes of the thyroid gland in patients with Hashimoto's thyroiditis.

We evaluated 20 patients (17 women, 3 men) with Hashimoto's thyroiditis which has been diagnosed by the presence of elevated thyroid antibodies serum level and thyroid ultrasound imaging. Among all included subjects, 12 patients presented a normal TSH serum level and 8 patients presented an elevated TSH concentration. All subjects presented a normal triiodothyronine and thyroxine serum levels. None of the subjects were treated with levothyroxine before the ^{18}F-FDG PET scan. Control subjects consisted of patients who have been in carcinoma remission and simultaneously underwent neck imaging with a PET scan due to reasons other than diagnosing or evaluating thyroid diseases.

The SUVmax of the thyroid parenchyma was measured using ^{18}F-FDG PET. The SUVmax was significantly higher in subjects with AITD than in control subjects (4.25 (IQR 2.79–5.91 vs. 1.76 (IQR 1.33–2.36), $p = 0.05$). There was no significant SUVmax differences between patients who had elevated TSH concentration and normal TSH serum level. The highest reported SUVmax (14, 76) was presented by a patient with no hormonal abnormalities and slight clinical manifestations of the thyroid disorder. Each of 20 subjects presented diffuse type 18 -FDG uptake.

Yasuda et al. (8) and consecutively Seji et al. (22) have reported that diffuse type of thyroid 18-FDG uptake pattern may be associated with chronic thyroiditis. Yasuda et al. (8) also suggested that subclinical chronic thyroiditis may be diagnosed accidentally during whole-body PET scan. According to the results obtained and presented by Choi et al. (23) diffuse thyroid ^{18}F-FDG uptake pattern most likely indicates benign thyroid lesion. Our results also indicate that diffuse ^{18}F-FDG pattern uptake may support AITDs diagnosis.

The mechanism of ^{18}F-FDG uptake in AITD is still unknown. In a research focused on activated inflammatory cells, an increased FDG uptake has been observed, probably due to enhanced expression of the Glucose Transporters Type 1 (GLUT-1), described by Chakrabarti and al. in human peripheral blood lymphocytes enriched in T cells after phytohemagglutinins stimulation (24).

The limitations of our study was a small number of performed PET scans due to low availability and high cost of PET imaging. In Poland there are 26 PET-CT systems per 37,4 milions citizens.

Summing it up, ^{18}F-FDG -PET scan in AITDs patients shows abnormal diffuse FDG uptake pattern in thyroid parenchyma. Abnormal thyroid PET scan pattern may indicate autoimmune diseases in subjects with no previous medical history or may support the diagnosis of an AITD in patients with subtle clinical signs with normal hormone levels and/or elevated thyroid antibodies. Although, we judge it necessary to obtain more data about the usage of PET imaging in the management and follow-up of the AITDs. Moreover, it seems to be crucial to know the techniques to differentiate ^{18}F-FDG -PET uptake patterns in patients with neoplastic lesions associated with AITD. The American Thyroid Association (ATA) recommends that nodules which has at least 10 mm in size should be investigated with ultrasound (US) and needle aspiration (FNAB) (13).

AUTHOR CONTRIBUTIONS

BM and RJ concept and design. ZS ultrasound imaging. SS, RG, RJ, and RŁ recrutation of patients. SS, RG, and RJ analysis and interpretation of data. SS, RG, and RJ manuscript writing. RJ review of final manuscript. All authors literature review and refinement of manuscript.

REFERENCES

1. Swain M, Swain T, Mohanty BK. Autoimmune thyroid disorders - An update. *Ind J Clin Biochem*. (2005) 1:9–17. doi: 10.1007/BF02893034
2. Benvenga S, Antonelli A, Vita R. Thyroid nodules and thyroid autoimmunity in the context of environmental pollution. *Rev Endocr Metab Disord.* (2015) 16:319–40. doi: 10.1007/s11154-016-9327-6
3. Caturegli P, De Remigis A, Rose NR. Hashimoto thyroiditis: clinical and diagnostic criteria. *Autoimmun Rev.* (2014) 13:391–7. doi: 10.1016/j.autrev.2014.01.007
4. Ferrari SM, Fallahi P, Ruffilli I, Elia G, Ragusa F, Benvenga S, et al. The association of the autoimmune diseases in patients with Graves' disease (with or without ophthalmopathy): review of the literature and report of alargeseries. *Autrev*. (2019) 18:287–92. doi: 10.1016/j.autrev.2018.10.001
5. Czepczynski R. Nuclear medicine in the diagnosis of benign thyroid diseases. *Nuclear Med Rev.* (2012) 2:113–9.
6. Garberoglio S, Testori O. Role of nuclear medicine in the diagnosis of benign thyroid diseases. *Front Horm Res.* (2016) 45:24–36. doi: 10.1159/000442275
7. Rosenbaum SJ, Lind T, Antoch G, Bockisch A. False-Positive FDG PET Uptake - the Role of PET/CT. *Eur Radiol.* (2006) 16:1054–65. doi: 10.1007/s00330-005-0088-y
8. Yasuda S, Shohtsu A, Ide M, Takagi S, Takahashi W, Suzuki Y, et al. Chronic thyroiditis: diffuse uptake of FDG at PET. *Radiology.* (1998) 207:775–8. doi: 10.1148/radiology.207.3.9609903

9. Glaudemans AW, de Vries EF, Galli F, Dierckx RA, Slart RH, Signore A. The use of ^{18}F-FDG-PET/CT for diagnosis and treatment monitoring of inflammatory and infectious diseases. *Clin Dev Immunol*. (2013) 2013:623036. doi: 10.1155/2013/623036
10. Slman R, Monpeyssen H, Desarnaud S, Haroche J, Fediaevsky Ldu P, Fabrice M, et al. Ultrasound, elastography, and fluorodeoxyglucose positron emission tomography/computed tomography imaging in Riedel's thyroiditis: report of two cases. *Thyroid*. (2011) 7:799–804. doi: 10.1089/thy.2010.0242
11. Song YS, Jang SJ, Chung JK, Lee DS. F-18 fluorodeoxyglucose (FDG) positron emission tomography (PET) and Tc-99m pertechnate scan findings of a patient with unilateral subacute thyroiditis. *Clin Nucl Med*. (2009) 7:456–8. doi: 10.1097/RLU.0b013e3181a7d24a
12. Yeo SH, Lee SK, Hwang I, Ahn EJ. Subacute thyroiditis presenting as a focal lesion on [18F] fluorodeoxyglucose whole-body positron-emission tomography/CT. *AJNR Am J Neuroradiol*. (2011) 4:E58–60. doi: 10.3174/ajnr.A2017
13. Wong J, Liu K, Siu C, Jones S, Sovka M, Wilson D, et al. Management of PET diagnosed thyroid incidentalomas in British Columbia Canada: critical importance of the PET report. *Am J Surg*. (2017) 213:950e957. doi: 10.1016/j.amjsurg.2017.03.015
14. Rohren EM, Turkington TG, Coleman RE. Clinical applications of PET in oncology. *Radiology*. (2004) 231:305–32. doi: 10.1148/radiol.2312021185
15. Fischer BM, Siegel BA, Weber WA, von Bremen K, Beyer T, Kalemis A. PET/CT is a cost-effective tool against cancer: synergy supersedes singularity. *Eur J Nucl Med Mol Imaging*. (2016) 43:1749–52. doi: 10.1007/s00259-016-3414-5
16. Szurowska E, Teodorczyk J, Dziadziuszko K, Pieńkowska J, Romanowicz G, Lass P. Positron emission tomography in oncology with use of radiotracers alternative to 18F-fluorodeoxyglucose. *Onkol Prak Klin*. (2013) 9:197–99. Available online at: https://journals.viamedica.pl/oncology_in_clinical_practice/article/view/36382
17. Okayasu I, Saegusa M, Fujiwara M, Hara Y, Rose NR. Enhanced cellular proliferative activity and cell death in chronic thyroiditis and thyroid papillary carcinoma. *J Cancer Res Clin Oncol*. (1995) 121:746–52. doi: 10.1007/BF01213321
18. Mane M, O'Neill AC, Tirumani SH, Shi M, Shinagare AB, Fisher DC. Thyroid lymphoma on a background of Hashimoto's thyroiditis: PET/CT appearances. *Clin Imag*. (2014) 38:864–7. doi: 10.1016/j.clinimag.2014.03.004
19. Kim TY, Kim WB, Ryu JS, Gong G, Hong SJ, Shong YK. 18F-fluorodeoxyglucose uptake in thyroid from positron emission tomogram (PET) for evaluation in cancer patients: high prevalence of malignancy in thyroid PET incidentaloma. *Laryngoscope*. (2005) 115:1074–8. doi: 10.1097/01.MLG.0000163098.01398.79
20. Akosman C, Selcuk NA, Ordu C, Ercan S, Ekici ID, Oyan B. Unicentric mixed variant Castleman disease associated with Hashimoto disease: the role of PET/CT. *Cancer Imag*. (2011) 11:52–55. doi: 10.1102/1470-7330.2011.0011
21. Schmid DT, Kneifel S, Stoeckli SJ, Padberg BC, Merrill G, Goerres GW. Increased 18F-FDG uptake mimicking thyroid cancer in a patient with Hashimoto's thyroiditis. *Eur Radiol*. (2003) 13:2119–21. doi: 10.1007/s00330-002-1619-4
22. Kurata S, Ishibashi M, Hiromatsu Y, Kaida H, Miyake I, Uchida M, et al. Diffuse and diffuse-plus-focal uptake in the thyroid gland identifi ed by using FDG-PET: prevalence of thyroid cancer and Hashimoto's thyroiditis. *Ann Nucl Med*. (2007) 21:325–30. doi: 10.1007/s12149-007-0030-2
23. Choi JY, Lee KS, Kim HJ, Shim YM, Kwon OJ, Park K, et al. Focal thyroid lesions incidentally identified by integrated 18F-FDG PET/CT: clinical significance and improved characterization. *J Nucl Med*. (2006) 47:609–15.
24. Chakrabarti R, Jung CY, Lee TP, Liu H, Mookerjee BK. Changes in glucose transport and transporter isoforms during the activation of human peripheral blood lymphocytes by phytohemagglutinin. *J Immunol*. (1994) 152:2660–8.

Conflict of Interest Statement: The authors declare that the research was conducted in the absence of any commercial or financial relationships that could be construed as a potential conflict of interest.

frontiers in Endocrinology

ORIGINAL RESEARCH
published: 10 April 2019
doi: 10.3389/fendo.2019.00223

Sonographic and Elastographic Features of Extra- and Intrathyroidal Ectopic Thymus Mimicking Malignancy: Differential Diagnosis in Children

*Magdalena Stasiak[1], Zbigniew Adamczewski[1,2], Renata Stawerska[1], Tomasz Krawczyk[3], Monika Tomaszewska[4] and Andrzej Lewiński[1,2]**

[1] Department of Endocrinology and Metabolic Diseases, Polish Mother's Memorial Hospital-Research Institute, Lodz, Poland, [2] Department of Endocrinology and Metabolic Diseases, Medical University of Lodz, Lodz, Poland, [3] Department of Pathology, Polish Mother's Memorial Hospital-Research Institute, Lodz, Poland, [4] Department of Pediatrics, Oncology, Hematology and Diabetology, Central Teaching Hospital of the Medical University of Lodz, Lodz, Poland

OPEN ACCESS

Edited by:
Marek Ruchala, Poznan University of Medical Sciences, Poland

Reviewed by:
Guia Vannucchi, Istituto Auxologico Italiano (IRCCS), Italy
Grzegorz Wiktor Kaminski, Military Institute of Medicine (Poland), Poland

***Correspondence:**
Andrzej Lewiński
alewin@csk.umed.lodz.pl

Specialty section:
This article was submitted to Thyroid Endocrinology, a section of the journal Frontiers in Endocrinology

Received: *28 November 2018*
Accepted: *20 March 2019*
Published: *10 April 2019*

Citation:
Stasiak M, Adamczewski Z, Stawerska R, Krawczyk T, Tomaszewska M and Lewiński A (2019) Sonographic and Elastographic Features of Extra- and Intrathyroidal Ectopic Thymus Mimicking Malignancy: Differential Diagnosis in Children. Front. Endocrinol. 10:223. doi: 10.3389/fendo.2019.00223

Thyroid nodules with ultrasound (US) cancer risk features and extra-thyroid lesions suggesting malignant lymph nodes, require prompt diagnosis, especially in children. The US pattern of intrathyroidal ectopic thymus (IET) can strongly suggest papillary thyroid carcinoma (PTC). The extra-thyroid ectopic thymic tissue (EET) can mimic pathological lymph nodes in US. The aim of the study has been to demonstrate US features and diagnostic methods, allowing finally to confirm the presence of IET and EET in children. The US and elastographic features of 16 ectopic thymic tissue (ET) lesions were analyzed so as to describe the typical characteristics of ET and to define the best method to differentiate ET and malignant lesions. Among 16 analyzed lesions, 11 lesions were IET, and 5 were EET adjacent to the thyroid connective tissue capsule. Most of IET were located in the middle part of the right lobe and were fusiform or oval in shape. All the lesions were solid, hypoechoic, and heterogeneous with bright internal echoes. Among IET, 73% of lesions had well- or very well-defined margins. In strain elastography of IET lesions, the strain ratio was similar in all lesions, and its value ranged from 0.95 to 1.09. Despite the low prevalence of IET and cervical EET, clinicians and radiologists should be aware of US characteristics of such lesions. The confirmation of their benign character is absolutely required. Elastography is a useful tool to initially differentiate PTC and IET. However, due to high risk of malignancy in thyroid lesions in children, similarity of US features of PTC and IET, and due to the possibility of malignancy in ET, only cytological evaluation provides definitive diagnosis.

Keywords: ectopic thymus, thyroid, elastography, ultrasound, thyroid cancer, metastatic lymph node

INTRODUCTION

Ultrasonography (US) is an accurate non-invasive diagnostic method commonly used in neck imaging. This is the first line tool in the diagnosis of thyroid gland nodules. In children, a frequent reason for neck US is the diagnosis of enlarged lymph nodes or other palpable neck nodules, but US is sometimes performed also due to family history of thyroid diseases or as a

part of population studies. The increasing availability of US examination results in accidental findings of many more thyroid lesions than there used to be. Estimates from US and postmortem examinations suggest that 1–1.5% of children and up to 13% of older adolescents or young adults have thyroid nodules (1). The risk of cancer in thyroid nodules in children is 22–26% and is much higher than in adults (up to 5–10%) (1). Thus, in accordance with current guidelines, any thyroid lesion found in a child, except for pure cysts, requires thorough diagnosis including fine needle aspiration biopsy (FNAB). The size of the thyroid nodule cannot be a qualification criterion for FNAB because the child's body and thyroid are smaller than an adult's. Therefore, even small but suspicious nodules should undergo FNAB. Bilateral occurrence of focal lesions in a child does not reduce diagnostic alertness because thyroid cancer in children is often multifocal and bilateral (1, 2). In children, disease progression at the time of diagnosis is usually significant, with the presence of lymph node metastases in most cases and—in over 20% of cases—also distant lung metastases (1, 2). Hence, careful US examination of lymph nodes is required in every child with thyroid lesions. Sonographic features suggesting malignant thyroid lesion include solid and hypoechoic tumor pattern, irregular tumor margins, tumor shape (taller than wide), presence of microcalcifications, and increased tumor vascularization. Abnormal, hypoechogenic structure within the neck, containing microcalcifications, and not showing central vascularization may correspond to a pathological neoplastic lymph node.

A thymus is a lymphatic organ involved in the differentiation of T lymphocytes. During embryogenesis, the thymus is formed from the ectoderm of the third branchial cleft and the endoderm of the third branchial pouch. The definitive thymus is formed by fusion of the right and left thymic primordials. Then it descends to the upper anterior mediastinum (3, 4). Aberrant thymic migration may lead to ectopic thymus location, including intrathyroidal locus. The prevalence of ectopic neck thymic tissue (ET) in children is very low and was reported as 0.99% (5) to 1.8% (6).

The US pattern of intrathyroidal ectopic thymus (IET) can strongly suggest papillary thyroid carcinoma (PTC), which is the most common thyroid cancer in children. The IET is usually a hypoechogenic lesion, with pronounced numerous punctate or linear bright internal echoes that suggest microcalcifications. In addition, the lesion margins may be irregular. Such features suggest PTC and require precise differential diagnosis. The extra-thyroid ectopic thymic tissue (EET) is most often located in the vicinity of the thyroid gland, usually close to the lower pole of the one of the lobes. For an inexperienced ultrasonographer, the US image of such a structure may suggest the presence of a pathological lymph node.

Strain elastography is a method which evaluates tissue stiffness (elasticity) by measuring the degree of tissue deformation in response to mechanical compression (7, 8). In this method, the stiffness of the thyroid lesion is compared to the adjacent healthy thyroid tissue and the difference in relative stiffness is presented as the strain ratio (SR). A SR value close to 1.0 means a similar relative stiffness for both evaluated tissues, and the higher the SR, the more suspicious the examined lesion is.

The aim of the study has been to present US features and diagnostic methods that will finally allow for confirmation of the presence of ET in children who were referred to our center in order to definitively diagnose suspicious thyroid nodules. Most of the presented children had already been scheduled for thyroid surgery in other centers.

MATERIALS AND METHODS

Medical data of nine children with 16 lesions, who were referred to the Department of Endocrinology and Metabolic Diseases, Polish Mothers' Memorial Hospital–Research Institute, Lodz, Poland, with suspected PTC or suspicion of neoplastic lymph node were analyzed. In 11 of the cases, the US image of thyroid gland required differentiation with IET and in the remaining 5, the EET mimicked metastatic lymph nodes. After admission, patients had laboratory tests performed, including thyrotropin (TSH), free triiodothyronine (FT3), free thyroxine (FT4), parathyroid hormone (PTH) levels, anti-thyroglobulin antibodies (aTg), anti-thyroid peroxidase antibodies (aTPO), and TSH receptor antibodies (TRAb). All parameters were measured by electrochemiluminescence immunoassay (ECLIA) with a Cobas e601 analyzer (Roche Diagnostics, USA). Ultrasound examination was performed in every patient using a 7–14 MHz linear transducer (AplioXG, Toshiba Medical Systems Corp., Shimoishigami, Otawara-shi, Tochigi-ken, Japan). Scanning was performed in supine position with a pad under the patients' shoulders to provide optimum neck extension. Strain elastography was performed in all IET lesions (AplioXG, Toshiba Medical Systems Corp., Shimoishigami, Otawara-shi, Tochigi-ken, Japan).

FNAB with US guidance was performed in all patients using a 23-gauge needle. In all patients FNAB procedures were performed under moderate sedation or general anesthesia. All cytological evaluations were carried out by the same pathologist, who had more than 20 years of experience. Smears were cytologically evaluated and the presence of small lymphocytes with scattered epithelioid cells, without the presence of macrophages, histiocytes, or other cell types (e.g., eosinophils and plasma cells) was considered as a result typical for thymic tissue. The absence of lymphocytes of different stages of differentiation together with the absence of macrophages and other cells typically occurring in lymph nodes were required for differentiation with lymph nodes or other lymphatic tissues. The absence of oncotic follicular cells and plasma cells allowed us to cytologically exclude lymphocytic thyroiditis.

In all cases, written informed consent for all performed procedures was obtained from the patients' parents.

RESULTS

Clinical Features

The mean age of our patients was 5.8 years, ranging from 6 months to 11 years. The male to female ratio was 3:1.

Abbreviations: EET, extrathyroidal ectopic thymic tissue; ET, ectopic thymic tissue; IET, intrathyroidal ectopic thymus; PD, power Doppler; PTC, papillary thyroid carcinoma; SR, strain ratio; US, ultrasound.

TABLE 1 | Ultrasound characteristics of the patients with ectopic thymic tissue.

Case	Age	Gender	No of lesions in one child	Location	Size (mm)	Bilateral
1	6 mo	F	1	EET below RL	12 × 8 × 18	No
2	5 yr	M	2	RL inferior part	RL: 5 × 4 × 5	Yes
				LL middle part	LL: 5 × 2 × 5	
3	7 yr	M	3	RL middle part	RL: 5 × 2 × 6	Yes
				LL middle part	LL: 11 × 2 × 12	
				EET below the RL	Below RL: 10 × 5 × 12	
4	4 yr	M	2	RL middle part	RL: 4 × 2 × 6	No
				EET below RL	Below RL: 5 × 4 × 7	
5	10 yr	F	1	RL middle part	6 × 2 × 7	No
6	4 yr	M	3	RL inferior part	RL inferior: 3 × 2 × 4	Yes
				RL middle part	RL middle: 7 × 3 × 6	
				LL inferior part	LL: 5 × 6 × 11	
7	5 yr	F	1	LL inferior part	7 × 6 × 14	No
8	11 yr	M	2	EET below RL	Below RL: 9 × 9 × 17	Yes
				EET below LL	Below LL: 7 × 13 × 16	
9	6 yr	M	1	RL middle part	6 × 4 × 7	No

EET, extrathyroidal ectopic thymus; F, female; IET, intrathyroidal ectopic thymus; LL, left lobe; M, male; mo, months; RL, right lobe; yr, years.

None of the children had any family history of thyroid cancer nor did they have medical history of irradiation. We did not measure calcitonin levels in the evaluated patients, as routine calcitonin assessment in diagnostics of thyroid nodules in children not harboring germline *RET* proto-oncogene mutation is not recommended (2). However, in 4 children the level of calcitonin was assessed in other centers and in all of them it was lower than 10 pg/ml, ranging from 4 to 7 pg/ml. In all patients in whom thyroid hormone tests were performed, all the results were normal for the patients' age. Anti-thyroid antibodies were negative in all cases. Clinical characteristics of the patients are presented in **Supplementary Table 1**.

Ultrasonographic Features

A total of 16 ectopic thymic tissues were found in 9 patients. Eleven lesions were IET and five were EET adjacent to the thyroid capsule. Ultrasound features of the studied lesions are presented in **Tables 1**, **2**. IET size varied from 4 to 14 mm with the mean largest dimension at 6.5 mm, while EET size ranged from 7 to 18 mm with a mean largest dimension of 14 mm. Among IET, 7 lesions were located in right lobe and 4 in left lobe, 7 were found in the middle part of thyroid lobe, 4 in the lower part, and none in the upper part of the thyroid lobe. In three children, IET was located bilaterally, while in four children IET was unilateral. Extrathyroidal lesions were unilateral in 3 children, and all of them were located directly below the right lobe. In one child EET was bilateral. Coexistence of EET and IET was found in 2 children (**Table 1**).

Most of the cases of IET were fusiform (4 lesions) (**Figure 3A**) or oval (5 lesions) (**Figure 4A**) in shape, while extrathyroidal thymic tissue lesions were triangular (2 lesion) (**Figure 1D**), or oval (3 lesion). Among IET cases, there was one lesion of non-typical heart shape and one lesion of very characteristic longitudinal shape (**Figure 1A**), which strongly suggested ectopic tissue. In US, all the lesions were solid, hypoechoic, and heterogeneous with bright internal echoes (**Figures 1**–**4**). In all lesions, linear bright echoes were present, while punctual echoes were observed in 6 lesions only. The number of bright echoes varied, from numerous to only a few (3–4) echoes. In 6 lesions, the bright echoes were located in the middle of the lesion, with a hypoechoic margin (**Figure 1A**), while in the remaining 9 lesions they were scattered, in 7 cases unevenly (**Figures 2A**, **3A**). Among IET cases, 73% (8/11) had well or very well-defined margins and only 3 lesions had blurred margins (27%) (**Figure 4A**). All extrathyroidal lesions had well-defined margins (**Figure 1D**). In 6 of the IET nodules, blood flow in power Doppler (PD) evaluation was decreased, and in the remaining 5 IET cases no blood flow was observed (**Table 2**). All extrathyroidal lesions had decreased blood flow in PD (**Table 2**). In all cases, the EET resembled an US appearance of a normal thymus, which was present in a normal location in every patient (**Figure 1C**).

Elastographic Features

In strain elastography of IET lesions, the SR was similar in all lesions, and its value ranged from 0.95 to 1.09, mean 1.02 (**Table 2**, **Figures 1B**, **2B**, **3B**, **4B**), thus the stiffness of IET was comparable to adjacent thyroid tissue.

Cytomorphological Features

The cytology findings included lymphoid cells that were usually numerous, always with a predominance of small lymphocytes with scattered epithelioid cells (**Figures 2C**, **3C**, **4C**). None of the smears included thyroid follicular cells, macrophages, histiocytes or other cell types (e.g., eosinophils and plasma cells). The absence of lymphocytes of different stages of differentiation, macrophages and other cells typically occurring in lymph nodes allowed for differentiation with lymph nodes or other lymphatic tissues. The absence of thyroid follicular cells, oncotic

TABLE 2 | Ultrasound features and strain ratio (SR) of lesions diagnosed as ectopic thymic tissue.

No	Size (mm)	Shape	Internal echoes	Margins	Vascularity	Elastography SR	Cytology
1	5 × 4 × 5	Heart	A few linear bright echoes in the middle, hypoechoic margin	Well-defined	low	0.97	Typical for thymus
2	5 × 2 × 5	Fusiform	A few linear bright echoes in the middle, hypoechoic margin	Very well-defined	low	1.09	Typical for thymus
3	5 × 2 × 6	Fusiform	Numerous punctual and linear bright internal echoes scattered unevenly	Blurred	low	1.06	Typical for thymus
4	11 × 2 × 12	Longitudinal	Numerous punctual and linear bright internal echoes scattered mainly in the medial part	Very well-defined	low	0.95	Typical for thymus
5	4 × 2 × 6	Fusiform	Several punctual and linear bright internal echoes scattered unevenly	Well-defined	low	0.96	Typical for thymus
6	6 × 2 × 7	Oval	Three linear bright internal echoes in the middle, hypoechoic margin	Well-defined	no	1.06	Typical for thymus
7	3 × 2 × 4	Oval	Very few linear bright internal echoes in the middle, hypoechoic margin	Blurred	no	0.99	Typical for thymus
8	7 × 3 × 6	Fusiform	A few linear bright internal echoes in the middle, hypoechoic margin	Well-defined	low	1.09	Typical for thymus
9	5 × 6 × 11	Oval	A few linear bright internal echoes scattered mainly in the middle, hypoechoic margin	Well-defined	low	1.01	Typical for thymus
10	7 × 6 × 14	Oval	Several punctual and linear bright internal echoes scattered unevenly	Well-defined	low	0.97	Typical for thymus
11	6 × 4 × 7	Oval	A few scattered linear bright internal echoes	Blurred	low	1.03	Typical for thymus
12	12 × 8 × 18	Oval	A few linear bright echoes scattered unevenly	Well-defined	low	NA	Typical for thymus
13	7 × 4 × 5	Triangular	A few punctual and linear bright internal echoes scattered unevenly	Very well-defined	low	NA	Typical for thymus
14	10 × 5 × 12	Triangular	Several punctual and linear bright internal echoes scattered unevenly	Very well-defined	low	NA	Typical for thymus
15	9 × 9 × 17	Oval	Several linear bright internal echoes scattered quite unevenly	Very well-defined	low	NA	Typical for thymus
16	7 × 13 × 16	Oval	Several linear bright internal echoes scattered quite evenly	Very well-defined	low	NA	Typical for thymus

Lesions are presented according to the location: first 11 lesions are IET, second 5 lesions are EET.
EET, extrathyroidal ectopic thymus; LL, left lobe; NA, not applicable; RL, right lobe; SR, strain ratio.

cells, histiocytes, macrophages and plasma cells allowed us to cytologically exclude autoimmune thyroiditis. In all cases, the material was sufficient for cytological analysis and a cytological confirmation of ET was possible.

DISCUSSION

In children, finding of a pathological lesion in the thyroid or in another cervical location always arouses diagnostic alertness. Many extrathyroidal lesions on a child's neck are reactive lymph nodes that only require observation. However, thyroid nodules other than pure cysts and every cervical mass with suspicious US features require further accurate diagnosis to exclude malignancy.

There are a few reports on the prevalence and ultrasound characteristics of IET, which were carried out on large groups of patients, but the presence of IET was confirmed in them only on the basis of US imagery without cytological evaluation (4, 5). In many reports on the US characteristics of ET, cytological evaluation was not performed although the number of analyzed lesions was similar or even lower than ours (3, 9, 10). This approach involves the potentially high risk of misdiagnosis of children with suspicious thyroid lesions, some of which can be malignant. Reports in which IET suspicion was confirmed cytologically include small groups of patients with a dozen or so (2–15 subjects) IET lesions analyzed (6, 11–13). The group presented in this study is therefore one of the largest with cytological IET confirmation described so far. To the best of our knowledge, this is the first study in which elastography was used in the diagnosis of IET, and the first study that demonstrated the usefulness of this method in the initial evaluation of IET-like lesions. We have shown that the stiffness of IET tissue is similar to the stiffness of the surrounding healthy thyroid tissue (mean SR 1.02). This is of great importance in the differentiation of IET and PTC, since PTC is known to be significantly stiffer than thyroid tissue (14). Follicular cancer, which is often soft in elastography

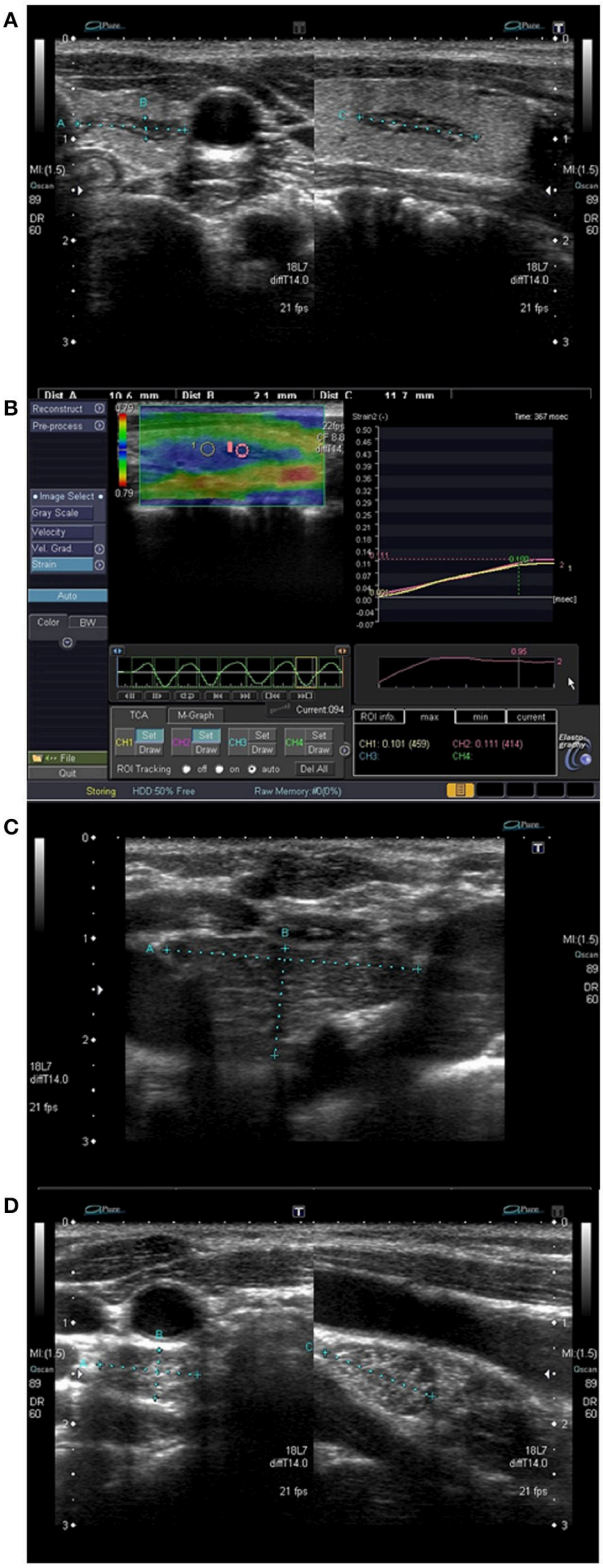

FIGURE 1 | Patient No. 3 (**Table 1**). **(A)** A longitudinal intrathyroid ectopic thymus (IET) of the left thyroid lobe; **(B)** Elastography of the IET; **(C)** Normal thymus in physiologic location; **(D)** Extrathyroid ectopic thymus below the right thyroid lobe.

and different in US pattern, is extremely rare in children. The usefulness of elastography is therefore even greater, because it can be assumed that a US IET-like lesion with stiffness similar to the thyroid tissue is actually IET. If the stiffness of the lesion is greater than the surrounding thyroid tissue, we should suspect PTC, even if the US pattern of the lesion resembles IET.

The US differential diagnosis between IET and suspicious thyroid nodules is challenging. Children with hypoechoic nodules with microcalcification-like echoes are often referred for surgery due to strong suspicion of malignancy.

In our study, the analyzed IET cases were located mostly in the middle part of the thyroid lobe (7 lesions) and less frequently in the lower part (4 lesions). In nearly half of the patients with IET, lesions were bilateral. Most extrathyroidal lesions were located directly below the right lobe. These observations are not fully consistent with previously published ones, because IET locations described by other authors varied. Bang et al. (11) found all 15 IET lesions in the inferior part of the thyroid lobe and IET was bilateral only in four patients. Similarly, all eight IET lesions described by Escobar et al. (6) were located in the inferior part of the thyroid, but strangely no subject had bilateral lesions. On the contrary, Kabaalioğlu et al. (4) reported a similar occurrence of IET in the middle and lower parts of the thyroid lobes. Interestingly, among 14 cases, only two IET cases were bilateral (4). Kim et al. (3) reported four IET cases in the middle part of the thyroid lobe while the remaining 8 IET cases were in the inferior part. Bilateral IET was observed in 3 cases (3). The predominance of IET occurrence in the middle part of the thyroid lobe was observed by Yildiz et al. (10), who reported 11 IET cases, among which 10 were located in the middle part and one in the inferior part of the lobe. Once again, none of the IET cases were bilateral (10). In two of 12 children with IET described by Frates et al. (12), the lesions were bilateral, and—interestingly—one of the lesions was located in the upper part of the thyroid. Comparing our observations and other authors' findings, it is clearly visible that IET is located in the middle or in the inferior part of the thyroid lobe, and extremely rarely it occurs in the upper part. However, it is a surprising issue that some of the authors did not observe the existence of bilateral IET (6, 10). Even when considering all our ET lesions together (extra-and intrathyroidal), the frequency of bilateral and unilateral ET occurrence is similar in our group. Perhaps this discrepancy is due to the fact that some very small lesions, located in the inferior pole of the thyroid lobes, were difficult to visualize and may have been neglected in other studies. The age does not seem to be decisive for the frequency of bilateral IET, as in our group the patients with bilateral lesions were 4–7 years old, similarly as in other authors' reports (4–9 years) (4), while in much younger children no bilateral IET cases were reported (11). It seems, therefore, that at least until the onset of puberty when the physiological process of thymic involution begins, the age does not affect the incidence and location of IET.

In US, most of our analyzed IET lesions were fusiform or ovular in shape, and one lesion had a very characteristic longitudinal shape which strongly suggested ectopic tissue rather than thyroid nodule. All the lesions were solid, hypoechoic, and heterogeneous with bright internal punctual or linear echoes. Generally, linear echoes are easier to differentiate from

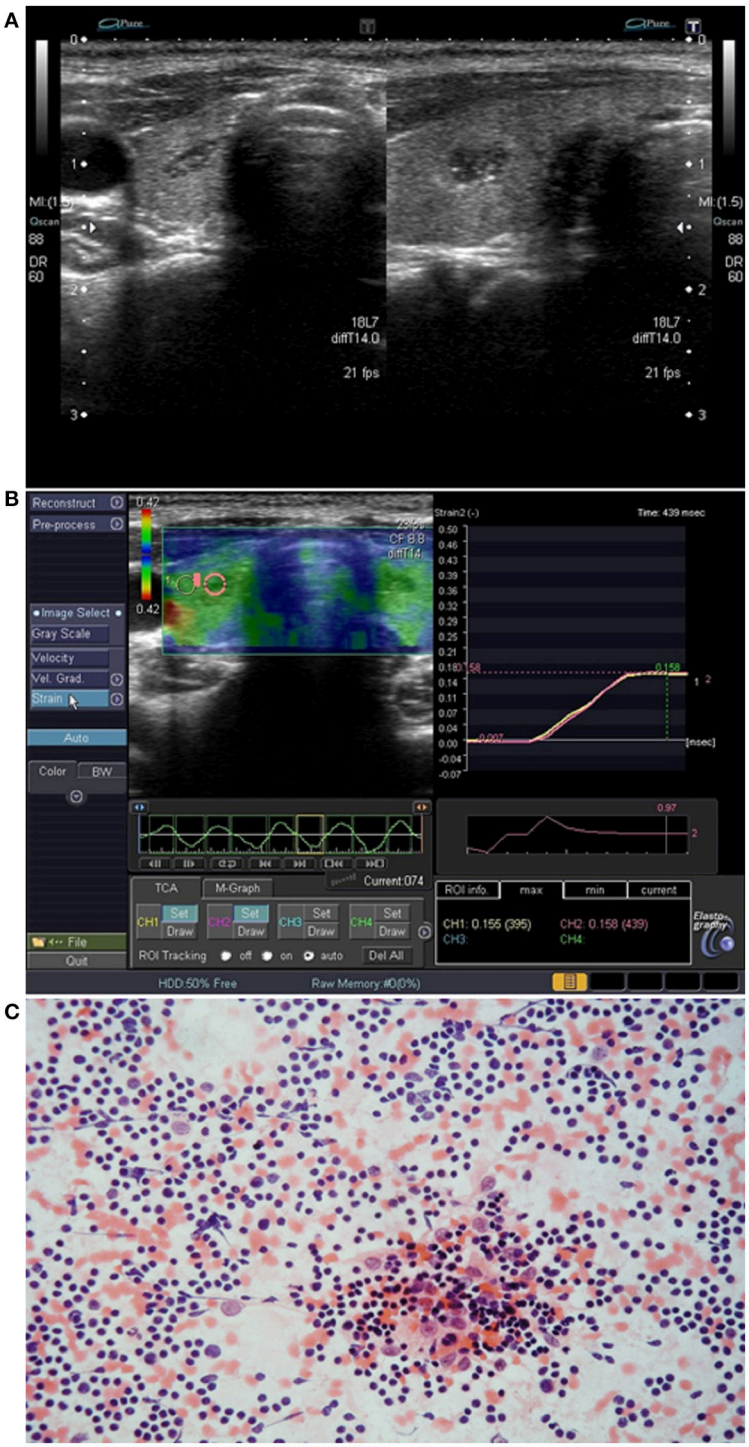

FIGURE 2 | Patient No. 2 (**Table 1**). **(A)** Intrathyroid ectopic thymus (IET) with well-defined margins in the right thyroid lobe; **(B)** Elastography of the IET; **(C)** Cytological smear shows numerous small lymphocytes with scattered epithelioid cells (hematoxylin-eosin staining; light microscopy, magnification ×80).

microcalcifications while punctual ones can look exactly like microcalcifications. It is known that both bright echoes in ET and microcalcifications in thyroid nodules are not evenly distributed within the lesions and can occur at one (in IET mainly central) or more parts of the lesion or can be scattered unevenly.

Most of ETs typically have well-defined margins, but sometimes the margins can be blurred or irregular, which can additionally suggest malignancy. Blood flow in PD is known to be decreased or absent. Our observations are similar to other authors' findings (3–6, 9–13). In our

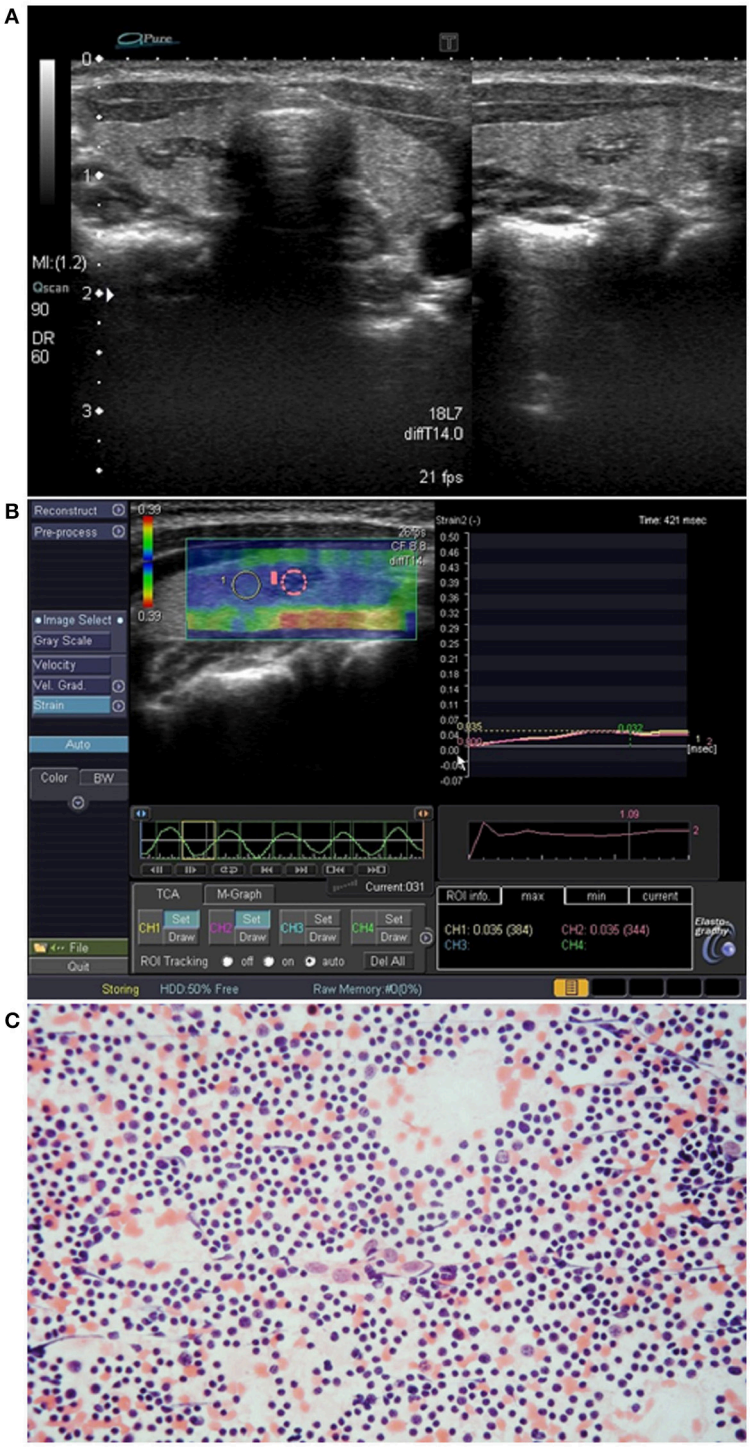

FIGURE 3 | Patient No. 6 (**Table 1**). **(A)** Intrathyroid ectopic thymus (IET) in the right thyroid lobe; **(B)** Elastography of the IET; **(C)** Cytological smear shows numerous small lymphocytes with scattered epithelioid cells (hematoxylin-eosin staining; light microscopy, magnification ×80).

group, IET cases were hypovascular or no vascularity was visible on PD. Yildiz et al (9, 10) reported a group of patients in whom a few lesions were isovascular comparing to the thyroid parenchyma. Unfortunately, most authors did not report IET-related vascularity at all.

In our analyzed group of children, and in other described cohorts (5), the prevalence of IET was higher in males than

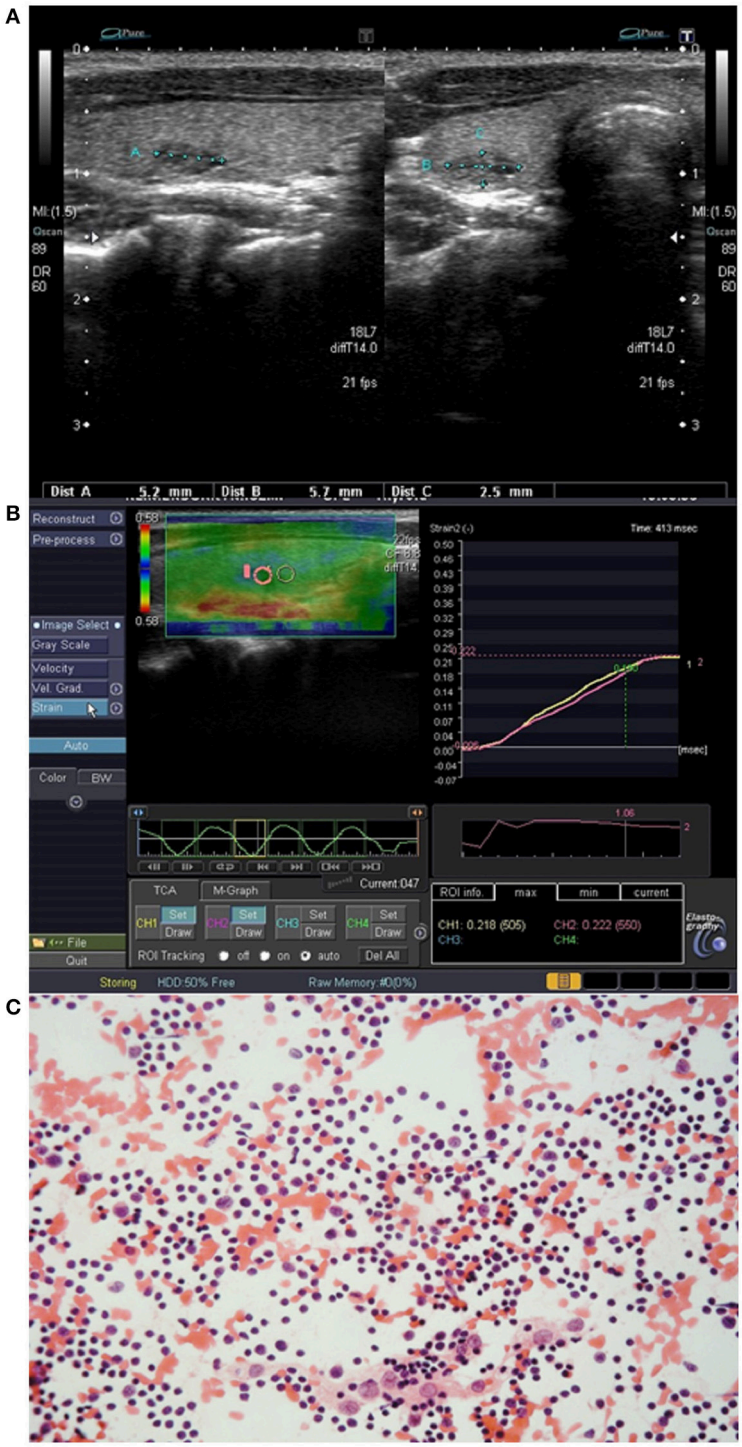

FIGURE 4 | Patient No. 3 (**Table 1**). **(A)** Intrathyroid ectopic thymus (IET) with blurred margins in the right thyroid lobe; **(B)** Elastography of the IET; **(C)** Cytological smear shows numerous small lymphocytes with scattered epithelioid cells (hematoxylin-eosin staining; light microscopy, magnification ×80).

females, although a few authors reported higher frequency in females (3). The mean age was also similar to those reported by other authors (3–6, 9–13). The largest dimension of ET lesion in or group was 4–18 mm, while other authors reported ET size from 3 to 33 mm (3, 4, 6, 11, 12). The largest ET dimensions were reported by Bang et al. (11), and in this group half of the patients were younger than 1 year old. In older children the size of ET was smaller but still very diverse (3–27 mm) and did not seem to

depend on the age of the child at the time of diagnosis (3, 4, 6, 12). In all our cases, the ET tissue was similar in the US pattern to the normal descended thymus which was visible in every subject.

It is known that the IET tissue actually resembles the US pattern of papillary carcinoma and EET mimics metastatic lymph nodes. Distinguishing the suspicious thyroid nodule from IET in US requires a lot of experience. The lack of visible metastatic lymph nodes, which are typically present in children with PTC, cannot be used to exclude malignancy. Punctual bright internal echoes in ET are virtually impossible to differentiate from microcalcifications in US. In ET with linear bright echoes, such differentiation is possible, but only if a very experienced sonographer is available. However, in pediatric patients with hypoechoic thyroid nodule containing bright internal echoes resembling microcalcifications, the exclusion of malignancy cannot be based only on US examination. In our study, the usefulness of elastography in the differential diagnosis of IET and PTC has been demonstrated, but this method still does not provide a definitive diagnosis. Clinicians and radiologists should be aware of typical locations, US patterns and elastography features of ET, so as not to trigger unnecessary anxiety in the patient and his/her parents, and not to suggest the presence of PTC and unnecessarily refer to surgery. However, due to the high risk of cancer in thyroid nodules in children (1, 2), one should not determine the diagnosis only on the US image, neglecting further evaluation. It seems that such an approach can be recommended only when the US evaluation is done by a very experienced ultrasonographer, as there is a possibility of regular US monitoring, and—at the same time—there are contraindications to FNAB, resulting—for example—from contraindications to even short-term sedation in a very young child. One should always remember that ET and PTC may look similar. Moreover, it should be underlined that rare cases of thymoma, thymic carcinoma and lymphoblastic lymphoma arising from ET were reported (4, 15–18). Therefore, whenever possible, the diagnosis of cervical ET should be confirmed cytologically, although it may be difficult to aspirate diagnostic material from ET. Only cytological confirmation ensures that the evaluated lesion is a benign ET that requires simple periodical US monitoring. There are known cases when thyroidectomy was performed due to the lack of diagnostic material from FNAB in IET with suspicious US findings (19).

In conclusion, despite the low prevalence of IET and cervical EET, clinicians and radiologists should be aware of US characteristics of such lesions and of the necessity of confirmation of their benign character. Elastography is a useful tool to initially differentiate PTC and IET. However, due to the high risk of malignancy in thyroid lesions in children, similarity of US features of PTC and IET, and because of the possibility of malignancy in ET, only cytological evaluation provides definitive diagnosis and prevents, on one hand, unnecessary frequent diagnostic procedures and/or surgery and, on the other hand, missing malignant lesions.

ETHICS STATEMENT

This study was carried out in accordance with the recommendations of WHO′ Standards and operational guidance for ethics review of health-related research with human participants, with written informed consent from all subjects' parents. All subjects' parents gave written informed consent in accordance with the Declaration of Helsinki. The protocol was approved by the Ethic Committee of Polish Mother's Memorial Hospital–Research Institute, Lodz, Poland.

AUTHOR CONTRIBUTIONS

MS was responsible for study design, data collection, data analysis, and writing of the manuscript. ZA, RS, and MT contributed to data collection and data analysis. TK contributed to data collection and was responsible for cytology smear assessment. AL contributed to study design, and writing of the manuscript. All authors were involved in writing the paper and approved the submitted final versions.

ACKNOWLEDGMENTS

The study was financially supported by the statutory funds from the Polish Mother's Memorial Hospital–Research Institute, Lodz, Poland, and from the Medical University of Lodz, Lodz, Poland (503/1-107-03/503-11-001-18).

SUPPLEMENTARY MATERIAL

The Supplementary Material for this article can be found online at: https://www.frontiersin.org/articles/10.3389/fendo.2019.00223/full#supplementary-material

REFERENCES

1. Francis GL, Waguespack SG, Bauer AJ, Angelos P, Benvenga S, Cerutti JM, et al. American thyroid association guidelines task force. management guidelines for children with thyroid nodules and differentiated thyroid cancer. *Thyroid.* (2015) 25:716–59. doi: 10.1089/thy.2014.0460
2. Niedziela M, Handkiewicz-Junak D, Małecka-Tendera E, Czarniecka A, Dedecjus M, Lange D, et al. Diagnostics and treatment of differentiated thyroid carcinoma in children - guidelines of polish national societies. *Endokrynol Pol.* (2016) 67:628–42. doi: 10.5603/EP.2016.0072
3. Kim HG, Kim MJ, Lee MJ. Sonographic appearance of intrathyroid ectopic thymus in children. *J Clin Ultrasound.* (2012) 40:266–71. doi: 10.1002/jcu.21898
4. Kabaalioğlu A, Öztek MA, Kesimal U, Çeken K, Durmaz E, Apaydın A. Intrathyroidal ectopic thymus in children: a sonographic survey. *Med Ultrason.* (2017) 19:179–84. doi: 10.11152/mu-913
5. Fukushima T, Suzuki S, Ohira T, Shimura H, Midorikawa S, Ohtsuru A, et al. Thyroid examination unit of the radiation medical center for the fukushima health management survey. prevalence of ectopic intrathyroidal thymus in japan: the fukushima health management survey. *Thyroid.* (2015) 25:534–7. doi: 10.1089/thy.2014.0367

6. Escobar FA, Pantanowitz L, Picarsic JL, Craig FE, Simons JP, Viswanathan PA, et al. Cytomorphology and sonographic features of ectopic thymic tissue diagnosed in paediatric FNA biopsies. *Cytopathology.* (2018) 29:241–6. doi: 10.1111/cyt.12529
7. Adamczewski Z, Dedecjus M, Skowrońska-Jóźwiak E, Lewiński A. Metastases of renal clear-cell carcinoma to the thyroid–a comparison of shear-wave and quasi-staticelastography. *Pol Arch Med Wewn.* (2014) 124:485–6. doi: 10.20452/pamw.2413
8. Ruchała M, Szmyt K, Sławek S, Zybek A, Szczepanek-Parulska E. Ultrasound sonoelastography in the evaluation of thyroiditis and autoimmune thyroid disease. *Endokrynol Pol.* (2014) 65:520–6. doi: 10.5603/EP.2014.0071
9. Yildiz AE, Elhan AH, Fitoz S. Prevalence and sonographic features of ectopic thyroidal thymus in children: a retrospective analysis. *J Clin Ultrasound.* (2018) 46:375–9. doi: 10.1002/jcu.22590
10. Yildiz AE, Ceyhan K, Sıklar Z, Bilir P, Yağmurlu EA, Berberoğlu M, et al. Intrathyroidal ectopic thymus in children: retrospective analysis of grayscale and doppler sonographic features. *J Ultrasound Med.* (2015) 34:1651–6. doi: 10.7863/ultra.15.14.10041
11. Bang MH, Shin J, Lee KS, Kang MJ. Intrathyroidal ectopic thymus in children: a benign lesion. *Medicine.* (2018) 97:e0282. doi: 10.1097/MD.0000000000010282
12. Frates MC, Benson CB, Dorfman DM, Cibas ES, Huang SA. Ectopic intrathyroidal thymic tissue mimicking thyroid nodules in children. *J Ultrasound Med.* (2018) 37:783–91. doi: 10.1002/jum.14360
13. Chng CL, Kocjan G, Kurzawinski TR, Beale T. Intrathyroidal ectopic thymic tissue mimicking thyroid cancer in children. *Endocr Pract.* (2014) 20:e241–5. doi: 10.4158/EP14236.CR
14. Tian W, Hao S, Gao B, Jiang Y, Zhang X, Zhang S, et al. Comparing diagnostic accuracy of RTE and SWE in differentiating malignant thyroid nodules from benign ones: a meta-analysis. *Cell Physiol Biochem.* (2016) 39:2451–63. doi: 10.1159/000452513
15. Wu SL, Gupta D, Connelly J. Adult ectopic thymus adjacent to thyroid and parathyroid. *Arch Pathol Lab Med.* (2001) 125:842–3. doi: 10.1043/0003-9985(2001)125<0842:AETATT>2.0.CO;2
16. Büyükyavuz I, Otçu S, Karnak I, Akçören Z, Senocak ME. Ectopic thymic tissue as a rare and confusing entity. *Eur J Pediatr Surg.* (2002) 12:327–9. doi: 10.1055/s-2002-35961
17. Hirokawa M, Miyauchi A, Minato H, Yokoyama S, Kuma S, Kojima M. Intrathyroidal epithelial thymoma/carcinoma showing thymus-like differentiation; comparison with thymic. *APMIS.* (2013) 121:523–30. doi: 10.1111/apm.12017
18. Pan XB, Lang ZQ, Cai L. Primary T lymphoblastic lymphoma arising from ectopic thymus in the neck of a child. *Zhonghua Er Bi Yan Hou Tou Jing Wai Ke Za Zhi.* (2011) 46:159–60.
19. Durmaz E, Barsal E, Parlak M, Gurer I, Karaguzel G, Akcurin S, et al. Intrathyroidal ectopic thymic tissue may mimic thyroid cancer: a case report. *J Pediatr Endocrinol Metab.* (2012) 25:997–1000. doi: 10.1515/jpem-2012-0207

Conflict of Interest Statement: The authors declare that the research was conducted in the absence of any commercial or financial relationships that could be construed as a potential conflict of interest.

Advantages of publishing in Frontiers

OPEN ACCESS
Articles are free to read for greatest visibility and readership

FAST PUBLICATION
Around 90 days from submission to decision

HIGH QUALITY PEER-REVIEW
Rigorous, collaborative, and constructive peer-review

TRANSPARENT PEER-REVIEW
Editors and reviewers acknowledged by name on published articles

Frontiers
Avenue du Tribunal-Fédéral 34
1005 Lausanne | Switzerland

Visit us: www.frontiersin.org
Contact us: info@frontiersin.org | +41 21 510 17 00

REPRODUCIBILITY OF RESEARCH
Support open data and methods to enhance research reproducibility

DIGITAL PUBLISHING
Articles designed for optimal readership across devices

FOLLOW US
@frontiersin

IMPACT METRICS
Advanced article metrics track visibility across digital media

EXTENSIVE PROMOTION
Marketing and promotion of impactful research

LOOP RESEARCH NETWORK
Our network increases your article's readership